Stochastic Image Models and Texture Synthesis

Bruno Galerne

Ecole Normale Supérieure de Cachan

Thèse

Présentée par

Bruno GALERNE

pour obtenir le grade de

Docteur de l'Ecole Normale Supérieure de Cachan
Domaine : MATHÉMATIQUES APPLIQUÉES

Modèles d'image aléatoires et synthèse de texture

Stochastic Image Models and Texture Synthesis

Soutenue le 9 décembre 2010 devant le jury composé de :

Rapporteurs :	Gabriel PEYRÉ	-	CNRS - Université Paris Dauphine
	François ROUEFF	-	Télécom ParisTech
	Volker SCHMIDT[1]	-	Universität Ulm
Président du jury :	Lionel MOISAN	-	Université Paris Descartes
Examinateurs :	Christian LANTUÉJOUL	-	Mines ParisTech
	Sylvain LEFEBVRE	-	INRIA Nancy
	Elena VILLA	-	Università degli Studi di Milano
Directeur :	Jean-Michel MOREL	-	Ecole Normale Supérieure de Cachan
Codirecteur :	Yann GOUSSEAU	-	Télécom ParisTech

---

[1]Non présent à la soutenance

Remerciements

En tout premier lieu je tiens à exprimer toute ma gratitude à Jean-Michel Morel et Yann Gousseau qui ont tous deux dirigé mes travaux de thèse. Je les remercie sincèrement pour la qualité de leur encadrement durant ces trois dernières années. Les échanges et les discussions qui ont ponctué l'avancée de ma thèse n'ont pas seulement été riches de l'étendue de leur connaissances et de leur intuitions scientifiques mais aussi de leurs qualités humaines. Enfin, je remercie Jean-Michel Morel et Yann Gousseau pour m'avoir toujours soutenu et encouragé dans mes projets de thèse tout en m'ayant laissé la liberté de choix des sujets traités.

Je souhaite également remercier les membres de mon jury de thèse. Je tiens tout d'abord à exprimer ma reconnaissance à Gabriel Peyré, François Roueff et Volker Schmidt pour m'avoir fait l'honneur de rapporter ma thèse. Je remercie sincèrement les examinateurs, Christian Lantuéjoul, Sylvain Lefebvre, Lionel Moisan et Elena Villa d'avoir accepté de prendre part au jury. Des travaux de chacun d'eux ont eu une place importante au cours de l'élaboration de ma thèse, et je suis donc particulièrement honoré par leur présence.

Si ces trois années de thèse m'ont donné goût à la recherche, c'est aussi grâce aux divers échanges que j'ai pu avoir avec certains chercheurs et enseignants-chercheurs. Merci donc à Jean-François Aujol, Hermine Biermé, Antoni Buades, Pierre Calka, Antonin Chambolle, Jérôme Darbon, Julie Delon, Agnès Desolneux, Anne Estrade, Saïd Ladjal, Simon Masnou, Lionel Moisan, Gabriel Peyré, Frédéric Richard et François Roueff. Enfin je tiens tout particulièrement à remercier George Drettakis, Ares Lagae et Sylvain Lefebvre pour m'avoir accueilli quelques jours à l'INRIA Sophia-Antipolis et avoir répondu favorablement à ma demande de collaboration. Je remercie également l'ensemble de l'équipe du projet ANR MATAIM auquel j'ai la chance de participer.

Je me dois bien évidemment de remercier les personnes qui m'ont accompagné au quotidien pour ce travail de thèse. Cela concerne tout d'abord le personnel du CMLA et de Télécom ParisTech. Pour leur gentillesse et leur bienveillance merci à toutes les secrétaires : Carine, Micheline, Sandra, Véronique et Virginie au CMLA, et Patricia à Télécom. Merci aussi à Christophe et Pascal, les spécialistes de l'informatique. Effectuer mon monitorat au département de mathématiques de l'ENS Cachan a été une expérience enrichissante. Merci donc à Frédéric Pascal, Sylvie Fabre, Claudine Picaronny, et, une fois de plus, à Jean-Michel Morel.

J'ai évidemment une pensée particulière pour tous les doctorants du CMLA, de Télécom et d'ailleurs avec qui j'ai passé de très bons moments. Les anciens d'abord : Ayman, F.-X., Frédéric, Frédérique, Gaël, Jean-Pascal, Jérémie, Julien, Neus, Rafa, Thomas, auxquels je dois ajouter Julie et Joseph qui viennent de soutenir leur thèse. Et tous les autres (à qui je souhaite bon courage !) : Adina, Aude, Baptiste M., Baptiste C., Benjamin, Charles, Eric, Gui-Song, Marc, Mathieu, Morgan, Nicolas C., Nicolas L., Mauricio, Saad, Vincent, Yohann, Yves, Zhongwei. . . avec mes excuses à tous ceux qui ne figurent pas sur cette liste !

Bien sûr, ce travail n'aurait pas vu le jour sans les encouragements et le soutien

de mes proches. En premier lieu je voudrai remercier mes parents à qui ce projet de thèse tient beaucoup à cœur. La présence de ma sœur à ma soutenance me touche particulièrement et je lui en remercie. Je tiens également à exprimer ma reconnaissance à mes beaux-parents, Jean-Paul et Jocelyne, qui ont toujours exprimé de l'intérêt pour mes divers projets. Merci aussi à Vincent et Elodie pour leur écoute et leur bonne humeur. Je les félicite une fois encore pour avoir donné naissance à Luce, la petite dernière de la famille. Merci également à mes amis Thibaut et Gelsomina ainsi qu'à leur petite Sophie dont j'ai l'honneur d'être le parrain. Enfin, à Amélie, merci infiniment pour ton soutien sans faille tout au long de cette thèse.

Contents

Introduction

Contents

This thesis is a study of stochastic image models with a view toward texture synthesis. Most of the stochastic texture models under investigation are germ-grain models.

In the first part of the thesis, texture synthesis algorithms relying on the shot noise model are developed. The subject of the second part is to introduce and study a new germ-grain model involving a transparency principle. Finally, in the third part of the thesis, general results on random fields of bounded variation are established. As particular cases of interest, these general results permit the computation of the mean perimeter of random sets and of the mean variation of classical germ-grain models.

Before describing in further details the contributions of the thesis, general facts on texture synthesis and germ-grain models are recalled.

1.1 Texture Synthesis

1.1.1 What is a Texture?

There is no clear definition of textures as image models. A minimal definition of a texture image is an "image containing repeated patterns" [152], where the family of patterns reflects a certain amount of randomness depending on the nature of the texture. Among the family of textures, one discriminates two main subclasses. First, the *micro-textures*, also called stochastic textures, typical examples of which are images of sand, clouds, or a water surface. The second main family of textures

(a) Pebbles micro-texture   (b) Pebbles macro-texture   (c) Some pebbles
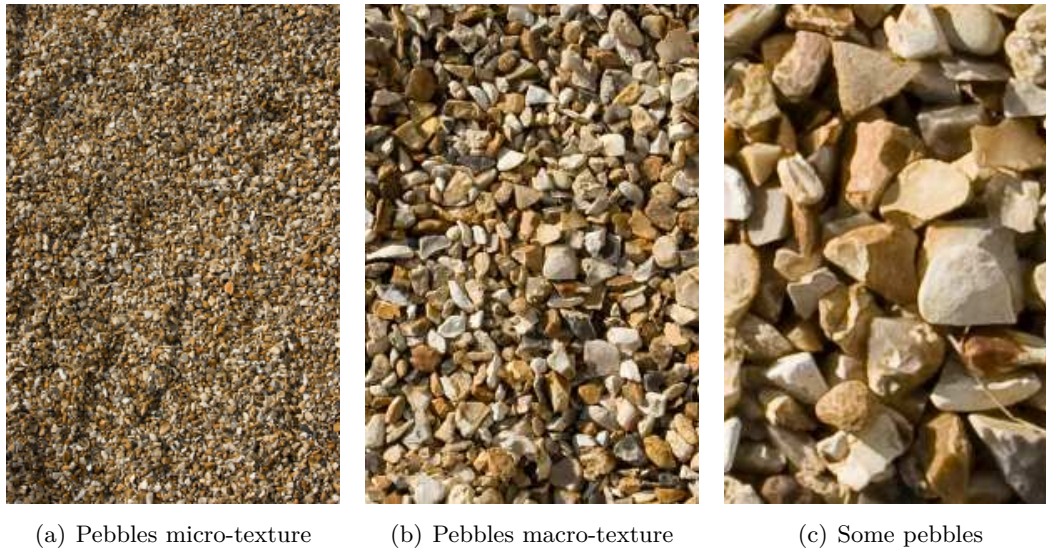
Figure 1.1: Micro-texture and macro-texture: Three different scales of observation taken from a single high-resolution image of pebbles (there is a scale factor of 3 from one image to the other). This example illustrates that the nature of a texture is highly dependent of the scale of observation: seen from a long distance, the pebbles form a micro-texture, as one gets closer they become a macro-texture, whereas at a very short distance individual pebbles are perceived as individual objects and are no more grouped together.

are the *macro-textures*, that is textures which are constituted of several small but discernible objects. Let us observe that the delimitation between the micro-textures and the macro-textures does not only depend on the nature of the observed objects but also on the scale of observation. As an illustration, Fig. 1.1 displays three different images extracted from the same high resolution picture of pebbles. Depending on the viewing distance, the same objects are perceived as either a micro-texture, a macro-texture or a collection of individual objects.

1.1.2 Texture Synthesis Algorithms

Texture synthesis[1] consists in reproducing a texture from one sample. More precisely, the texture synthesis problem can be formulated as follows: Given an input texture image, produce an output texture image being both visually similar to and pixel-wise different from the input texture. As illustrated by the abstract representation of Fig. 1.2, the output image should ideally be perceived as another part of the same large piece of homogeneous material the input texture is taken from.

One can roughly separate the existing texture synthesis methods in two families. The one which has been very popular over the last decade is the family of

---

[1]In computer graphics one may speak of example-based texture synthesis or texture synthesis by example to differentiate from the generation of texture from procedural noise functions (see the next section).
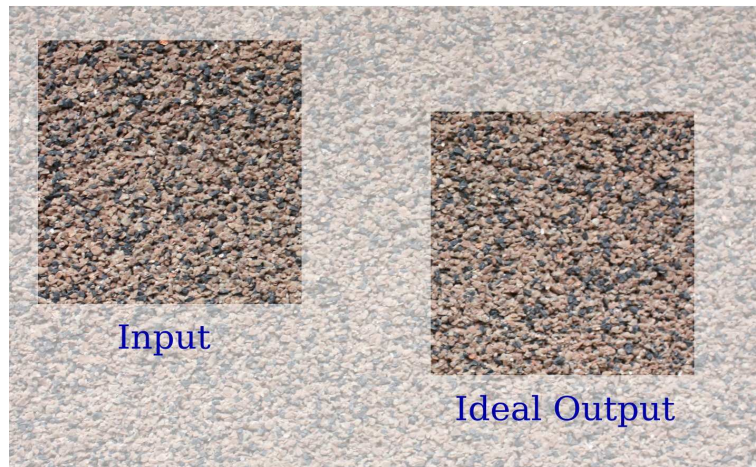
Figure 1.2: Texture synthesis: Given an input texture, a texture synthesis algorithm should ideally provide an output texture image perceived as another part of the same large piece of material.

neighborhood-based synthesis algorithms. These algorithms are non parametric Markovian methods: they assume a Markov random field model for the textures but do not rely on an explicit model, contrary to former approaches, e.g. [38]. They synthesize the output texture image by sequentially copying pixels or patches of the input texture. At each step, a pixel or a patch of the input image is chosen among the ones which have their neighborhood similar to the corresponding neighborhood in the output texture. These methods were first developed by Efros and Leung [51] and Wei and Levoy [153] for one-pixel-at-a-time synthesis, and by Efros and Freeman [50] and Kwatra *et al.* [94] for patch-based methods. We refer to [152] for a complete state of the art on the subject.

The second main approach to texture synthesis algorithms is based on texture modeling by statistical constraints. These algorithms typically consist in estimating a set of statistical constraints from the input texture, and then produce an output texture as a random image satisfying these statistical constraints [125]. As a seminal example, Heeger and Bergen [74] introduced an algorithm for which the constraints are the histogram of colors and the ones of wavelet coefficients of the input texture. Several improvements of this method have been proposed [41, 125, 124, 128], involving higher-order statistics between coefficients and more evolved decompositions of images.

Neighborhood-based algorithms are the ones which produce the most impressive results since they are able to synthesize a large class of textures, and notably many structured macro-textures. Yet, the quality of the output textures depends on several parameters which must be carefully chosen for each input texture, and some of the methods can produce erratic results [51]. On the opposite, algorithms based on statistical constraints are only able to reproduce a certain subclass of textures, but produce visually stable results: all the output textures obtained from the same

input texture are visually similar.

The random phase noise algorithm, initially introduced by van Wijk [146] and further developed in Chapter 2 of this thesis to enable the synthesis of realistic textures, belongs to this second family of algorithms. Indeed, it is defined as follows: conserve the constraints given by the Fourier modulus of the input texture and replace the phase by a random phase (see Chapter 2 for details).

1.1.3   Procedural Texture Synthesis

In computer graphics, textures are most of the time designed from procedural noise functions [49, 95]. The main practical interest of these noise functions is precisely that they are *procedural*, that is defined by an algorithm which can be evaluated at any point at a fixed computational cost, and thus they are ideal tools for texturing 3D objects in virtual environments (animation movies, video games, etc.) [49]. Yet, one should mention that some elaborated neighborhood-based methods share most of the assets of procedural noise functions, notably local evaluation and real-time synthesis [101, 45].

The first author who defined a procedural noise function and demonstrated its interest was Perlin [123]. Albeit Perlin noise is still very popular today, over the last few years several new procedural noise functions have been proposed by the computer graphics community to cope with the shortcomings of this model: *wavelet noise* [36], *anisotropic noise* [65], and lastly *Gabor noise* [96].

Even though procedural noise functions are the ideal technical tool for computing textures for virtual environments, determining the parameters of a procedural noise which would produce a given texture is not an easy task. Indeed it requires an acquaintance with the model, not to mention some artistic skills. Hence, an important practical problem is to derive procedural texture models from input texture images. This is a relatively new problem, precisely formulated in the recent paper [99], even though previous works have already tackled this problem, e.g. [44]. One of the contribution of this thesis is the elaboration of a procedural example-based texture synthesis algorithm based on the recent Gabor noise model (see Chapter 4). Although the early results that will be presented are limited to textures in 2D, this new algorithm would potentially enable the synthesis of a large class of micro-textures directly on 3D surfaces.

1.2   Germ-Grain Models and Texture Synthesis

As mentioned above the main contribution of the first part of this thesis is the elaboration of texture synthesis algorithms relying on shot noise models. As we will see, shot noise models are limited to micro-textures, and therefore it is of interest to investigate other germ-grain models as generic models for textures.

The formal definition of germ-grain models is delayed to Chapter 5. For now let us just say that a germ-grain model defines a random field by combining a family of colored random sets, called *grains*, according to some interaction principle. For

example, the shot noise model is the germ-grain model for which the interaction principle is addition. Other classical germ-grain models include the Boolean random field model, the dead leaves model, and colored tessellations. The corresponding interaction principles of these models are respectively supremum, occultation, and juxtaposition.

Apart from shot noise models, other classical germ-grain models have appeared in texture modeling and texture synthesis, although more exceptionally. Tessellations models have been studied by Ahuja and Rosenfeld [3], and Poisson-Voronoi tessellations are at the center of the cellular texture methods developed by Worley [156, 49] for solid texture synthesis, i.e. synthesis of volumetric textures. In another direction, a texture synthesis algorithm inspired from the dead leaves model has been proposed by Gousseau [66].

One of the main motivation for the study of the dead leaves model is that it is solely based on the occultation principle, a central principle in natural image formation [18, 68]. Another principle which is at stake in the formation of natural images is transparency. The transparency phenomenon may also be encountered in other imaging modality where images are obtained through successive reflexion-transmission steps, as in microscopy or ultrasonic imaging. In addition, in computer graphics, the simulation for certain material such as hair or foliage relies on the superimposition of numerous transparent objects [52]. Transparency is an interesting interaction principle since it is non linear, as is occultation in the dead leaves model. On the other hand, similarly to the addition in shot noise models, the final color which results from the superposition of several transparent objects depends on the color of all the superposed objects.

This motivates the definition of a new germ-grain model where the random objects are superimposed by transparency. The study of this model, called the transparent dead leaves (TDL) process, is the subject of the second part of the thesis. Our main result shows that the TDL process is a transition model between two classical models, the dead leaves model and the Gaussian limit of high intensity shot noises, as illustrated by Fig. 1.3. Indeed, varying the transparency of the random objects from opaque to total transparency, the TDL process varies from the colored dead leaves model to the Gaussian random field which is the limit of the high intensity shot noise having the same grain distribution.

1.3   Functional Spaces and Texture Models

As mentioned above, a class of texture synthesis algorithms is based on a set of statistical constraints estimated from the input texture sample [146, 74, 125]. More generally, in image processing an image model is often given as a functional space for the image to live in. Classical image models are Besov spaces [46, 31, 35] or the space of functions of bounded variation [133, 6, 7, 32]. In fact, statistical constraints used for texture synthesis are often implicitly related to some particular functional spaces. For example, in conserving the modulus of the Fourier coefficients of an

(a) Shot noise   (b) Transparent dead leaves   (c) Dead leaves model
                                  process
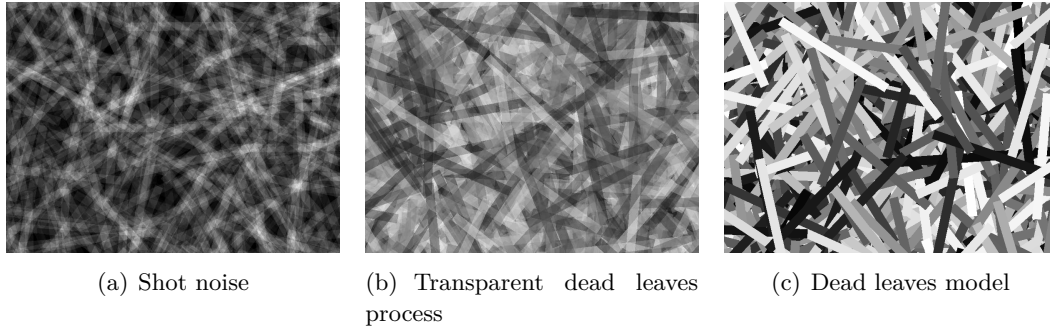
Figure 1.3:   Realizations of three different germ-grain models having the same grain distribution: shot noise, transparent dead leaves process (see Chapter 6), and dead leaves model. The transparent dead leaves model is a transition model between the Gaussian limit of high intensity shot noises and the dead leaves model.

image, the output textures are in the same Sobolev space as the input image, whereas conserving the first-order distributions of wavelet coefficients at each scale is related to Besov spaces.

An alternative widespread model initially proposed by Meyer [112] is to decompose an image into the sum of two functions, one cartoon part and one texture part. The chosen functional space for the cartoon part is generally the space of functions of bounded variation whereas the texture part belongs to a functional space in which oscillatory images have a low norm (see e.g. [148, 8, 9, 23]). The corresponding functional space is thus wider than the space of functions of bounded variation which is not appropriate to fully represent the details of natural images [67]. Notice that the cartoon plus texture model explicitly assumes that the textures present in natural images are not of bounded variation, or at least that their total variation is very high, which is confirmed by the multifractal analysis of some textures (see e.g. [154] and the references therein).

Hence the total variation of textures is generally considered to be high or even infinite. However, simple geometric texture models which do not contain oscillations turn out to be of bounded variation. For example, dead leaves models are piecewise constant random images, and thus they are intuitively of bounded variation when the size and shape of the grains are regular enough, as in the example of Fig. 1.3(c). Yet the total variation of the dead leaves model is infinite when the size of grains are distributed according to a scaling law, as shown by Gousseau and Roueff [68].

Determining if a stochastic texture model is of bounded variation and computing its mean total variation is the main motivation of the third part of this thesis. In this third part, the general study of random fields of bounded variation will be developed. Our main result provides a general expression for the mean variation per unit volume of a stationary random field. In the special case of germ-grain models, the obtained expression makes explicit the somewhat intuitive relation between the geometry of the grains and the variation per unit volume.

1.4   Main Contributions of the Thesis

- In Chapter 2, two texture synthesis algorithms are elaborated, namely the asymptotic discrete spot noise (ADSN) and the random phase noise (RPN). A theoretical and experimental study clarifies their properties as well as the links between these two models previously defined by van Wijk for data visualization [146]. Our main contribution is to make the algorithms work for realistic textures. First, an extension of both algorithms to color images is given. Second, the artifacts due to the non-periodicity of real-world texture samples are eliminated. This is done by replacing the input texture samples by their periodic component, as defined by Moisan [113]. Third, a method for synthesizing output textures of arbitrary size is proposed. The resulting algorithms are robust and fast, as demonstrated by an on-line demo of the RPN algorithm [60]. Numerous experiments show that both algorithms produce visually similar textures and that they reproduce satisfyingly well a large class of micro-textures.

- Chapter 3 is devoted to the study of the normal convergence of Poisson shot noise and its application to procedural texture synthesis. Following the approach of Heinrich and Schmidt [75], the normal convergence rate of a Poisson shot noise is controlled by the Berry-Esseen theorem for Poisson shot noise. Our main theoretical contribution is to give a new sharp upper bound of the Berry-Esseen constant for Poisson shot noises. In addition, experiments demonstrate that from the upper bound provided by the Berry-Esseen theorem one can determine the good order of magnitude for the intensity which corresponds to the beginning of the "visual convergence" of the shot noise to the limit Gaussian texture.

- In Chapter 4, a new algorithm for procedural texture synthesis by example relying on the recent Gabor noise model [96] is presented. This algorithm coined *Gabor noise by example* makes use of the contributions of both Chapter 3 and Chapter 2: control of the normal convergence, extension to color images, and replacement of the sample by its periodic component. The presented early results demonstrate that the computed procedural textures reproduce the same class of textures than the RPN algorithm of Chapter 2. Thus the proposed algorithm should enable the synthesis of a large class of micro-textures directly on 3D surfaces by using the surface noise procedure for Gabor noise [96].

- Chapter 6 is devoted to the study of the transparent dead leaves (TDL) process, a new germ-grain model based on transparency. Properties of this new model are established and a simulation algorithm is proposed. In particular the covariance of the TDL process is computed using a generalization of the no memory property of one-dimensional Poisson processes, as an alternative to Palm calculus. Our main result is to show that, when varying the transparency of the grains, the TDL process provides a family of models varying

from the dead leaves model to a Gaussian random field.

- In Chapter 7, general results on random fields (r.f.) of bounded variation are established. Our main result shows that the mean variation of a stationary r.f. f is equal to a constant $\theta_V(f)$, called the *variation intensity* of f, times the Lebesgue measure, and a practical expression of $\theta_V(f)$ is established. More precisely, the derived expression of $\theta_V(f)$ only involves the limits of mean absolute difference quotients of f, and in particular it only depends on the family of second-order distributions of f.

- Several applications of the general results of Chapter 7 are developed. As shown in Chapter 8, when restricted to the case of random sets, the established results lead to rigorous generalizations of formulas for the mean perimeter of random sets initially stated by Matheron [107]. To return to our initial motivation and to illustrate that the derived formulas are generic, the variation intensities of Gaussian random fields and classical germ-grain models are computed in Chapter 9. For germ-grain models, the obtained expressions make explicit the intuitive relation between the geometry of the grains and the total variation of the random fields.

1.5 Detailed Outline of the Thesis

This section provides a detailed and illustrated outline of the thesis. The brief paragraphs summarizing each chapter will be largely used for the abstracts and introductions of the corresponding chapters.

Part I: Shot Noise and Texture Synthesis

The main subject of the first part of this manuscript is the use of the shot noise model for texture synthesis.

Chapter 2: Random Phase Textures: Theory and Synthesis

This first chapter explores the mathematical and algorithmic properties of two sample-based texture models: *random phase noise* (RPN) and *asymptotic discrete spot noise* (ADSN). Given a texture sample h, the RPN associated with h is the random image obtained by replacing the phase of the discrete Fourier transform (DFT) of h by a random phase, whereas the ADSN associated with h is the Gaussian limit of the discrete spot noises obtained in summing independently randomly translated copies of h.

Both models arguably derive from linearized versions of two early Julesz texture discrimination theories, and they both permit to synthesize *random phase textures*, that is textures which are visually robust to randomization of their DFT phase.

These algorithms have been initially introduced by van Wijk [146] to synthesize various textures from simple geometric patterns for the purpose of scientific

visualization. Contrarily to van Wijk statements, it is shown that RPN and ADSN are different stochastic processes. Nevertheless, numerous experiments suggest that the textures obtained by RPN and ADSN algorithms from identical samples are perceptually similar. This shows that the theoretical differences between the two processes, that is the multiplication of the DFT modulus by a Rayleigh white noise, has no influence on the perception of random phase textures, a perceptual result that, to the best of our knowledge, is new.

In addition to this comparative study of the RPN and ADSN algorithms, our main contribution is to provide solutions to obstacles that prevented the use of RPN or ADSN to emulate textures. First, RPN and ADSN algorithms are extended to color images. The extensions of both algorithms to color images lead to the following observation: conserving the phase displacements between color channels permits to respect the color range of random phase textures. Second, a preprocessing technique is proposed to avoid artifacts due to the non-periodicity of real-world texture samples. This preprocessing consists in replacing the texture sample by its periodic component as defined by Moisan [113]. Finally, the method is extended to synthesize textures with arbitrary size from a given sample.

The resulting color ADSN and RPN algorithms are fast algorithms which produce textures of any given size, as illustrated by Fig. 1.4. An additional noticeable properties of these algorithms is that they produce visually stable results, in the sense that all the textures obtained from the same sample are visually similar. In comparison with neighborhood-based methods [51], the developed ADSN and RPN algorithms only reproduce a restricted range of textures, but they are fast and robust, as demonstrated by the on-line demo of the RPN algorithm [60].

Chapter 3: Poisson Shot Noise

The ADSN algorithm developed in Chapter 2 illustrates the interest of the Gaussian limit of discrete shot noise models for image texture synthesis. The aim of this second chapter is to study the corresponding shot noise model defined on the continuous domain, and more particularly its convergence to a Gaussian random field (r.f.). We focus on shot noise processes driven by independently marked Poisson point processes[2]. These shot noise models, called *Poisson shot noises*, are defined by

$$f(x) = \sum_{(x_j, \kappa_j) \in \Pi} h(x - x_j, \kappa_j), \ x \in \mathbb{R}^d,$$

where h is a measurable function and Π is an independently marked Poisson process over $\mathbb{R}^d \times K$, K being the mark space.

The Poisson shot noise model is extensively used in procedural texture synthesis [102, 123, 146, 96, 95], where it is often called *sparse convolution model* in reference to the work of Lewis [102]. The fundamental reason why shot noise models are used in procedural texture synthesis is that, as for the discrete shot noise

---

[2]Appendix B recalls basic definitions and properties of Poisson point processes.

(a) Original sample h (b) RPN associated with h
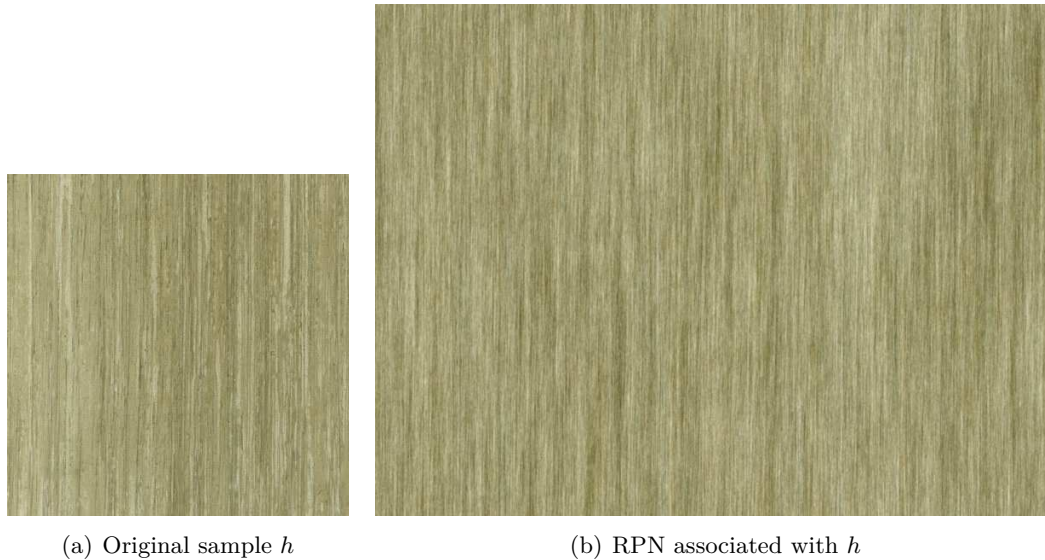
Figure 1.4: Example of texture synthesis with the RPN algorithm from a wood texture sample. Notice that the size of the output texture is larger than the size of the original sample.

model, the Poisson shot noise tends to a Gaussian r.f. when increasing the intensity of impulses [119, 75].

Hence to simulate a Gaussian texture, one can use a Poisson shot noise with high intensity. However the computational cost of shot noise simulation algorithms is typically linearly proportional to the impulse intensity λ. One must therefore find a trade-off between the quality of the Gaussian approximation and the computational cost. The main motivation of this chapter is to demonstrate that one can automatically determine a value for the intensity λ which would satisfy this trade-off in estimating the normal convergence rate of the Poisson shot noise. Following the approach of Heinrich and Schmidt [75], the shot noise normal convergence is estimated from the upper bound given by the Berry-Esseen theorem for Poisson shot noises. Our main theoretical contribution is to show that the Berry-Esseen constant for Poisson shot noises is the same as the Berry-Esseen constant for Poisson random sums. As a consequence, thanks to a recent result due to Korolev and Shevtsova [92], we reduce by a factor seven the upper bound of the Berry-Esseen constant for Poisson shot noises previously derived in [75].

An experimental section completes the theoretical study of the normal convergence of Poisson shot noise. It is mainly shown that the Berry-Esseen bound provides the good order of magnitude for the beginning of the "visual convergence" to the limit Gaussian texture. This observation might enable procedural texture synthesis software relying on shot noise models to automatically evaluate a range of interest for the value of the intensity parameter.

Chapter 4: Gabor Noise by Example

This chapter tackles the problem of procedural texture synthesis *from a sample texture* using the recent Gabor noise model [96]. The Gabor noise model is a particular Poisson shot noise model with Gabor kernels as impulse functions. More precisely, a Gabor noise is a random function of the form

$$f(y) = \sum_{(x_j, w_j, \omega_j, \theta_j) \in \Pi} w_j e^{-\pi a^2 \|y - x_j\|^2} \cos\left(2\pi \langle y - x_j, \omega_j \rangle + \theta_j\right),$$

where the random marks w_j, ω_j and θ_j are independent and respectively follow some probability distributions. These probability distributions are the parameters of the Gabor noise model. Since it determines the frequency content of the noise, the main parameter of the Gabor noise model is the probability distribution P_ω of the frequencies ω_j.

Given a texture sample h, an automatic solution is provided for determining Gabor noise parameters such that the procedural texture is visually similar to h. The developed algorithm for Gabor noise by example relies on a rather simple idea: the probability distribution P_ω associated with h is given by the normalized power spectrum of the texture sample h. In other words, the frequencies ω_j are drawn according to their relative importance in the spectrum of the discrete sample h.

The complete elaboration of Gabor noise by example makes use of three contributions of Chapter 2 and Chapter 3. First the Gaussian convergence of the high intensity Gabor noise is controlled by the Berry-Esseen bound derived in Chapter 3. Second, as for the random phase noise (RPN) algorithm of Chapter 2, the periodic component of h [113] is used in place of the original texture sample h, in order to obtain a discrete Fourier transform without cross structure. Third, as for the color RPN algorithm, the phase displacements between RGB color channels is enforced in order to ensure color consistency when extending the Gabor noise to the case of color textures.

Numerical experiments show that the procedural models obtained by the developed algorithm for Gabor noise by example produce textures that are visually similar to the output of the RPN algorithm (see Fig. 1.5), and thus enables to reproduce any texture sample which is well-reproduced by the RPN algorithm. The main advantage of the Gabor noise by example over the algorithms of Chapter 2 is of course the locality of its basic elements, offering the possibility to synthesize aliasing-free textures on arbitrary surfaces [96].

Part II: The Transparent Dead Leaves Process: a New Germ-Grain Model

The first part of the thesis shows that shot noise models are good models for micro-textures, but are limited to this class of textures. To overcome this limitation, it is natural to turn to other models relying on non linear procedures, in particular to germ-grain models. As illustrated in the second part of the thesis, one of the interest

(a) Original image h (b) RPN
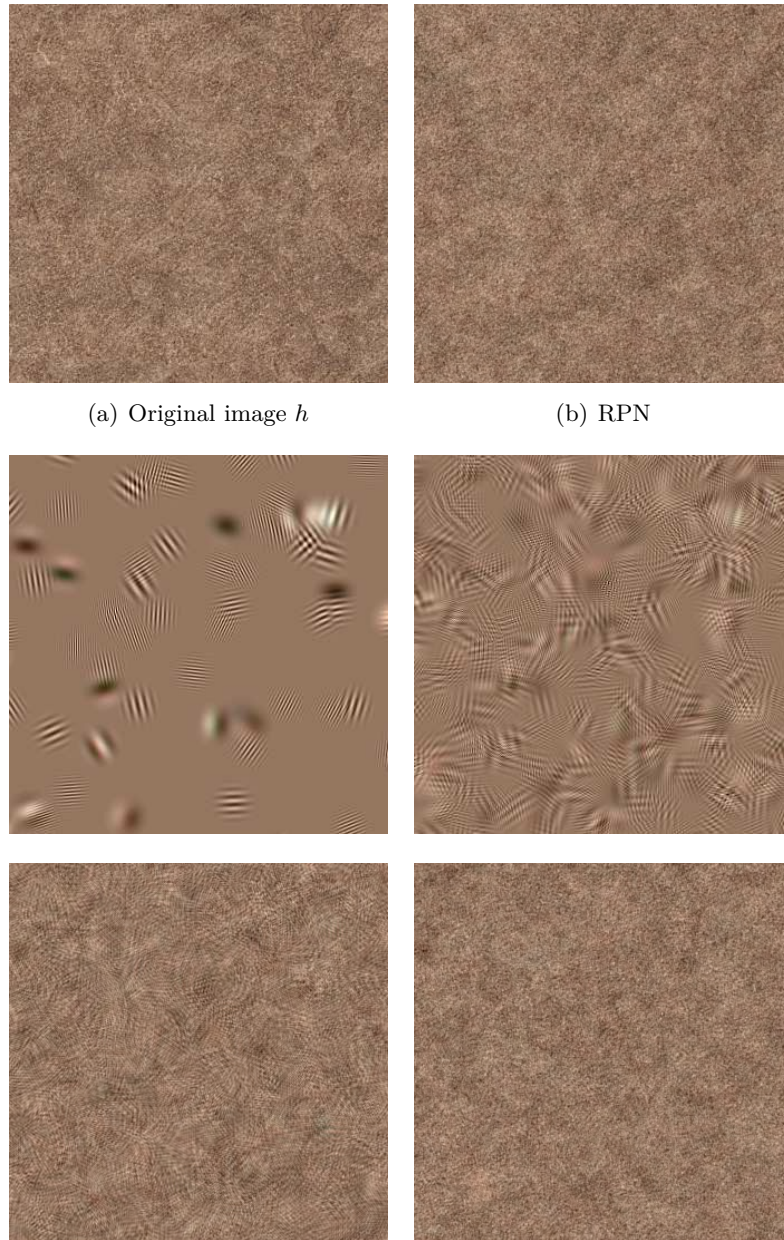
Figure 1.5: Illustration of the convergence of the color Gabor noise by example: Top row original leather texture sample and its associated RPN (as defined in Chapter 2); Middle row and bottom row: Gabor noises associated with h. From one Gabor noise to the other the number of Gabor kernels is multiplied by a factor 10. The last example corresponds to the bound derived from the Berry-Esseen theorem (see Chapter 3). The size of the image is 340×340 and the radius of the Gabor kernels is 20.

of germ-grain models is that they permit to investigate separately the interaction principles involved in natural image formation.

Chapter 5: Classical Germ-Grain Models

The main object of this chapter is to define and illustrate several classical germ-grain models. It does not expose new results, but presents these models in a unified framework. The considered germ-grain models are Poisson shot noises of random sets, Boolean models, colored dead leaves models, and colored tessellations. Each one of these models combine random colored sets, called *grains*, according to an interaction principle. The respective interaction principles are addition for shot noise, supremum for Boolean random fields (which generalizes the set union used for Boolean random sets), occultation for the dead leaves model, and, arguably, juxtaposition for colored tessellations. Numerical simulations show that only varying this interaction principle produces geometric images with very different visual aspects.

This introductory chapter on germ-grain models is followed by Chapter 6 which introduces the transparent dead leaves process, a new germ-grain model for which the interaction principle is transparency. The variation intensities, that is the mean variation per unit volume, of all the mentioned germ-grain models will be computed in Chapter 9.

Chapter 6: The Transparent Dead Leaves Process

This chapter introduces a new-germ grain model which is based on an elementary operation involved in natural image formation: the transparency.

The motivation for defining this new germ-grain model is threefold: First, it permits to study the properties of images solely constructed with the transparency principle, a principle which is at stake in natural image formation as well as in other image modalities such as microscopy or ultrasonic imaging. Second, superimposing semi-transparent objects is done in practice in computer graphics to simulate material such as hair or foliage [52], but the corresponding limit process has never been studied. Third, as our main result rigorously shows, transparency appears as an intermediate interaction principle between the occultation principle of the dead leaves model and the addition principle of the shot noise model.

The transparent dead leaves (TDL) process is defined as the germ-grain model obtained in sequentially superimposing transparent objects, called *leaves* in this context. The TDL process has already been informally introduced and illustrated by Fig. 1.3(b). In Chapter 6, a simulation procedure for the TDL process is proposed, and several properties of the process are established. In particular, we compute the covariance of the process in making use of a generalization of the no memory property of Poisson processes, which provides an alternative to Palm calculus in this context.

An important parameter of the TDL process is the transparency coefficient

$\alpha \in (0, 1]$ associated with the colored leaves. When $\alpha = 1$, that is when the leaves are opaque, the TDL process is the colored dead leaves model. On the other extreme case, the main result of Chapter 6 establishes that, when properly normalized, the TDL process tends to a Gaussian random field when the leaves tend to be fully transparent, this Gaussian random field being the limit of the high intensity shot noise having the same grain distribution. Hence, by varying the transparency of the grain from opacity to total transparency, the TDL process ranges from the dead leaves model to a Gaussian random field.

Part III: Variation of Random Fields

Even though the total variation of textures is generally considered to be high or even infinite, to the best of our knowledge little is known on the total variation of classical texture models such as Gaussian random fields, shot noises, or other classical germ-grain models presented in Chapter 5. However the random geometric images corresponding to germ-grain models are clearly images of bounded variation when the grains are regular enough, and intuitively their total variation depends on the geometry of the grains. It is therefore natural to address the computation of the mean total variation of the germ-grain models presented in Chapter 5.

   This is the goal of the third part of the thesis. To enable such computations, we had to formulate the general definition of a random field of bounded variation, a notion that is hardly touched in the literature.

Chapter 7: Random Fields of Bounded Variation

This chapter presents a general framework for the study of random fields (r.f.) of bounded variation defined over $\mathbb{R}^d$. Our general strategy is first to deal with directional variations $|D_u f|$, $u \in S^{d-1}$ and then to integrate these over all directions $u \in S^{d-1}$ to obtain results on the variation $|Df|$. The advantage of dealing with directional variations is first that it yields simple expressions and second that it provides information on the anisotropy of the r.f. f.

   The first section of this chapter recalls classical results from the theory of functions of bounded directional variation. Relations between the directional variation $|D_u f|$ of a function f and the integral of its difference quotients are emphasized, yielding to the fundamental relation

$$|D_u f|\left(\mathbb{R}^d\right) = \lim_{r \to 0} \int_{\mathbb{R}^d} \frac{|f(x + ru) - f(x)|}{|r|} dx,$$

a relationship that happens to be known by the geometric measure theory community but is not stated in the literature. After this preliminary study of deterministic functions of bounded directional variation, random fields of (locally) bounded (directional) variation are defined and characterized. In particular, one defines the *directional variation intensity measure* $\Theta_{V_u}(f, \cdot)$ of a r.f. f as the expectation of

the directional variation of f, and, in the case where the r.f. f is a.s. of bounded variation over the whole space $\mathbb{R}^d$, it is shown that

$$\Theta_{V_u}\left(f, \mathbb{R}^d\right) = \mathbb{E}\left(|D_u f|\left(\mathbb{R}^d\right)\right) = \lim_{r \to 0} \int_{\mathbb{R}^d} \frac{\mathbb{E}\left(|f(x+ru) - f(x)|\right)}{|r|} dx.$$

A particular interest is then given to stationary r.f. f of locally bounded (directional) variation. If f is such a r.f., it is proved that the mean directional variation of f on every domain U is proportional to the Lebesgue measure of U. The constant of proportionality is called the *directional variation intensity* of the stationary r.f. f and is denoted $\theta_{V_u}(f)$. Along with the definition of $\theta_{V_u}(f)$, a practical formula is derived:

$$\theta_{V_u}(f) = \lim_{r \to 0} \frac{\mathbb{E}(|f(ru) - f(0)|)}{|r|}.$$

In particular, the directional variation intensity $\theta_{V_u}(f)$ only depends on the family of second-order distributions of the stationary random field f.

Chapter 8: Variation of Random Sets

This chapter focuses on the mean directional and non directional variations of random sets. Applying the results of Chapter 7, one proves several formulas which equate the directional variations of random sets to the directional derivatives at the origin of functions related to the second-order property of random sets, namely the mean covariogram for random sets with finite mean Lebesgue measure and the variogram for stationary random sets. These formulas show that classical results on the mean perimeter of random closed sets due to Matheron [107, 110] extend rigorously to any measurable random set, provided the perimeter is understood as the variational perimeter.

In a last part, one also establishes a coarea formula for variation intensities: the mean total variation of a r.f. is equal to the integral of the mean perimeter of its excursion sets.

Chapter 9: Applications: Variation Intensities of Classical Germ-Grain Models

The aim of this chapter is to compute the variation intensities of various stationary r.f. models by applying the results of Chapter 7 and Chapter 8. The considered stationary r.f. are Gaussian r.f., Poisson shot noise of random sets, Boolean models, colored dead leaves, transparent dead leaves, and colored tessellations.

For germ-grain models, the obtained expressions make explicit the somewhat intuitive relation between the geometry of the grains and the total variation. In particular, for all the considered germ-grain models they show that there are only two geometric features influencing the mean total variation of the germ-grain r.f.: the mean perimeter and Lebesgue measure of the grains.

1.6 Publications

The works presented in this thesis have lead to the following publications and prepublications:

- The results of Chapter 2 have been published in the journal IEEE Transactions on Image Processing [61].

- An on-line demo of the random phase noise algorithm defined in the same chapter has been submitted to Image Processing on Line [60].

- Most of the results of Chapter 8 can be found in the paper [58], accepted for publication in Image Analysis and Stereology. The proofs presented in this paper do not rely on the results of Chapter 7 (which were not written at that time).

- The study of the transparent dead leaves process presented in Chapter 6 is the subject of the preprint [59], submitted to the journal Advances in Applied Probability.

- The developed algorithm for Gabor noise by example gave rise to an ongoing collaboration with A. Lagae, S. Lefebvre and G. Drettakis, three of the authors of the original Gabor noise paper [96].

Part I

Shot Noise and Texture Synthesis

Random Phase Textures: Theory and Synthesis

Contents

Abstract: This chapter explores the mathematical and algorithmic properties of two sample-based texture models: *random phase noise* (RPN) and *asymptotic discrete spot noise* (ADSN). These models permit to synthesize *random phase textures*. They arguably derive from linearized versions of two early Julesz texture discrimination theories. The ensuing mathematical analysis shows that, contrarily to some statements in the literature, RPN and ADSN are different stochastic processes. Nevertheless, numerous experiments also suggest that the textures obtained by these algorithms from identical samples are perceptually similar. The relevance of this study is enhanced by three technical

contributions providing solutions to obstacles that prevented the use of RPN or ADSN to emulate textures. First, RPN and ADSN algorithms are extended to color images. Second, a preprocessing is proposed to avoid artifacts due to the non-periodicity of real-world texture samples. Finally, the method is extended to synthesize textures with arbitrary size from a given sample.

The content of this chapter is mostly from [61].

2.1 Introduction

2.1.1 Texture Perception Axioms and their Formalization

Oppenheim and Lim [118] state that "spectral magnitude and phase tend to play different roles" for digital images and that, in some situations, the phase contains many of the important features of images. This is suggested by the classic experiment which consists to exchange the Fourier modulus and phase of two images [118, 126]. However when it comes to textures, perception theory suggests that some of the main texture characteristics are contained in their Fourier magnitude. In his early work on texture discrimination Julesz [85] demonstrated that many texture pairs having the same second-order statistics could not be discerned by human preattentive vision. This hypothesis is referred to as the first Julesz axiom for texture perception [85]. As a consequence, textures having the same second-order statistics share a common auto-covariance and therefore a common Fourier magnitude. Even though counterexamples to the first Julesz axiom exist [85, 87, 158], it is believed that Fourier magnitude is more important than phase for the perception of textures [86]. This conclusion is still considered valid by several more recent contributions [144, 151]. For example, working on texture classification, Tang and Stewart [144] conclude that "the Fourier transform magnitudes contain enough texture information for classification" whereas "the Fourier phase information is a noise signal for texture classification."

Thus, a weak form of the first Julesz assumption is that the perception of a texture is characterized by its Fourier modulus. Under this assumption, its perception should not vary when the texture phase is randomized. This fact turns out to be true for a large class of textures which we shall call in the sequel *micro-textures*. More generally, any two images obtained by randomizing the phase of any given sample image are perceptually very similar. As the experiments displayed here show, this is true regardless of whether the sample image is a texture or not. We shall call in the sequel *random phase texture* any image that is obtained by a phase randomization.

The second Julesz approach to texture preattentive discrimination theory introduced the notion of textons (blobs, terminators, line crossings, etc.) [87]. The texton theory assumes that the density of local indicators (the textons) is responsible for texture preattentive discrimination: images with the same texton densities should not be discriminated. A main axiom of the texton theory is that texture perception
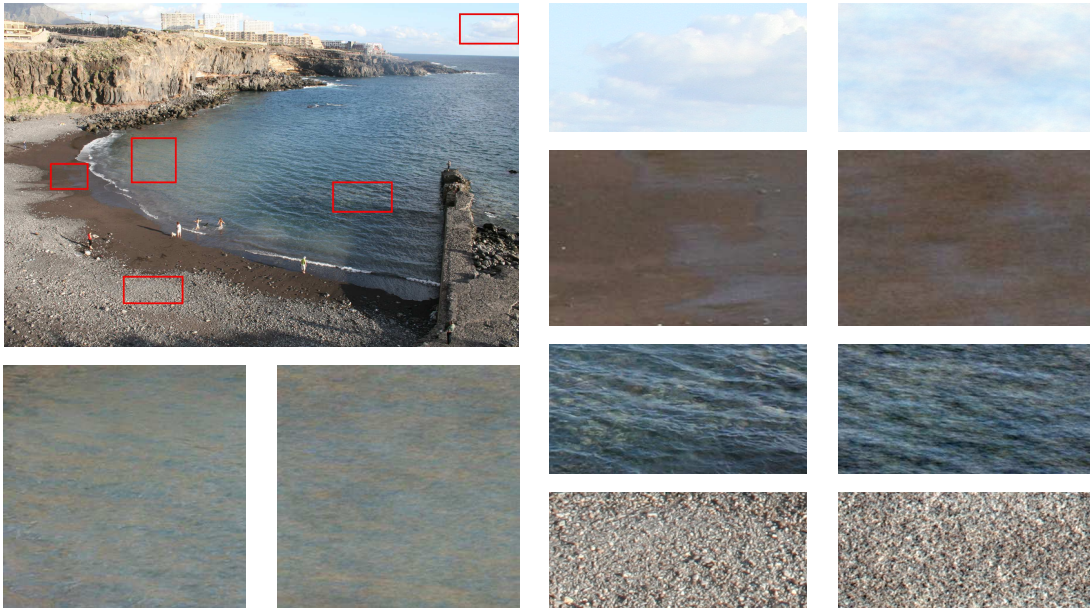
Figure 2.1: Some examples of micro-textures taken from a single image (water with sand, clouds, sand, waves with water ground, pebbles). The emplacements of the original textures are displayed with red rectangles. Each micro-texture is displayed together with an outcome of the RPN algorithm to its right. These micro-textures are reasonably well emulated by RPN. Homogeneous regions that have lost their geometric details due to distance are often well simulated by RPN.

is invariant to random shifts of the textons [87]. The shift invariance of this second Julesz theory can be made into a synthesis algorithm building a texture from initial shapes by random shifts. In the Julesz toy algorithm used in his discrimination experiments, this construction was a mere juxtaposition of simple shapes on a regular grid, with random shifts avoiding overlap. This random shift principle can be used to make realistic textures provided a linear superposition is authorized, by which the colors of overlapping objects are averaged. Textures obtained by the combined use of random shifts and linear superposition will be called *random shift textures*. We shall discuss thoroughly their relation to *random phase textures*.

Random phase and random shift textures belong to a linear world where the superposition principle dominates. A sound objection is that linear superposition is not always adapted for natural image formation. Several authors prefer an occlusion principle yielding the stochastic dead leaves model [108, 137, 18]. Indeed, most visible objects do not add up visually in the image ; they hide each other.

However, thin, small, or semitransparent objects obey an additive superposition principle due to the blur inherent to image formation. More generally, all homogeneous image regions made of small objects, when seen at a distance where individual shapes vanish, obey the linear superposition principle. Indeed, when individual texture constituents are close to pixel size, the camera blur linearly superposes their colors and geometric features. Thus, many homogeneous regions

in any image should be *micro-textures* obeying the linear superposition principle and the random shift principle. Fig. 2.1 shows an example. Five rectangles belonging to various homogeneous regions were picked in a high resolution landscape (1762×1168 pixels). These textures are displayed in pairs where on the left is the original sub-image and on the right is a simulation obtained by the *random phase noise* (RPN) algorithm elaborated in this chapter. These micro-textures are reasonably well emulated by the RPN algorithm. This success encourages RPN simulation attempts on the homogeneous regions of any image. Yet, many images or image parts usually termed *textures* do not fit to the micro-texture requisites. Typically, periodic patterns with big visible elements, such as brick walls, are not micro-textures. More generally, textures whose building elements are spatially organized, such as the branches of a tree, are not micro-textures (see Fig. 2.15). In addition, *random phase textures* don't contain clear edges, and more generally, according to the global phase coherence indicator introduced by Blanchet, Moisan and Rougé [17], *random phase textures* have a poor sharpness. Nonetheless, each textured object has a critical distance at which it becomes a micro-texture. For instance, as illustrated in Fig. 2.2, tiles at a close distance are a *macro-texture*, and are not amenable to phase randomization. The smaller tiles extracted from the roofs in Fig. 2.18 can instead be emulated.

2.1.2 Random Phase and Random Shift Algorithms

The two texture models under study have been used either to create new textures from initial spots, or to analyze texture perception. Emulating real texture samples by these algorithms requires the solution of several technical obstacles which will be treated in Section 2.5. Here, we first sketch the mathematical and algorithmic discussion.

Random phase textures are produced by *random phase noise* (RPN) which is a very simple algorithm performing phase randomization. Random shift textures correspond to a classical model in signal processing called *shot noise* [39]. *Spot noise*, the two-dimensional *shot noise*, was introduced in computer graphics by van Wijk [146, 42] to create new textures from simple spot images (Fig. 2.3). In this chapter we call *discrete spot noise* (DSN) the corresponding discrete model.

Van Wijk [146] claimed that the asymptotics of discrete spot noise (DSN) is obtained by uniformly randomizing the phases of all Fourier coefficients. In short, it is claimed that the DSN asymptotic process is the random phase noise (RPN). Our first result here is that the limit of DSN is <u>not</u> RPN but is another process, which we shall call *asymptotic discrete spot noise* (ADSN). The difference between the two models lies in the modulus of the Fourier transform of their outcomes. For RPN, it is given by the Fourier magnitude of the spot whereas for ADSN, it is subject to pointwise multiplication by a Rayleigh noise.

It will be shown that ADSN and RPN, in spite of their theoretical differences, give perceptually similar results and therefore justify van Wijk's approach [146] (see Fig. 2.5 and 2.10). These experiments show that the perception of random phase

(a) Input   (b) RPN ×1.5

(c) Input   (d) RPN ×1.5

(e) Input   (f) RPN ×1
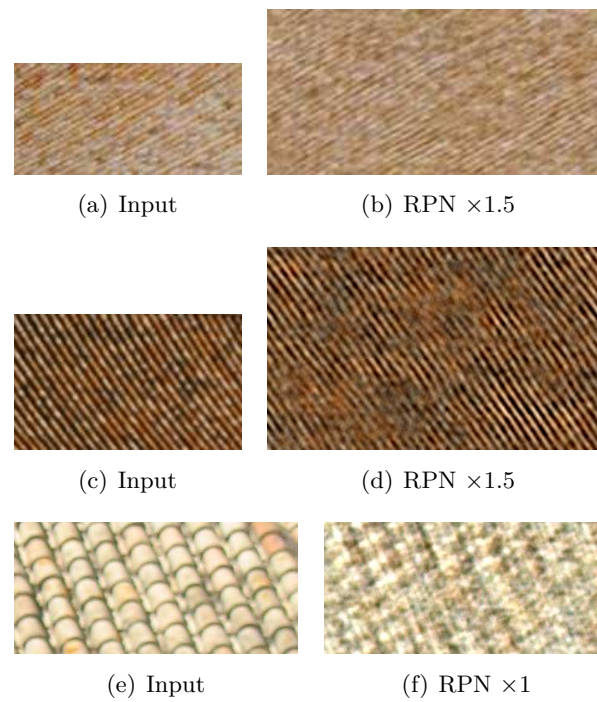
Figure 2.2: The first two inputs are rectangles taken from the tiled roofs in Fig. 2.18. The third input is again a piece of tiled roof taken at a shorter distance. RPN does well on tiles viewed at a distance at which they make a micro-texture. RPN fails instead on the third sample, which is a macro-texture.

textures is actually robust to the pointwise multiplication of the Fourier magnitude by a Rayleigh noise. By contrast, natural images containing macroscopic structures are in no way robust to this same perturbation (Fig. 2.18). Hence the perceptual invariance of random phase textures to a multiplicative noise on their magnitude possibly characterizes this kind of texture.

In short, mathematical arguments clarify the asymptotics of DSN and also establish a link between Julesz's first and second texture perception theories: their linearized versions give perceptually equivalent textures.

This mathematical and experimental study is completed by three important improvements of the texture synthesis algorithms that stem from both considered randomization processes. The ADSN and RPN algorithms are first extended to color images. The study of the color ADSN shows that this extension should be performed by preserving the phase coherence between color channels (Fig. 2.6). Second, artifacts induced by the non periodicity of the input sample are avoided by replacing the input sample with its periodic component [113]. Eventually, a natural extension of the method permits to synthesize RPN and ADSN textures with arbitrary size.

The resulting algorithms are fast algorithms based on fast Fourier transform (FFT). They can be used as powerful texture synthesizers starting from any input image. Both these claims are asserted by the companion online demo [60] which enables to test the RPN texture synthesis algorithm. As explained above, the algorithms under consideration do not reproduce all classes of textures: they are restricted to the so-called micro-textures. Exemplar-based methods like those of [51] and the numerous variants that have followed, see *e.g.* [152], successfully reproduce a wide range of textures, including many micro- and macro-textures. However, these methods are also known to be relatively slow, highly unstable, and to often produce garbage results or verbatim copy of the input (see Fig. 2.16). In contrast, RPN and ADSN are limited to a class of textures, but are fast, non iterative and parameter free. They are also robust, in the sense that all the textures synthesized from the same original sample are perceptually similar. Speed and stability are especially important in computer graphics, where the classical *Perlin noise* model [123] has been massively used for 25 years. Similarly to ADSN, the Perlin noise model (as well as its numerous very recent variants [36, 65, 96, 95]) relies on stable and fast noise filters.

The plan of this chapter is as follows. The two discrete mathematical models corresponding to Julesz first and second axioms are presented in Sections 2.2 and 2.3. The mathematical difference between these two processes is emphasized in Section 2.4. The corresponding micro-texture synthesis algorithms are introduced in Section 2.5, and their performance illustrated in Section 2.6.

(a) $n = 10$ (b) $n = 10^2$ (c) $n = 10^3$ (d) $n = 10^4$ (e) $n = 10^5$
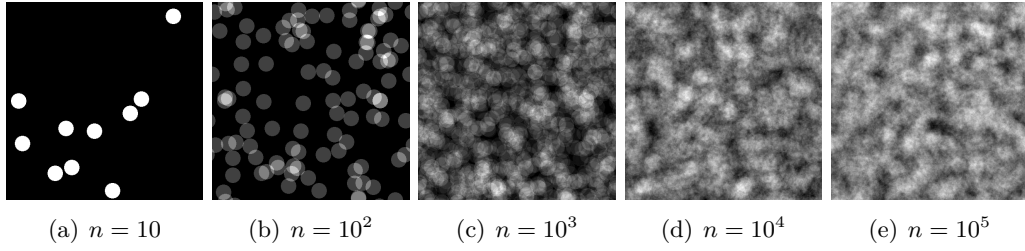
Figure 2.3: Outcomes of the DSN associated with the binary image of a small disk for different values of n. As n increases the random images f_n converge towards a stationary texture.

2.2 Asymptotic Discrete Spot Noise

2.2.1 Discrete Spot Noise

We consider the space $\mathbb{R}^{M \times N}$ of discrete, real-valued and periodic rectangular images. The components of an image $f \in \mathbb{R}^{M \times N}$ are indexed on the set $\Omega = \{0, \ldots, M-1\} \times \{0, \ldots, N-1\}$, and by periodicity $f(x) = f(x_1 \mod M, x_2 \mod N)$ for all $x = (x_1, x_2) \in \mathbb{Z}^2$.

Let h be a real-valued image and let X_p, $p = 1, 2, \ldots$ be independent identically distributed (i.i.d.) random variables (r.v.), uniformly distributed on the image domain Ω. We define the *discrete spot noise* (DSN) of order n associated with the *spot h* as the random image

$$f_n(x) = \sum_{p=1}^{n} h(x - X_p), \ x \in \Omega. \tag{2.1}$$

Fig. 2.3 shows several realizations of the DSN for different values of n where the spot h is the binary image of a small disk. It appears clearly that as n increases the random images f_n converge towards a texture-like image. Our purpose is to rigorously define this limit random texture and determine an efficient synthesis algorithm.

2.2.2 Definition of the Asymptotic Discrete Spot Noise

In order to define an interesting limit to the DSN sequence we need to normalize the images f_n. As f_n is the sum of n i.i.d. random images, the normalization is given by the central limit theorem. This limit will be called the *asymptotic discrete spot noise* (ADSN) associated with h.

Let X be a uniform r.v. on Ω and let $H(x) = h(x - X)$. A direct computation shows that the expected value of H is $\mathbb{E}(H) = m\mathbf{1}$ where m denotes the arithmetic mean of h and $\mathbf{1}$ is the image whose components are all equal to 1. Similarly the covariance of the random image H is shown to be equal to the autocorrelation of

h, that is for all $(x, y) \in \Omega^2$

$$\mathrm{Cov}\left(H(x), H(y)\right) = C_h(x, y),$$

where

$$C_h(x, y) = \frac{1}{MN} \sum_{u \in \Omega} \left(h(x - u) - m\right)\left(h(y - u) - m\right). \tag{2.2}$$

The central limit theorem ensures that the random sequence $n^{-1/2}\left(f_n - nm\mathbf{1}\right)$ converges in distribution towards the MN-dimensional normal distribution $\mathcal{N}(0, C_h)$, yielding the following definition.

Definition 2.1 (Asymptotic discrete spot noise). *With the above notations, the asymptotic discrete spot noise (ADSN) associated with h is the normal distribution $\mathcal{N}(0, C_h)$.*

2.2.3 Simulation of the ADSN

It is well known that applying a spatial filter to a noise image results in synthesizing a stochastic texture, the characteristic features of which are inherited from the filter and from the original noise [157, 53]. In this section we show that the ADSN associated with h can be simulated as a convolution product between a normalized zero-mean copy of h and a Gaussian white noise. We recall that the convolution of two (periodic) images f, g of $\mathbb{R}^{M \times N}$ is defined by

$$\left(f * g\right)(x) = \sum_{u \in \Omega} f(x - u)g(u), \ x \in \Omega.$$

Theorem 2.1 (Simulation of ADSN). *Let $Y \in \mathbb{R}^{M \times N}$ be a Gaussian white noise, that is, a random image whose components are i.d.d. with distribution $\mathcal{N}(0, 1)$. Let h be an image and m be its arithmetic mean. Then the random image*

$$\frac{1}{\sqrt{MN}}\left(h - m\mathbf{1}\right) * Y \tag{2.3}$$

is the ADSN associated with h.

Proof. Denote

$$\tilde{h} := \frac{1}{\sqrt{MN}}(h - m\mathbf{1})$$

and $Z := \tilde{h} * Y$ the random image defined by Equation (2.3). Since the convolution product is a linear operator, Z is Gaussian and $\mathbb{E}(Z) = \tilde{h} * \mathbb{E}(Y) = 0$. Besides, for all $(x, y) \in \Omega$,

$$\mathrm{Cov}\left(Z(x), Z(y)\right) = \mathbb{E}\left(Z(x)Z(y)\right)$$

$$= \mathbb{E}\left[\left(\sum_{u \in \Omega} \tilde{h}(x - u)Y(u)\right)\left(\sum_{v \in \Omega} \tilde{h}(y - v)Y(v)\right)\right]$$

$$= \sum_{u \in \Omega} \tilde{h}(x - u)\tilde{h}(y - u),$$

since $\mathbb{E}\left(Y(u)Y(v)\right) = 1$ if $u = v$ and 0 otherwise. Using Equation (2.2) and the definition of $\tilde{h}$, we obtain $\mathrm{Cov}\left(Z(x), Z(y)\right) = C_h(x, y)$. Hence Z is Gaussian with distribution $\mathcal{N}(0, C_h)$. $\qquad\square$

2.3 Random Phase Noise

In this section we analyze a stochastic process, the *random phase noise* (RPN) which was used by van Wijk and his co-workers as a technique to synthesize stationary textures [146, 77]. Using a random phase to obtain a texture from a given Fourier spectrum was first evoked by Lewis [102].

The RPN associated with a discrete image h is a random real image that has the same Fourier modulus as h but has a random phase. We first define a uniform random phase, which is a uniform random image constrained to be the phase of a real-valued image.

Definition 2.2 (Uniform random phase)**.** *We say that a random image $\theta \in \mathbb{R}^{M \times N}$ is a* uniform random phase *if:*

1. *θ is odd: $\forall x \in \Omega$, $\theta(-x) = -\theta(x)$.*

2. *Each component $\theta(x)$ is either uniformly distributed on the interval $(-\pi, \pi]$ if $x \notin \left\{(0,0), \left(\frac{M}{2}, 0\right), \left(0, \frac{N}{2}\right), \left(\frac{M}{2}, \frac{N}{2}\right)\right\}$, or uniform on the set $\{0, \pi\}$ otherwise.*

3. *For every subset $\mathcal{S}$ of the Fourier domain which does not contain distinct symmetric points, the family of r.v. $\{\theta(x) | x \in \mathcal{S}\}$ is independent.*

Definition 2.3 (Random phase noise)**.** *Let $h \in \mathbb{R}^{M \times N}$ be an image. A random image Z is a* random phase noise *(RPN) associated with h if there exists a uniform random phase θ such that*

$$\hat{Z}(\xi) = \hat{h}(\xi) e^{i\theta(\xi)}, \ \xi \in \Omega.$$

It is equivalent to define RPN as the random image Z such that $\hat{Z}(\xi) = \left|\hat{h}(\xi)\right| e^{i\theta(\xi)}$, where θ is a uniform random phase. This is because if ϕ is the phase of a real-valued image and θ is a uniform random phase then the random image $(\theta + \phi) \mod 2\pi$ is also a uniform random phase. One of the assets of this second definition is to emphasize that the RPN associated with an image h only depends on the Fourier modulus of this image. However, as developed in Section 2.5.1, the first definition permits to extend RPN to color images.

2.4 Spectral Representation of ADSN and RPN

The ADSN associated with an image h is a convolution of a normalized zero-mean copy of h with a Gaussian white noise whereas the RPN is obtained by multiplying each Fourier coefficient of h by a uniform random phase.

(a) Gaussian spot   (b) ADSN   (c)   (d)
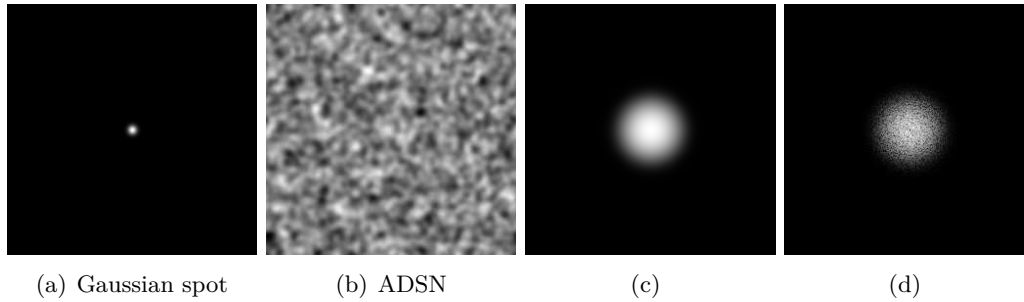
Figure 2.4:   ADSN 2.4(b) associated with a Gaussian spot 2.4(a) and their respective Fourier modulus 2.4(d) and 2.4(c) represented on logarithmic scale. The modulus of the ADSN is the pointwise multiplication of the modulus of h by a white Rayleigh noise.

ADSN is easily described in the Fourier domain. A Gaussian white noise image has a uniform random phase, its Fourier modulus is a white Rayleigh noise and its Fourier phase and modulus are independent [120, Chapter 6]. Consequently, the convolution theorem ensures that the phase of the ADSN is a uniform random phase whereas its Fourier modulus is the pointwise multiplication of the Fourier modulus of h by a Rayleigh noise.

Thus the phases of ADSN and RPN are both uniform random phases. However, the Fourier modulus of the two processes have different distributions: The Fourier modulus of the RPN is by definition equal to the Fourier modulus of the original image h whereas the Fourier modulus of the ADSN is the modulus of h degraded by a pointwise multiplication by a white Rayleigh noise (see Fig. 2.4). This characteristic of the limit process is clearly visible on Fig. 12 of the recent paper [95] where the noisy Fourier spectra of some *spot noise* textures are displayed.

To highlight the differences between ADSN and RPN, consider the effect of both processes on a single oscillation $h(x) = \sin(\lambda x_1 + \mu x_2)$. Because of the phase shift, the RPN associated with h is a random uniform translation $\sin(\theta + \lambda x_1 + \mu x_2)$ of h whereas the ADSN associated with h is a random uniform translation of h multiplied by a random Rayleigh amplitude R that is $R\sin(\theta + \lambda x_1 + \mu x_2)$. In the same way, if h is the sum of two oscillations then the RPN is still a translation of h whereas the ADSN may favor one of the two frequencies as illustrated by Fig. 2.5.

2.5   Texture Synthesis Algorithms

Theorem 2.1 and Definition 2.3 yield two fast synthesis algorithms based on FFT. To preserve the mean of outcomes, the mean value m of the input image is added to the ADSN outcomes, while for RPN, the condition $\theta(x) = 0$ is enforced if $x = (0, 0)$. Observe that both processes can produce values outside the initial range. These values are usually very few and are simply cut off. An alternative yielding visually similar results is to stretch the histogram of outcomes.

(a) Input   (b) RPN   (c) ADSN   (d) ADSN
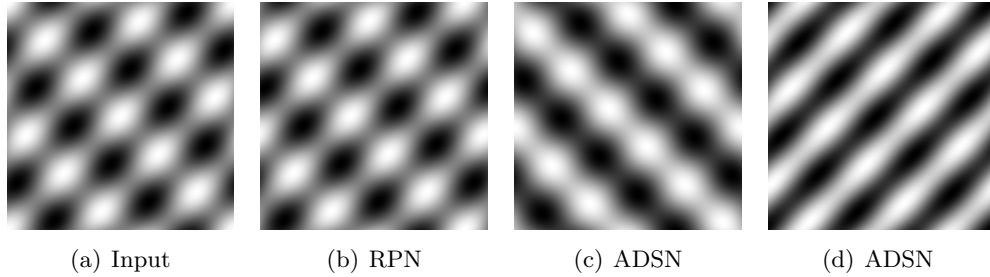
Figure 2.5:   Differences between the outcomes of the RPN and the ADSN associated with the bisinusoidal image 2.5(a). The RPN 2.5(b) is always a translation of the original image 2.5(a) whereas the ADSN randomly favors one of the two frequencies (two different realizations are displayed in 2.5(c) and 2.5(d)).

Two important practical points for the simulation of ADSN and RPN associated with non periodic color images are addressed next, and then we consider the issue of synthesizing ADSN and RPN textures having larger size than their initial sample.

2.5.1   Extension to Color Images

Color ADSN   First observe that the definition of the discrete spot noise (DSN) is easily extended to color images by summing colored spots, that is by using vector-valued spots $\mathbf{h} = (h_r, h_g, h_b)$ in Formula (2.1). This operation is performed in the RGB space that roughly corresponds to the frequency content of images. This obviously induces correlations between the color channels of the resulting image. Henceforth, the color ADSN is defined as the limit of the normalized DSN, as in Section 2.2. The central limit theorem then applies as before and the limit is a Gaussian multivariate field, with covariance matrix

$$C_h(x,y) = \frac{1}{MN} \sum_{u \in \Omega} \left(\mathbf{h}(x-u) - \mathbf{m}\right)^T \left(\mathbf{h}(y-u) - \mathbf{m}\right),$$

where as before $\mathbf{m} = (m_r, m_g, m_b)$ is the arithmetic mean of $\mathbf{h}$. Theorem 2.1 straightforwardly generalizes to this setting, and the limit is obtained as

$$\frac{1}{\sqrt{MN}} \left(\mathbf{h} - \mathbf{m1}\right) * Y, \tag{2.4}$$

where as before Y is a <u>scalar</u> Gaussian white noise of dimension $M \times N$.

In other words, the color ADSN is obtained by convolving each color channel with the <u>same</u> realization of a Gaussian white noise. Note that this procedure is much simpler than a classical approach to color texture synthesis relying on a PCA transform of the color space [74, 53]. As will be illustrated in the experimental section, this procedure permits to preserve the color content of the input image. This provides an interesting alternative to the use of color lookup tables, the standard way to obtain colored noises in computer graphics [123, 49, 96].

(a) Input   (b) RPN   (c) Wrong RPN

(d) Input   (e) RPN   (f) Wrong RPN
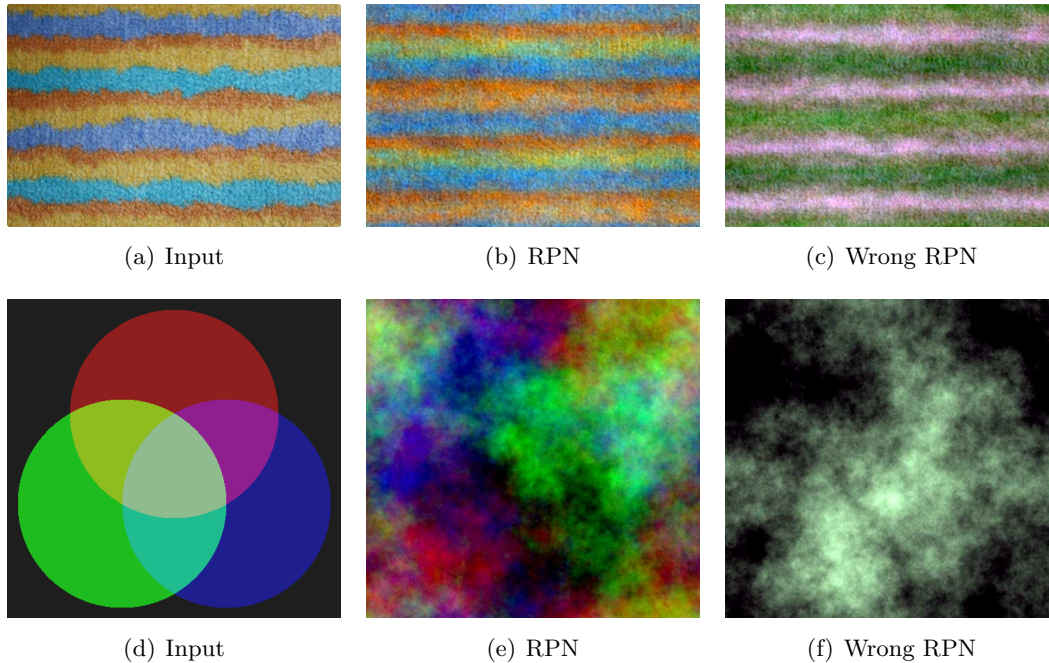
Figure 2.6: RPN associated with color images. Images 2.6(a) and 2.6(d): input RGB images; Images 2.6(b) and 2.6(e): associated color RPN, obtained by adding the same random phase to each phase of the three color channels. In contrast, if one imposes the same random phase to each color channel one obtains images 2.6(c) and 2.6(f), the colors of which are not consistent with the original images.

Color RPN   The mathematical extension of the RPN to the color case is less clear than for ADSN. The question is how to define a random phase in the vector-valued case. First observe that the phase of each channel of the color ADSN is a scalar random phase, as in Definition 2.2. Moreover, Formula (2.4) and the convolution theorem implies that the same random phase is added to the phase of each color channel of **h**. By analogy, the color RPN is defined by adding the same random phase to the phase of each color channel of the spot. Recall that in the gray level case, as explained at the end of Section 2.3, adding a random phase to the phase of the spot is equivalent to replacing the phase of the spot by a random phase. In the color setting, this second option (replacing the phase of each color channel by a random phase) would yield false colors, as illustrated by Fig. 2.6. In contrast, adding the same random phase to the original phases of each color channel preserves the phase displacements between channels, which is important for color consistency (see Fig. 2.6).

2.5.2   Avoiding Artifacts Due to Non Periodicity

Since both ADSN and RPN are based on FFT the periodicity of the input sample is a critical requirement. A digital image can always be considered as a periodic

image but this results in creating artificial discontinuities at its boundary. In our case it is not possible to avoid this problem using a symmetrization of the image because this would change the features of the output, for example by creating new characteristic directions.

The goal here is to slightly change the input sample h to enforce its periodicity. This is done by replacing h with its periodic component $p = \text{per}(h)$ as introduced by Moisan in [113]. In the original paper [113], p is defined as the solution of a variational problem. As shown in the Appendix A, p can also be defined as the unique solution of the Poisson problem

$$\begin{cases} \Delta p = \Delta_i h \\ \text{mean}(p) = \text{mean}(h) \end{cases} \tag{2.5}$$

where Δ is the usual discrete periodic Laplacian and Δ_i is the discrete Laplacian in the interior of the domain. For a periodic image f, these discrete operators are defined by

$$\Delta f(x) = 4f(x) - \sum_{y \in N_x} f(y)$$

and

$$\Delta_i f(x) = |N_x \cap \Omega| f(x) - \sum_{y \in N_x \cap \Omega} f(y),$$

where $N_x \subset \mathbb{Z}^2$ denotes the 4-connected neighborhood of x and $|N_x \cap \Omega|$ the number of those neighbors that are in Ω. Note that Δf and $\Delta_i f$ only differ at the boundary of the image domain. As a consequence (2.5) ensures that p and h have a similar behavior inside the image domain. In particular if h is constant at its boundary we have $p = h$.

In the general case p is computed directly by the classical FFT-based Poisson solver [127] since in the Fourier domain (2.5) becomes

$$\begin{cases} \left(4 - 2\cos\left(\frac{2\xi_1 \pi}{M}\right) - 2\cos\left(\frac{2\xi_2 \pi}{N}\right)\right) \hat{p}(\xi) = \widehat{\Delta_i h}(\xi), \ \xi \in \Omega, \\ \hat{p}(0) = \hat{h}(0). \end{cases}$$

The definition of p given by (2.5) is preferable, in the context of this chapter, to the original one of [113]. Indeed it enables the direct computation of the discrete Fourier transform of p, which is useful in view of the synthesis algorithm.

Using the periodic component p in place of the initial image h permits to avoid strong artifacts due to the non periodicity of the input samples, as illustrated by Fig. 2.7. From now on, this preprocessing will be used in all numerical experiments.

Observe that other solutions exist in the literature for finding a "good" periodic representative of h, especially for solving the periodic tiling problem (see [121] for example). Nevertheless the periodic component p is particularly adapted to our problem since it has been defined to eliminate the "cross structure" present in the discrete Fourier transform [113].

(a) Input h (b) p (c) $s + \mathrm{mean}(h)$

(d) ADSN(h)   (e) ADSN(p)   (f) s+ADSN(p)
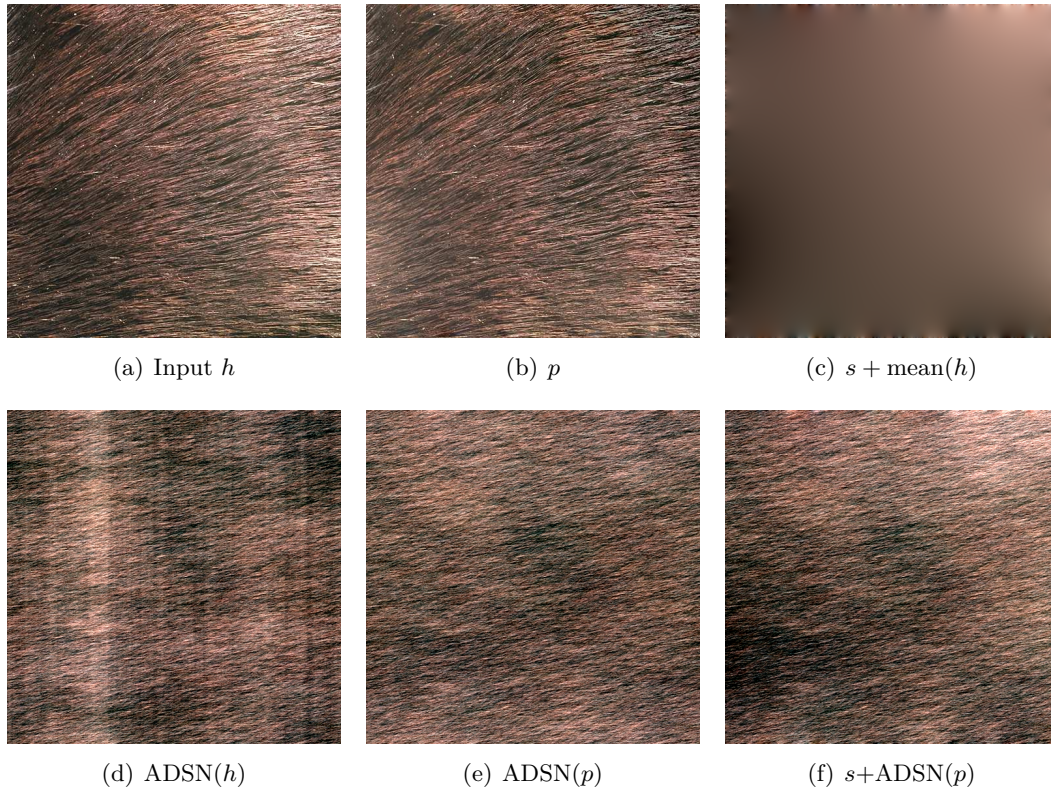
Figure 2.7:   First row: periodic and smooth component of the input sample $h = p + s$ [113]. The mean of h is added to the smooth component s for visualization. Second row: ADSN associated with the original texture sample h and ADSN associated to its periodic component p. In 2.7(d) the vertical stripes are due to the change of lighting between the left and the right sides of the input sample 2.7(a). When using the preprocessed decomposition (2.7(e)) this artifact due to the non periodicity of the input sample does not appear (results are similar for the RPN algorithm). Note that for rendering purpose one can add back the smooth component s to the ADSN associated with p 2.7(f).
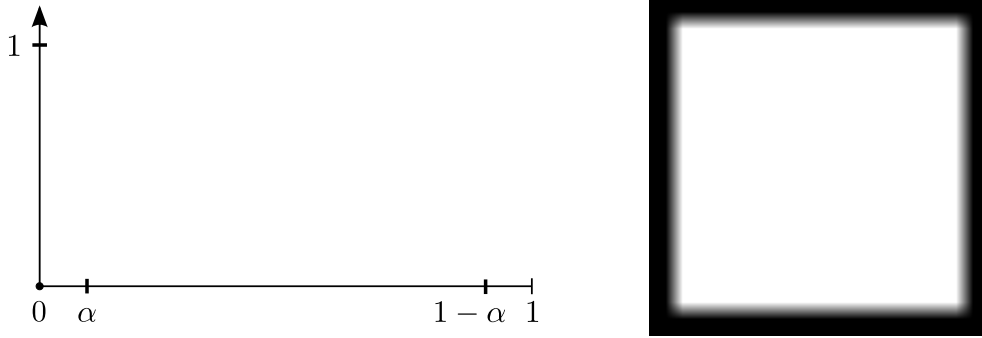
Figure 2.8: Cross section and gray-level representation of the smooth transition function φ_α used to attenuate the spot along the border of the image. On the interval $[0, \alpha]$ the function varies as the primitive of the standard $\mathcal{C}^\infty$ function $t \mapsto \exp\left(-1/\left(1 - (2t/\alpha - 1)^2\right)\right)$, and it is symmetrically defined on the interval $[1 - \alpha, 1]$. To preserve the variance of the spot, φ_α is normalized so that its L^2-norm equals 1.

2.5.3 Synthesizing Textures With Arbitrary Sizes

So far both discussed algorithms synthesize output textures which have the same size as the original input sample. However, an important issue in texture synthesis is to synthesize textures with arbitrary large size from a given sample. In this section we propose a practical method which solves this problem for ADSN and RPN textures simply by extending the spot (see Fig. 2.9).

Given a spot h of size $M_1 \times N_1$ and an output size $M_2 \times N_2$, with $M_2 > M_1$ and $N_2 > N_1$, we synthesize ADSN (resp. RPN) textures of size $M_2 \times N_2$ by computing the ADSN (resp. RPN) associated with an extended spot $\tilde{h} \in \mathbb{R}^{M_2 \times N_2}$ which represents suitably the original spot $h \in \mathbb{R}^{M_1 \times N_1}$. The extended spot $\tilde{h} \in \mathbb{R}^{M_2 \times N_2}$ is constructed by pasting a normalized copy of the periodic component p of h in the center of an image constant to m. More precisely:

$$\tilde{h}(x) = m + \sqrt{\frac{M_2 N_2}{M_1 N_1}} \left(p(x) - m\right) \mathbb{1}_{R_1}(x), \tag{2.6}$$

where $\mathbb{1}_{R_1}$ denotes the indicator function of R_1, the centered rectangle of size $M_1 \times N_1$ included in $\Omega_2 = \{0, \dots, M_2 - 1\} \times \{0, \dots, N_2 - 1\}$. As defined by Equation (2.6), $\tilde{h}$ has the same mean and variance as p, and the autocorrelation of both spots is close for small distances. However $\tilde{h}$ has discontinuities along the border of R_1 which is undesirable since, as illustrated by Fig. 2.7, those discontinuities can lead to artifacts after randomization.

In order to wear off this brusque transition the inner spot $p - m$ is progressively attenuated at its border. This is done by multiplying $p - m$ by a smooth transition function φ_α. The function φ_α, which is precisely described in Fig. 2.8, is constant at the center of the domain and decreases smoothly to zero at the border. All experiments in this chapter are performed using $\alpha = 0.1$.

(a) Spot h (b) Extended Spot $\tilde{h}$

(c) RPN(h)   (d) RPN$\big(\tilde{h}\big)$
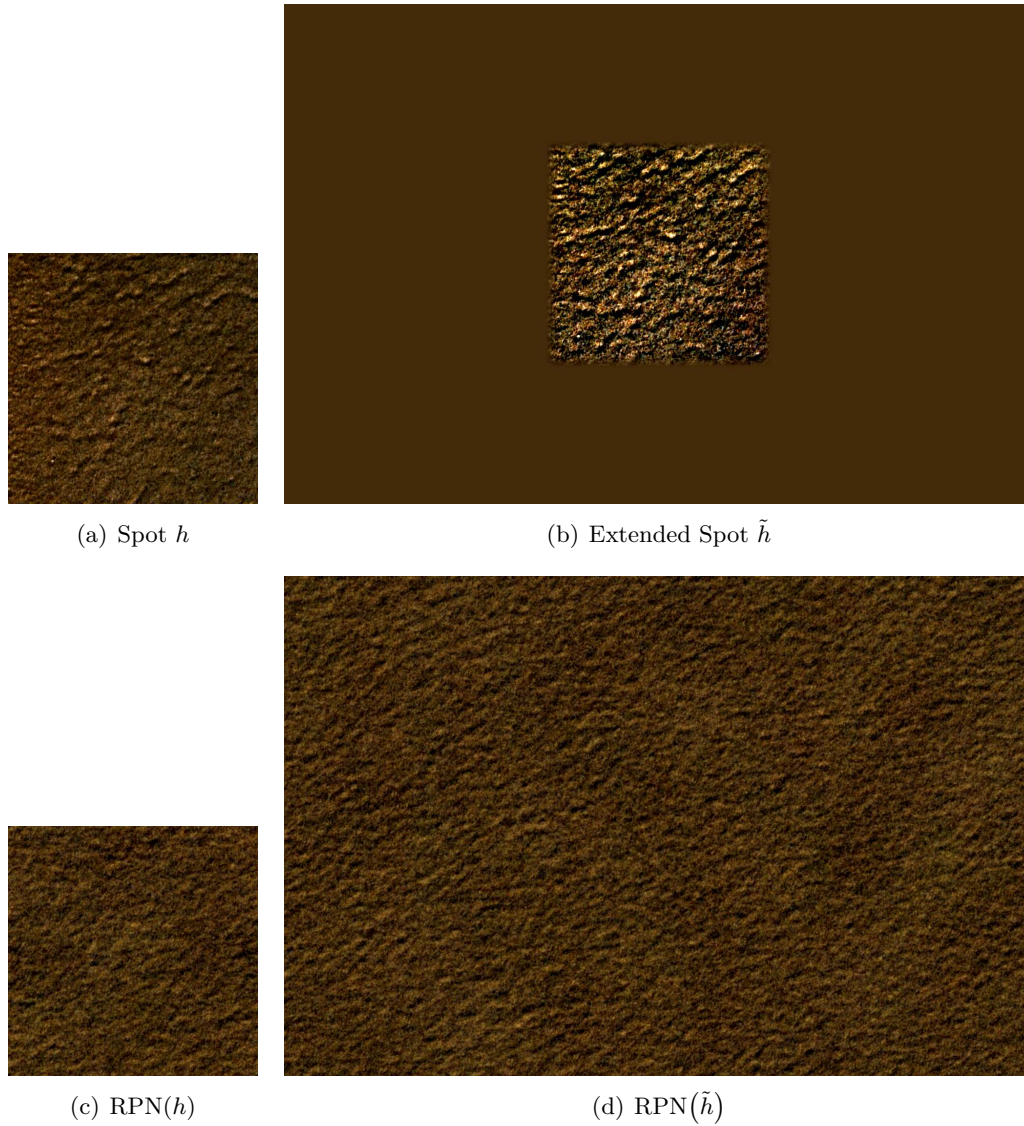
Figure 2.9:   Spot extension technique: the original spot h 2.9(a) is extended into the spot 2.9(b) by copying its periodic component p in the center, normalizing its variance (see Equation (2.6)), and smoothing the transition at the border of the inner frame by multiplying by the function φ_α (here $\alpha = 0.1$). The RPN associated to the extended spot is visually similar to the RPN associated with the original spot and has an higher size. Results are similar for the ADSN algorithm.

The resulting spot extension technique is illustrated in Fig. 2.9. Again, in this example $\alpha = 0.1$. Experiments show that the value of this parameter is not critical and that for most images $\alpha = 0.1$ seems a good compromise between wave artifact correction and information loss.

Summary of the synthesis method: To conclude this section we summarize the whole procedure for both ADSN and RPN texture synthesis algorithms. The input of both algorithms is a color input sample h of size $M_1 \times N_1$, the size $M_2 \times N_2$ of the output texture and (optionally) a value for the parameter α involved in the smooth transition function φ_α.

1. Compute the periodic component p of h.

2. Extends p into $\tilde{h}$ using Equation (2.6) and the pointwise multiplication by the smooth transition function φ_α.

3.
   - **ADSN**: Simulate a Gaussian white noise Y and return $Z = m + \frac{1}{\sqrt{M_2 N_2}} \left(\tilde{h} - m \right) * Y$, the convolution being applied to each color channel of $\tilde{h} - m$.
   - **RPN**: Simulate a random phase θ with $\theta(0) = 0$ and compute Z by adding θ to the phase of each color channel of $\tilde{h}$.

Note that step 1) and step 3) are based on FFT whereas step 2) has linear complexity. Eventually both algorithms have a complexity of $\mathcal{O}\left(M_2 N_2 \log\left(M_2 N_2\right)\right)$. The slight advantage of RPN is that it only necessitates the generation of about $\frac{M_2 N_2}{2}$ uniform variables versus the $M_2 N_2$ Gaussian variables necessary for the ADSN. Moreover, with RPN the Fourier modulus of the original sample is conserved. As already mentioned, an online demo [60] enables the interested reader to test the RPN texture synthesis algorithm.

2.6 Numerical Results

2.6.1 Perceptual Similarity of ADSN and RPN

Even though the two processes ADSN and RPN have different Fourier modulus distributions (see Section 2.4), they produce visually similar results when applied to natural images as shown by Fig. 2.10. In order to better illustrate this perceptual similarity, we display for each input image the corresponding ADSN and RPN to which the *same* uniform random phase was imposed. Recall that it was shown in Fig. 2.5 that perceptual similarity does not hold in the case of images having a sparse Fourier spectrum.

2.6.2 RPN and ADSN as Micro-Texture Synthesizers

This section investigates the synthesis of real-world textures using RPN. As mentioned above, ADSN produces visually similar results.
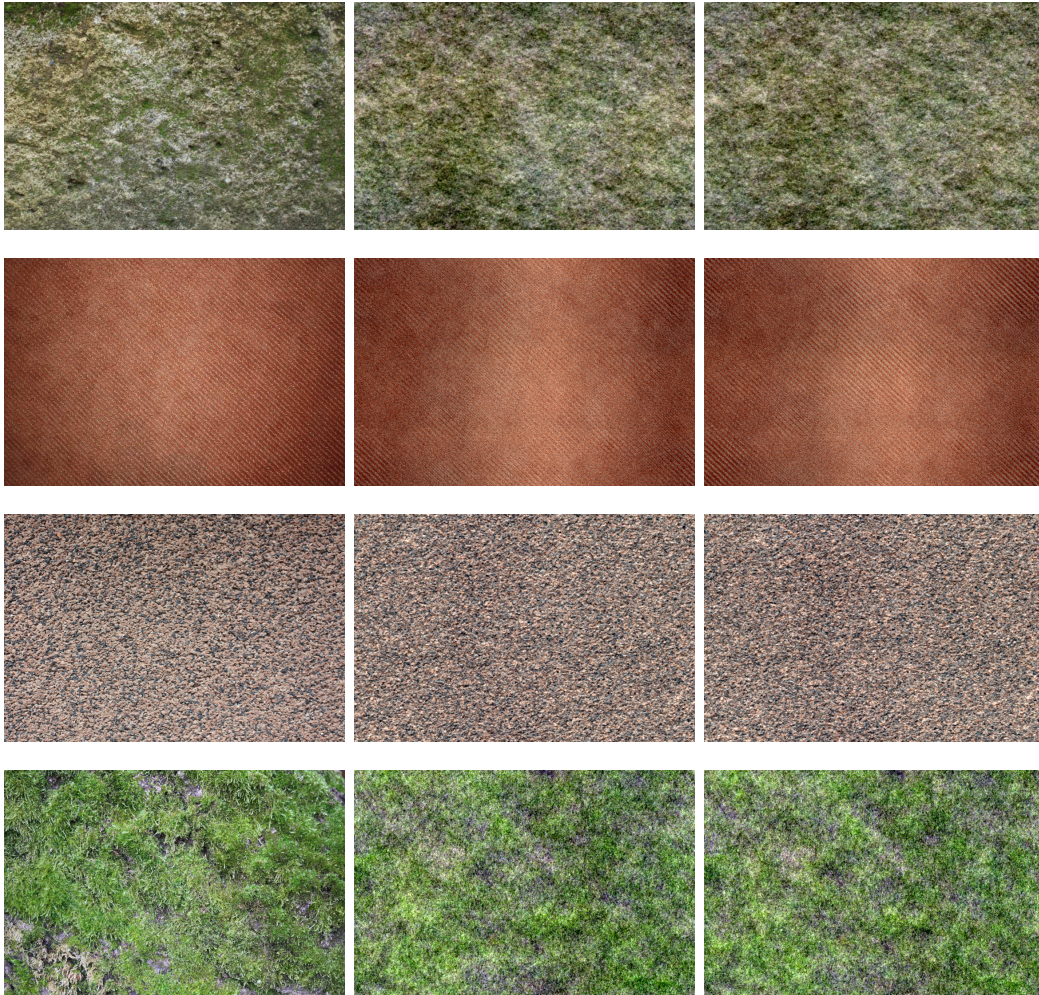
Figure 2.10: ADSN (middle) and RPN (right) associated with several input textures (left): stone, carpet, pink concrete, and moss. In order to compare the results the same uniform random phase is imposed to both ADSN and RPN. Observe that there is nearly no perceptual difference between the outcome of both algorithms. This perceptual similarity has been observed for every ADSN and RPN outcomes associated with natural textures, showing that random phase and random shift textures are perceptually the same class of texture.

Figure 2.11: Examples of well-reproduced textures of walls: RPN (right) associated with different input textures (left). All these textures are satisfyingly reproduced by the RPN algorithm, which indicates that they are random phase textures. Observe that some local details are lost for the last texture. See also the next three figures (Fig. 2.12, Fig. 2.13, and Fig. 2.14) as well as the online demo webpage [60] for more examples of successful synthesis.
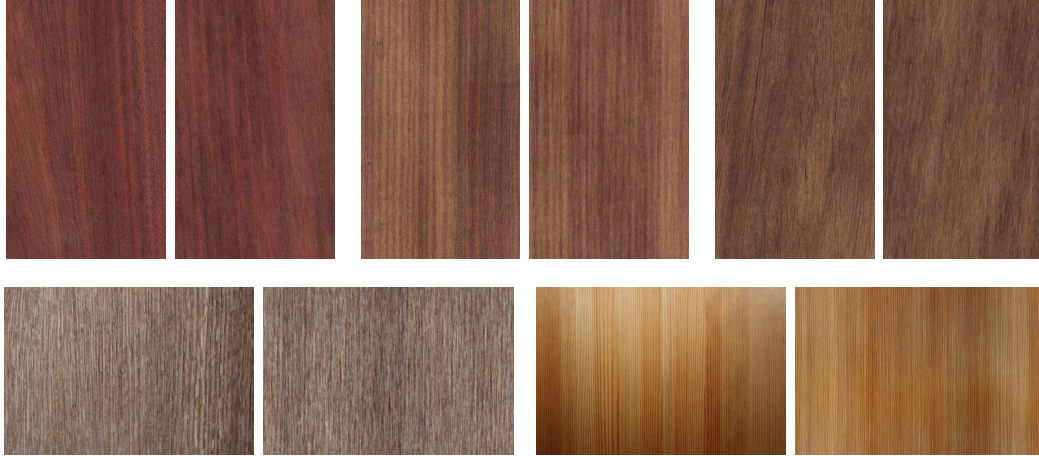
Figure 2.12: Examples of well-reproduced wood textures: RPN (right) associated with
different input textures (left). Again all these textures are satisfyingly reproduced by the
RPN algorithm, which indicates that they are random phase textures.

Figure 2.13: Examples of well-reproduced textures of fabrics and carpets: RPN (right)
associated with different input textures (left).
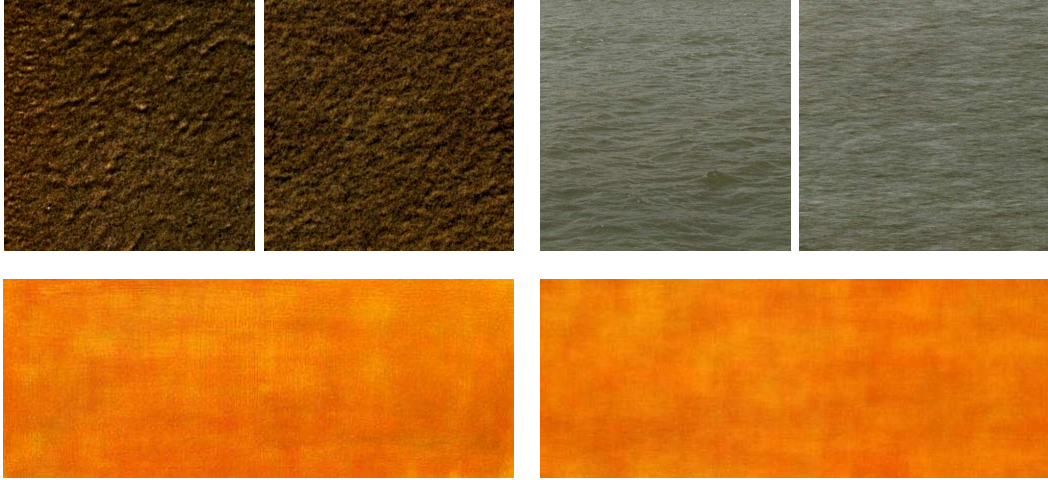
Figure 2.14: Examples of well-reproduced miscellaneous textures (sand, water, and paint on canvas): RPN (right) associated with different input textures (left).

The series of figures from Fig. 2.11 to Fig. 2.14 show that the RPN algorithm can be used to synthesize various micro-textures similar to a given original sample. Indeed the RPN algorithm can reproduced satisfyingly well textures of wallpaper, marble and concrete (Fig. 2.11), as well as wood textures (Fig. 2.12), fabric and carpet textures (Fig. 2.13), water, sand, and paint on canvas (Fig. 2.14).

However, as illustrated by Fig. 2.15, the RPN algorithm gives poor results with macro-textures. For this kind of texture, resampling algorithms (*e.g.* [51] or [50]) can give impressive results if the parameters (window or patch size, initialization, scanning order, ...) are well-chosen for each input image. However, as said in the introduction, these algorithms are also known for their tendency to sometimes produce erratic results or to excessively use verbatim copying (see Fig. 2.16), not to mention their computational cost. Recent inpainting algorithms [122, 152] partially solve these issues, but instabilities remain in the case of texture synthesis.

In contrast RPN (as well as ADSN), despite being limited to the synthesis of specific textures, is parameter-free and non iterative. Besides, it is very fast with a complexity of $\mathcal{O}(MN \log(MN))$. Last but not least, RPN (as well as ADSN) produces visually stable results: for any given image it always produces perceptually similar results, as illustrated by Fig. 2.17. As said in the introduction, this property is important in view of an automatic use in the context of computer graphic applications and explain why older and very simple synthesis procedures such as Perlin noise [123], also relying on noise filtering, are still popular today [36, 65, 96].

2.6.3 A Perceptual Robustness of Phase Invariant Textures

In Section 2.4 we showed that the ADSN associated to a spot can be obtained from its RPN by a pointwise product of the Fourier modulus with a Rayleigh noise.
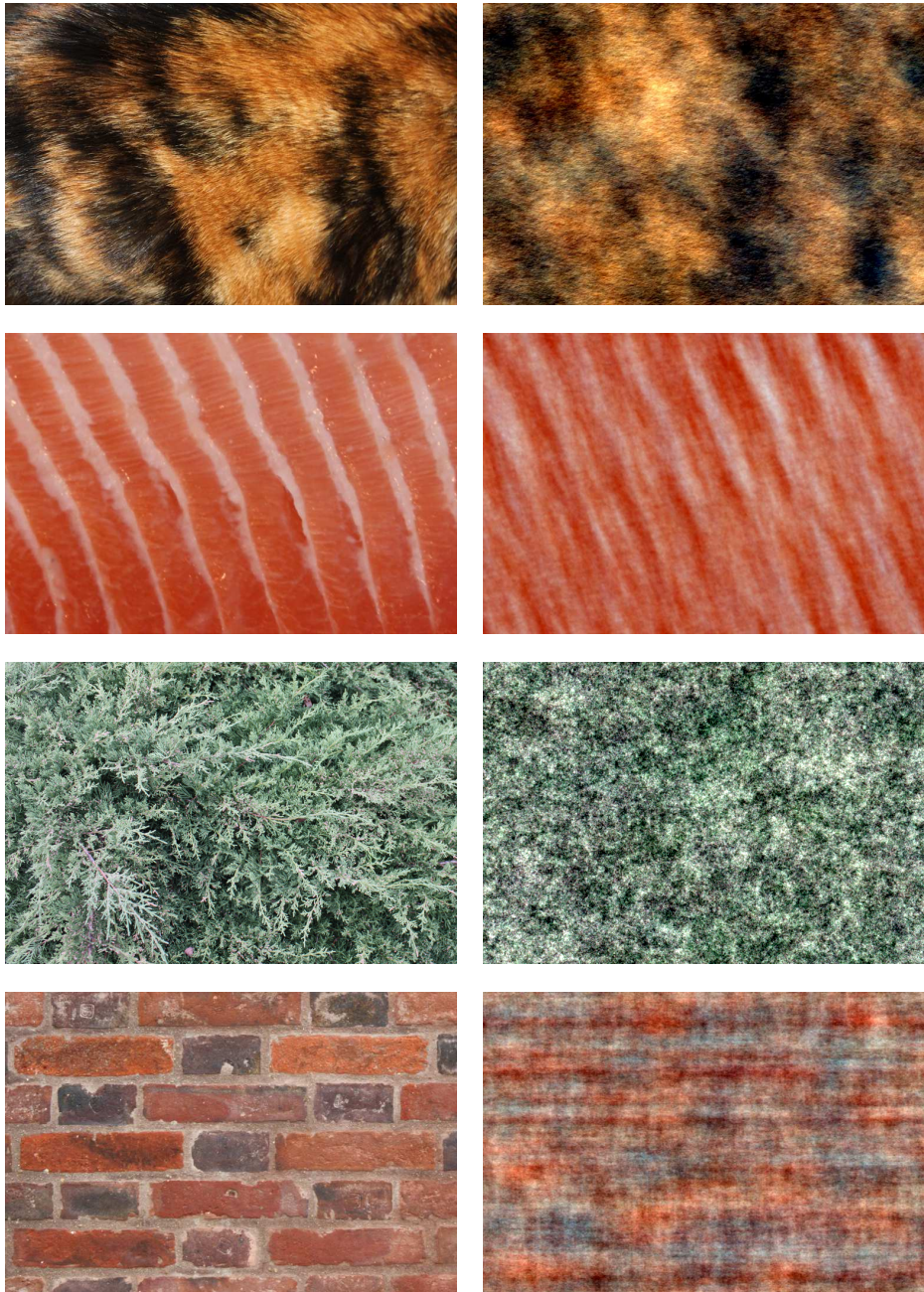
Figure 2.15: Examples of failures: RPN (right) associated with different input textures (left): cat fur, salmon, thuja, and bricks. All input textures are, to some extent, not well reproduced by the RPN algorithm and therefore are not random phase textures. On the third and fourth line are displayed two highly structured textures to which the algorithm is clearly not adapted. See [60] for more examples of failures.

(a) Input image   (b) $w = 9$ (c) $w = 15$ (d) $w = 21$ (e) RPN
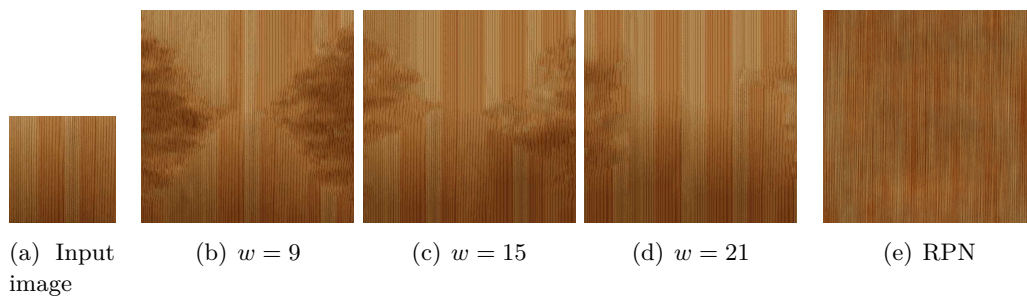
Figure 2.16: Illustrations of the limitations of exemplar-based algorithms. The pinewood texture 2.16(a) of size 256×256 pixels was used to synthesize twice larger textures using the Efros-Leung algorithm [51] with several values for the window width w (2.16(b), 2.16(c), and 2.16(d)). These algorithms are prone to grow garbage at times, as well as to produce verbatim copies of the input textures. In contrast, as illustrated by 2.16(e), the RPN algorithm is stable.

Figure 2.17: Several outcomes of the RPN associated with the same input image (top left). RPN (as well as ADSN) is a visually stable algorithm: indeed even though the output images are locally quite different they are always visually similar.
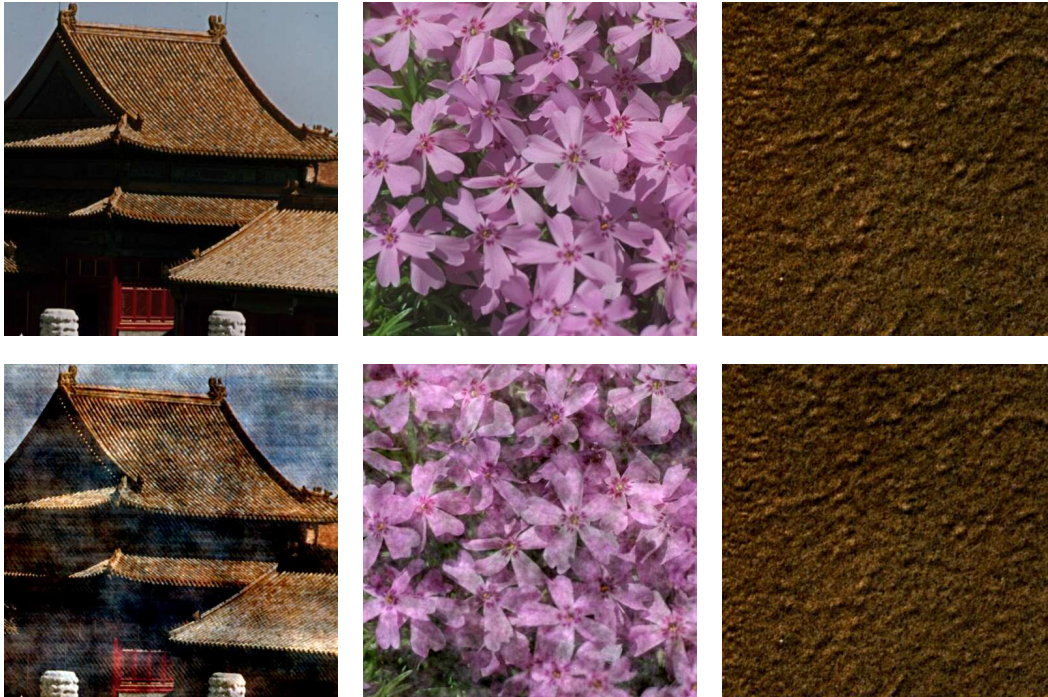
Figure 2.18: Effect of the pointwise multiplication of the Fourier modulus by a Rayleigh noise. The non random phase images (left and middle) are damaged whereas the random phase texture (right) is perceptually robust to this transformation.

Hence the observed visual similarity of the outcomes of the ADSN and the RPN (see Fig. 2.10) leads us to claim that the perception of random phase or random shift textures is actually robust to pointwise multiplication of the Fourier modulus by a Rayleigh noise.

One can wonder wether this robustness is also observed for every image. The answer is no and Fig. 2.18 illustrates that non random phase images are damaged by this multiplication. Thus, the perceptual invariance of random phase textures to a multiplicative noise on their magnitude may be a characteristic of this kind of texture.

2.7 Conclusion

This chapter presented a mathematical analysis of *spot noise* texture models and synthesis methods. Two texture perception models stemming from Julesz's theories were recalled. The first one is the random phase model, which leads exactly to the RPN algorithm. The second one is the shift invariant texton model. When applied in conjunction with the superposition principle, we have seen that this last model yields a stationary texture model which we called ADSN. Experimental evidence has shown that random phase textures and random shift textures generated from

the same sample are indistinguishable. Consequently, an unexpected additional perceptual invariance property of random phase textures was uncovered: random phase textures are perceptually invariant under a multiplicative noise on the Fourier modulus. To the best of our knowledge, this surprising fact had never been pointed out.

As for the texture synthesis algorithms, three significant technical points have been developed permitting the synthesis of textures from real-world texture samples. The first was the extension of ADSN and RPN to color images in preserving the phase displacement between the DFT of color channels. The second was the replacement of the original texture sample by its periodic component in order to avoir artifacts due to non periodicity. The third was a practical solution to synthesize ADSN and RPN textures of arbitrary large size. Numerical results have shown that ADSN and RPN reproduce satisfyingly well a relatively large range of textures, namely the micro-textures. The algorithms are ideally fast and produce visually stable results, two properties which are crucial for computer graphics applications.

Several perspectives open up. First, one should investigate if the technical methods developped for ADSN and RPN can be applied to other texture synthesis algorithms based on Fourier analysis. Chapter 4 will show that the extension to color images as well as replacing the sample by its periodic component enable procedural texture synthesis from sample using the state of the art model, namely the Gabor noise model [96]. Second, a similar study should be conducted on perceptually based texture synthesis methods relying on wavelet decompositions, following the seminal work of [74].

To conclude let us mention that a strong limitation of the models discussed here is the exclusive use of a linear superposition principle. It would therefore be of interest to investigate asymptotic properties of more elaborate generative texture models involving an occlusion principle or random transparent templates. This will be the object of Chapter 6 of this thesis where we will introduce the transparent dead leaves model.

Poisson Shot Noise

Contents

Abstract: The ADSN algorithm developed in Chapter 2 illustrates the interest of the Gaussian limit of discrete shot noise models for image texture synthesis. This chapter deals with the Poisson shot noise model, the continuous counterpart of the discrete shot noise. This model is often used in procedural texture synthesis, mainly because it converges to a Gaussian random field when the impulse intensity increases. Focus is put on this normal convergence for which classical results are recalled, notably the Berry-Esseen theorem for Poisson shot noise. Our main theoretical contribution is to significantly improve the upper bound of the Berry-Esseen constant for Poisson shot noise. It is also shown that, under additional hypotheses, multiplying the impulses of the shot noise by random weights accelerates the normal convergence. As a practical contribution to procedural texture synthesis, experiments show that the Berry-Esseen bound provides the good order of magnitude for the "visual convergence" to the limit Gaussian texture. However, multiplying the impulses by random weights does not seem to accelerate the visual convergence.

3.1   Introduction

The previous chapter has illustrated the interest of the Discrete Spot Noise (DSN) model for texture synthesis (See Chapter 2). The developed ADSN algorithm relies on the limit Gaussian process of the DSN sequence when the number of impulses tends to infinity.

   The goal of this chapter is to define and study the corresponding shot noise model defined on the continuous domain, and more particularly its convergence to a Gaussian random field (r.f.) (in this theoretical chapter, the general terminology *shot noise* will be used in place of the terminology *spot noise* which is only encountered for texture synthesis [146]). The family of shot noise models is very large, including several degrees of complexification. As a common characteristic, all shot noise models are made of the sum of several (possibly random) functions translated by random vectors scattered all over the space. Here we focus on shot noise processes driven by independently marked Poisson point processes[1]. Hence the studied model, called *Poisson shot noise*, takes the form

$$f(x) = \sum_{(x_j, \kappa_j) \in \Pi} h(x - x_j, \kappa_j), \ x \in \mathbb{R}^d,$$

where h is a measurable function and Π is an independently marked Poisson process over $\mathbb{R}^d \times K$, K being the mark space. This means that to each point x_j is attached a random mark κ_j following some probability distribution P_κ. One should think of the mark κ_j as a random parameter to select the impulse function among a family of functions $\{y \mapsto h(y, \kappa), \ \kappa \in K\}$. For example the random mark κ_j may encode a random amplitude, random orientation, scale, frequency, indicator of random set, etc.

   The Poisson shot noise model is used in many different areas. For examples, it has been used to model current through some electronic device [39], Internet traffic [12], as well as the roughness of paper [22, 84]. It is also a classical model in geostatistics (see the random token model in [100] and the references therein).

   The Poisson shot noise model has also been and is still extensively used in procedural texture synthesis [102, 123, 146, 96, 95], where it is often called sparse convolution model in reference to the work of Lewis [102]. The main practical reason why shot noise models are used as procedural noise functions is that, when the impulses have a compact support, the shot noise f can be evaluated at any point x for a fixed computational cost. This is done by only simulating the impulses influencing the noise at the point x. From a theoretical point of view, shot noise models are used in procedural texture synthesis since, as for the discrete shot noise model, when increasing the intensity of impulses the Poisson shot noise tends to a Gaussian r.f. Hence if the intensity of the Poisson shot noise is high enough, it is an approximation of a Gaussian r.f. which is defined on the whole continuous domain. Note that the fact that the r.f. is defined and computable on every

---

[1]Appendix B recalls basic definitions and properties of Poisson point processes.

point of the continuous domain is an important requirement for computer graphics applications such as texturing objects of a 3D virtual environment [95]. This is a main difference with the ADSN model of Chapter 2 as well as the classical exact simulation algorithms for Gaussian r.f. [155, 43] based on FFT: they only permit to simulate a Gaussian r.f. on a finite grid.

Hence to simulate a Gaussian texture, one can use a Poisson shot noise with high intensity. However the computational cost of shot noise simulation algorithms is typically linearly proportional to the impulse intensity λ. One must therefore find a trade-off between the quality of the Gaussian approximation and the computational cost. Determining automatically a value for the intensity λ which would satisfy this trade-off is a crucial problem. The main practical contribution of this chapter is to demonstrate that this problem can be solved by using a classical result from probability theory, namely the Berry-Esseen theorem for Poisson shot noise [119, 75].

After recalling the general properties of Poisson shot noise, its convergence toward a Gaussian r.f. is studied in detail in this chapter. Known theoretical results on the rate of the normal convergence are recalled [119, 75]. Our main contribution on the subject is to show that the Berry-Esseen constant for Poisson shot noises is the same as the Berry-Esseen constant for Poisson random sums. As a consequence, thanks to a recent result due to Korolev and Shevtsova [92], we reduce by a factor seven the upper bound of the Berry-Esseen constant for Poisson shot noises previously derived by Heinrich and Schmidt [75].

The Berry-Esseen theorem provides a bound which tends to zero proportionally to $\lambda^{-\frac{1}{2}}$, where λ is the intensity of the Poisson point process. As an attempt to reach a faster rate of convergence, we also investigate conditions for which the normal convergence is of order 1 instead of order $\frac{1}{2}$. It is demonstrated that, under broad hypotheses, an asymptotic normal convergence rate of order 1 is always achieved in multiplying the random impulses $h(x_j, \kappa_j)$ by i.i.d. random weights w_j.

The theoretical study of the normal convergence of Poisson shot noise is completed with an experimental section. Its goal is to determine whether the theoretical results on the normal convergence rate have applications for procedural texture synthesis based on shot noise models. First, it is shown that the Berry-Esseen bound provides the good order of magnitude for the "visual convergence" to the limit Gaussian texture. This might be integrated in procedural texture synthesis software relying on shot noise models to propose a range of interest for the value of the intensity λ. Second it is shown that, unfortunately, multiplying the impulses by random weights does not seem to accelerate the "visual convergence" of the shot noise sequence. Hence our result permitting to reach a normal convergence rate of order 1 would be interesting in practice only if some high statistical precision is needed, which is *a priori* not the case in computer graphics.

The plan of this chapter is as follows. Section 3.2 defines the Poisson shot noise model and gives its covariance and power spectrum. Section 3.3 recalls and proves the normal convergence of Poisson shot noise with increasing intensity. The

rate of this normal convergence is then studied in detailed in Section 3.4. In particular the two above mentioned theoretical contributions are stated and proved. Finally, applications to procedural texture synthesis are discussed and illustrated in Section 3.5.

3.2   Mean, Covariance, and Power Spectrum of Poisson Shot Noise

We consider an independently marked Poisson process[2] $\Pi = \{(x_j, \kappa_j)\} \subset \mathbb{R}^d \times K$ having intensity measure $\lambda \mathcal{L}^d \otimes P_\kappa$, where $\lambda > 0$ is the intensity of the stationary unmarked Poisson process $\{x_j\}$ and P_κ is a probability distribution. We also consider a measurable function $h : \mathbb{R}^d \times K \to \mathbb{R}$ which will be called the *impulse function*.

Definition 3.1 (Poisson shot noise)**.** *The* shot noise *associated with the independently marked Poisson process $\Pi = \{(x_j, \kappa_j)\} \subset \mathbb{R}^d \times K$ and the impulse function $h : \mathbb{R}^d \times K \to \mathbb{R}$ is the random field f defined by*

$$f(x) = \sum_{(x_j, \kappa_j) \in \Pi} h(x - x_j, \kappa_j).$$

Let us introduce some notation. The expectation with respect to the distribution of Π is denoted by $\mathbb{E}$ whereas the distribution with respect to P_κ is denoted by E. $\tilde{h}$ denotes the function defined by $\tilde{h}(y, \kappa) = h(-y, \kappa)$. In addition, $\hat{h}$ denotes the Fourier transform of h with respect to the spatial variable y, that is

$$\hat{h}(\xi, \kappa) = \int_{\mathbb{R}^d} h(y, \kappa) e^{-2i\pi\langle \xi, y \rangle} dy.$$

Since it will always be assumed that

$$\int_{\mathbb{R}^d \times K} |h(y, \kappa)| \, dy P_\kappa(d\kappa) < +\infty,$$

Fubini's theorem ensures that the function $\hat{h}$ is P_κ-a.s. defined.

Proposition 3.1 (Mean, covariance and power spectrum of the shot noise process)**.** *Suppose that*

$$\int_{\mathbb{R}^d \times K} |h(y, \kappa)|^k \, dy P_\kappa(d\kappa) < +\infty$$

for $k = 1$ and $k = 2$. Then for all $x \in \mathbb{R}^d$, the sum $f(x)$ is a.s. absolutely convergent which ensures that f is well-defined. f is a stationary random field and it has a finite variance. Its expectation is given by

$$\mathbb{E}(f(x)) = \lambda \int_{\mathbb{R}^d \times K} h(y, \kappa) dy P_\kappa(d\kappa),$$

---

[2]Appendix B recalls basic definitions and properties of Poisson point processes.

while its covariance function C is given by

$$C(\tau) := \operatorname{Cov}(f(x+\tau), f(x)) = \lambda \int_{\mathbb{R}^d \times K} h(y+\tau, \kappa) h(y, \kappa) dy P_\kappa(d\kappa) = E\left(\tilde{h} * h(\tau, \kappa)\right).$$

The power spectrum S of the shot noise f is equal, up to a factor λ, to the mean power spectrum of the random integrable function $h(\cdot, \kappa)$, that is

$$S(\xi) := \int_{\mathbb{R}^d} C(\tau) e^{-2i\pi \langle \xi, \tau \rangle} d\tau = \lambda E\left(\left|\hat{h}(\xi, \kappa)\right|^2\right).$$

Proof. We provide the proof of these standard results for the sake of completeness. For all $x \in \mathbb{R}^d$, we can apply Campbell's theorem (see Theorem B.2) with the Poisson process Π and the function $h_x : (y, \kappa) \mapsto h(x - y, \kappa)$. The hypothesis of integrability ensures that h_x is integrable and thus the sum

$$f(x) = \sum_{(x_j, \kappa_j) \in \Pi} h(x - x_j, \kappa_j) = \sum_{(y_j, \kappa_j) \in \Pi} h_x(y_j, \kappa_j)$$

is a.s. absolutely convergent and

$$\mathbb{E}(f(x)) = \lambda \int_{\mathbb{R}^d \times K} h(x - y, \kappa) dy P_\kappa(d\kappa) = \lambda \int_{\mathbb{R}^d \times K} h(y, \kappa) dy P_\kappa(d\kappa).$$

For all $\tau \in \mathbb{R}^d$ and $x \in \mathbb{R}^d$, by hypothesis $h_{x+\tau}$ and h_x are square-integrable with respect to the intensity measure, hence Corollary B.1 ensures that

$$\begin{aligned}
C(\tau) &= \operatorname{Cov}(f(x+\tau), f(x)) \\
&= \lambda \int_{\mathbb{R}^d \times K} h(x + \tau - y, \kappa) h(x - y, \kappa) dy P_\kappa(d\kappa) \\
&= \lambda \int_{\mathbb{R}^d \times K} h(z + \tau, \kappa) h(z, \kappa) dz P_\kappa(d\kappa).
\end{aligned}$$

Using Fubini's theorem one remarks that

$$C(\tau) = \lambda \int_K \left(\int_{\mathbb{R}^d} h(y - \tau, \kappa) h(y, \kappa) dy \right) P_\kappa(d\kappa) = \lambda E\left(\tilde{h} * h(-\tau, \kappa)\right) = \lambda E\left(\tilde{h} * h(\tau, \kappa)\right).$$

To compute the power spectrum S of f we first use Fubini's theorem

$$S(\xi) = \int_{\mathbb{R}^d} C(\tau) e^{-2i\pi \langle \xi, \tau \rangle} d\tau = \lambda E\left(\int_{\mathbb{R}^d} \tilde{h} * h(\tau, \kappa) e^{-2i\pi \langle \xi, \tau \rangle} d\tau \right) = \lambda E\left(\widehat{\tilde{h} * h}(\xi, \kappa)\right).$$

Since the convolution theorem ensures that $\widehat{\tilde{h} * h}(\xi, \kappa) = \left|\hat{h}(\xi, \kappa)\right|^2$ we have

$$S(\xi) = \lambda E\left(\left|\hat{h}(\xi, \kappa)\right|^2\right).$$

$\square$

3.3   Normal Convergence of High Density Shot Noise

In this section we establish the convergence of the normalized Poisson shot noise to a Gaussian random field when the intensity λ tends to $+\infty$. The proof follows the outline given by [131, p. 558]. This result extends to more general shot noise models involving non Poisson point processes [75].

We consider a family of independently marked Poisson processes $\Pi_\lambda \subset \mathbb{R}^d \times K$, $\lambda > 0$, each Poisson process having intensity measure $\lambda \mathcal{L}^d \otimes P_\kappa$. The considered shot noise processes are

$$f_\lambda(x) = \sum_{(x_j,\kappa_j) \in \Pi_\lambda} h(x - x_j, \kappa_j),$$

where $h : \mathbb{R}^d \times K \to \mathbb{R}$ is a measurable function which is both integrable and square-integrable.

Centering and normalizing the processes f_λ we define the family of normalized shot noise

$$g_\lambda(x) = \frac{f_\lambda(x) - \mathbb{E}(f_\lambda)}{\sqrt{\lambda}}.$$

The expectation of $g_\lambda(x)$ is zero and its covariance, which does not depend on λ, is

$$\mathrm{Cov}(g_\lambda(x+\tau), g_\lambda(x)) = \frac{1}{\lambda}\mathrm{Cov}(f_\lambda(x+\tau), f_\lambda(x)) = \int_{\mathbb{R}^d \times K} h(y+\tau, \kappa)h(y, \kappa)dyP_\kappa(d\kappa)$$

Theorem 3.1 (Normal convergence of high density shot noise)**.** *Suppose that*

$$\int_{\mathbb{R}^d \times K} |h(y, \kappa)|^k \, dyP_\kappa(d\kappa) < +\infty$$

for $k = 1$ and $k = 2$. Then, as λ tends to $+\infty$, the family of random fields $(g_\lambda)_{\lambda \in]0,+\infty[}$ converges in the sense of finite dimensional distributions to a stationary Gaussian random field having null expectation and covariance function

$$C(\tau) = \int_{\mathbb{R}^d \times K} h(y + \tau, \kappa)h(y, \kappa)dyP_\kappa(d\kappa), \ \tau \in \mathbb{R}^d.$$

The proof of Theorem 3.1 is divided in two parts. First it is shown that each r.v. $g_\lambda(x)$ converges in distribution to a normal distribution. Second this result is extended to any linear combination $\sum_{k=1}^p w_k g_\lambda(x_k)$.

Lemma 3.1. *For all $x \in \mathbb{R}$ and for all $n \in \mathbb{N}$ we have*

$$\left| e^{ix} - 1 - ix - \cdots - \frac{(ix)^{n-1}}{(n-1)!} \right| \leq \frac{|x|^n}{n!}.$$

Proof. This elementary lemma stated in [119] is easily proved by induction. Indeed, for $n = 0$, $\left|e^{ix}\right| \leq 1$ is always true. If the inequality is true at rank n, then

$$\left|e^{ix} - 1 - ix - \cdots - \frac{(ix)^n}{n!}\right| = \left|\int_0^x ie^{it}dt - \int_0^x idt - \cdots - \int_0^x i\frac{(it)^{n-1}}{(n-1)!}dt\right|$$

$$\leq \int_0^x \left|e^{it} - 1 - \cdots - \frac{(it)^{n-1}}{(n-1)!}\right|dt$$

$$\leq \int_0^x \frac{|t|^n}{n!}dt$$

$$\leq \frac{|x|^{n+1}}{(n+1)!}.$$

$\square$

Lemma 3.2 (Normal convergence of the first-order distribution)**.** *Under the assumptions of Theorem 3.1, for all $x \in \mathbb{R}^d$, the family of r.v. $(g_\lambda(x))_\lambda$ converges in distribution to a normal r.v. with null expectation and variance*

$$\int_{\mathbb{R}^d \times K} h(y, \kappa)^2 dy P_\kappa(d\kappa).$$

Proof. By definition

$$g_\lambda(x) = \left(\sum_{(x_i, \kappa_i) \in \Pi_\lambda} \frac{1}{\sqrt{\lambda}} h(x - x_i, \kappa_i)\right) - \lambda \int_{\mathbb{R}^d \times K} \frac{1}{\sqrt{\lambda}} h(x - y, \kappa) dy P_\kappa(d\kappa).$$

Hence $g_\lambda(x)$ is the difference between a particular shot noise and a constant. By Campbell's theorem, the characteristic function of $g_\lambda(x)$ is for all $t \in \mathbb{R}$

$$\log\left(E\left(e^{itg_\lambda(x)}\right)\right)$$

$$= \int_{\mathbb{R}^d \times K} \left(e^{it\frac{1}{\sqrt{\lambda}}h(x-y,\kappa)} - 1\right) \lambda dy P_\kappa(d\kappa) - it\lambda \int_{\mathbb{R}^d \times K} \frac{1}{\sqrt{\lambda}} h(x - y, \kappa) dy P_\kappa(d\kappa)$$

$$= \int_{\mathbb{R}^d \times K} \lambda \left(e^{it\frac{1}{\sqrt{\lambda}}h(y,\kappa)} - 1 - it\frac{1}{\sqrt{\lambda}} h(y, \kappa)\right) dy P_\kappa(d\kappa).$$

Let us compute the limit of this last integral as $\lambda \to +\infty$ using the Lebesgue convergence theorem. First note that for all $(y, \kappa) \in \mathbb{R}^d \times K$ we have

$$\lim_{\lambda \to +\infty} \lambda \left(e^{it\frac{1}{\sqrt{\lambda}}h(y,\kappa)} - 1 - it\frac{1}{\sqrt{\lambda}} h(y, \kappa)\right) = -\frac{t^2}{2} h(y, \kappa)^2.$$

Besides using Lemma 3.1 we have the inequality

$$\lambda \left|e^{it\frac{1}{\sqrt{\lambda}}h(y,\kappa)} - 1 - it\frac{1}{\sqrt{\lambda}} h(y, \kappa)\right| \leq \frac{t^2}{2} h(y, \kappa)^2.$$

Since by hypothesis the right-hand side is integrable, we can apply the dominated convergence theorem to get

$$\lim_{\lambda \to +\infty} \log\left(E\left(e^{itg_\lambda(x)}\right)\right) = -\frac{t^2}{2} \int_{\mathbb{R}^d \times K} h(y, \kappa)^2 dy P_\kappa(d\kappa).$$

This limit is precisely the logarithm of the characteristic function of a normal distribution having the announced parameters. Lévy's theorem ensures the convergence in distribution. □

We are now able to prove Theorem 3.1.

Proof of Theorem 3.1. Let $x_1, \ldots, x_p$ be points in $\mathbb{R}^d$ and let $w_1, \ldots, w_p$ be real numbers. To prove the result we have to show that

$$Z_\lambda = \sum_{k=1}^{p} w_k g_\lambda(x_k)$$

converges in distribution to a Gaussian distribution having null expectation and variance

$$\sum_{k=1}^{p} \sum_{l=1}^{p} w_k w_l C(x_k - x_l).$$

Now remark that the linear combination of a particular shot noise can be seen as the value in $x = 0$ of another shot noise:

$$\sum_{k=1}^{p} w_k f_\lambda(x_k) = \sum_{(x_j, \kappa_j) \in \Pi_\lambda} \sum_{k=1}^{p} w_k h(x_k - x_j, \kappa_j) = \sum_{(x_j, \kappa_j) \in \Pi_\lambda} H(0 - x_j, \kappa_j),$$

where H is the measurable function

$$H : (y, \kappa) \mapsto \sum_{k=1}^{p} w_k h(y + x_k, \kappa).$$

By linearity H has the same integrability properties as h. Hence Lemma 3.2 applies to Z_λ: Z_λ converges in distribution to a Gaussian with null expectation and variance σ^2 given by

$$\sigma^2 = \int_{\mathbb{R}^d \times K} H(y, \kappa)^2 dy P_\kappa(d\kappa) = \sum_{k=1}^{p} \sum_{l=1}^{p} w_k w_l C(x_k - x_l).$$

□

3.4   Rate of Normal Convergence

In all this section σ is defined by

$$\sigma^2 = \int_{\mathbb{R}^d \times K} h(y, \kappa)^2 dy d\kappa$$

and it is assumed that $0 < \sigma < +\infty$, which means that the shot noise with impulse function h is non null and has a finite variance. For any fixed $x \in \mathbb{R}^d$ we define

$$Y_\lambda = \frac{f_\lambda(x) - \mathbb{E}(f_\lambda)}{\sigma \sqrt{\lambda}}$$

(note that the distribution of Y_λ does not depend on x, thanks to the stationarity of the shot noise f_λ). Theorem 3.1 shows that $(Y_\lambda)_{\lambda>0}$ converges in distributions to the normal distribution $\mathcal{N}(0,1)$. The goal of this section is to provide some estimations of the rate of this convergence (under additional hypotheses).

Following [119] and [75], the deviation between the distribution of the normalized shot noise and the standard normal distribution is measured using the Kolmogorov-Smirnov distance, as it is usual for Berry-Esseen theorems (which are recalled in Section 3.4.2).

3.4.1 Measuring the Deviation From Gaussianity: Kolmogorov-Smirnov Distance

Definition 3.2 (Kolmogorov-Smirnov distance). *Let P_1 and P_2 be two distributions of some r.v. X_1 and X_2, and let F_1 and F_2 be their respective cumulative distribution functions. The* Kolmogorov-Smirnov distance *between the distributions P_1 and P_2 is defined as*

$$d_{KS}(P_1, P_2) = \sup_{u \in \mathbb{R}} |F_1(u) - F_2(u)| = \|F_1 - F_2\|_\infty.$$

By convention, if $X_1 \sim P_1$ and $X_2 \sim P_2$ are two r.v., then $d_{KS}(X_1, X_2)$ denotes $d_{KS}(P_1, P_2)$. Convergence for the Kolmogorov-Smirnov distance implies convergence in distribution. Indeed, if (X_n) and X are such that $d_{KS}(X_n, X) \to 0$, then for all $x \in \mathbb{R}$ $F_n(x) \to F(x)$. In particular, this is true in all point of continuity of F, and thus X_n converges in distribution to X.

A fundamental and practical result for the estimation of Kolmogorov-Smirnov distances is Esseen's inequality (see e.g. [57, Lemma 2 p. 538] or [104, p. 297]). Here we recall this inequality in the case where one of the distributions is the standard normal distribution.

Lemma 3.3 (Esseen's inequality for normal distribution). *Let P be a distribution with null expectation, and let φ be its characteristic function. Then for all $a > 0$,*

$$d_{KS}(P, \mathcal{N}(0,1)) \leq \frac{2}{\pi} \int_0^a \frac{\left|\varphi(t) - \exp\left(-\frac{t^2}{2}\right)\right|}{t} dt + \frac{24}{\pi\sqrt{2\pi}a}.$$

This lemma is the key argument of the classical proof of the Berry-Esseen theorem, which we recall in the next section.

3.4.2 Two Berry-Esseen Theorems

Let us recall the classical Berry-Esseen theorem which provides a bound for the rate of normal convergence for the central limit theorem in the case where the i.i.d. r.v. have a finite third moment (see e.g. [57, p. 542] or [104, p. 300]).

Theorem 3.2 (Berry-Esseen theorem)**.** *Let (X_n) be a sequence of i.i.d. r.v. such that $\mathbb{E}(X_1) = 0$, $\mathbb{E}\left(X_1^2\right) > 0$, and $\mathbb{E}\left(|X_1|^3\right) < +\infty$. Let (Y_n) be the normalized sequence*

$$Y_n = \frac{X_1 + \cdots + X_n}{\sqrt{\mathbb{E}\left(X_1^2\right) n}}.$$

Then there exists a universal minimal constant $\Gamma_{BE} > 0$ (called the Berry-Esseen constant) such that

$$d_{KS}(Y_n, \mathcal{N}(0,1)) \le \Gamma_{BE} \frac{\mathbb{E}\left(|X_1|^3\right)}{\mathbb{E}(X_1^2)^{\frac{3}{2}} \sqrt{n}}.$$

Here the expression "universal constant" means that the constant Γ_{BE} does not depend on the the distribution of X_1. The exact computation of the Berry-Esseen constant Γ_{BE} is an open problem. Estimation of this constant has received and still receive a lot of attention, as the recent paper [145] and the references therein show. According to [145] the last to date estimation of Γ_{BE} is $0.409 \le \Gamma_{BE} \le 0.4785$.

The Berry-Esseen theorem can be generalized in several ways. As it will be demonstrated in the next section, one case of interest for the Poisson shot noise is the Berry-Esseen theorem for Poisson random sums. We refer to [93] and [92] for historical references on this result as well as to [92] for the last to date upper bound of the corresponding universal constant.

Theorem 3.3 (Berry-Esseen theorem for Poisson random sums)**.** *Let (X_n) be a sequence of i.i.d. r.v. such that $\mathbb{E}\left(X_1^2\right) > 0$, and $\mathbb{E}\left(|X_1|^3\right) < +\infty$. Let N_λ be an independent Poisson r.v. with parameter $\lambda > 0$. Define*

$$S_\lambda = \sum_{k=1}^{N_\lambda} X_k.$$

Then $\mathbb{E}(S_\lambda) = \lambda \mathbb{E}(X_1)$, and $\mathrm{Var}(S_\lambda) = \lambda \mathbb{E}\left(X_1^2\right)$. Define T_λ as the normalized sequence associated to S_λ,

$$T_\lambda = \frac{S_\lambda - \lambda \mathbb{E}(X_1)}{\sqrt{\lambda \mathbb{E}\left(X_1^2\right)}}.$$

Then there exists a universal minimal constant $\Gamma_{PRS} > 0$ such that

$$d_{KS}(T_\lambda, \mathcal{N}(0,1)) \le \Gamma_{PRS} \frac{\mathbb{E}\left(|X_1|^3\right)}{\mathbb{E}(X_1^2)^{\frac{3}{2}} \sqrt{\lambda}}.$$

Besides $\Gamma_{PRS} \le 0.3051$ [92].

3.4.3   The Berry-Esseen Theorem for Poisson Shot Noises

As defined at the beginning of this section,

$$Y_\lambda = \frac{f_\lambda(x) - \mathbb{E}(f_\lambda)}{\sigma \sqrt{\lambda}}$$

for some $x \in \mathbb{R}^d$. We first state the Berry-Esseen theorem for Poisson shot noises established by Heinrich and Schmidt [75, Theorem 7], the proof of which relies on Lemma 3.3.

Theorem 3.4 (Berry-Esseen theorem for Poisson shot noises)**.** *Suppose that the measurable function $h : \mathbb{R}^d \times K \to \mathbb{R}$ satisfies*

$$\int_{\mathbb{R}^d \times K} |h(y, \kappa)|^k \, dy P_\kappa(d\kappa) < +\infty$$

for $k = 1$, $k = 2$, and $k = 3$. Write

$$\sigma^2 = \int_{\mathbb{R}^d \times K} h(y, \kappa)^2 dy P_\kappa(d\kappa) > 0 \quad and \quad E_3 = \int_{\mathbb{R}^d \times K} |h(y, \kappa)|^3 \, dy P_\kappa(d\kappa).$$

Then there exists a universal minimal constant $\Gamma_{PSN} > 0$ such that

$$d_{KS}(Y_\lambda, \mathcal{N}(0, 1)) \le \Gamma_{PSN} \frac{E_3}{\sigma^3 \sqrt{\lambda}}.$$

This theorem was first established, in a less general framework, by Papoulis [119], with the bound $\Gamma_{PSN} \le \frac{4}{3}\sqrt{2\pi} \le 3.35$. The upper bound given by Heinrich and Schmidt [75, Theorem 7] is $\Gamma_{PSN} \le 2.21$. Our first contribution concerning the normal convergence of Poisson shot noises is to provide the sharper bound $\Gamma_{PSN} \le 0.3051$, thanks to the recent result of Korolev and Shevtsova [92] (see Theorem 3.3).

Proposition 3.2. *The Berry-Esseen constant for Poisson shot noises is equal to the Berry-Esseen constant for Poisson random sums:*

$$\Gamma_{PSN} = \Gamma_{PRS}.$$

As a consequence, $\Gamma_{PSN} \le 0.3051$.

Proof. Let us begin with the easiest inequality: $\Gamma_{PSN} \ge \Gamma_{PRS}$. Let (X_n) be any sequence of i.i.d. r.v. with distribution Q and such that $\mathbb{E}\left(X_1^2\right) > 0$, and $\mathbb{E}\left(|X_1|^3\right) < +\infty$. Let N_λ be an independent Poisson r.v. with parameter λ, and define S_λ and T_λ as in Theorem 3.3. Let us show that the distribution of S_λ is the first-order distribution of some Poisson shot noise. Consider Π_λ a Poisson point process over $\mathbb{R}^d \times \mathbb{R}$ with intensity measure $\lambda \mathcal{L}^d \otimes Q$, and define f_λ as the shot noise associated to Π_λ and the impulse function $h(y, \kappa) = \kappa \mathbb{1}_{[0,1]^d}(y)$, that is the shot noise

$$f_\lambda(x) = \sum_{(x_j, \kappa_j) \in \Pi_\lambda} \kappa_j \mathbb{1}_{[0,1]^d}(x - x_j).$$

Then for all $x \in \mathbb{R}^d$, $f_\lambda(x)$ is the sum of a random number of i.i.d. r.v. having distribution Q, and this random number follows a Poisson distribution with parameter $\lambda \int_{\mathbb{R}^d} \mathbb{1}_{[0,1]^d}(x - y) dy = \lambda$. Hence $f_\lambda(x)$ has the same distribution as S_λ. Since

$$\sigma^2 = \int_{\mathbb{R}^d \times \mathbb{R}} \kappa^2 \mathbb{1}_{[0,1]}(y) dy Q(d\kappa) = \int_{\mathbb{R}} \kappa^2 Q(d\kappa) = \mathbb{E}\left(X_1^2\right),$$

and similarly $E_3 = \mathbb{E}\left(|X_1|^3\right)$, by Theorem 3.4

$$d_{KS}(T_\lambda, \mathcal{N}(0,1)) \leq \Gamma_{PSN} \frac{\mathbb{E}\left(|X_1|^3\right)}{\mathbb{E}(X_1^2)^{\frac{3}{2}}\sqrt{\lambda}},$$

which shows that $\Gamma_{PSN} \geq \Gamma_{PRS}$.

Let us now turn to the reverse inequality. Let us first restrict to the case where the impulse function h has compact spatial support: there exists a compact set $A \subset \mathbb{R}^d$ such that $y \notin A \Rightarrow h(y,\kappa) = 0$ for all $\kappa \in K$. Let us fix a point $x \in \mathbb{R}^d$ and consider the distribution of

$$f_\lambda(x) = \sum_{(x_j,\kappa_j)\in\Pi_\lambda} h(x-x_j,\kappa_j).$$

Then, $x_j \notin x \oplus \check{A} \Rightarrow h(x-x_j,\kappa_j) = 0$. Consequently, we can restrict the sum defining $f_\lambda(x)$ to the restriction of Π_λ to the set $x \oplus \check{A} \times K$. $\Pi_\lambda \cap \left(x \oplus \check{A} \times K\right)$ is a finite Poisson process and its cardinal follows a Poisson distribution with parameter $\lambda \mathcal{L}^d\left(x \oplus \check{A}\right) = \lambda \mathcal{L}^d(A)$. Besides, given that $\#\left\{\Pi_\lambda \cap \left(x \oplus \check{A} \times K\right)\right\} = n \geq 1$, the points $(x_j,\kappa_j) \in \Pi_\lambda \cap \left(x \oplus \check{A} \times K\right)$ are i.i.d. with distribution $Unif\left(x \oplus \check{A}\right) \otimes P_\kappa$. Hence, for each point (x_j,κ_j) of the considered restriction of Π_λ, $h(x-x_j,\kappa_j)$ is a r.v. with distribution Q, say, the push-forward measure of $Unif\left(x \oplus \check{A}\right) \otimes P_\kappa$ by the measurable function h. To sum up, $f_\lambda(x)$ is the sum of a Poisson random number of parameter $\lambda \mathcal{L}^d(A)$ of i.i.d. r.v. of distribution Q, that is $f_\lambda(x)$ is a Poisson random sum. Write H a r.v. with distribution Q. We have

$$\mathbb{E}(H) = \frac{1}{\mathcal{L}^d(A)} \int_{x\oplus\check{A}\times K} h(x-y,\kappa)dyP_\kappa(d\kappa) = \frac{1}{\mathcal{L}^d(A)} \int_{\mathbb{R}^d\times K} h(y,\kappa)dyP_\kappa(d\kappa).$$

Similarly,

$$\mathbb{E}\left(|H|^p\right) = \frac{1}{\mathcal{L}^d(A)} \int_{\mathbb{R}^d\times K} |h(y,\kappa)|^p dyP_\kappa(d\kappa),$$

for $p = 2$ and $p = 3$. By the Berry-Esseen theorem for Poisson random sums (Theorem 3.3) we have

$$d_{KS}(Y_\lambda, \mathcal{N}(0,1)) \leq \Gamma_{PRS} \frac{\mathbb{E}\left(|H|^3\right)}{\mathbb{E}\left(H^2\right)^{\frac{3}{2}}\sqrt{\mathcal{L}^d(A)\lambda}}$$

$$= \Gamma_{PRS} \frac{\mathcal{L}^d(A)^{-1}E_3}{\left(\mathcal{L}^d(A)^{-1}\sigma^2\right)^{\frac{3}{2}}\sqrt{\mathcal{L}^d(A)\lambda}}$$

$$= \Gamma_{PRS} \frac{E_3}{\sigma^3\sqrt{\lambda}}.$$

In conclusion, the class of Poisson shot noises having an impulse function of compact support satisfies the Berry-Esseen inequality with a constant less than Γ_{PRS}. To conclude the proof we need to show that this last inequality is true for any Poisson shot noise. This is done in approximating any shot noise by a shot noise having

compact support. More precisely, let us now consider a general Poisson shot noise f_λ with impulse function h. For all $R > 0$, let B_R denote the ball of center 0 and radius R. Define $h_R(y, \kappa) = \mathbb{1}_{y \in B_R} h(y, \kappa)$, as well as $f_{\lambda,R}$ the shot noise associated to h_R and the Poisson process Π_λ. Then, by Proposition 3.1 the difference $f_\lambda(x) - f_{\lambda,R}(x)$ is a shot noise with variance

$$\lambda \int_{\mathbb{R}^d \times K} \mathbb{1}_{y \notin B_R} h^2(y, \kappa) dy P_\kappa(d\kappa),$$

and this variance tends to 0 as R tends to $+\infty$ by dominated convergence. Hence $f_{\lambda,R}(x)$ converges to $f_\lambda(x)$ in L^2, as well as the corresponding normalized r.v. $Y_{\lambda,R}$ and Y_λ. In particular $Y_{\lambda,R}$ converges to Y_λ in distribution. Let us note $F_{\lambda,R}$, F_λ, and Φ the cumulative distribution functions of $Y_{\lambda,R}$, Y_λ, and $\mathcal{N}(0, 1)$. For all $u \in \mathbb{R}$, and $R > 0$,

$$|F_\lambda(u) - \Phi(u)| \leq |F_\lambda(u) - F_{\lambda,R}(u)| + |F_{\lambda,R}(u) - \Phi(u)|.$$

Let $E_{3,R}$ and σ_R^2 denote the corresponding moments of h_R. As shown above, since h_R has compact support

$$|F_{\lambda,R}(u) - \Phi(u)| \leq \Gamma_{PRS} \frac{E_{3,R}}{\sigma_R^3 \sqrt{\lambda}}.$$

Clearly, as $R \to +\infty$, $E_{3,R} \to E_3$ and $\sigma_R \to \sigma$. Hence, from the convergence in distribution, letting $R \to +\infty$ we obtain that for all continuity point u of F_λ,

$$|F_\lambda(u) - \Phi(u)| \leq \Gamma_{PRS} \frac{E_3}{\sigma^3 \sqrt{\lambda}}.$$

But since F_λ is right-continuous and Φ is continuous, the above inequality is valid for all $u \in \mathbb{R}$. This shows that $\Gamma_{PSN} \leq \Gamma_{PRS}$ and concludes the proof.

$\square$

3.4.4 Reaching Normal Convergence of Order One

The Berry-Esseen theorem for Poisson shot noises provides an error control for approximating the limit Gaussian random field by the shot noise of intensity λ. It might be used in practice to simulate an approximation of the limit Gaussian r.f. However the error bound only decreases according to $\lambda^{-\frac{1}{2}}$, which might prohibit high precision approximation.

In this section we investigate conditions for which the normal convergence is of order 1 instead of order $\frac{1}{2}$. It is demonstrated that as soon as the impulse function h has finite moments up to order four, an asymptotic normal convergence rate of order 1 is achieved by multiplying the random impulses $h(x_j, \kappa_j)$ by i.i.d. random weights w_j.

First let us demonstrate a technical lemma.

Lemma 3.4. *Suppose that the measurable function $h : \mathbb{R}^d \times K \to \mathbb{R}$ satisfies*

$$\int_{\mathbb{R}^d \times K} |h(y,\kappa)|^k \, dy P_\kappa(d\kappa) < +\infty$$

for $k = 1$, $k = 2$, $k = 3$, and $k = 4$. In addition suppose that

$$\int_{\mathbb{R}^d \times K} h(y,\kappa)^3 dy P_\kappa(d\kappa) = 0. \tag{3.1}$$

Note

$$\sigma^2 = \int_{\mathbb{R}^d \times K} h(y,\kappa)^2 dy P_\kappa(d\kappa) \quad and \quad E_4 = \int_{\mathbb{R}^d \times K} h(y,\kappa)^4 dy P_\kappa(d\kappa).$$

Besides let $\varphi(t)$ be the characteristic function of the shot with impulse function $\frac{h}{\sigma}$ and intensity $\lambda = 1$, that is

$$\varphi(t) = \exp\left(\int_{\mathbb{R}^d \times K} \left(e^{i \frac{th(y,\kappa)}{\sigma}} - 1 \right) dy P_\kappa(d\kappa) \right).$$

Let

$$q = \sup\left\{ |\varphi(t)|, \ t \geq \sqrt{\frac{6\sigma^4}{E_4}} \right\}.$$

Then we have for all $\lambda \geq \frac{E_4}{6\sigma^4}$

$$d_{KS}(Y_\lambda, \mathcal{N}(0,1)) \leq \underbrace{\left(\frac{2}{3\pi} + \frac{4}{\pi\sqrt{2\pi}} \right)}_{\leq 0.721} \frac{E_4}{\sigma^4} \frac{1}{\lambda} + \frac{1}{\pi} \ln\left(\frac{6\sigma^4}{E_4}\lambda \right) q^\lambda.$$

In particular, if $q < 1$, $d_{KS}(Y_\lambda, \mathcal{N}(0,1)) = \mathcal{O}\left(\frac{1}{\lambda} \right)$.

Proof. The proof of this lemma is close to the one of Theorem 3.4 given in [75, p. 726]. In our case the hypothesis (3.1) of vanishing third moment enables to use Lemma 3.1 with an higher order. To obtain an error bound term in $\frac{1}{\lambda}$ we follow the method to establish Edgeworth expansions in Feller's textbook [57, (4.14) p. 541].

Fix $x \in \mathbb{R}^d$. Let $Y_\lambda = \frac{f_\lambda(x) - \mathbb{E}(f_\lambda)}{\sigma\sqrt{\lambda}}$, and let $F_\lambda(u) = \mathbb{P}(Y_\lambda \leq u)$ and $\varphi_\lambda(t) = \mathbb{E}\left(e^{itY_\lambda} \right)$ be respectively the cumulative distribution function and the characteristic function of Y_λ. Recall that from Campbell's theorem (see Theorem B.2) we have

$$\log(\varphi_\lambda(t)) = \lambda \int_{\mathbb{R}^d \times K} \left(\exp\left(\frac{it}{\sigma\sqrt{\lambda}} h(y,\kappa) \right) - 1 - \frac{it}{\sigma\sqrt{\lambda}} h(y,\kappa) \right) dy P_\kappa(d\kappa).$$

Now remark that one can write

$$\frac{t^2}{2} = \lambda \int_{\mathbb{R}^d \times K} -\frac{1}{2} \left(\frac{it}{\sigma\sqrt{\lambda}} h(y,\kappa) \right)^2 dy P_\kappa(d\kappa).$$

Besides from the hypothesis (3.1) we have

$$\int_{\mathbb{R}^d \times K} \left(\frac{it}{\sigma\sqrt{\lambda}} h(y,\kappa) \right)^3 dy P_\kappa(d\kappa) = 0.$$

Hence

$$\log\left(\varphi_\lambda(t)\right) + \frac{t^2}{2} = \lambda \int_{\mathbb{R}^d \times K} \exp\left(\frac{it}{\sigma\sqrt{\lambda}} h(y,\kappa) \right) - 1 - \frac{it}{\sigma\sqrt{\lambda}} h(y,\kappa) - \dots$$

$$\dots \frac{1}{2}\left(\frac{it}{\sigma\sqrt{\lambda}} h(y,\kappa) \right)^2 - \frac{1}{6}\left(\frac{it}{\sigma\sqrt{\lambda}} h(y,\kappa) \right)^3 dy P_\kappa(d\kappa).$$

Hence applying Lemma 3.1 with $x = \frac{t}{\sigma\sqrt{\lambda}} h(y,\kappa)$ and $n = 4$ we get

$$\left| \log\left(\varphi_\lambda(t)\right) + \frac{t^2}{2} \right| \leq \lambda \int_{\mathbb{R}^d \times K} \frac{1}{24} \left(\frac{t}{\sigma\sqrt{\lambda}} h(y,\kappa) \right)^4 dy P_\kappa(d\kappa) = \frac{t^4 E_4}{24\sigma^4\lambda}.$$

Using the inequality $|e^z - 1| \leq |z|e^{|z|}$ we have

$$\left| \varphi_\lambda(t) - \exp\left(-\frac{t^2}{2} \right) \right| = \left| \exp\left(\log\left(\varphi_\lambda(t)\right) + \frac{t^2}{2} \right) - 1 \right| \exp\left(-\frac{t^2}{2} \right)$$

$$\leq \left| \log\left(\varphi_\lambda(t)\right) + \frac{t^2}{2} \right| \exp\left(\left| \log\left(\varphi_\lambda(t)\right) + \frac{t^2}{2} \right| - \frac{t^2}{2} \right)$$

$$\leq \frac{t^4 E_4}{24\sigma^4\lambda} \exp\left(\left| \log\left(\varphi_\lambda(t)\right) + \frac{t^2}{2} \right| - \frac{t^2}{2} \right).$$

Let us define the constant

$$C = \sqrt{\frac{6\sigma^4}{E_4}}$$

and note $L = L(\lambda) = C\sqrt{\lambda}$. Then for all $|t| \leq L = C\sqrt{\lambda}$ we have

$$\left| \log\left(\varphi_\lambda(t)\right) + \frac{t^2}{2} \right| - \frac{t^2}{2} \leq \frac{t^4 E_4}{24\sigma^4\lambda} - \frac{t^2}{2} \leq L^2 \frac{t^2 E_4}{24\sigma^4\lambda} - \frac{t^2}{2} \leq \frac{t^2}{4} - \frac{t^2}{2} \leq -\frac{t^2}{4}.$$

Hence for all $|t| \leq L = C\sqrt{\lambda}$

$$\left| \varphi_\lambda(t) - \exp\left(-\frac{t^2}{2} \right) \right| \leq \frac{t^4 E_4}{24\sigma^4\lambda} \exp\left(-\frac{t^2}{4} \right). \tag{3.2}$$

From now on we suppose that $L \geq 1$, that is $\lambda \geq \frac{E_4}{6\sigma^4}$. Let us now apply Lemma 3.3 with the interval of integration $[0, L^2]$. We have

$$d_{KS}(Y_\lambda, \mathcal{N}(0,1)) \leq \frac{2}{\pi} \int_0^{L^2} \frac{\left| \varphi_\lambda(t) - \exp\left(-\frac{t^2}{2} \right) \right|}{t} dt + \frac{24}{\pi\sqrt{2\pi}C^2\lambda}.$$

Let us divide in two parts the integral on the right-hand side.

$$\int_0^{L^2} \frac{\left| \varphi_\lambda(t) - \exp\left(-\frac{t^2}{2} \right) \right|}{t} dt = \int_0^{L} \frac{\left| \varphi_\lambda(t) - \exp\left(-\frac{t^2}{2} \right) \right|}{t} dt + \int_L^{L^2} \frac{\left| \varphi_\lambda(t) - \exp\left(-\frac{t^2}{2} \right) \right|}{t} dt.$$

Using Inequality (3.2), we have

$$\int_0^L \frac{\left|\varphi_\lambda(t) - \exp\left(-\frac{t^2}{2}\right)\right|}{t}dt \leq \int_0^L \frac{t^3 E_4}{24\sigma^4\lambda}\exp\left(-\frac{t^2}{4}\right)dt.$$

Now

$$\int_0^L t^3 \exp\left(-\frac{t^2}{4}\right)dt \leq \int_0^{+\infty} t^3 \exp\left(-\frac{t^2}{4}\right)dt = 4.$$

Hence

$$\int_0^L \frac{\left|\varphi_\lambda(t) - \exp\left(-\frac{t^2}{2}\right)\right|}{t}dt \leq \frac{E_4}{6\sigma^4\lambda}.$$

Let us now bound the integral over $[L, L^2]$ (recall that $L = C\sqrt{\lambda}$). First we simply decompose the integral

$$\int_L^{L^2} \frac{\left|\varphi_\lambda(t) - \exp\left(-\frac{t^2}{2}\right)\right|}{t}dt. \leq \int_L^{L^2} \frac{|\varphi_\lambda(t)|}{t}dt + \int_L^{L^2} \frac{1}{t}\exp\left(-\frac{t^2}{2}\right)dt.$$

We have

$$\int_L^{L^2} \frac{1}{t}\exp\left(-\frac{t^2}{2}\right)dt \leq \int_L^{+\infty} \frac{t}{t^2}\exp\left(-\frac{t^2}{2}\right)dt$$

$$\leq \frac{1}{L^2}\int_L^{+\infty} t\exp\left(-\frac{t^2}{2}\right)dt$$

$$\leq \frac{1}{L^2}\exp\left(-\frac{L^2}{2}\right)$$

$$\leq \frac{1}{L^2}.$$

The upper bound of the integral of $\dfrac{|\varphi_\lambda(t)|}{t}$ is more delicate. First remark that we have

$$\varphi_\lambda(t) = \left(\varphi\left(\frac{t}{\sqrt{\lambda}}\right)\right)^\lambda,$$

where φ is the function defined in the proposition (φ is the characteristic function of the shot noise with impulse $\dfrac{h}{\sigma}$ and intensity $\lambda = 1$). Hence, using the change of variable $u = \dfrac{t}{\sqrt{\lambda}}$ we have

$$\int_L^{L^2} \frac{|\varphi_\lambda(t)|}{t}dt = \int_{C\sqrt{\lambda}}^{C^2\lambda} \frac{\left|\varphi\left(\frac{t}{\sqrt{\lambda}}\right)\right|^\lambda}{t}dt = \int_C^{C^2\sqrt{\lambda}} \frac{|\varphi(u)|^\lambda}{u}du.$$

Introducing $q = \sup\limits_{t\in[C,+\infty[} |\varphi(t)| \leq 1$, we have

$$\int_C^{C^2\sqrt{\lambda}} \frac{|\varphi(u)|^\lambda}{u}du \leq q^\lambda \int_C^{C^2\sqrt{\lambda}} \frac{1}{u}du = q^\lambda \ln\left(C\sqrt{\lambda}\right) = \frac{1}{2}q^\lambda \ln\left(C^2\lambda\right).$$

Eventually adding all the established upper bounds and replacing L by its expression we obtain that for all $\lambda \geq \frac{E_4}{6\sigma^4}$

$$d_{KS}(Y_\lambda, \mathcal{N}(0,1)) \leq \underbrace{\left(\frac{2}{3\pi} + \frac{4}{\pi\sqrt{2\pi}}\right)}_{\leq 0.721} \frac{E_4}{\sigma^4} \frac{1}{\lambda} + \frac{1}{\pi} \ln\left(\frac{6\sigma^4}{E_4}\lambda\right) q^\lambda.$$

$\square$

Lemma 3.4 above only applies if the shot noise has a null third order moment and is only interesting if the supremum q is less than 1. However, as the next proposition shows, given any Poisson shot noise the impulse function of which has finite moments up to order $k = 4$, one can easily derive another shot noise process converging to the same Gaussian process and satisfying all these technical conditions. The new shot noise process is simply obtained by multiplying each random impulses $h(\cdot, \kappa_j)$ by some random weight w_j which follows some symmetric distribution. In short, multiply the impulses by random weights permits to ensure the convergence rate of order one towards the targeted Gaussian random field. Hence, in most cases, multiply the impulses by random weights accelerates the normal convergence of shot noise processes.

As above consider a shot noise f_λ with Poisson point process Π_λ of intensity $\lambda \mathcal{L}^d \otimes P_\kappa$ and impulse function h. Let P_w be a probability distribution over $\mathbb{R}$. Let us define

$$f_\lambda^w(x) = \sum_{(x_i, \kappa_i, w_i) \in \Pi_\lambda^w} w_i h(x - x_i, \kappa_i)$$

the corresponding randomly weighted shot noise with weight distribution P_w, that is the shot noise with Poisson process $\Pi_\lambda^w \subset \mathbb{R}^d \times K \times \mathbb{R}$ of intensity $\lambda \mathcal{L}^d \otimes P_\kappa \otimes P_w$ and impulse function $h^w : (y, \kappa, w) \mapsto w h(y, \kappa)$.

Proposition 3.3 (Normal convergence rate for randomly weighted shot noises)**.** *Suppose that the measurable function $h : \mathbb{R}^d \times K \to \mathbb{R}$ satisfies*

$$\int_{\mathbb{R}^d \times K} |h(y, \kappa)|^k \, dy P_\kappa(d\kappa) < +\infty$$

for $k = 1$, $k = 2$, $k = 3$, and $k = 4$, and note

$$\sigma^2 = \int_{\mathbb{R}^d \times K} h(y, \kappa)^2 dy P_\kappa(d\kappa) \quad and \quad E_4 = \int_{\mathbb{R}^d \times K} h(y, \kappa)^4 dy P_\kappa(d\kappa).$$

Suppose also that the weight distribution P_w has a density and is such that $E(w^4) < +\infty$, $E(w) = E(w^3) = 0$, and $E(w^2) = 1$. Then, as λ tends to $+\infty$, the normalized sequence of r.f. $\left(x \mapsto \frac{f_\lambda^w(x)}{\sqrt{\lambda}}\right)$ converges to the same Gaussian random field as the sequence $\left(x \mapsto \frac{f_\lambda(x) - \mathbb{E}(f)}{\sqrt{\lambda}}\right)$. Besides, for all $x \in \mathbb{R}^d$, the convergence rate of $\left(\frac{f_\lambda^w(x)}{\sigma\sqrt{\lambda}}\right)$ is of order one, that is

$$d_{KS}\left(\frac{f_\lambda^w(x)}{\sigma\sqrt{\lambda}}, \mathcal{N}(0,1)\right) = \underset{\lambda \to +\infty}{\mathcal{O}}\left(\frac{1}{\lambda}\right).$$

Proof. Remark that for $k = 1, \ldots, 4$,

$$E_k^w := \int_{\mathbb{R}^d \times K \times \mathbb{R}} |h^w(y, \kappa, w)|^k \, dy P_\kappa(d\kappa) P_w(dw)$$

$$= E(|w|^k) \int_{\mathbb{R}^d \times K} |h(y, \kappa)|^k \, dy P_\kappa(d\kappa) < +\infty.$$

Besides,

$$\int_{\mathbb{R}^d \times K \times \mathbb{R}} (h^w(y, \kappa, w))^3 \, dy P_\kappa(d\kappa) P_w(dw) = E(w^3) \int_{\mathbb{R}^d \times K} h(y, \kappa)^3 dy P_\kappa(d\kappa) = 0.$$

Hence Lemma 3.4 applies to the shot noise f_λ^w. To conclude the proof it only remains to show that the constant q of Lemma 3.4 is less than one. Here the function φ is

$$\varphi(t) = \exp\left(\int_{\mathbb{R}^d \times K \times \mathbb{R}} \left(e^{i \frac{twh(y,\kappa)}{\sigma}} - 1 \right) dy P_\kappa(d\kappa) P_w(dw) \right),$$

and

$$q = \sup \left\{ |\varphi(t)|, \ t \geq C \right\},$$

where C denotes the constant $\sqrt{\frac{6\sigma^4}{E(w^4) E_4}}$. In what follows we note $\psi(t) = \ln(\varphi(t))$. Since $|\varphi(t)| = \exp(\mathrm{Re}\,(\psi(t)))$, to show that $q < 1$ it is enough to show that

$$\sup \left\{ \mathrm{Re}\,(\psi(t)), \ t \geq C \right\} < 0.$$

As noted by several authors [70, 14], the characteristic function φ_w of the random weights w_j appears naturally in the characteristic function of the randomly weighted shot noise. Indeed, by Fubini's theorem

$$\psi(t) = \int_{\mathbb{R}^d \times K} \left(\varphi_w \left(\frac{th(y, \kappa)}{\sigma} \right) - 1 \right) dy P_\kappa(d\kappa).$$

For all $u > 0$, define

$$M_w(u) = \sup \left\{ |\varphi_w(t)|, \ t \geq u \right\}.$$

By hypothesis P_w has a density, hence by Riemann-Lebesgue lemma (see e.g. [57, Lemma 4 p. 514]),

$$\lim_{t \to +\infty} \varphi_w(t) = 0.$$

By [57, Lemma 4 p. 501], this implies that for all $u > 0$, $M_w(u) < 1$. Let us now bound $\mathrm{Re}\,(\psi(t))$.

$$\mathrm{Re}\,(\psi(t)) = \int_{\mathbb{R}^d \times K} \mathrm{Re}\left(\varphi_w \left(\frac{th(y, \kappa)}{\sigma} \right) - 1 \right) dy P_\kappa(d\kappa)$$

$$\leq \int_{\mathbb{R}^d \times K} -1 + \left| \varphi_w \left(\frac{th(y, \kappa)}{\sigma} \right) \right| dy P_\kappa(d\kappa).$$

Let $u > 0$. Using the bound

$$\left| \varphi_w \left(\frac{th(y, \kappa)}{\sigma} \right) \right| \leq \begin{cases} M_w(u) & \text{if } \left| \frac{th(y,\kappa)}{\sigma} \right| \geq u, \\ 1 & \text{otherwise,} \end{cases}$$

we obtain

$$\operatorname{Re}\left(\psi(t)\right) \leq (-1 + M_w(u))\mathcal{L}^d \otimes P_\kappa\left(\left\{(y,\kappa),\ \ |h(y,\kappa)| \geq \frac{u\sigma}{t}\right\}\right).$$

As a consequence, for all $t \geq C > 0$, we have

$$\operatorname{Re}\left(\psi(t)\right) \leq (-1 + M_w(u))\mathcal{L}^d \otimes P_\kappa\left(\left\{(y,\kappa),\ \ |h(y,\kappa)| \geq \frac{u\sigma}{C}\right\}\right).$$

As u tends to 0, $\mathcal{L}^d \otimes P_\kappa\left(\{(y,\kappa),\ |h(y,\kappa)| \geq \frac{u\sigma}{C}\}\right)$ tends to $+\infty$. Hence there exists some $u > 0$ such that the above term is positive. But then for this value of u,

$$\sup\left\{\operatorname{Re}\left(\psi(t)\right),\ t \geq C\right\} \leq (-1 + M_w(u))\mathcal{L}^d \otimes P_\kappa\left(\left\{(y,\kappa),\ \ |h(y,\kappa)| \geq \frac{u\sigma}{C}\right\}\right) < 0,$$

which concludes the proof. $\qquad\qquad\qquad\qquad\qquad\qquad\qquad\qquad\qquad\qquad\qquad\square$

3.5   Applications to Texture Synthesis

As mentioned in the introduction of this chapter, shot noise models are used in procedural texture synthesis to approximate Gaussian r.f. [102, 146, 96, 95]. In this section we investigate the potential applications of the results of Section 3.4 for controlling the visual convergence of shot noise toward their limit Gaussian texture.

3.5.1   Determining the Value of the Intensity λ

When approximating some Gaussian r.f. by a Poisson shot noise, the problem of determining a good value for the intensity λ is critical. Indeed, on one hand, if there are too few impulses the quality of the texture would be poor (or at least not Gaussian enough), whereas, on the other hand, the more impulses there are the more computation time is needed. Hence choosing the value for the intensity λ is really a trade-off between computation speed and visual quality, as expressed in [96].

   Here we demonstrate with two experiments that the Berry-Esseen bound for Poisson shot noises of Theorem 3.4 can be used to determine a good value for the intensity λ. More precisely, we use the bounds

$$d_{KS}(Y_\lambda, \mathcal{N}(0,1)) \leq \Gamma_{PSN}\frac{E_3}{\sigma^3\sqrt{\lambda}}$$

and $\Gamma_{PSN} \leq 0.3051$ of Theorem 3.4 and Proposition 3.2 to obtain a value for the intensity λ. One issue is to decide which bounding value of $d_{KS}(Y_\lambda, \mathcal{N}(0,1))$ should be required. We chose $d_{KS}(Y_\lambda, \mathcal{N}(0,1)) \leq 2.5\%$ which implies that the probability of the normalized shot noise to be in any given interval is equal to the corresponding probability for the standard normal distribution with a margin of 5%. The corresponding value for λ is thus

$$\lambda_{BE}(2.5\%) := \frac{E_3^2}{\sigma^6}\frac{0.3051^2}{0.025^2}. \qquad\qquad\qquad (3.3)$$

Fig. 3.1 shows four different examples with varying intensity of Poisson shot noises where the impulse function is the indicator of a disc. One observes that for the intensity $\lambda = \lambda_{BE}(2.5\%)$ the individual discs start not to be discriminable. Hence in this example the intensity derived from the Berry-Esseen bound provides the good order of magnitude for the beginning of the "visual convergence" to the limit Gaussian texture.

Fig. 3.2 presents the same experiments but with the isotropic Gabor noise [96]. This shot noise is obtained as the sum of Gabor kernels which all have the same frequency and a random orientation [96]. The corresponding limit Gaussian r.f. is the same as the one associated with the Poisson shot noise of the non random impulse function represented by Fig. 3.2(b) (this function is called isotropic Gabor kernel in [98] where it is shown to be the product between a Gaussian kernel and the Bessel functions J_0). Hence the corresponding Gaussian r.f. is easily simulated on a grid using the ADSN algorithm (see Chapter 2).

With Fig. 3.2, one observes that the intensity $\lambda = \lambda_{BE}(2.5\%)$ derived from the Berry-Esseen bound provides again a good order of magnitude for the "visual convergence". Contrary to the case of discs, the isotropic Gabor noise texture with ten times less kernels (Fig. 3.2(d)) already have a satisfying quality. Intuitively this might be explained by the fact that in this second case the impulse function is more regular[3]. This example permits to recall that the Berry-Esseen theorem is a "worst case theorem": for some cases of interest, the bound might be a crude overestimation, as suggested by Proposition 3.3.

To conclude our observations, we have shown that the bound provided by the Berry-Esseen theorem for Poisson shot noises can be used to determine the order of magnitude of the intensity λ for which the "visual convergence" to the limit Gaussian texture occurs. This might be used by procedural texture synthesis software relying on shot noise models to automatically compute an interesting range of value for the intensity λ.

3.5.2 Accelerating the Convergence with Random Weights?

Our next experiment is an attempt to use the convergence acceleration procedure suggested by Proposition 3.3, that is, multiplying each impulse by a random weight. However as it will be shown and discussed, the conclusions of this experiment are negative.

Fig. 3.3 shows side by side the four shot noises of Fig. 3.1 and four realizations of the corresponding randomly weighted shot noise with uniformly distributed weights. Contrary to what might have been expected, the "visual convergence" of the randomly weighted sequence is not faster than the one of the original sequence. Even worse, observing the textures 3.3(e) and 3.3(f) for which $\lambda = \lambda_{BE}(2.5\%)$, one

---

[3]It would require further investigation to see if the normal convergence rate is faster when the impulse function is "regular". A first result in this sense is due to Papoulis [119] who showed that the Berry-Esseen bound can be improved when restricting to band-limited impulse functions.

(a) Impulse function: a disc

(b) $\lambda = 0.01\lambda_{BE}(2.5\%)$

(c) $\lambda = 0.1\lambda_{BE}(2.5\%)$

(d) $\lambda = \lambda_{BE}(2.5\%)$

(e) $\lambda = 10\lambda_{BE}(2.5\%)$
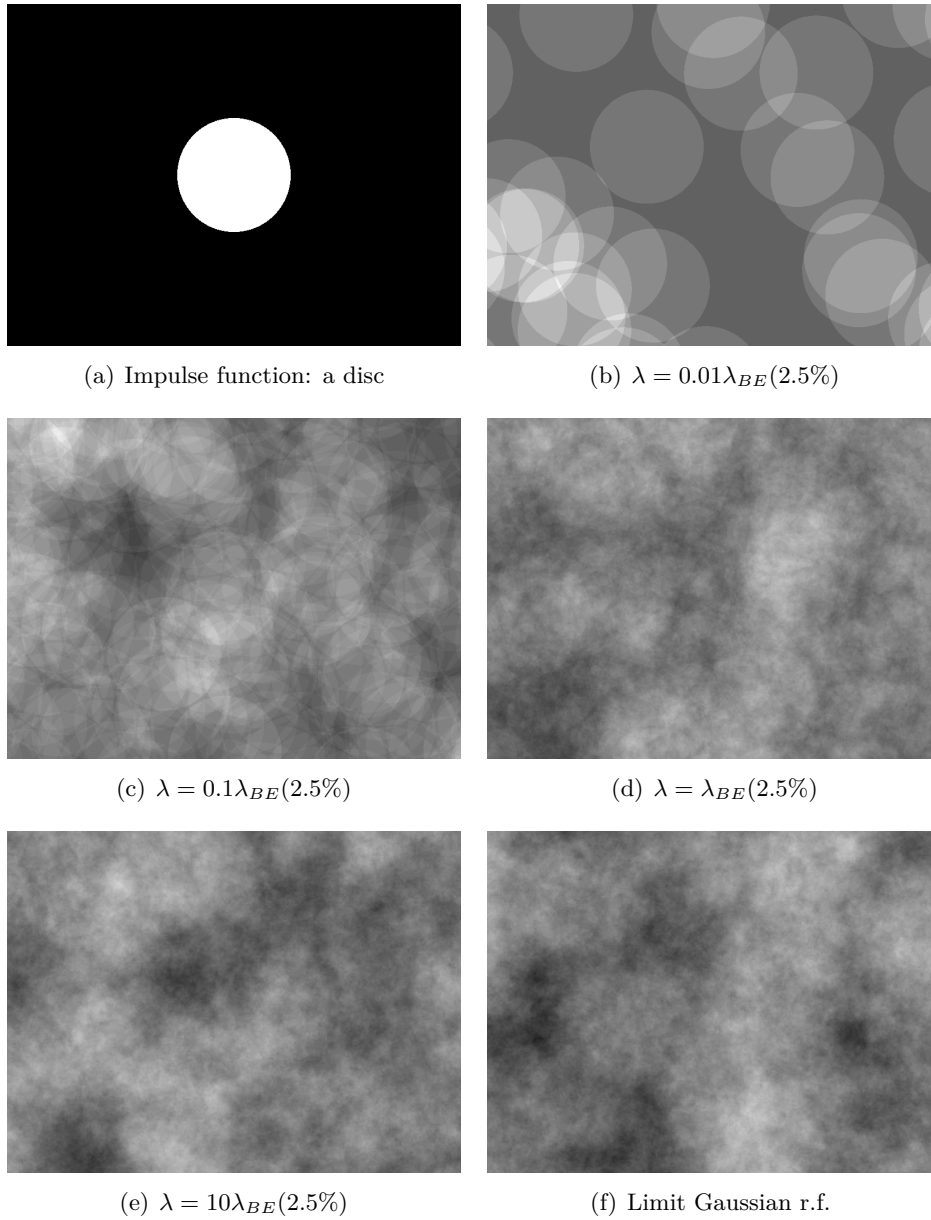
(f) Limit Gaussian r.f.

Figure 3.1: Four different realizations of Poisson shot noises with discs, and their common limit Gaussian r.f. From one realization to the next, the intensity λ is increased by factor 10. One observes that $\lambda = \lambda_{BE}(2.5\%)$ roughly corresponds to the beginning of the "visual convergence" to the limit Gaussian r.f. 3.1(f). Indeed, with ten times less discs, individual discs are visible whereas with ten times more discs the texture looks very similar to the limit Gaussian r.f. 3.1(f).

(a) A Gabor kernel

(b) Isotropic Gabor kernel

(c) $\lambda = 0.01\lambda_{BE}(2.5\%)$

(d) $\lambda = 0.1\lambda_{BE}(2.5\%)$

(e) $\lambda = \lambda_{BE}(2.5\%)$

(f) $\lambda = 10\lambda_{BE}(2.5\%)$
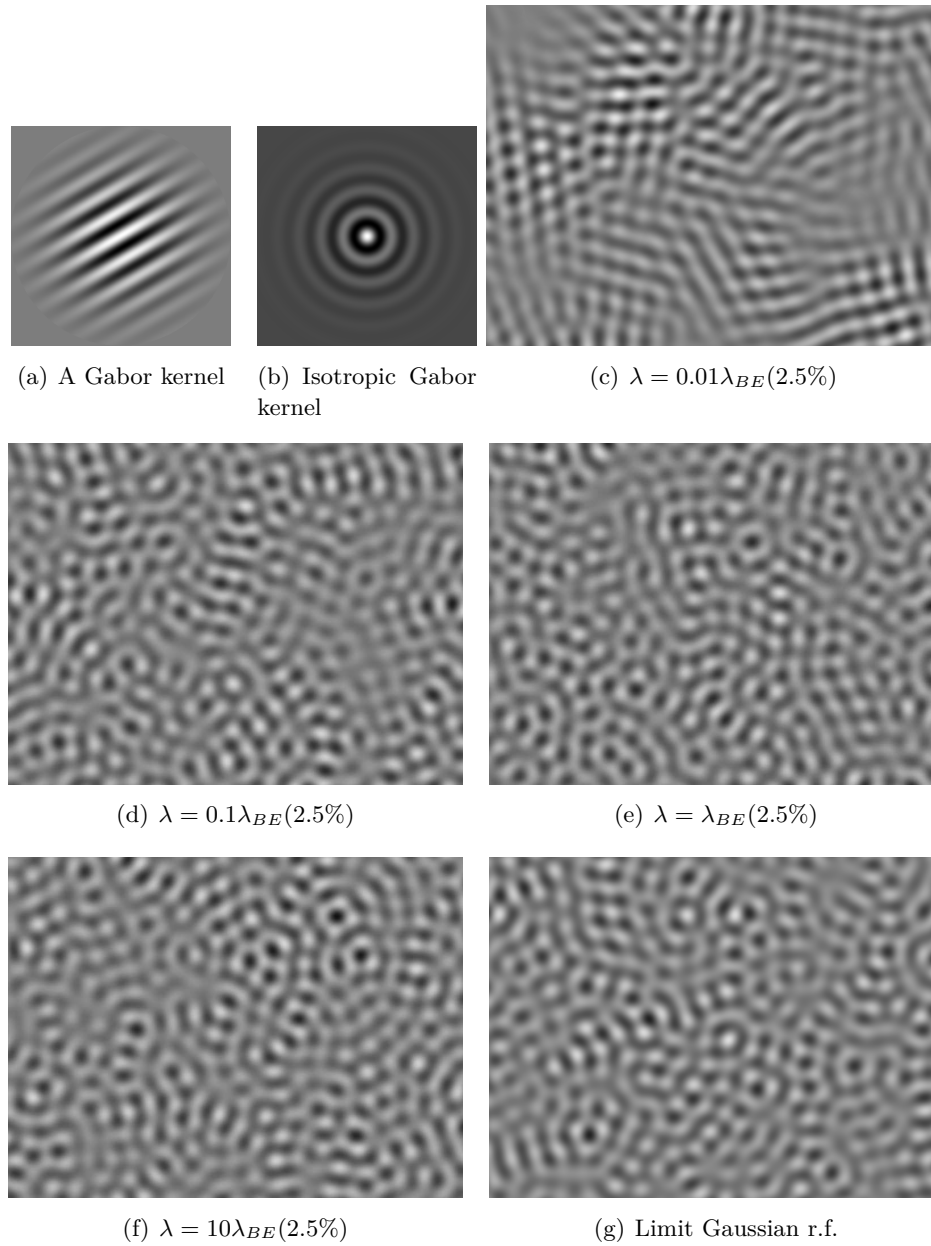
(g) Limit Gaussian r.f.

Figure 3.2: Four different realizations of isotropic Gabor noise [96], and the limit Gaussian r.f. Each Gabor noise is the sum of several Gabor kernels such as 3.2(a) and having a random orientation. The corresponding Gaussian r.f. is the one associated to the isotropic Gabor kernel 3.2(b) (see [98] for more details). As for Fig. 3.1, each Gabor noise has a different intensity λ. In this example, the visual criterion for estimating the quality of the Gaussian approximation is the anisotropy of the texture. Here the Berry-Esseen bound provides an intensity for which the "visual convergence" seems to be reached, but even with ten times less kernels the quality of the texture is satisfying.

observes that the randomly weighted shot noise presents more contrasted discontinuities.

Let us clarify that this last observation is not in contradiction with the previous section, since the bound given by the Berry-Essen theorem is not the same for the randomly weighted shot noise than for the non-weighted one (in Formula (3.3), the moment E_3 should be multiplied by the factor $E(w^3) = 4.5$, which roughly multiplies the intensity $\lambda_{BE}(2.5\%)$ by 20). And as the image 3.3(h) shows, with more impulses the quality of the Gaussian approximation is satisfying.

In conclusion, Fig. 3.3 suggests that the asymptotic normal convergence acceleration of the randomly weighted sequence is of no interest for reaching the "visual convergence". Hence the result of Proposition 3.3 would be interesting in practice only if some high statistical precision is needed. *A priori* this would never be the case in texture synthesis for computer graphics.

3.6 Conclusion and Perspectives

This chapter presented a systematic study of the normal convergence of high intensity Poisson shot noise. A new sharper upper bound of the Berry-Esseen constant for Poisson shot noises have been established. It has also been shown that, under broad additional assumptions, multiply each impulse by a random weight ensures a normal convergence rate of order one. Applications of these results to texture synthesis have also been discussed. In particular it has been demonstrated that the Berry-Esseen bound provides a good order of magnitude for the beginning of the "visual convergence" to the limit Gaussian texture.

The results of this theoretical and experimental study will be applied in Chapter 4 to a recent shot noise model developed for procedural texture synthesis: the Gabor noise model [96].

As mentioned in the introduction, Poisson shot noise are only a peculiar model of the family of shot noise processes. It would certainly be of interest to investigate the possible applications in texture synthesis of other shot noise models. For example, when introducing some scaling laws, non Gaussian limit regimes exist for the Poisson shot noise (see e.g. [15, 88, 16] and the references therein). Another direction to more general models would be to discard the Poisson assumption on the point process [131, 75, 116]. For example the use of cluster point processes [21] might yield to different textures.

To finish let us say that even though the general statistics of Poisson shot noises are well-known, understanding the geometry of these random fields is not an easy problem, even in dimension 1 as shown by the recent paper [14]. In the last part of this thesis, the problem of evaluating the mean total variation per unit volume of Poisson shot noises will be tackled (see Chapter 9).

(a) $\lambda = 0.01\lambda_{BE}(2.5\%)$

(b) $\lambda = 0.01\lambda_{BE}(2.5\%)$, r.w.

(c) $\lambda = 0.1\lambda_{BE}(2.5\%)$

(d) $\lambda = 0.1\lambda_{BE}(2.5\%)$, r.w.

(e) $\lambda = \lambda_{BE}(2.5\%)$

(f) $\lambda = \lambda_{BE}(2.5\%)$, r.w.

(g) $\lambda = 10\lambda_{BE}(2.5\%)$

(h) $\lambda = 10\lambda_{BE}(2.5\%)$, r.w.
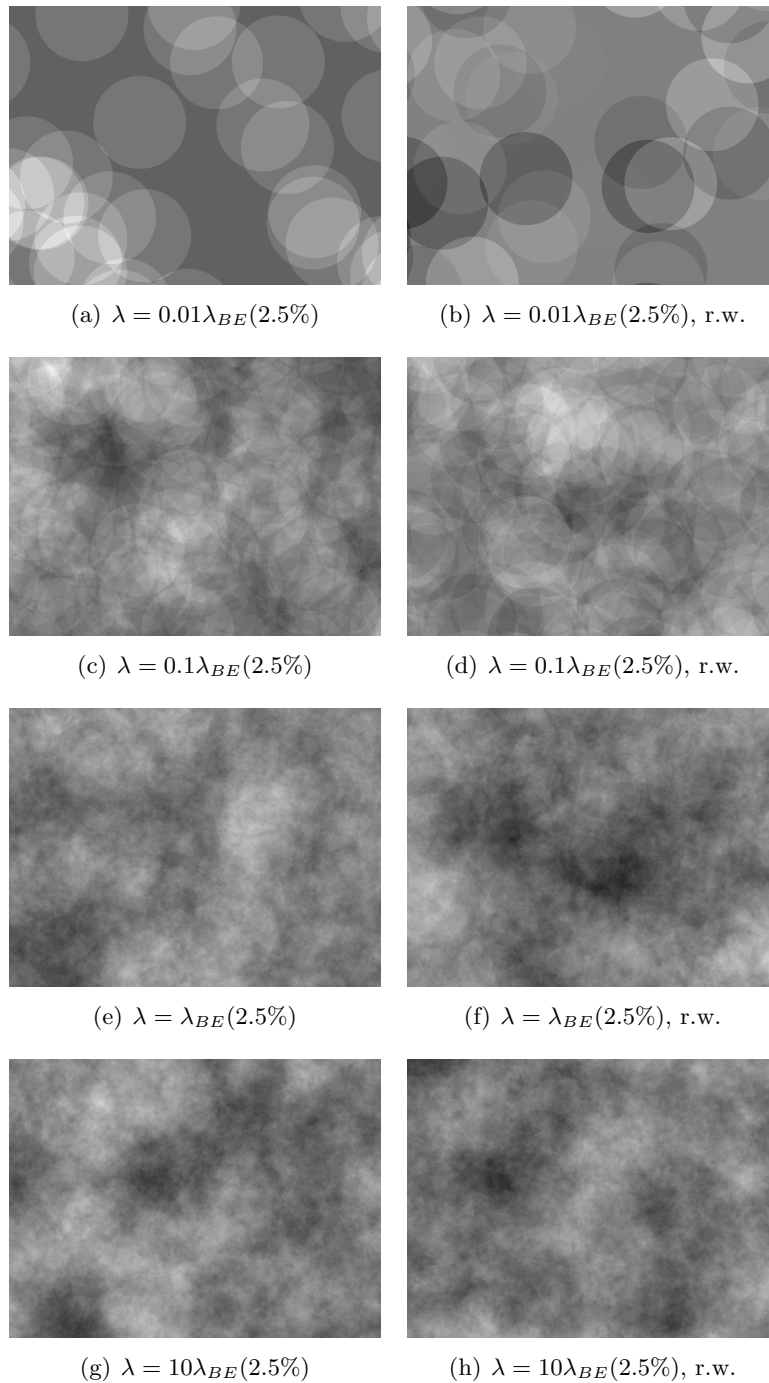
Figure 3.3: Comparison of the four realizations of Poisson shot noises with discs of Fig. 3.1 (left) and their corresponding randomly weighted (r.w.) shot noises (right). The weights are uniformly distributed over $[-\sqrt{3}, \sqrt{3}]$. The "visual convergence" of the randomly weighted sequence is not faster. On the contrary, a detailed observation of the two textures 3.3(e) and 3.3(f) shows that the randomly weighted shot noise presents more contrasted discontinuities.

Gabor Noise by Example

Contents

Abstract: This chapter tackles the problem of procedural texture synthesis from sample using the recent Gabor noise model [96]. Given a texture sample, an automatic solution is provided for determining Gabor noise parameters such that the procedural texture is visually similar to the sample. The developed algorithm relies on three contributions

from Chapter 2 and Chapter 3 of this manuscript: First the Gaussian convergence of the high intensity Gabor noise is controlled by the Berry-Esseen bound derived in Chapter 3, second, the periodic component [113] is used in place of the original texture sample in order to obtain of a discrete Fourier transform without cross structure as in the random phase noise (RPN) algorithm of Chapter 2, and third, as for color RPN, the phase displacements between RGB color channels is enforced in order to ensure color consistency. Numerical results show that the procedural models given by our algorithm produce texture visually similar to the output of the RPN algorithm, and thus it enables to reproduce any texture sample which is well-reproduced by the RPN algorithm.

The work presented in this chapter has not been submitted and requires further developments. In particular we do not present examples of color Gabor noise textures on 3D surface, even though this is the main targeted application of this work. The early results presented here yielded to an ongoing collaboration with three of the authors of the original Gabor noise paper [96], namely A. Lagae, S. Lefebvre and G. Drettakis.

4.1   Introduction

Procedural noise functions are the basic tool in computer graphics to synthesize textures on the surface of 3D objects [95]. Ever since the seminal work of Perlin [123], several procedural noise functions have been proposed: *wavelet noise* [36], *anisotropic noise* [65], and lastly *Gabor noise* [96].

Even though procedural noise functions are used to design textures, manually tuning the parameters of a procedural texture model in order to synthesize a given natural texture requires both a perfect knowledge of the model as well as ad hoc techniques [49]. In entertainment companies, this task is reserved to the so-called *texture artists*. To add to the difficulty of the task, producing different kind of textures usually necessitates to use different procedural algorithms relying on different sets of parameters [49].

Since all the users of procedural texture softwares are not as trained and skilled as professional texture artists, it is of practical importance to provide automatic tools for determining the parameters of a procedural texture model which permit to reproduce a given texture sample. Contrary to image texture synthesis by example (see e.g. [152] and the references of Chapter 2), there is very few literature on procedural texture synthesis by example. The problem of procedural texture synthesis by example has recently been clearly formulated and addressed in [99]. As for the short list of related previous works, let us mention [44] and refer to [99] for a more complete bibliography.

The algorithm developed in [99] determines the parameters of a wavelet noise [36] from a given texture sample. Since wavelet noise is an isotropic procedural noise

function [36], one of the main drawback of this method is that it only deals with isotropic and structureless textures. In this chapter we provide an automatic solution for selecting the parameters of the recent Gabor noise model [96] in order to reproduce a micro-texture from one sample. While working on the content of this chapter, a short paper also addressing Gabor noise texture synthesis by example has been published [64]. Let us clarify however, that the solution proposed in this short paper is completely different from our approach. Indeed, the method developed in [64] simplifies drastically the frequency content of the texture sample, reducing it to a dozen of frequencies. This results in a very compact representation of the procedural texture, which is obtained from a crude and questionable spectral decomposition of the texture sample [64, Section 3]. The price to pay for this compact representation is that the output textures does not really look realistic. On the opposite the method that we develop here does not provide a compact representation of the procedural texture, but is much more faithful to the frequency content of the original sample. As a result, we are able to reproduce complex natural micro-textures.

Let us now describe more precisely the content of this chapter. The first part is a general study of the Gabor noise model. From a theoretical point of view, the Gabor noise model is a Poisson shot noise with random Gabor kernels as impulse functions. Based on the classical results on Poisson shot noises recalled in Chapter 3, we derive general properties of the model. In particular we study the Gaussian convergence of the Gabor noise model and we show how to control the normal convergence of high intensity Gabor noise. It is also observed that the power spectrum of the limit Gaussian r.f. of a Gabor noise is determined by the probability distribution of the frequencies of the Gabor kernels. Note that it is really similar to the classical spectral method of Shinozuka for Gaussian r.f. simulation [139, 140, 100], where sums of cosine waves are used in place of sums of Gabor kernels.

In a second part, the problem of Gabor noise by example for gray-level textures is tackled. Quite naturally we propose to determine the probability distribution of the frequencies of the random Gabor kernels from the discrete spectrum of the texture sample. As for the ADSN and RPN algorithms of Chapter 2, we demonstrate that a practical key point is to replace the texture sample with its periodic component in order to obtain a discrete Fourier transform without cross structure [113].

In the last section, the proposed algorithm for Gabor noise by example is extended to reproduce color texture samples. In procedural texture synthesis, color textures are most of the time obtained in applying a non linear color map to a gray-level procedural noise function, that is in associating an RGB color to a gray-level [123, 49, 97], whereas in the two previous works on procedural texture synthesis by example [99, 64], color textures are synthesized using a PCA decomposition of the color space, similarly to the Heeger-Bergen image texture synthesis algorithm [74]. Here we propose a simpler and more realistic alternative where color Gabor noises are directly defined in the RGB space. Our key insight is to use the observation uncovered in Chapter 2: Fourier phase displacements between color channels are related to the color range of random phase textures.

Results show that the proposed color Gabor noise by example reproduces any texture sample that is also well-reproduced by the RPN algorithm presented in Chapter 2, that is a large class of micro-textures. In fact, given any texture sample, the color Gabor noise by example provides a procedural model visually similar to the RPN associated with the texture sample. Let us precise that this similarity with the results of the RPN algorithm does not reduce the interest of the developed method. Indeed, color Gabor noises are procedural texture models, as recalled in Section 4.3 below, and they potentially could be used to render any 3D surface with the texture they reproduce [96]. Another advantage of the proposed algorithm is that the whole process is linear, consequently enabling to use the intrinsic anti-aliasing of the Gabor noise model [96]. On the opposite, as mentioned in [96], once a non-linear color map has been applied to a gray-level Gabor noise, the intrinsic anti-aliasing scheme of Gabor noise is not rigorously well-funded. Filtering the resulting texture then necessitates additional techniques (e.g. [73]).

The plan of this chapter is as follow. Section 4.2 gives the definition and general properties of the Gabor noise model [97]. In particular, the normal convergence of high intensity Gabor noise models is highlighted. Section 4.3 briefly recalls the procedural evaluation algorithm of Gabor noise model. The algorithm is then described for gray-level texture samples in Section 4.4 and extended to color texture samples in Section 4.5. Finally, Section 4.6 summarizes the results presented in this chapter and precises several guidelines for improving the proposed algorithm.

4.2 The Gabor Noise Model

In all this chapter we work on the two-dimensional space $\mathbb{R}^2$, the targeted application being 2D texture synthesis. However, all the results are valid in the d-dimensional space $\mathbb{R}^d$ for all $d \geq 1$. In particular they are valid for $d = 3$ and therefore provide theoretical insight for solid texture synthesis.

4.2.1 Gabor Kernels

A Gabor kernel is a function $g : \mathbb{R}^2 \to \mathbb{R}$ of the form

$$g(x) = we^{-\pi a^2 \|x\|^2} \cos\left(2\pi \langle x, \omega \rangle + \theta\right),$$

where $w \in \mathbb{R}$, $a > 0$, $\omega \in \mathbb{R}^2$, and $\theta \in (-\pi, \pi]$. The Fourier transform $\hat{g}$ of a Gabor kernel g is

$$\hat{g}(\xi) = \frac{w}{2a^2} \left(e^{-\frac{\pi}{a^2} \|\xi - \omega\|^2} e^{i\theta} + e^{-\frac{\pi}{a^2} \|\xi + \omega\|^2} e^{-i\theta} \right), \ \xi \in \mathbb{R}^2. \tag{4.1}$$

The role of each parameter is the following:

- w is the amplitude or weight of the kernel.

- a^{-1} represents the width of the Gaussian envelope (a is the width of the Gaussian envelopes in the Fourier domain).

- $\omega \in \mathbb{R}^2$ is the frequency of the Gabor kernel.

- θ is the phase of the kernel.

In the following we will consider a Poisson shot noise the impulse functions of which are Gabor kernels with different parameters. The width a will be the same for all the kernels, whereas the other parameters will be chosen randomly. Hence we note

$$g(x; w, \omega, \theta) = w e^{-\pi a^2 \|x\|^2} \cos\left(2\pi \langle x, \omega \rangle + \theta\right).$$

4.2.2 Definition of the Gabor Noise Model

The Gabor noise model of [96] is a peculiar Poisson shot noise with Gabor kernels as impulse functions.

Let $a > 0$ be a real number. Let Π be an independently marked Poisson process[1] $\Pi = \{(x_j, w_j, \omega_j, \theta_j)\} \subset \mathbb{R}^2 \times \mathbb{R} \times \mathbb{R}^2 \times (-\pi, \pi]$. The unmarked Poisson process $\{x_j\} \subset \mathbb{R}^2$ is stationary and has intensity λ. The marks $(w_j, \omega_j, \theta_j)$ are mutually independent and

- $w_j \in \mathbb{R}$ are i.i.d. real r.v. with distribution P_w.

- $\omega_j \in \mathbb{R}^2$ are i.i.d. random points distributed according to a distribution P_ω symmetric with respect to the origin, that is for all Borel set $B \subset \mathbb{R}^2$, $P_\omega(B) = P_\omega(-B)$.

- θ_i are i.i.d. r.v. uniformly distributed over the interval $(-\pi, \pi]$.

For the sake of convenience, and in accordance with the notation of Chapter 3, the mark space $\mathbb{R} \times \mathbb{R}^2 \times (-\pi, \pi]$ will be denoted by K, a mark $(w_j, \omega_j, \theta_j)$ will be sometimes denoted by κ_j, and the mark distribution $P_w \otimes P_\omega \otimes P_\theta$ will be denoted P_κ.

Definition 4.1 (Gabor noise model). *The Gabor noise model associated with the independently marked Poisson process* $\Pi = \{(x_j, w_j, \omega_j, \theta_j)\}$ *is the Poisson shot noise*

$$f(x) = \sum_{(x_j, w_j, \omega_j, \theta_j) \in \Pi} g(x - x_j; w_j, \omega_j, \theta_j),$$

where $g : \mathbb{R}^2 \times K \to \mathbb{R}$ *is the Gabor kernel*

$$g(x; w, \omega, \theta) = w e^{-\pi a^2 \|x\|^2} \cos\left(2\pi \langle x, \omega \rangle + \theta\right).$$

Remark. In the original model of [96] $\theta_j = 0$. As it will be shown in Section 4.5, this new random phase parameter is of capital importance to synthesize color Gabor noise textures since it permits to introduce phase shift displacements between color channels. Another difference with the original model is that we do not impose that

---

[1]Let us remind that Appendix B recalls basic definitions and properties of Poisson point processes.

the r.v. w_j have mean zero. As next proposition shows, this is because the uniform distribution of the random phases θ_j already ensures that the Gabor noise model has mean zero (see Proposition 4.1 below).

4.2.3 Power Spectrum and Covariance of the Gabor Noise

Since the Gabor noise is a peculiar Poisson shot noise, Proposition 3.1 gives its expectation, covariance function and power spectrum.

Proposition 4.1 (Power spectrum and covariance of the Gabor noise). *Suppose that the random weights w_i are r.v. with finite variance, that is $E(w^2) < +\infty$. Then the Gabor noise f is a well-defined stationary random field, f has finite variance, and $\mathbb{E}(f) = 0$. The power spectrum S of f is equal to*

$$S(\xi) = \lambda \frac{E(w^2)}{2a^4} \int_{\mathbb{R}^2} e^{-\frac{2\pi}{a^2}\|\xi-\omega\|^2} P_\omega(d\omega), \ \xi \in \mathbb{R}^2.$$

The covariance function C of f is given by

$$C(\tau) = \lambda \frac{E(w^2)}{4a^2} \int_{\mathbb{R}^2} e^{-\frac{\pi a^2}{2}\|\tau\|^2} \cos\left(2\pi\langle\tau,\omega\rangle\right) P_\omega(d\omega), \ \tau \in \mathbb{R}^2.$$

In particular the variance of f is

$$C(0) = \lambda \frac{\mathbb{E}\left(w^2\right)}{4a^2}.$$

Proof. For $k = 1$ and $k = 2$,

$$\int_{\mathbb{R}^2 \times K} |g(x;\kappa)|^k \, dx P_\kappa(d\kappa) = \int_{\mathbb{R}^2 \times K} \left|we^{-\pi a^2\|x\|^2} \cos\left(2\pi\langle x,\omega\rangle + \theta\right)\right|^k dx P_\kappa(d(w,\omega,\theta))$$

$$\leq \int_{\mathbb{R}^2 \times K} |w|^k e^{-k\pi a^2\|x\|^2} dx P_w(dw)$$

$$\leq \frac{1}{ka^2} E\left(|w|^k\right).$$

Hence as soon as $E\left(w^2\right) < +\infty$ the Gabor noise satisfies the hypothesis of Proposition 3.1. Hence f is a well-defined stationary random field, and integrating with respect to θ,

$$\mathbb{E}(f) = \int_{\mathbb{R}^2 \times K} we^{-\pi a^2\|x\|^2} \cos\left(2\pi\langle x,\omega\rangle + \theta\right) dx P_\kappa(d\kappa) = 0.$$

By Proposition 3.1,

$$S(\xi) = \lambda E\left(|\hat{g}(\xi,\kappa)|^2\right).$$

By the expression of the Fourier transform $\hat{g}$ (see Equation (4.1)),

$$|\hat{g}(\xi;w,\omega,\theta)|^2 = \frac{w^2}{4a^4} \left|e^{-\frac{\pi}{a^2}\|\xi-\omega\|^2}e^{i\theta} + e^{-\frac{\pi}{a^2}\|\xi+\omega\|^2}e^{-i\theta}\right|^2.$$

Integrating with respect to w gives a factor $E(w^2)$. Using the formula $\left| r_1 e^{i\theta} + r_2 e^{-i\theta} \right|^2 = r_1^2 + r_2^2 + 2r_1 r_2 \cos(2\theta)$,

$$\frac{1}{2\pi} \int_{-\pi}^{\pi} \left| e^{-\frac{\pi}{a^2}\|\xi-\omega\|^2} e^{i\theta} + e^{-\frac{\pi}{a^2}\|\xi+\omega\|^2} e^{-i\theta} \right|^2 d\theta = e^{-\frac{2\pi}{a^2}\|\xi-\omega\|^2} + e^{-\frac{2\pi}{a^2}\|\xi+\omega\|^2}.$$

Hence

$$S(\xi) = \lambda \frac{E(w^2)}{4a^4} \int_{\mathbb{R}^2} \left(e^{-\frac{2\pi}{a^2}\|\xi-\omega\|^2} + e^{-\frac{2\pi}{a^2}\|\xi+\omega\|^2} \right) P_\omega(d\omega).$$

Finally, by symmetry of the distribution P_ω

$$\int_{\mathbb{R}^2} e^{-\frac{2\pi}{a^2}\|\xi+\omega\|^2} P_\omega(d\omega) = \int_{\mathbb{R}^2} e^{-\frac{2\pi}{a^2}\|\xi-\omega\|^2} P_\omega(d\omega),$$

and thus

$$S(\xi) = \lambda \frac{E(w^2)}{2a^4} \int_{\mathbb{R}^2} e^{-\frac{2\pi}{a^2}\|\xi-\omega\|^2} P_\omega(d\omega).$$

Fubini's theorem shows that the integral of the power spectrum S is finite:

$$\int_{\mathbb{R}^2} S(\xi) d\xi = \lambda \frac{E(w^2)}{2a^4} \int_{\mathbb{R}^2} \left(\int_{\mathbb{R}^2} e^{-\frac{2\pi}{a^2}\|\xi-\omega\|^2} d\xi \right) P_\omega(d\omega)$$

$$= \lambda \frac{E(w^2)}{2a^4} \int_{\mathbb{R}^2} \frac{a^2}{2} P_\omega(d\omega)$$

$$= \lambda \frac{E(w^2)}{4a^2} < +\infty.$$

Hence the covariance function C is integrable as well as its Fourier transform S. The inversion theorem (see e.g. [62]) ensures that C is equal to the inverse Fourier transform of S,

$$C(\tau) = \int_{\mathbb{R}^2} S(\xi) e^{2i\pi\langle\tau,\xi\rangle} d\tau$$

$$= \lambda \frac{E(w^2)}{4a^4} \int_{\mathbb{R}^2} \left(\int_{\mathbb{R}^2} \left(e^{-\frac{2\pi}{a^2}\|\xi-\omega\|^2} + e^{-\frac{2\pi}{a^2}\|\xi+\omega\|^2} \right) e^{2i\pi\langle\tau,\xi\rangle} d\xi \right) P_\omega(d\omega)$$

$$= \lambda \frac{E(w^2)}{4a^4} \int_{\mathbb{R}^2} \frac{a^2}{2} e^{-\frac{\pi a^2}{2}\|\tau\|^2} 2\cos\left(2\pi\langle\tau,\omega\rangle\right) P_\omega(d\omega)$$

$$= \lambda \frac{E(w^2)}{4a^2} \int_{\mathbb{R}^2} e^{-\frac{\pi a^2}{2}\|\tau\|^2} \cos\left(2\pi\langle\tau,\omega\rangle\right) P_\omega(d\omega).$$

$\square$

Remark that the Power spectrum of f

$$S(\xi) = \lambda \frac{E(w^2)}{2a^4} \int_{\mathbb{R}^2} e^{-\frac{2\pi}{a^2}\|\xi-\omega\|^2} P_\omega(d\omega)$$

is equal to the variance $C(0)$ times the convolution between the two probability distributions P_ω and $\frac{2}{a^2} e^{-\frac{2\pi}{a^2}\|\xi\|^2} d\xi$. Hence the power spectrum of the Gabor noise f is a kind of regularized version of the probability distribution P_ω. Note that in the classical spectral method of Shinozuka [139, 140, 100], where cosine waves are used in place of Gabor kernels, there is a strict equality between the power spectrum of the simulated random field and the frequency distribution.

4.2.4 Normal Convergence of the Gabor Noise Model

In this section we consider a family of Gabor noise models $(f_\lambda)_{\lambda>0}$ which share the same parameters (*i.e.* having same kernel width a and same distributions P_w and P_ω) except for their intensity λ. The next proposition shows that the normalized Gabor noise models $\frac{f_\lambda}{\sqrt{\lambda}}$ converges in distribution towards a Gaussian random field.

Proposition 4.2 (Normal convergence of Gabor noise models)**.** *If $E(w^2) < +\infty$ then as λ tends to $+\infty$ the normalized sequence of Gabor noises $\left(\frac{f_\lambda}{\sqrt{\lambda}}\right)_{\lambda>0}$ converges in distribution towards a stationary Gaussian random field having null expectation and power spectrum S given by*

$$S(\xi) = \frac{E(w^2)}{2a^4} \int_{\mathbb{R}^2} e^{-\frac{2\pi}{a^2}\|\xi-\omega\|^2} P_\omega(d\omega).$$

Proof. Apply Theorem 3.1 to the considered shot noise. $\qquad\square$

As it has been discussed in Chapter 3, the upper bound given by the Berry-Esseen theorem provides the good order of magnitude for the beginning of the "visual convergence" of Poisson shot noise toward the limit Gaussian texture. The next proposition makes explicit the Berry-Esseen bound in the case of Gabor noise.

Proposition 4.3 (Berry-Esseen bound for Gabor noise)**.** *Suppose that $E\left(|w|^3\right) < +\infty$. Then for all $y \in \mathbb{R}^2$,*

$$d_{KS}\left(\frac{f_\lambda(y)}{\sqrt{\lambda}}, \mathcal{N}(0,1)\right) \leq \Gamma_{PSN} \frac{32 E\left(|w|^3\right)}{9\pi E\left(w^2\right)^{\frac{3}{2}}} \frac{a}{\sqrt{\lambda}},$$

where $\Gamma_{PSN} \leq 0.3051$.

We first compute the integral of the powers of Gabor kernels.

Lemma 4.1. *For any $k \in \mathbb{N}$,*

$$E_k := \int_{\mathbb{R}^2 \times K} |g(y; w, \omega, \theta)|^k \, dy P_\kappa(d(w, \omega, \theta)) = \frac{2}{\pi}\left(\int_0^{\frac{\pi}{2}} \cos^k \theta d\theta\right) \frac{E\left(|w|^k\right)}{ka^2}.$$

In particular, $E_2 = \frac{1}{4}\frac{E\left(w^2\right)}{a^2}$ and $E_3 = \frac{4}{9\pi}\frac{E\left(|w|^3\right)}{a^2}$.

Proof.

$$E_k = \int_{\mathbb{R}^2 \times K} |w|^k e^{-k\pi a^2 \|y\|^2} |\cos\left(2\pi\langle y, \omega\rangle + \theta\right)|^k \, dy P_\kappa(d(w, \omega, \theta)).$$

Integrating with respect to w gives a factor $E\left(|w|^k\right)$. A simple change of variable shows that

$$\frac{1}{2\pi}\int_{-\pi}^{\pi} |\cos\left(2\pi\langle y, \omega\rangle + \theta\right)|^k \, d\theta = \frac{2}{\pi}\int_0^{\frac{\pi}{2}} \cos^k \theta d\theta.$$

As a consequence, the integration with respect to ω becomes trivial. Hence

$$E_k = \frac{2}{\pi} \left(\int_0^{\frac{\pi}{2}} \cos^k \theta d\theta \right) E\left(|w|^k\right) \int_{\mathbb{R}^2} e^{-k\pi a^2 \|y\|^2} dy = \frac{2}{\pi} \left(\int_0^{\frac{\pi}{2}} \cos^k \theta d\theta \right) \frac{E\left(|w|^k\right)}{ka^2}.$$

Using Wallis cosine formulas we obtain the algebraic expressions of E_k. □

Proof of Proposition 4.3. Apply the Berry-Esseen theorem for Poisson shot noises (see Theorem 3.4) to the Gabor noise model. Recall that $\Gamma_{PSN} \leq 0.3051$ by Proposition 3.2. □

As in Section 3.5.1, we derive the following intensity $\lambda_{BE}(2.5\%)$ from Proposition 4.3:

$$\lambda_{BE}(2.5\%) = \frac{1}{0.025^2} \left(\Gamma_{PSN} \frac{32E\left(|w|^3\right)}{9\pi E\left(w^2\right)^{\frac{3}{2}}} a \right)^2 \simeq 190 \frac{E\left(|w|^3\right)^2}{E\left(w^2\right)^3} a^2. \qquad (4.2)$$

As it will be justified in Section 4.4, the random weights w will typically be chosen to be constant. Hence the ratio of the moments of w would cancel out in the above formula. Besides, in practice, the Gabor kernels will be truncated to 0 outside the disc of radius a^{-1}, as in the original Gabor noise paper [96]. With this approximation, the mean number of Gabor kernels influencing the value of $f_\lambda(y)$ is $\lambda 2\pi a^{-2}$. For the above value $\lambda_{BE}(2.5\%)$ this gives a mean number of approximately 1200 Gabor kernels of influence per point.

The normal convergence of a Gabor noise model has already been illustrated with Fig. 3.2 in Chapter 3. Fig. 4.1 presents another example.

4.3   Procedural Evaluation of a Gabor Noise Model

The Gabor noise model is a *procedural noise function* [49, 95], that is a random function described by a computational process and not by some data structure. An ideal procedural noise function should fulfill several requirements such as being *compact*, i.e. requiring little memory, being defined on the whole plan, or also being non periodic [95]. In practice, one of the more important requirements for a procedural noise function is to be *randomly accessible*, that is that "it can be evaluated in a constant time, regardless of the location of the point of evaluation, and regardless of previous evaluations" [95, Section 2.3].

In this section we recall in detail how a given Gabor noise model is evaluated at any point $y \in \mathbb{R}^2$. The main reference of this section is the original paper [96] and no new result is presented here.

We suppose that a Gabor noise model is given and that procedures to simulate r.v. following the distributions P_w and P_ω from a pseudo random number generator are known.

(a) $\lambda = 0.01\lambda_{BE}(2.5\%)$ (b) $\lambda = 0.1\lambda_{BE}(2.5\%)$

(c) $\lambda = \lambda_{BE}(2.5\%)$ (d) $\lambda = 10\lambda_{BE}(2.5\%)$
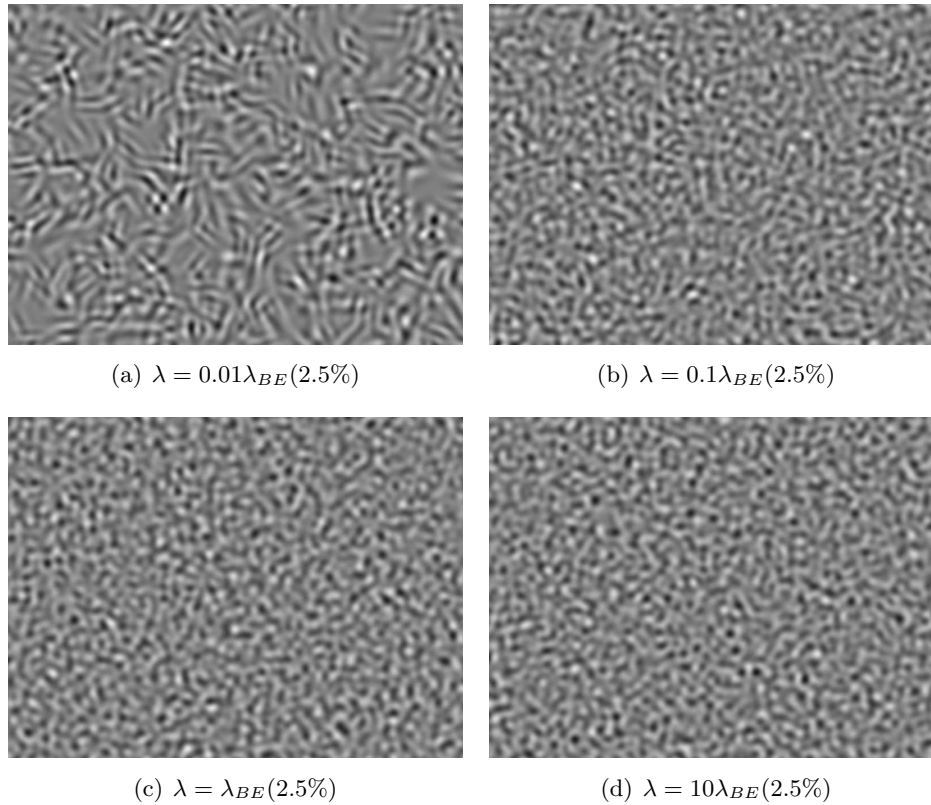
Figure 4.1: Four different realizations of Gabor noises with various intensities λ. The random weight w_j are constant to 1 and the frequencies are uniformly distributed over a thick ring of the spectral plane. From one realization to the next, the intensity λ is increased by a factor 10. For $\lambda = 0.01\lambda_{BE}(2.5\%)$, individual Gabor kernels are visible, for $\lambda = 0.1\lambda_{BE}(2.5\%)$ individual Gabor kernels are no more visible but the texture is locally less isotropic than the following realizations. The case $\lambda = \lambda_{BE}(2.5\%)$ corresponds to the beginning of the "visual convergence": there is no difference with the next realization for which $\lambda = 10\lambda_{BE}(2.5\%)$.

4.3.1 Truncation of the Gabor Kernels

Theoretically, since the support of any Gabor kernel is the whole space $\mathbb{R}^2$, the value $f(y)$ of a Gabor noise at any point $y \in \mathbb{R}^2$ is a sum of infinitely many Gabor kernels. In practice the Gaussian envelope of each Gabor kernel is truncated so that the kernels have compact support. In [96], the considered compact support is the disc $B(0, a^{-1})$ of radius a^{-1}. At the boundary of this disc the Gaussian envelope equals $e^{-\pi} \simeq 0,043$ which is considered negligible.

A precise analysis of the error induced by this truncation is provided in the technical report [98, Section 4.1]. The authors establish a formula relating the truncation radius r_t and the corresponding relative noise error. In all the experiments of this chapter, we simply used $r_t = 1/a$ as in the original paper [96].

4.3.2 Grid Partition and Pseudo-Random Number Generator Initialization

Thanks to the truncation of the Gabor kernels, the simulation of the r.v. $f(y)$ becomes easy: It consists in simulating the finite number of points $\Pi = \{(x_j; w_j, \omega_j, \theta_j)\}$ such that x_j is in the disc $B(y, a^{-1})$ and add all the corresponding Gabor kernels. Up to the error induced by the kernel truncation, this sketched algorithm would provide a simulation of $f(y)$. However a major difficulty remains: once $f(y)$ is computed, how can we simulate the value $f(z)$ at another point $z \in \mathbb{R}^2$ of the same realization f of the Gabor noise model?

The underlying problem is to ensure that the simulated points $\{(x_j; w_j, \omega_j, \theta_j)\}$ are from the same realization of Π when rerunning the algorithm for another point z close to y. In general, in order to obtain twice the same random objects with an algorithm, one needs to call the same pseudo-random number generator (PRNG) with the same seed s. We recall that for any integer s, a PRNG provides a sequence $(u_n(s))_{n \in \mathbb{N}}$ of pseudo-random numbers uniformly distributed in $[0, 1]$. In addition, here it is required that the restriction on any disc $B(y, a^{-1})$ of the realization of the Poisson process Π can be simulated at will.

To fulfill this requirement, a classical solution [49, 96] consists in partitioning the plane $\mathbb{R}^2$ in square cells with corners in $a^{-1}\mathbb{Z}^2$, that is

$$\mathbb{R}^2 = \bigcup_{(k,l) \in \mathbb{Z}^2} C_{k,l},$$

where $C_{k,l} = [a^{-1}k, a^{-1}(k+1)) \times [a^{-1}l, a^{-1}(l+1))$. This partition is referred to as a *grid*. Given a grid, one associates a seed $s(k, l)$ to each cell $C_{k,l}$ using an injective map $s : \mathbb{Z}^2 \to \mathbb{N}$ (see [96, Section 4] for details). To simulate the restriction of Π to the cell $C_{k,l}$, one initializes a PRNG with the cell seed $s(k, l)$ and then draw the points and their marks. There are two key points here: first for any cell the same seed is used to draw the points, ensuring that the same random points $\{(x_j; w_j, \omega_j, \theta_j)\}$ will be drawn at each evaluation, second, each cell has a different seed, ensuring that the set of points in each cell is different.

To finish remark that any point $y \in \mathbb{R}^2$ belongs to a unique cell $C(y) := C_{k,l}$ of the grid, and the disc $B(y, a^{-1})$ is contained in the union of $C(y)$ and the eight neighboring cells of $C(y)$. This observation is at the center of the procedural evaluation algorithm detailed in the next section.

4.3.3 Procedural Evaluation Algorithm

Below is the detailed algorithm for the evaluation of a Gabor noise model. As already mentioned, we suppose that procedures to simulate r.v. following the distributions P_w and P_ω from the PRNG are known.

The input of the algorithm is any point $y \in \mathbb{R}^2$.

1. Initialization: $f(y) \leftarrow 0$.

2. Determination of the set $\mathcal{C}$ of cells of interest:

    (a) $\mathcal{C} \leftarrow \{C(y)\}$ where $C(y)$ is the cell containing y.

    (b) For each cell C of the 8 neighboring cells of $C(y)$: if $C \cap B(y, a^{-1}) \neq \emptyset$, $\mathcal{C} \leftarrow \mathcal{C} \cup \{C\}$.

3. Iterative sums of Gabor kernels: for each cell $C \in \mathcal{C}$:

    (a) Initialize the PRNG with the seed $s(k,l)$ of the cell $C = C_{k,l}$.

    (b) Draw $N \sim \mathcal{P}(\lambda a^{-2})$ the number of points of Π in C.

    (c) For $j = 1$ to N:

        i. Draw a point x_j uniformly distributed in C.
        ii. Draw a random weight $w_j \sim P_w$.
        iii. Draw a random phase $\theta_j \sim Unif(-\pi, \pi)$.
        iv. Draw a random frequency $\omega_j \sim P_\omega$.
        v. Add the truncated Gabor kernel: if $|x_j - y| \leq a^{-1}$,

$$f(y) \leftarrow f(y) + g(y - x_j; w_j, \omega_j, \theta_j).$$

4. Return $f(y)$.

Thanks to the superposition property of independent Poisson processes (see e.g. [11, p. 18]), if f_1 and f_2 are two independent outcomes of the same Gabor noise model with respective intensities λ_1 and λ_2, then the sum $f = f_1 + f_2$ is an outcome of the considered Gabor noise model with intensity $\lambda = \lambda_1 + \lambda_2$. This property can be used to ensure the convergence towards the Gaussian distribution: if the output texture quality is not satisfying due to a poor intensity, it can still be used as an initialization for the simulation of a Gabor noise with higher intensity.

4.4 Texture Synthesis from Samples Using Gabor Noise

4.4.1 Problem Statement

As mentioned in the introduction, the goal of this chapter is to tackle the following problem: given a discrete texture sample h of size $M \times N$ can we find adapted Gabor noise parameters such that the Gabor noise looks like the sample texture h?

To begin let us note that the problem is ill-posed. First, as always the notion of texture sample is not clear. Second, we are trying to construct a random function defined on the whole space $\mathbb{R}^2$ from just one discrete sample $h = \{h(m,n) | (m,n) \in [\![0, M-1]\!] \times [\![0, N-1]\!]\}$. Nevertheless as it will be shown, we can give a solution to this problem when restricting to samples of random phase textures as defined in Chapter 2.

In this section, in accordance with Definition 4.1, we only consider the case of a gray-level Gabor noise. The proposed method will then be extended to color images in Section 4.5.

Hence given a discrete gray-valued texture image

$$h = \{h(m,n), \ (m,n) \in [\![0, M-1]\!] \times [\![0, N-1]\!]\}$$

we want to derive Gabor noise parameters such that the normalized Gabor noise

$$\text{mean}(h) + \frac{f}{\sqrt{\lambda}}$$

is visually similar to the original texture sample h. Recall that the parameters of the Gabor noise model are:

- The kernel intensity λ.

- The kernel width a.

- The probability distribution of the weights P_w.

- The probability distribution of the frequencies P_ω.

We first suppose that the parameter a is given (the influence of this parameter will be illustrated in Section 4.5.4). Besides, given the parameters a and P_w and using Equation (4.2), the intensity λ will be always chosen high enough so that the Gabor noise is close to its associated limit Gaussian texture.

In the following of this section we tackle the two remaining problems: determine P_w and P_ω from the discrete gray-valued texture h. In the first place however, let us clarify the range of textures which might be reproduced by high intensity Gabor noise.

<div align="center">

(a) $\lambda = 0.01\lambda_{BE}(2.5\%)$ (b) Associated RPN

</div>

<div align="center">

(c) $\lambda = \lambda_{BE}(2.5\%)$ (d) Associated RPN

</div>
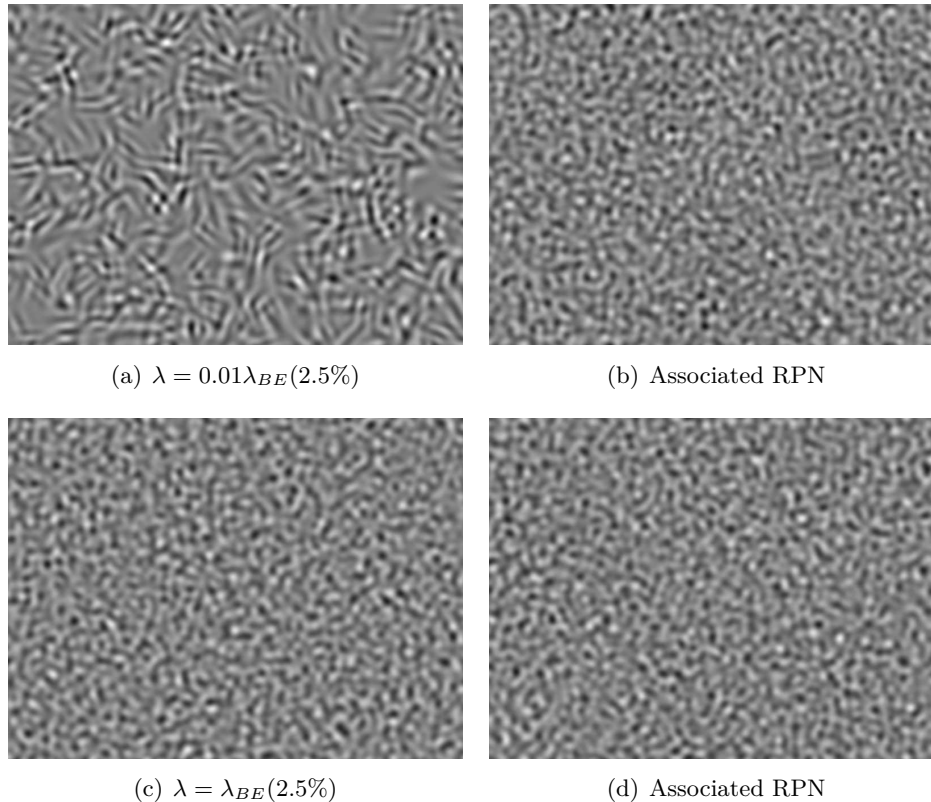
Figure 4.2:   Two Gabor noise textures of Fig. 4.1 and a realization of their associated RPN (see Chapter 2). Observe that both the RPN textures are visually similar to the high intensity Gabor noise. Hence high intensity Gabor noise textures are random phase textures.

4.4.2   High Intensity Gabor Noise Textures are Random Phase Textures

As all the procedural noise models, a Gabor noise is an approximation of a Gaussian random field [95]. By Proposition 4.2, the approximation is better when the intensity of kernels λ is high. Since Gaussian random fields are uniquely determined by their power spectra, high density Gabor noise textures sharing the same parameters are visually similar (see bottom row of Fig. 4.1).

In Chapter 2 it has been demonstrated that Gaussian textures could not be discriminated from their associated random phase noise[2] (RPN). As illustrated by Fig 4.2, discrete images obtained in properly sampling high density Gabor noise textures are visually similar to their associated RPN, whereas this is not the case for low density Gabor noise. One concludes that high intensity Gabor noise textures are random phase textures.

---

[2]We recall that the RPN algorithm consists in randomizing the phase of the discrete Fourier transform (DFT) of the discrete input image.

Therefore if a sample texture is reproducible by a high intensity Gabor noise model, it is also reproducible by the RPN algorithm. This observation suggests that given any sample image h, the best result that one can reach is to synthesize a Gabor noise texture visually similar to the RPN texture associated with the sample h (see Chapter 2). One might think that this remark would reduce the interest of Gabor noise by example. However this is not the case since, as mentioned in the introduction, RPN and Gabor noise belong to two distinct classes of algorithms: the first is an image texture synthesis algorithm whereas the second one is a procedural texture synthesis algorithm. Besides, Gabor noise enables the synthesis of a texture directly on a 3D surface [96] whereas RPN only produces flat texture images.

4.4.3 Distribution of the Random Weights

In the original paper [96], the distribution P_w of the weights w_j has been fixed to a uniform distribution over $[-1, 1]$. In fact the uniform distribution was chosen so that the Gabor noise f was centered. Here, thanks to the use of the uniformly distributed random phases θ_j, $\mathbb{E}(f) = 0$ is ensured for any choice of distribution P_w.

As suggested by the experiments of Section 3.5.2 in the previous chapter, despite multiplying the impulses of a Poisson shot noise by a random weight does not generally improve the visual convergence to the limit Gaussian texture. Fig. 4.3 illustrates that this conclusion is also valid for the Gabor noise model. Hence, in order to save calls to the random number generator, the random weights w_j are chosen to be constant to a value $w > 0$ (But any distribution P_w such that $E\left(|w|^3\right) < +\infty$ could be used).

It remains to determine the constant value w of the weights w_j. Let

$$\sigma_h^2 := \frac{1}{MN} \sum_{m=0}^{M-1} \sum_{n=0}^{N-1} \left(h(m, n) - \text{mean}(h)\right)^2$$

denotes the sample variance of h. Since we want the normalized Gabor noise $\text{mean}(h) + \frac{f}{\sqrt{\lambda}}$ to be visually similar to the original texture sample h, it is natural to enforce that $\text{mean}(h) + \frac{f}{\sqrt{\lambda}}$ has the same variance than h. By Proposition 4.1, this means that

$$\frac{\mathbb{E}\left(w^2\right)}{4a^2} = \sigma_h^2.$$

Hence, the weights w_j must be constant to $w = 2a\sigma_h$.

4.4.4 Distribution of the Frequencies

The distribution P_ω of the frequencies ω_j is the most critical parameter of the Gabor noise model. By proposition 4.1, the power spectrum S of f is given by

$$S(\xi) = \lambda \sigma_h^2 \int_{\mathbb{R}^2} \frac{2}{a^2} e^{-\frac{2\pi}{a^2}\|\xi - \omega\|^2} P_\omega(d\omega), \ \xi \in \mathbb{R}^2,$$

<div align="center">(a) $\lambda = 0.01\lambda_{BE}(2.5\%)$</div>

<div align="center">(b) Same λ, r.w.</div>

<div align="center">(c) $\lambda = 0.1\lambda_{BE}(2.5\%)$</div>

<div align="center">(d) Same λ, r.w.</div>

<div align="center">(e) $\lambda = \lambda_{BE}(2.5\%)$</div>

<div align="center">(f) Same λ, r.w.</div>

<div align="center">(g) $\lambda = 10\lambda_{BE}(2.5\%)$</div>

<div align="center">(h) Same λ, r.w.</div>
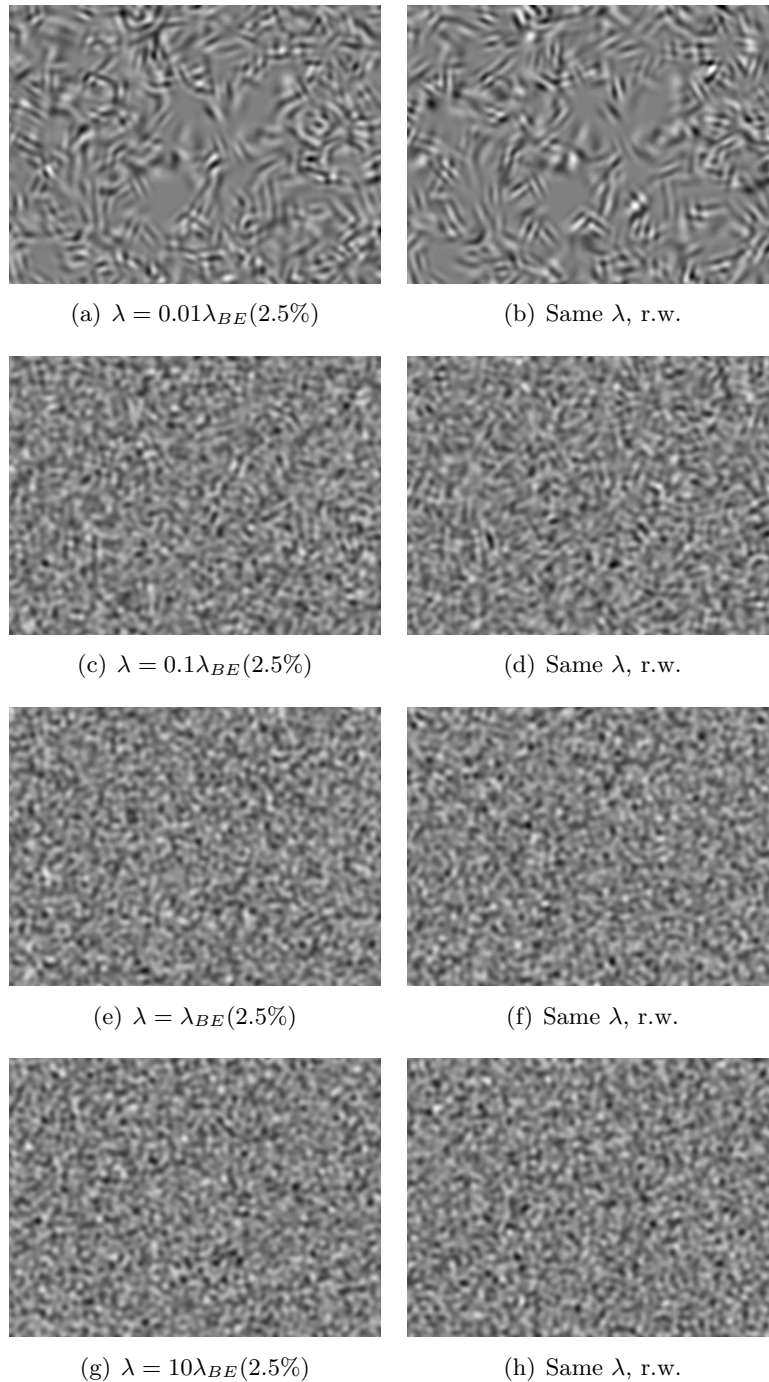
Figure 4.3: Four pairs of realizations of Gabor noise models similar to the ones of Fig. 4.1 with various intensities λ. On the left the weights of the Gabor noise model are constant to 1 whereas on the right they are uniformly distributed over $[-\sqrt{3}, \sqrt{3}]$. For each intensity λ the two textures are visually similar. Hence the Gaussian convergence is not faster when multiplying by random weights. In order to save calls to the random number generator, in the following of this chapter we will only use constant weights.

assuming that $E(w^2) = 4a^2\sigma_h^2$. From this expression one sees that the distribution P_ω gives the individual weights of each frequency ω, and that this weight is locally averaged according to a Gaussian convolution with kernel $\frac{2}{a^2}e^{-\frac{2\pi}{a^2}\|\xi-\omega\|^2}$ (note that this Gaussian kernel has a L_1-norm equal to 1).

Roughly speaking we would like the power spectrum of the Gabor noise to be close to the power spectrum of the non random discrete sample h. First let us clarify what is the power spectrum in the continuous domain of a non random discrete image.

In the discrete setting, the power spectrum of the discrete image h is simply its discrete Fourier transform (DFT) modulus to the square. Note $\hat{h} = \left\{ \hat{h}(k,l), \ (k,l) \in \left[\!\left[-\frac{M}{2}, \frac{M}{2}-1 \right]\!\right] \times \left[\!\left[-\frac{N}{2}, \frac{N}{2}-1 \right]\!\right] \right\}$ the DFT of h. In the continuous domain, h can be interpolated by its associated trigonometric polynomial

$$P_h(x) = \sum_{k=-\frac{M}{2}}^{\frac{M}{2}-1} \sum_{l=-\frac{N}{2}}^{\frac{N}{2}-1} \hat{h}(k,l)e^{2i\pi\langle(\frac{k}{M},\frac{l}{N}),x\rangle},$$

where we assume that M and N are both even integers. Recall that P_h is a real-valued function if and only if

$$\forall l \in \left[\!\left[-\frac{N}{2}, \frac{N}{2}-1 \right]\!\right], \ \hat{h}\left(-\frac{M}{2},l\right) = 0 \quad \text{and} \quad \forall k \in \left[\!\left[-\frac{M}{2}, \frac{M}{2}-1 \right]\!\right], \ \hat{h}\left(k,-\frac{N}{2}\right) = 0.$$

From now on this condition is supposed to be satisfied (in practice this condition must be imposed to the discrete sample h). P_h is not an integrable function over $\mathbb{R}^2$. However it is a tempered distribution and its Fourier transform $\widehat{P_h}$ is well-defined (see e.g. [62]) and given by

$$\widehat{P_h}(\xi) = \sum_{k=-\frac{M}{2}+1}^{\frac{M}{2}-1} \sum_{l=-\frac{N}{2}+1}^{\frac{N}{2}-1} \hat{h}(k,l)\delta_{\left(\frac{k}{M},\frac{l}{N}\right)}(\xi),$$

where δ is the Dirac delta function. Hence the power spectrum of P_h is

$$\left|\widehat{P_h}(\xi)\right|^2 = \sum_{k=-\frac{M}{2}+1}^{\frac{M}{2}-1} \sum_{l=-\frac{N}{2}+1}^{\frac{N}{2}-1} \left|\hat{h}(k,l)\right|^2 \delta_{\left(\frac{k}{M},\frac{l}{N}\right)}(\xi).$$

Actually the power spectrum of P_h is the discrete power spectrum $\left|\hat{h}(k,l)\right|^2$ of h distributed over the frequencies $\left(\frac{k}{M},\frac{l}{N}\right)$.

The expression we propose for the probability distribution P_ω naturally derives from the one of the power spectrum $\left|\widehat{P_h}(\xi)\right|^2$. From now on we suppose that the sample texture h has mean zero and that its associated trigonometric polynomial is real, that is

$$\begin{cases} \hat{h}(0,0) = 0, \\ \hat{h}\left(-\frac{M}{2},l\right) = 0, & l \in \left[\!\left[-\frac{N}{2}, \frac{N}{2}-1 \right]\!\right], \\ \hat{h}\left(k,-\frac{N}{2}\right) = 0, & k \in \left[\!\left[-\frac{M}{2}, \frac{M}{2}-1 \right]\!\right]. \end{cases} \tag{4.3}$$

In practice Conditions (4.3) are imposed on the sample h. Under Conditions (4.3), Parseval's identity becomes

$$\sigma_h^2 = \frac{1}{MN} \sum_{m=0}^{M-1} \sum_{n=0}^{N-1} h(m,n)^2 = \sum_{k=-\frac{M}{2}+1}^{\frac{M}{2}-1} \sum_{l=-\frac{N}{2}+1}^{\frac{N}{2}-1} \left| \hat{h}(k,l) \right|^2,$$

where σ_h^2 denotes the sample variance of h. The probability distribution of the frequencies P_ω is defined as the discrete distribution

$$P_\omega\left(\omega = \xi\right) = \begin{cases} \frac{|\hat{h}(k,l)|^2}{\sigma_h^2} & \text{if } \xi = \left(\frac{k}{M}, \frac{l}{N}\right), \ (k,l) \in \left[\!\left[-\frac{M}{2}+1, \frac{M}{2}-1\right]\!\right] \times \left[\!\left[-\frac{N}{2}+1, \frac{N}{2}-1\right]\!\right], \\ 0 & \text{otherwise.} \end{cases}$$

(4.4)

Note that P_ω is symmetric since $(k,l) \mapsto \left|\hat{h}(k,l)\right|^2$ is even. With this choice for the distribution P_ω, the power spectrum becomes

$$S(\xi) = \lambda \sum_{k=-\frac{M}{2}+1}^{\frac{M}{2}-1} \sum_{l=-\frac{N}{2}+1}^{\frac{N}{2}-1} \left|\hat{h}(k,l)\right|^2 \frac{2}{a^2} e^{-\frac{2\pi}{a^2}\left\|\xi - \left(\frac{k}{M}, \frac{l}{N}\right)\right\|^2}. \tag{4.5}$$

Hence $S(\xi)$ is the convolution between the discrete power spectrum of h and a Gaussian kernel $\frac{2}{a^2} e^{-\frac{2\pi}{a^2}\|\xi\|^2}$. Our choice for P_ω is very natural since the power spectrum of the Gabor kernel is close to the power spectrum of the sample.

Note that the parameter a controls the dilation effect over the power spectrum. For small values of a the power spectrum S of the Gabor noise is really close to the power spectrum of the sample h, whereas for large values of a the energy of various distinct frequencies contributes to $S(\xi)$. As always, there is a competition between localization in the Fourier domain and localization in the spatial domain: for small values of a, the Gabor kernels have a large support in the spatial domain, which should be proscribed to enable the synthesis of Gabor noise textures on surfaces. Indeed, for Gabor noise on surfaces the spatial width a^{-1} is assumed to be small in comparison with the radius of curvature of the surface [96].

Remark. Note that there is a clear control of the bandwidth of the Gabor noise: the support of the spectrum is mainly contained in the dilation by a disc of radius a of the support of the continuous spectrum of the discrete sample. Hence, if the input texture image is band-limited then the output texture is also band-limited. This property is essential for procedural texture synthesis [95].

4.4.5 Extracting a Quality Power Spectrum from the Input Texture Sample

As seen above, the probability distribution P_ω associated with the sample texture h uses the DFT modulus $\left|\hat{h}\right|$ to determine the relative importance of each frequencies of the Gabor noise model. Hence it is implicitly assumed that all the frequencies for

which the DFT modulus $\left|\hat{h}\right|$ is high are important frequencies for the texture image. Experiments show that this assumption is in general true, with the exception of the horizontal and vertical frequencies present in the cross structure inherent to any DFT modulus [113].

One of the main features of the periodic component $p = \mathrm{per}(h)$ defined by Moisan [113] is that the DFT $\hat{p}$ is obtained in filtering out the cross structure of the DFT $\hat{h}$ of h (both the DFT modulus and DFT phase does not have cross structure). In the case where the image h is a texture, the horizontal and vertical frequencies present in its DFT cross-structure are only due to border effects and does not correspond to proper frequencies of the texture. However, the frequencies which are active in the DFT $\hat{p}$ of the periodic component p only correspond to inner frequencies of the texture (see the two first rows of Fig. 4.4).

As in Chapter 2 for the ADSN and RPN algorithms, a natural solution to avoid problems due to the cross-structure of the DFT modulus $\left|\hat{h}\right|$ is to replace the DFT $\hat{h}$ by the DFT $\hat{p}$ of the periodic component[3] $p = \mathrm{per}(h)$ in the definition of the probability distribution P_ω (see Equation (4.4)). Of course before defining P_ω, Conditions (4.3) are enforced on $\hat{p}$.

Fig. 4.4 illustrates that replacing h by p is relevant: in the displayed example the Gabor noise associated with h suffers from oscillation artifacts due to horizontal and vertical frequencies present in its power spectrum, whereas the Gabor noise associated with p does not present these artifacts. In the remaining of this chapter, the texture sample h will always be replaced by its periodic component p in order to define the distribution P_ω, and the Gabor noise model associated with h will refer to the Gabor noise model associated with $p = \mathrm{per}(h)$.

The wood texture of Fig. 4.4 is relatively well-reproduced by the Gabor noise model associated with its periodic component. Before presenting further results, let us extend the Gabor noise by example method to color textures.

4.5   Color Gabor Texture Synthesis From Samples

4.5.1   Introduction and Notation

In procedural texture synthesis, designed color textures are generally obtained in applying a non linear color map to a gray-level procedural noise function, that is in associating an RGB color to a gray-level. In [99, 64], color textures are synthesized using a PCA decomposition of the color space, similarly to the Heeger-Bergen image texture synthesis algorithm [74]. In this section we propose a third alternative: a color Gabor noise is defined directly in the RGB space by enforcing some coherency between the color channels. Our key insight is to use the observation uncovered in Chapter 2: Fourier phase displacements between color channels are related to the

---

[3]We recall that it is shown in Appendix A that the DFT $\hat{p}$ can be computed with only one call to the FFT algorithm.

(a) Image h (b) Image $p = \text{per}(h)$ (c) Image $\text{mean}(h) + s$

(d) DFT modulus $\left|\hat{h}\right|$ (e) DFT modulus $|\hat{p}|$ (f) DFT modulus $|\hat{s}|$

(g) Gabor noise(h) (h) Gabor noise(p) (i) Gabor noise(s)
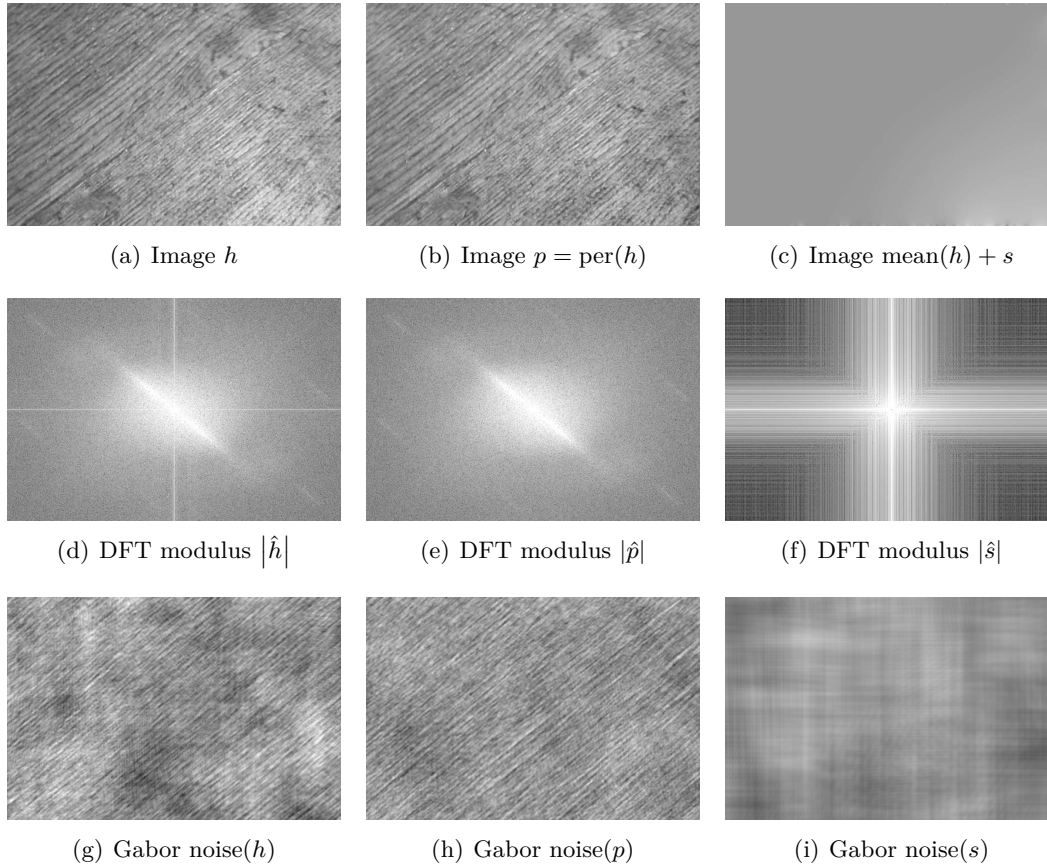
Figure 4.4: Gabor noise and periodic plus smooth decomposition. First row: Original image h, its periodic component p and its smooth component s (the mean is added for visualization purpose). Second row: Respective DFT moduli of the images of the first row. Third row: Gabor noise associated with each image of the first row. The image size is 768×512, the kernel size of the Gabor noises is $a^{-1} = 200$ and the intensity is $\lambda = 2\lambda_{BE}(2.5\%)$. Observe that, the cross structure present in the DFT modulus of the original image h is not present in the Fourier modulus of the periodic component p [113]. Due to this cross structure, the probability distribution P_ω associated with h defined by Equation (4.4) activates several horizontal and vertical frequencies. As a consequence the Gabor noise associated with h contains some horizontal and vertical oscillations, especially visible for the low frequencies in this example. On the opposite, these oscillation artifacts are not present in the Gabor noise associated with p. The Gabor noise associated with the smooth component reveals the artifacts which are removed from the Gabor noise when replacing the discrete sample h by its periodic component p.

color range of random phase textures.

The considered problem is the following: Given an RGB color texture sample

$$h_{RGB} = (h_R, h_G, h_B)$$

of size $M \times N$ we would like to define an associated color Gabor noise

$$f_{RGB} = (f_R, f_G, f_B)$$

which is visually similar to the texture sample h_{RGB}.

Clearly f_R, f_G and f_B should be gray-valued Gabor noises with parameters depending on the sample images h_R, h_G and h_B. In addition there must have some dependency relation between the three random color channels since the color channels of any natural texture are strongly correlated.

The dependence structure between the color channels of the proposed color Gabor noise model involves the three significant parameters of the Gabor kernels, that is the position x_j, the frequency ω_j and the phase. For each of these parameters, the enforced coherency is the following:

- Position coherency: The emplacements x_j of the Gabor kernels are the same for the three color channels f_R, f_G and f_B, that is to say that the color Gabor noise is a three-dimensional shot noise of three-dimensional Gabor kernels.

- Frequency coherency: The frequency in each channel of the three dimensional Gabor kernels is the same for the three channels. The probability distribution of the random frequencies takes into account the total energy of each frequency in the three color channels of the texture sample h_{RGB}.

- Phase coherency: The extension to color images of the RPN algorithm proposed in Chapter 2 highlighted a link between color consistency and phase displacements between color channels. This observation leads to enforce the phase displacements of the color channels of the sample h to each three-dimensional Gabor kernel (see below for details).

Before rigorously defining the color Gabor noise model associated with a color texture sample $h_{RGB} = (h_R, h_G, h_B)$, one needs to introduce several notation. We recall that $h_{RGB} = (h_R, h_G, h_B)$ has size $M \times N$, where M and N are supposed to be even. In addition, it is assumed that each color channel h_R, h_G, and h_B satisfies Conditions (4.3). We denote by S_h^R, S_h^G and S_h^B the respective power spectrum of the discrete images h_R, h_G, and h_B in the continuous domain, that is

$$S_h^C(\xi) = \begin{cases} \left| \hat{h}_C(k,l) \right|^2 & \text{if } \xi = \left(\frac{k}{M}, \frac{l}{M} \right), \\ 0 & \text{otherwise,} \end{cases}$$

where the index C denotes any of the three channels R, G, B (this notation will be used in all that follows). Besides we note S_h^{RGB} the function

$$S_h^{RGB}(\xi) = S_h^R(\xi) + S_h^G(\xi) + S_h^B(\xi).$$

The quantity $S_h^{RGB}(\xi)$ represents the total amount of energy of the image h at frequency ξ. Similarly σ_h^R, σ_h^G, σ_h^B denote the standard deviations of the color channels of h and

$$\left(\sigma_h^{RGB}\right)^2 = \left(\sigma_h^R\right)^2 + \left(\sigma_h^G\right)^2 + \left(\sigma_h^B\right)^2.$$

Note that $\left(\sigma_h^{RGB}\right)^2$ is the L^1-norm of S_h^{RGB}. Eventually ϕ_h^R, ϕ_h^G and ϕ_h^B denote the respective Fourier phase of h_R, h_G, and h_B, that is

$$\phi_h^C(\xi) = \begin{cases} \arg\left(\hat{h}_C(k,l)\right) & \text{if } \xi = \left(\frac{k}{M}, \frac{l}{M}\right), \\ 0 & \text{otherwise,} \end{cases}$$

where C denotes R, G or B.

4.5.2 Definition of the Color Gabor Noise Model

Definition 4.2 (Color Gabor noise model). *The color Gabor noise model associated with the discrete color image $h_{RGB} = (h_R, h_G, h_B)$, with intensity λ and kernel width a is the shot noise*

$$f_h^{RGB}(x) = \sum_{(x_j, w_j, \omega_j, \theta_j) \in \Pi} g_h^{RGB}(x - x_j; w_j, \omega_j, \theta_j),$$

where $\Pi = \{(x_j, w_j, \omega_j, \theta_j)\}$ is an independently marked Poisson process such that

- *$\{x_j\}$ is a stationary Poisson process over $\mathbb{R}^2$ with intensity λ,*

- *the r.v. w_j are constant to $2a\sigma_h^{RGB}$,*

- *the r.v. ω_j are distributed according to the density associated with S_h^{RGB}, that is*

$$P_\omega(\omega = \xi) = \frac{S_h^{RGB}(\xi)}{\left(\sigma_h^{RGB}\right)^2},$$

- *the r.v. θ_j are uniformly distributed over $(-\pi, \pi]$,*

and $g_h^{RGB} : \mathbb{R}^2 \times K \to \mathbb{R}^3$ is the measurable function defined by

$$g_h^{RGB}(x; w, \omega, \theta) = we^{-\pi a^2 \|x\|^2} \begin{pmatrix} \sqrt{\frac{S_h^R(\omega)}{S_h^{RGB}(\omega)}} \cos\left(2\pi\langle x, \omega\rangle + \theta + \phi_h^R(\omega)\right) \\ \sqrt{\frac{S_h^G(\omega)}{S_h^{RGB}(\omega)}} \cos\left(2\pi\langle x, \omega\rangle + \theta + \phi_h^G(\omega)\right) \\ \sqrt{\frac{S_h^B(\omega)}{S_h^{RGB}(\omega)}} \cos\left(2\pi\langle x, \omega\rangle + \theta + \phi_h^B(\omega)\right) \end{pmatrix}.$$

Let us briefly justify this definition. Except for some additional details, the definition of the color Gabor noise is similar to the one of the Gabor noise associated with a gray-valued sample image: it is a shot noise with a Gabor kernel as impulse

function and with an independently marked Poisson process which depends on h_{RGB}.

Here the distribution P_ω is chosen so that the probability of occurrence of a frequency ω is proportional to the total power of this frequency among the three color channels of the sample h_{RGB}. Of course, for each color channel this probability is unbalanced since a frequency ω can be more influent in one channel than in the others. This imbalance is corrected in multiplying by the term

$$\sqrt{\frac{S_h^C(\omega)}{S_h^{RGB}(\omega)}}.$$

Eventually the addition of the phases $\phi_h^R(\omega)$, $\phi_h^G(\omega)$, $\phi_h^B(\omega)$ is intended to conserve the Fourier phase displacements between the color channels of h_{RGB}, since it has been demonstrated in Section 2.5.1 that conserving these phase displacements helps preserving the color consistency of the sample color image h_{RGB}.

4.5.3 Power Spectrum of the Color Gabor Noise

Proposition 4.4. *The color Gabor noise $f_h^{RGB} = \left(f_h^R, f_h^G, f_h^B\right)$ is a well-defined stationary three-dimensional random field. Its has null expectation and is square-integrable. Besides, for all channel $C \in \{R, G, B\}$, the power spectrum S_f^C of f_h^C is given for all $\xi \in \mathbb{R}^2$ by*

$$S_f^C(\xi) = \lambda \sum_{k=-\frac{M}{2}+1}^{\frac{M}{2}-1} \sum_{l=-\frac{N}{2}+1}^{\frac{N}{2}-1} \left|\hat{h}_C(k,l)\right|^2 \frac{2}{a^2} e^{-\frac{2\pi}{a^2}\left\|\xi-\left(\frac{k}{M},\frac{l}{N}\right)\right\|^2}.$$

That is to say that for each color channel $C \in \{R, G, B\}$ the power spectrum of f_h^C is the same as the power spectrum of the Gabor noise associated with the gray-valued image h_C (see Equation (4.5)).

Proof. By Proposition 3.1,

$$S_f^C(\xi) = \lambda E\left(\left|\widehat{g_h^C}(\xi; w, \omega, \theta)\right|^2\right).$$

The Fourier transform of g_h^C is given by

$$\widehat{g_h^C}(\xi; w, \omega, \theta) = \frac{w}{2a^2}\sqrt{\frac{S_h^C(\omega)}{S_h^{RGB}(\omega)}}\left(e^{-\frac{\pi}{a^2}\|\xi-\omega\|^2}e^{i\left(\theta+\phi_h^C(\omega)\right)} + e^{-\frac{\pi}{a^2}\|\xi+\omega\|^2}e^{-i\left(\theta+\phi_h^C(\omega)\right)}\right).$$

We now follow the same step of computation as in the proof of Proposition 4.1. Integrating with respect to w and θ we have

$$S_f^C(\xi) = \lambda\frac{E(w^2)}{4a^4}\int_{\mathbb{R}^2}\frac{S_h^C(\omega)}{S_h^{RGB}(\omega)}\left(e^{-\frac{\pi}{a^2}\|\xi-\omega\|^2} + e^{-\frac{\pi}{a^2}\|\xi+\omega\|^2}\right)P_\omega(d\omega).$$

Using that $E(w^2) = 4a^2 \left(\sigma_h^{RGB}\right)^2$ as well as the expression and the symmetry of P_ω we get

$$S_f^C(\xi) = 2\lambda \frac{\left(\sigma_h^{RGB}\right)^2}{a^2} \sum_{k=-\frac{M}{2}+1}^{\frac{M}{2}-1} \sum_{l=-\frac{N}{2}+1}^{\frac{N}{2}-1} \frac{S_h^C((\frac{k}{M}, \frac{l}{N}))}{S_h^{RGB}((\frac{k}{M}, \frac{l}{N}))} e^{-\frac{\pi}{a^2}\|\xi - (\frac{k}{M}, \frac{l}{N})\|^2} \frac{S_h^{RGB}((\frac{k}{M}, \frac{l}{N}))}{\left(\sigma_h^{RGB}\right)^2}.$$

The enunciated formula is obtained in simplifying this last expression. □

Remark that the probability distribution of a channel f_h^C of the color Gabor noise f_h^{RGB} is not the same as the probability distribution of the Gabor noise associated with the gray-valued image h_C. Nevertheless both random fields share the same power spectrum and thus converge in distribution towards the same Gaussian random field when the intensity λ increases to $+\infty$ (see Theorem 3.1).

4.5.4   Numerical Results

This section presents several results of successful synthesis obtained with the proposed algorithm for color Gabor noise by example. As discussed in Section 4.4.2, the synthesis is restricted to micro-textures which are well-reproduced by the RPN algorithm, and for every texture sample we display its associated RPN as a reference result for the Gabor noise. Experiments show that failure examples for the RPN are also failure examples for the Gabor noise model.

Let us first illustrate the convergence of the algorithm. Fig. 4.5 shows several Gabor noises associated with a leather texture having different intensities λ. When the intensity increases, the Gabor noise texture tends to its limit Gaussian textures which, for this example, is visually similar to the input .

For all the subsequent examples of this section, the intensity λ will be set to $\lambda = 10\lambda_{BE}(2.5\%)$, where $\lambda_{BE}(2.5\%)$ is the intensity derived from the Berry-Esseen bound (see Equation (4.2)). This ensures that the synthesized textures are visually visually similar to the limit Gaussian texture.

Let us first discuss the influence of the parameter a (recall that a^{-1} is the spatial width of the Gabor kernels). Experiments show that this parameter is especially important for isotropic textures containing long oscillations such as wood or fabric textures. In order for the Gabor noise model to capture the long range correlation structures of these textures, the spatial width a^{-1} of the Gabor kernels must necessary be large. This is not surprising since if the distance between two points y and z is larger than $2a^{-1}$ then the Gabor noise values $f(y)$ and $f(z)$ are independent. The influence of the parameter a^{-1} is illustrated by Fig. 4.6 and Fig. 4.7. Fig. 4.6 shows that as the spatial width a^{-1} of the Gabor kernels increases the wood texture produces by the Gabor noise is more and more structured. On the opposite, for the structureless isotropic leather texture of Fig. 4.7, the value of a^{-1} has no influence on the quality of the result.

To complete this section, Fig. 4.8 and Fig. 4.9 show several examples of textures which are well-reproduced by the color Gabor noise. As for Fig. 4.6 and Fig. 4.7, for

(a) Original image h (b) RPN
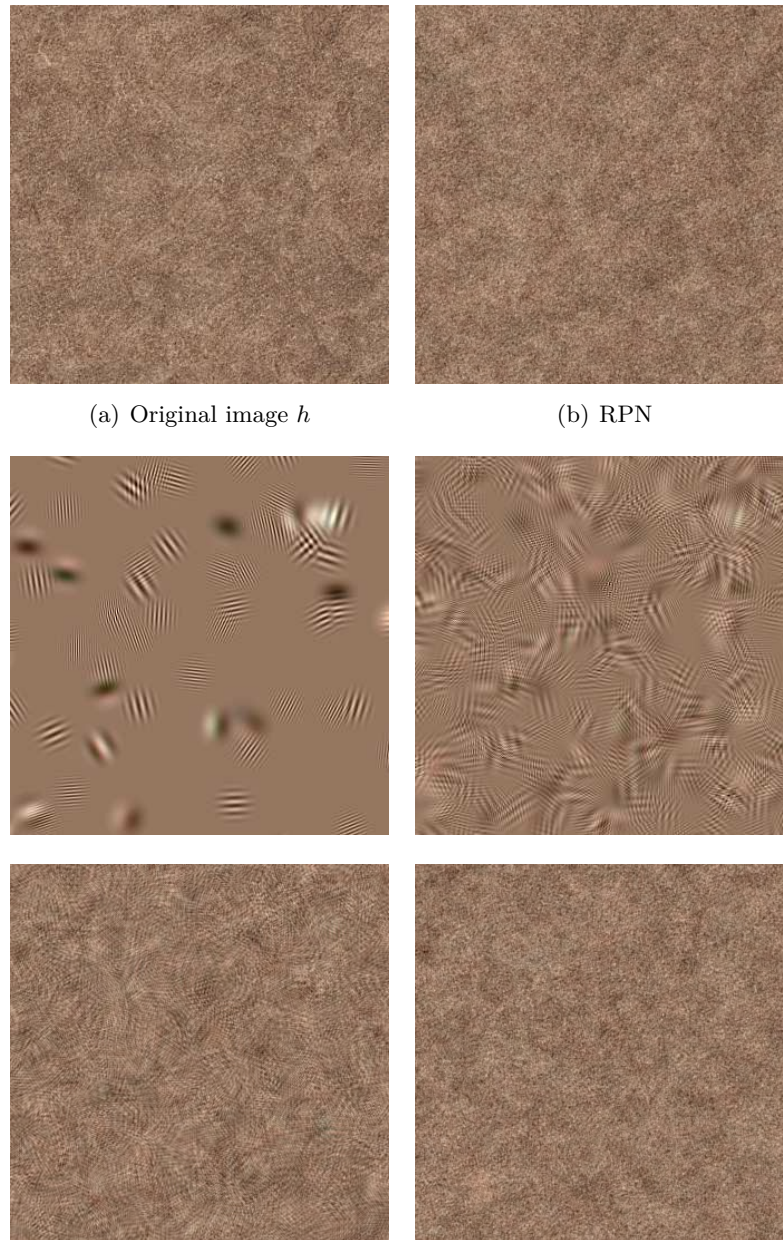
Figure 4.5: Illustration of the convergence of the color Gabor noise by example: Top row original leather texture sample and its associated RPN; Middle row and bottom row: Gabor noises associated with h. From one Gabor noise to the other the number of Gabor kernels is multiplied by a factor 10. The intensity λ of the last example is $\lambda = \lambda_{BE}(2.5\%)$ (see Equation (4.2)). The size of the image is 340×340 and the radius of the Gabor kernels is 20.

(a) Original image (459×283)

(b) RPN

(c) Gabor noise, $a^{-1} = 20$

(d) Gabor noise, $a^{-1} = 50$

(e) Gabor noise, $a^{-1} = 100$

(f) Gabor noise, $a^{-1} = 250$
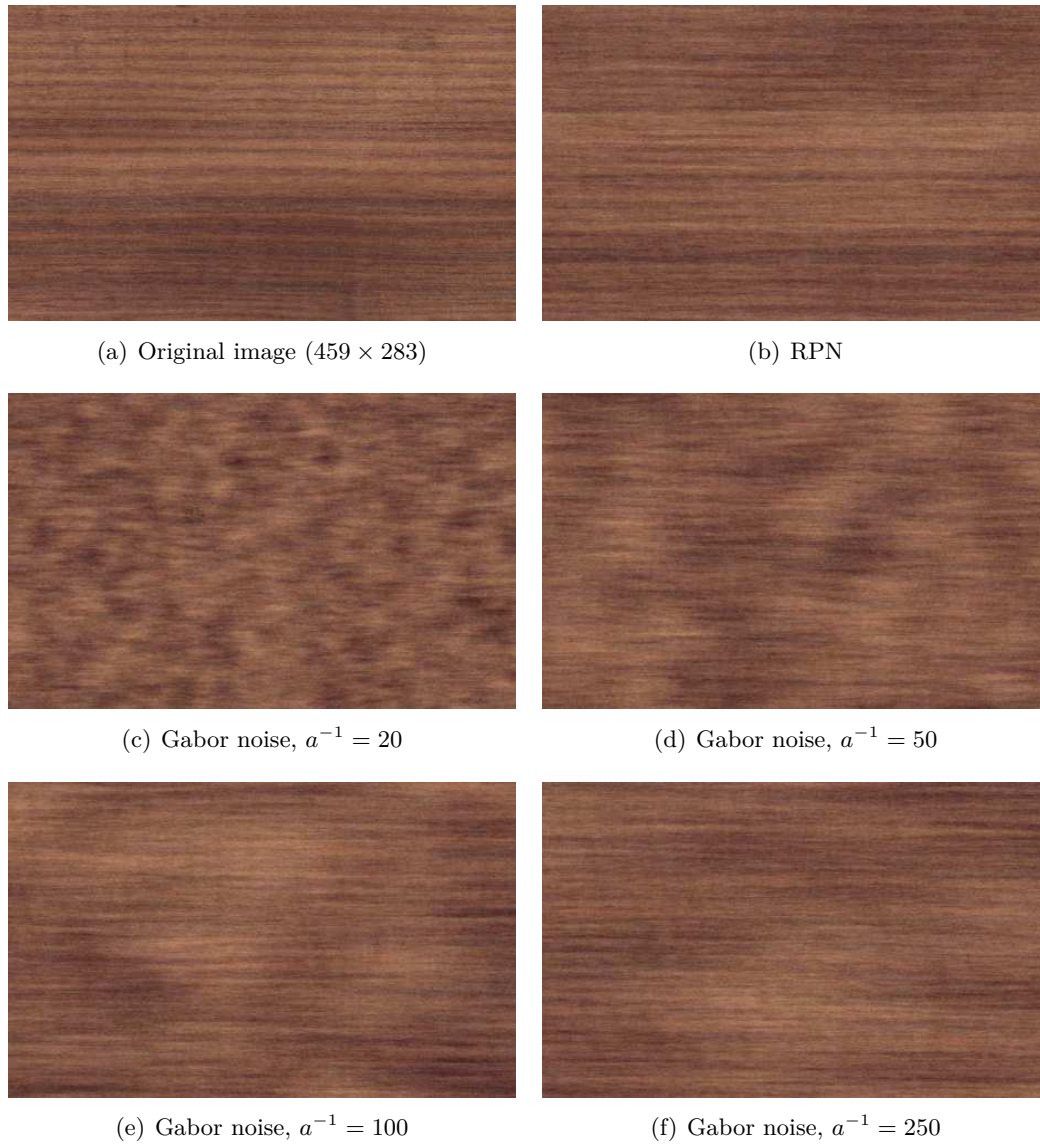
Figure 4.6: Influence of the spatial width a^{-1} of the Gabor kernels: As the spatial width a^{-1} increases the Gabor noise texture is more and more structured. This is justified by the fact that large Gabor kernels enable longer range dependencies. Hence the parameter a is especially important for oscillating textures such as wood or fabric. However for isotropic micro-textures increasing a does not necessary yields to better results (see Fig. 4.7).

(a) Original image (340×340)

(b) RPN

(c) Gabor noise, $a^{-1} = 20$

(d) Gabor noise, $a^{-1} = 50$

(e) Gabor noise, $a^{-1} = 100$

(f) Gabor noise, $a^{-1} = 250$
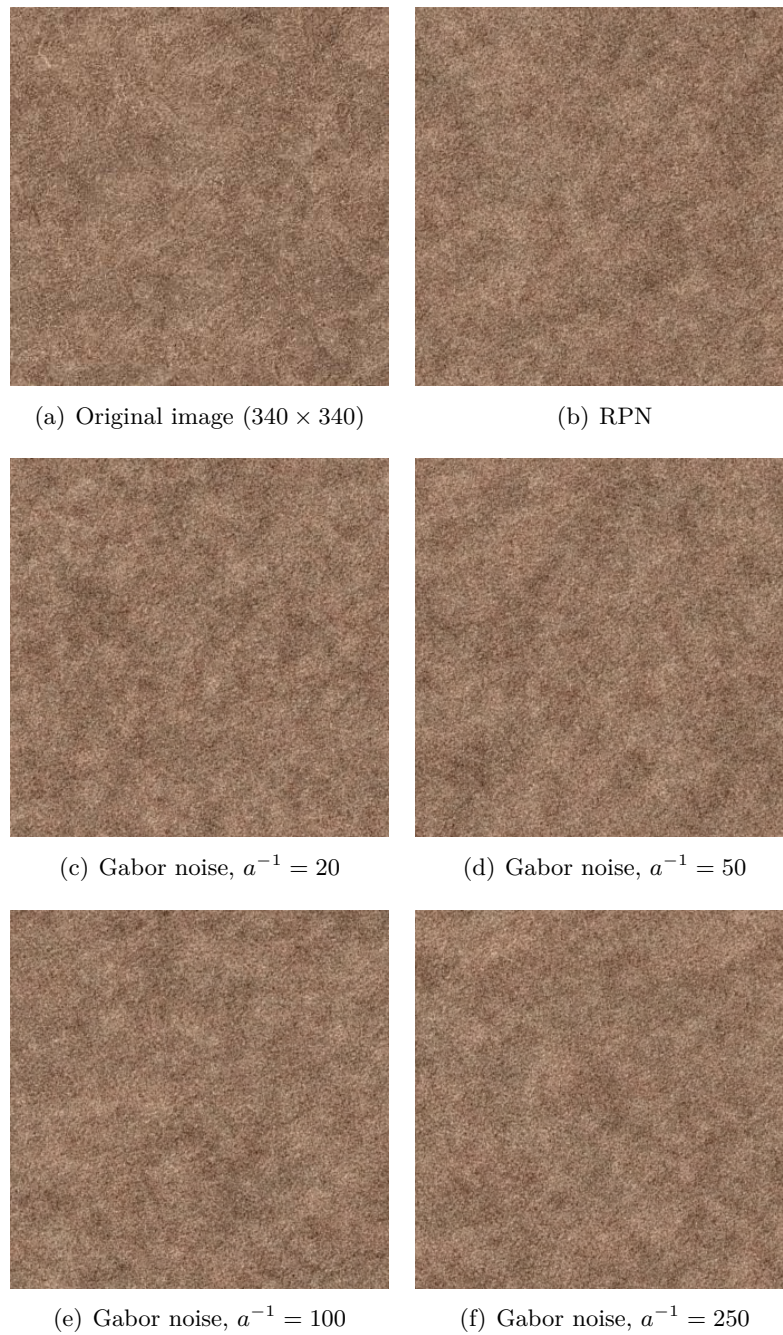
Figure 4.7: Influence of the spatial width a^{-1} of the Gabor kernels: Contrary to the wood texture of Fig. 4.6, this leather texture is well reproduced with any size of Gabor kernels. Hence using large Gabor kernels in the spatial domain is only important for textures having elongated structures.

each examples the kernel size 20, 50, 100 and 250 were tested, and the best result of the four has been selected. On the examples of Fig. 4.8 and Fig. 4.9 where there are slight differences between the original texture and its associated RPN, observe that the Gabor noise texture is always visually more similar to the RPN texture than to the original one.

In conclusion, the algorithm for color Gabor noise by example developed in this chapter provides a procedural texture model which is visually similar to the RPN texture associated with the discrete sample. In particular it permits to have a faithful procedural representation of all the micro-textures which are well-reproduced by the RPN algorithm of Chapter 2.

Another advantage of the color Gabor noise by example that has not been discussed yet is that the whole process is linear. As a consequence, it enables to use the intrinsic anti-aliasing of the Gabor noise model [96]. On the opposite, when applying a non-linear color map to a gray-level Gabor noise, the intrinsic anti-aliasing scheme of Gabor noise is not rigorously well-funded and filtering the resulting texture necessitates additional techniques [96, 73].

4.6   Conclusion and Future Works

This chapter introduced a new algorithm to derive a color Gabor noise model from a given texture sample. Relying on the general results on Poisson shot noises recalled or established in Chapter 3, properties of the Gabor noise model have been derived, with a particular emphasis on the normal convergence of high intensity Gabor noises.

As shown by the experiments, high intensity Gabor noise textures are visually reproducible by the RPN algorithm of Chapter 2. Conversely, using the same methods as for the RPN algorithms, that is replacing the texture sample by its periodic component and enforcing the phase displacement between the color channels of the sample to the Gabor kernels of the color Gabor noise, a color Gabor noise model visually similar to the RPN of the sample has been defined. Again let us clarify that the similarity of the results between Gabor noise by example and the RPN algorithm does not limit the interest of the methods. Indeed they are two different kind of algorithms. RPN is an algorithm which synthesizes numerical images, whereas Gabor noise by example defines a procedural texture model to be used in computer graphics softwares for rendering 3D surfaces.

As mentioned in the abstract, the content of this chapter yielded an ongoing collaboration with three of the authors of the original Gabor noise paper [96], namely A. Lagae, S. Lefebvre and G. Drettakis. A GPU implementation of the presented algorithm for color Gabor noise by example is being developed. The first version of this GPU implementation already enables to synthesize a whole image within a second, instead of several minutes for the Matlab implementation used to obtain the results presented in this chapter. Contrary to the performance of the Gabor noise model of [96], this first GPU implementation is not real-time. The main

(a) Original image (350×258)   (b) Gabor noise, $a^{-1} = 50$ (c) RPN

(d) Original image (247×250)   (e) Gabor noise, $a^{-1} = 50$ (f) RPN

(g) Original image (300×300)   (h) Gabor noise, $a^{-1} = 50$ (i) RPN

(j) Original image (300×300)   (k) Gabor noise, $a^{-1} = 250$ (l) RPN
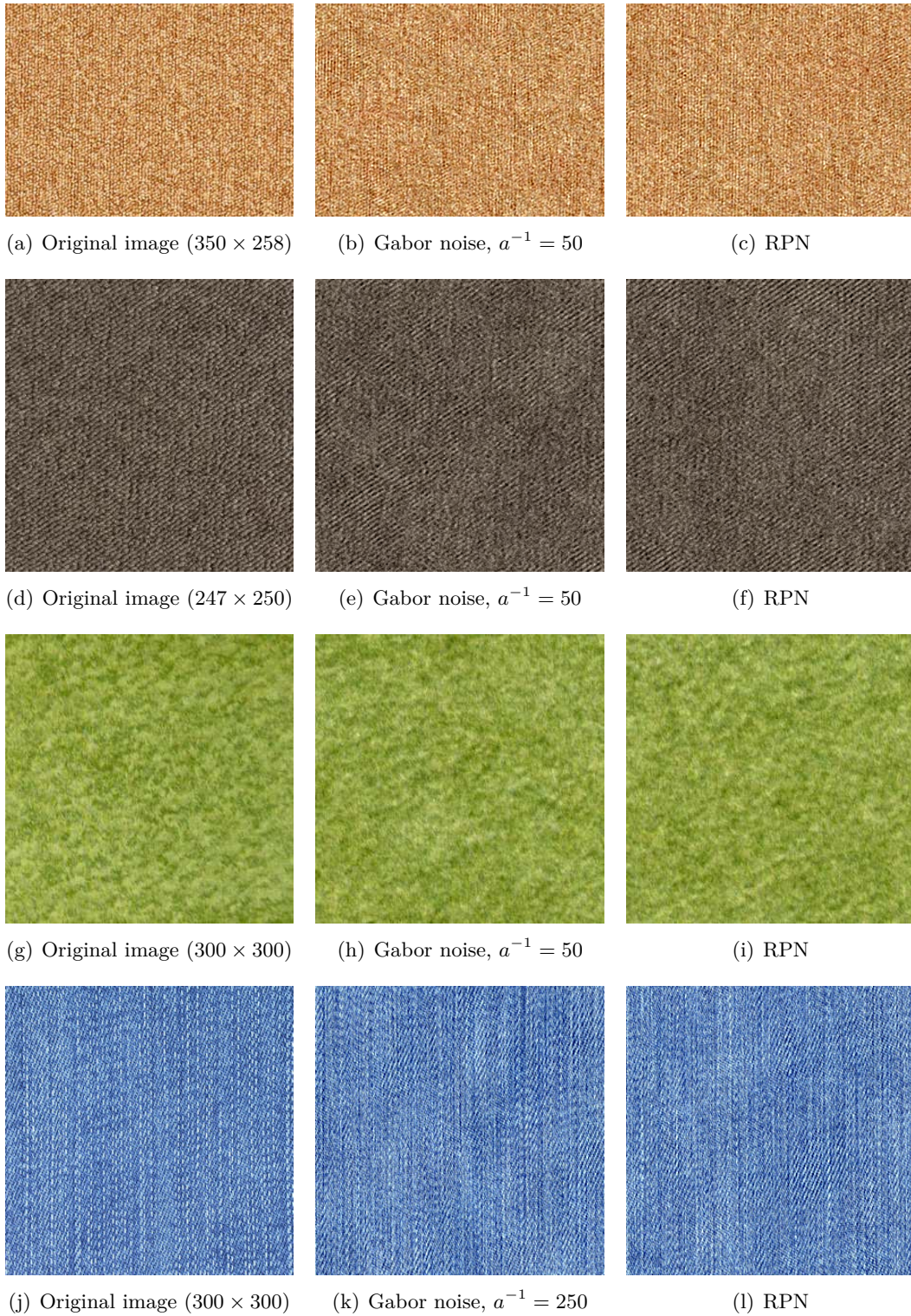
Figure 4.8: Several examples of fabric textures well-reproduced by the color Gabor noise algorithm. For each example the size of the image is specified as well as the spatial width of the Gabor kernels (chosen by hands in the cases). Note that for the blue fabric texture the kernel size is relatively large in order to reproduce the long waves of the texture.

(a) Original image (340×340) (b) Gabor noise, $a^{-1} = 20$ (c) RPN

(d) Original image (512×512) (e) Gabor noise, $a^{-1} = 100$ (f) RPN

(g) Original image (459×253) (h) Gabor noise, $a^{-1} = 100$ (i) RPN

(j) Original image (340×340) (k) Gabor noise, $a^{-1} = 50$ (l) RPN
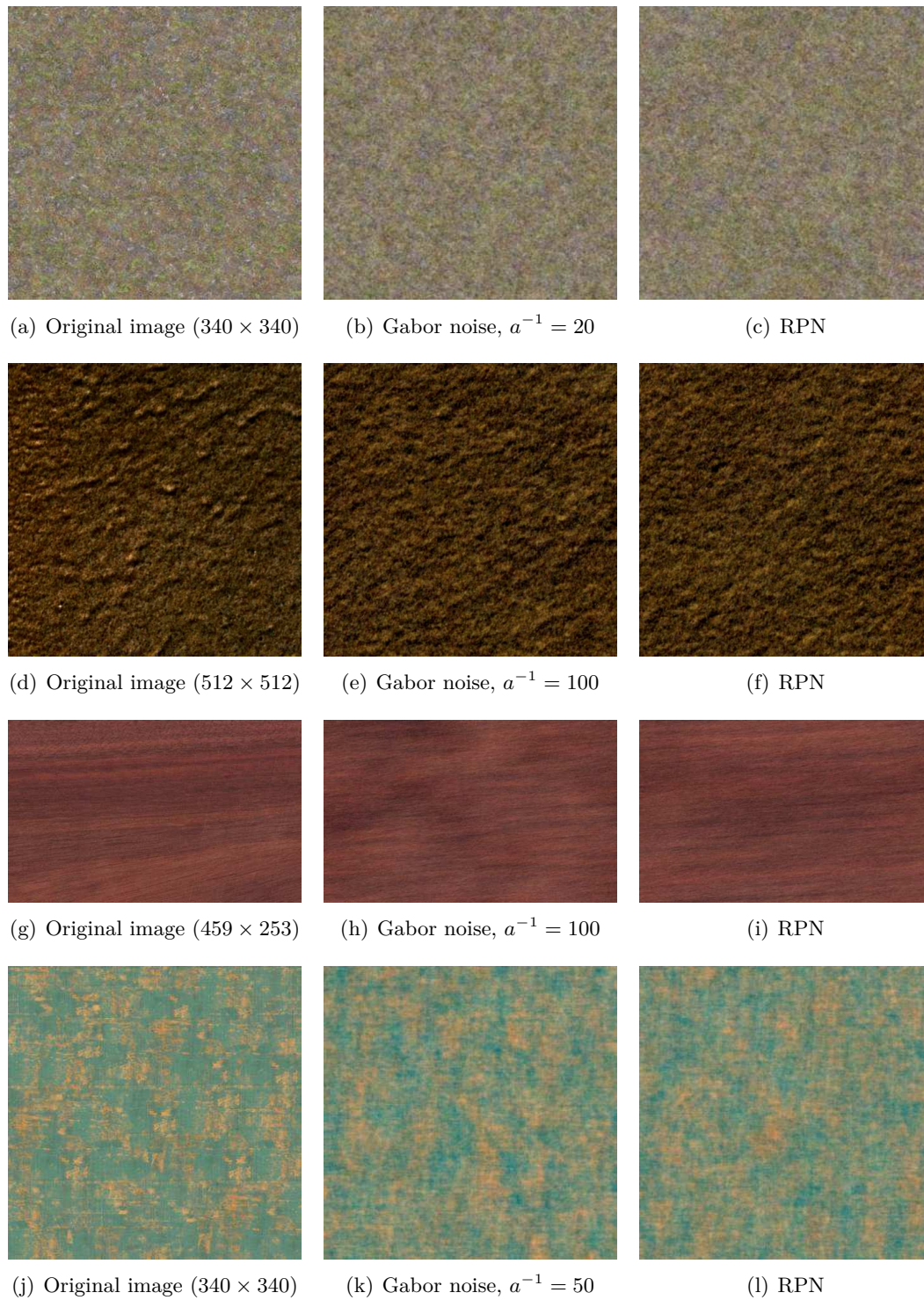
Figure 4.9: Same presentation as Fig. 4.8 with miscellaneous texture samples: mossy rock, sand, wood, and painted concrete.

reason is that, as discussed in Section 4.2.4, Gabor noise by example requires a really high intensity of Gabor kernels (typically two thousands of kernels for each point). Another issue is that the probability distribution for the frequency, as well as the phase displacements do not have a *compact* representation, in the sense that they require the memory space of a full discrete image. This is problematic for the GPU implementation since memory access are slow in comparison to computation cycles [95].

The Gabor noise by example model presented in this chapter also faces issues which are not purely computational. The main one is the fixed kernel width a, which has been shown to be sensible for oscillatory textures. For such textures large Gabor kernels are needed to reproduce oscillatory patterns whereas for structureless micro-textures small Gabor kernels are sufficient. In fact, as it is currently being investigated, it may certainly be more judicious to adapt the kernel radius for each frequency of the power spectrum of the texture sample: if the frequency is an isolated pick in the spectrum it might necessitates large Gabor kernels, whereas if the frequency lives in a flat zone of the power spectrum it can be mixed with the neighboring frequencies and small Gabor kernels might be used. A natural solution would be to decompose the power spectrum in two parts, quite similarly to 2D Wold decomposition (see e.g. [103]).

To finish, let us mention that one could make use of the locality of the Gabor noise model to develop a procedural texture mixing algorithm, enabling a continuous variation from one texture to the other [98].

As a general conclusion, a challenging problem would be to develop procedural texture synthesis methods able to reproduce textures being more structured than the random phase textures. To design such procedural texture methods from Gabor noise model would necessary involve to enforce some constraints on the phase of the Gabor kernels. Hence a direction for future work is to investigate the structure present in the phase of non random phase textures.

Part II

The Transparent Dead Leaves Process: a New Germ-Grain Model

Classical Germ-Grain Models

Contents

Abstract: This chapter presents different classical germ-grain random fields, namely shot noises of random sets, Boolean models, colored dead leaves models, and colored tessellations. These models all combine different colored random sets according to various interaction principles. The chapter also illustrates the wide range of images that are obtained by varying this interaction principle.

Let us precise that this introductory chapter to germ-grain models does not contain any contribution.

5.1 Introduction

This short chapter introduces and illustrates several classical germ-grain models. Each considered germ-grain model defines a random field by combining colored random sets according to an interaction principle. This interaction principle is addition for shot noise models, supremum for Boolean random fields (which generalizes set union for Boolean random sets), occultation for the dead leaves model, and, arguably, juxtaposition for colored tessellations.

The purpose of this chapter is threefold. First, it illustrates the wide range of images that are obtained by only varying the interaction principle. Second, it introduces germ-grain models sharing similarities with the new germ-grain model that will be introduced in the next chapter, namely the transparent dead leaves process, for which the interaction principle is transparency (see Chapter 6). Finally, under certain conditions, all the germ-grain models defined in this chapter are non trivial examples of random fields of bounded variation. Their mean total variation per

unit volume will be computed in Chapter 9 by making use of the formal definitions given in this chapter.

Germ-grain models rely on theoretical tools from stochastic geometry, namely point processes marked by random sets[1] [142, 136]. More precisely, in the simplest cases, a germ-grain model is constructed from a point process $\{(x_j, X_j)\}$ taking value in $\mathbb{R}^d \times \mathcal{F}$, where $\mathcal{F} = \mathcal{F}\left(\mathbb{R}^d\right)$ denotes the set of closed sets of $\mathbb{R}^d$. The random sets X_j are called the *grains* of the model, and the points x_j are the *germs*. A germ-grain models is then constructed in the following way: each grain X_j is placed at the germ x_j to form the set $x_j + X_j$, and the different translated grains $x_j + X_j$ are combined according to an interaction principle. For example, the interaction principle of the shot noise model is addition, which leads to the r.f.

$$f(y) = \sum_{(x_j, X_j)} \mathbb{1}(y \in x_j + X_j), \ y \in \mathbb{R}^d.$$

More generally, the random grains X_j can be "colored": to each random grain X_j is associated an intensity (or gray-level) $a_i \in \mathbb{R}$. In this case the underlying point process takes the form $\{(x_j, X_j, a_j)\} \subset \mathbb{R}^d \times \mathcal{F} \times \mathbb{R}$. In the example of the shot noise model, the corresponding random field would naturally be

$$f(y) = \sum_{(x_j, X_j, a_j)} a_j \mathbb{1}(y \in x_j + X_j), \ y \in \mathbb{R}^d.$$

Even more generally, the grains can be chronologically ordered by a time t_i, the point process having the form $\{(t_j, x_j, X_j, a_j)\} \subset (-\infty, 0) \times \mathbb{R}^d \times \mathcal{F} \times \mathbb{R}$. For example, this ordering is necessary for the dead leaves model for which the interaction principle is occultation: a grain (t_j, x_j, X_j, a_j) is placed above the grains (t_k, x_k, X_k, a_k) such that $t_k < t_j$ and below the grains such that $t_k > t_j$ (see Section 5.4 for details).

Even though the different germ-grain models are constructed according to the same scheme, the corresponding r.f. present different features determined by the interaction principle. For example, since high intensity shot noise tends to Gaussian random fields (see Chapter 3), the geometrical shape of the grains are not discernible in their realizations. On the opposite, the geometrical shapes of the grains are clearly discernible in Boolean random fields or dead leaves models. In fact, as it will be illustrated with various simulations[2], combining the same random sets with different interaction principles yields to very different kind of random geometric images.

All the presented germ-grain models have applications in a large variety of domains dealing with spatial data. Let us mention geostatistics, modeling of material, astrophysics, meteorology, or communication network (see e.g. [142] and the references therein). As for image models, tessellations models have been studied by Ahuja and Rosenfeld [3], and Poisson-Voronoi tessellations are at the center of the

---

[1]Basic definitions of point processes are recalled in Appendix B.

[2]We refer to the book of Lantuéjoul [100] for the description of the simulation algorithms of the considered models, as well as for further illustrations.
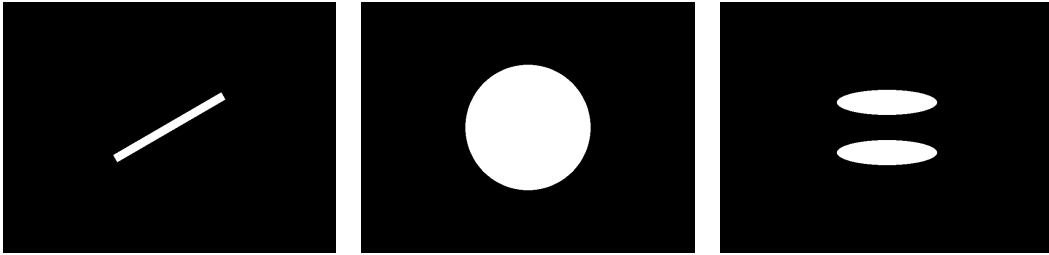
Figure 5.1: Representation of the three grain distributions used for the simulations of Poisson shot noises, Boolean random fields, and colored dead leaves models (see Fig. 5.2, Fig. 5.4, and Fig. 5.5). Left: a disc having a radius uniformly distributed over an interval $[0, r_{\max}]$; Middle: a rectangle randomly oriented according to a uniform distribution over $[0, \pi]$; Right: fixed set constituted of two disjoint ellipses.

cellular texture methods developed by Worley [156, 49] for the synthesis of volumetric textures. In another direction, an example-based texture synthesis algorithm inspired from the dead leaves model has been proposed by Gousseau [66].

5.2 Poisson Shot Noise of Colored Sets

As defined in the above introduction, the Poisson shot noise of colored random sets is the random field f_{PSN} obtained in summing the color a_j of each translated grain $x_j + X_j$. More formally,

$$f_{PSN}(y) = \sum_{(x_j, X_j, a_j) \in \Phi} a_j \mathbb{1}(y \in x_j + X_j),$$

where, similarly to the case of Boolean random fields, $\Phi = \{(x_j, X_j, a_j)\}$ is a Poisson process of $\mathbb{R}^d \times \mathcal{F} \times \mathbb{R}$ the intensity measure of which is $\lambda \mathcal{L}^d \otimes P_X \otimes P_a$.

As mentioned in Chapter 3, the statistics of f_{PSN} are known thanks to Campbell's theorem which provides an expression of the characteristic function of $f_{PSN}(x)$ (see Theorem B.2).

As said above, the main goal of this section is to illustrate and compare different germ-grain models. In particular we will show realizations of four germ-grain models using the same grain distributions P_X. These grain distributions are explicitly described in Fig. 5.1.

Fig. 5.2 shows several realization Poisson shot noises having the grain distributions described by Fig. 5.1. Note that with this model it is the accumulation of several objects which is highlighted. In particular, for high enough intensity the original shapes of the grains are not easily distinguished.
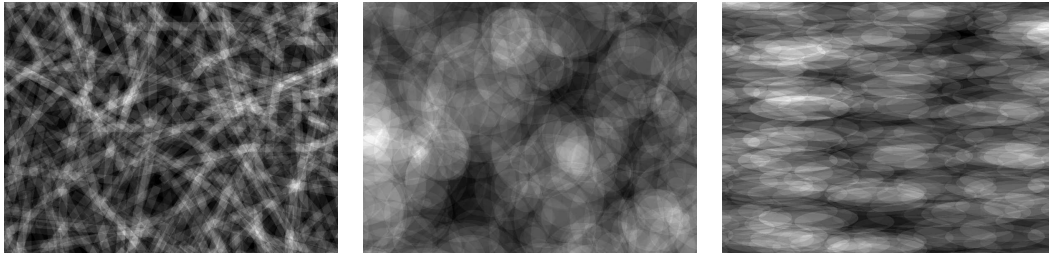
Figure 5.2:   Realizations of three different Poisson shot noises with uniformly distributed gray-levels. The grain distributions are the one presented in Fig. 5.1.
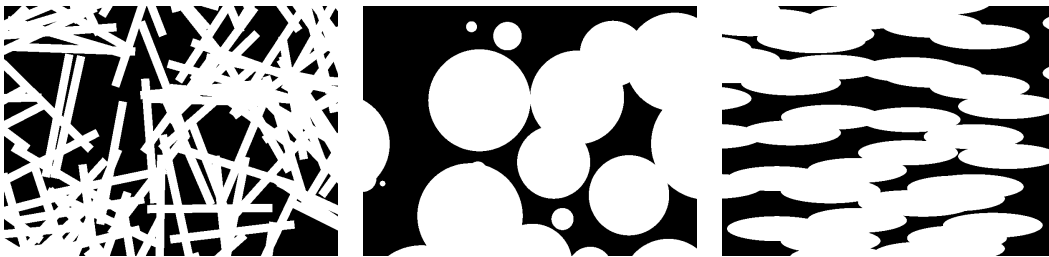
Figure 5.3:   Realizations of three different boolean random sets for which the grain distributions are the one presented in Fig. 5.1.

5.3   Boolean Models

Let us first introduce the *Boolean random set* [142, 136], a random set model which was first introduced by Matheron [107, 110, 143] and which combines the translated grains $x_j + X_j$ by union. The (homogeneous) *Boolean random set* with intensity λ and grain distribution P_X is the stationary random closed sets (RACS) Z_B defined by

$$Z_B = \bigcup_{j \in \mathbb{N}} x_j + X_j,$$

where $\{(x_j, X_j)\}$ is an independently marked stationary Poisson process in the space $\mathbb{R}^d \times \mathcal{F}$ having intensity measure $\lambda \mathcal{L}^d \otimes P_X$, $\lambda \geq 0$. Three examples of Boolean models constructed with the grain distributions described by Fig. 5.1 are represented in Fig. 5.3.

Several random field models can be considered as generalizations of Boolean random functions [138]. Here we consider a simple example called random Boolean islands. Let $\Phi = \{(x_j, X_j, a_j)\}$ be an independently marked Poisson process taking values in $\mathbb{R}^d \times \mathcal{F} \times [0, +\infty)$ and having intensity measure $\lambda \mathcal{L}^d \otimes P_X \otimes P_a$, $\lambda \geq 0$. We define the *Boolean random field* f_B associated to this process by

$$f_B(y) = \sup \left(\{0\} \cup \{a_j, \ y \in x_j + X_j\} \right).$$

Note that if $a_j = 1$ a.s., then f_B is the indicator function of the Boolean random

Figure 5.4:   Realizations of three different Boolean random fields with uniformly distributed gray-levels. The grain distributions are the one presented in Fig. 5.1.

set Z_B. More generally, remark that the upper-level sets of f_B are Boolean random sets: indeed, for all $t \geq 0$,

$$\{y,\ f_B(y) > t\} = \{y,\ \exists (x_j, X_j, a_j) \in \Phi,\ y \in x_j + X_j \text{ and } a_j > t\}$$
$$= \bigcup_{\Phi \cap \mathbb{R}^d \times \mathcal{F} \times (t, +\infty)} x_j + X_j,$$

that is to say $\{y,\ f_B(y) > t\}$ is the Boolean model associated with the Poisson process $\sum_\Phi \mathbb{1}\,(a_j > t)\,\delta_{x_j, X_j}$.

As explained in the introduction, the main goal of this chapter is to illustrate and compare different germ-grain models. In particular we will show realizations of three of these models using the same grain distributions P_X. These grain distributions are explicitly described in Fig. 5.1. Three examples of Boolean random fields having these grain distributions are represented by Fig. 5.4. Remark that with this model, the colored random sets are superimposed according to a hierarchy: the lighter sets are placed above the darker ones.

5.4   Colored Dead Leaves Model

The dead leaves model [37, 82, 18], also initially introduced by Matheron [108], is a germ-grain model where the interaction rule is occultation, that is where the grains $x_j + X_j$ hide each other. As mentioned in the introduction, for this germ-grain model the grains are chronologically ordered by a time $t_j \in (-\infty, 0)$, called *falling time*.

More precisely the leaves are the points of the Poisson process

$$\Phi = \{(t_j, x_j, X_j, a_j)\} \subset (-\infty, 0) \times \mathbb{R}^d \times \mathcal{F} \times \mathbb{R}$$

with intensity measure $\mathcal{L}^1 \otimes \mathcal{L}_d \otimes P_X \otimes P_a$. For each leaf (t_j, x_j, X_j, a_j), the random set $x_j + X_j$ is partially or totally hidden by its subsequent leaves, that is the leaves which fall after $t = t_j$. In the end, at time $t = 0$ the only remaining part of $x_j + X_j$
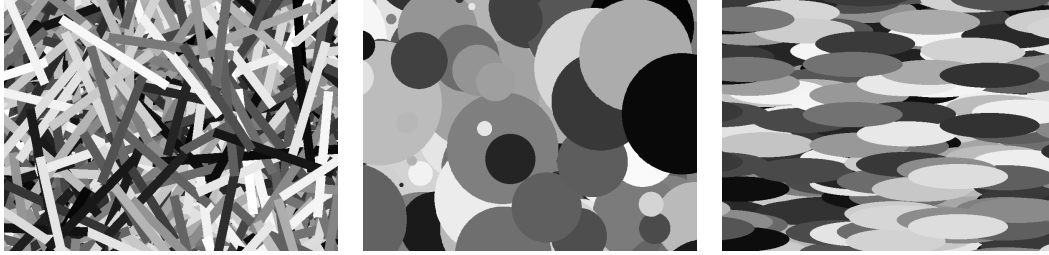
Figure 5.5:   Realizations of three different colored dead leaves r.f. with uniformly distributed gray-levels. The grain distributions are the one presented in Fig. 5.1.

is the *visible part* V_j, that is the set[3]

$$V_j = (x_j + X_j) \setminus \left(\bigcup_{(t_k,x_k,X_k,a_k)\in\Phi,\ t_k>t_j} x_k + X_k \right).$$

Let us precise that as soon as $E(\mathcal{L}^d(X)) > 0$, then all the Euclidean space $\mathbb{R}^d$ is covered by the random sets $x_j + X_j$, and consequently each point $y \in \mathbb{R}^d$ belongs to a unique visible part.

The *colored dead leaves r.f.* f_{CDL} is the r.f. defined in assigning to each $y \in \mathbb{R}^d$ the color a_j of the unique visible part V_j such that $y \in V_j$. More formally, f_{CDL} is defined by

$$f_{CDL}(y) = \sum_{(t_j,x_j,X_j,a_j)\in\Phi} a_j \mathbb{1}(y \in V_j),$$

but note that for each point y the sum has only one non null term.

As for the two previous models, three examples of colored dead leaves r.f. having the grain distributions described by Fig. 5.4 are shown in Fig. 5.5. Even though occultation between objects is also observable with Boolean r.f., remark that colored dead leaves r.f. vary from this first model. Indeed here the ordering of the objects is not related to their gray-level, and the whole domain is totally covered by objects.

5.5   Colored Tessellations

A colored tessellation is the random field obtained in assigning a random color to each subset of a random partition of the plane. The interaction principle which is at work for colored tessellations is arguably juxtaposition. We introduce below the formal definitions of the considered objects as they will be needed in Chapter 9.

A (random) tessellation is a random partition $\bigcup_j C_j = \mathbb{R}^d$ of the Euclidean space $\mathbb{R}^d$, the sets C_j being called *cells* of the tessellation. Even though random tessellations have been widely studied, there lacks a general acknowledged definition.

---

[3]Our definition of the *visible parts* V_j is slightly different from the one of [18]. This is because we do not enforce the visible parts to be closed sets.

This is principally because most studied tessellation models only involve convex cells [142, 136, 27]. Nevertheless, tessellations can be constituted of non convex (and even non connected) cells, such as the tessellation corresponding to the dead leaves model defined in [18]. Following [141, 18], we consider a quite general definition: A *(random) tessellation* is a point process $T = \sum_j \delta_{C_j}$ taking values in the set $\mathcal{K}'$ of non empty compact sets and which satisfies the following additional properties:

- For all compact set K, the number of sets C_i intersecting K is finite.

- For all $j \neq k$, $\mathrm{int}C_j \cap \mathrm{int}C_k \neq \emptyset$.

- $\bigcup_j C_k = \mathbb{R}^d$.

- For all j, $\mathcal{L}^d (\partial C_j) = 0$.

With these conditions, a.e. point $x \in \mathbb{R}^d$ belongs to a unique cell C_j. We will only consider *stationary* tessellations, that is tessellations such that for all $x \in \mathbb{R}^d$, $\sum_j \delta_{x+C_j} \overset{\mathrm{d}}{=} \sum_j \delta_{C_j}$. Thanks to the stationarity, for these tessellations every point $x \in \mathbb{R}^d$ a.s. belongs to a unique cell C_j.

Given a stationary tessellation $T = \sum_j \delta_{C_j}$ one defines a stationary random field f_T by associating a random intensity $a_j \in \mathbb{R}$ to each cell C_j. The real r.v. a_j are i.i.d. with common distribution P_a. More formally, the *colored tessellation* T_c associated to the tessellation T and with color distribution P_a is the independently marked point process $T_c = \sum_j \delta_{(C_j,a_j)}$, where the marks a_j have common distribution P_a. If μ denotes the intensity measure of the point process $\sum_j \delta_{C_j}$, then $T_c = \sum_j \delta_{(C_j,a_j)}$ has intensity measure $\mu \otimes P_a$. Its associated random field f_T is defined as follows: $f_T(x) = a_j$ where a_j is the color of the a.s. unique cell C_j containing x. Note that f_T can also be defined as a sum over the marked point process:

$$f_T(x) = \sum_j a_j \mathbb{1}\left(x \in C_j\right).$$

An example of a colored Poisson-Voronoi tessellation is reproduced in Fig. 5.6. Given a Poisson point process $\Pi = \{x_j\}$, the cells $\{C_j := C(x_j)\}$ of this tessellation are defined by

$$C(x_j) = \left\{ y \in \mathbb{R}^d,\ |y - x_j| \leq |y - x_k| \text{ for all } x_k \in \Pi \right\}.$$

We refer to [142, 136, 27] for further properties and references on Poisson-Voronoi tessellations.

5.6 Conclusion

Four different germ-grains models have been defined and illustrated. The interaction principle for these different models are supremum, addition, occultation and juxtaposition. Of course this list is not exhaustive. For example we could have mentioned multiplication for compound Poisson cascades [13, 29]. Moreover, in
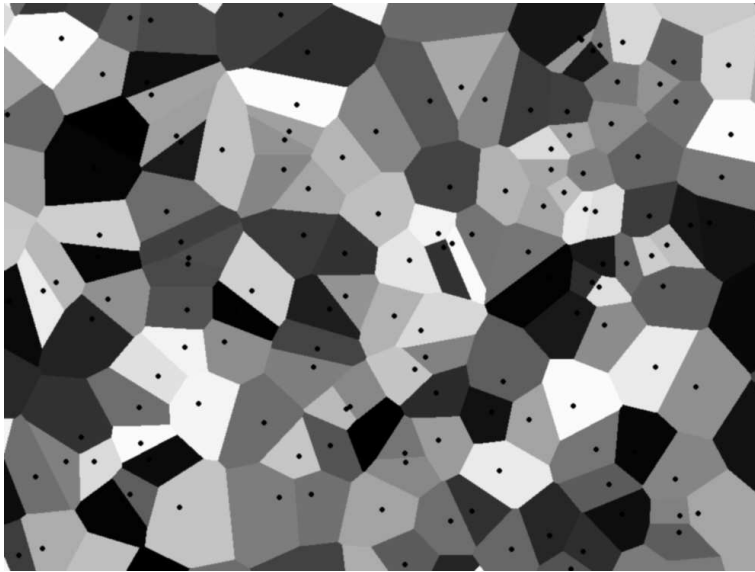
Figure 5.6: A realization of a colored Poisson-Voronoi tessellation with uniformly distributed gray levels. The points of the underlying Poisson point process are displayed in black.

the next chapter we will define and study a new germ-grain model for which the interaction principle is transparency (see Chapter 6).

Intuitively the realization of the germ-grain models defined in this chapter are functions of bounded variation when the grains have finite perimeter. This will be rigorously shown in Chapter 9 where the mean total variation per unit volume of all these germ-grain model will be computed.

As always, the presented models can be generalized in different ways. For example non Poisson point processes could be used. Besides, all the models can be generalized to the case where a random function is associated to each grain X_j in place of a constant color, as proposed by Jeulin [81, 82, 83].

The Transparent Dead Leaves Process

Contents

Abstract: This chapter introduces the transparent dead leaves (TDL) process, a new germ-grain model in which the grains are combined according to a transparency principle. Informally, this model may be seen as the superimposition of infinitely many semi-transparent objects. Properties of this new model are established and a simulation algorithm is proposed. A central limit theorem is then proved, showing that when varying the transparency of the grain from opacity to total transparency, the TDL process ranges from the dead leaves model to a Gaussian random field.

The work presented in this chapter is from the submitted paper [59].

6.1   Introduction

The main contribution of this chapter is the introduction and study of a new germ-grain model in which the grains are combined according to a transparency principle. To the best of our knowledge, this type of interaction between grains has not been studied before. As mentioned in the previous chapter (see Chapter 5),

| (a) A disc | (b) Initial scene | (c) Resulting scene |
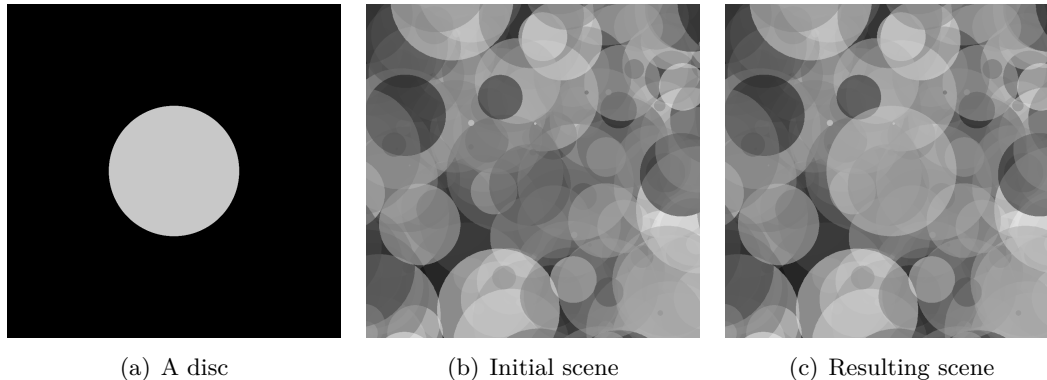
Figure 6.1: Addition of a transparent object. The transparency coefficient of the disc is $\alpha = 0.5$.

classical interaction principles between grains include *addition* for shot-noise processes [131, 75], *union* for Boolean models [142, 143, 136], *occultation* for dead leaves models [108, 82, 18] or *multiplication* for compound Poisson cascades [13, 29].

The proposed process, that we call *transparent dead leaves* (TDL), is obtained from a collection of grains (random closed sets) indexed by time, as for the dead leaves process of G. Matheron. We assume that each grain is given a random gray level (intensity). Informally, the process may be seen as the superimposition of *transparent* objects associated with the grains. Each time a new grain is added, new values are obtained as a linear combination of former values and the intensity of the added grain, as illustrated in Fig. 6.1. That is, when adding a grain X with gray level a, the current process $f : \mathbb{R}^2 \to \mathbb{R}$ is modified into g, defined for each $y \in \mathbb{R}^2$ as

$$g(y) = \begin{cases} \alpha a + (1 - \alpha)f(y) & \text{if } y \in X, \\ f(y) & \text{otherwise,} \end{cases} \tag{6.1}$$

where $\alpha \in (0, 1]$ is a transparency coefficient. The process is then defined as the sequential superimposition of grains of a suitable Poisson process $\sum_i \delta_{(t_i, x_i, X_i, a_i)}$.

The main motivation to define such a model originates from vision. Indeed, natural images are obtained from the light emitted by physical objects interacting in various ways. In the case of opaque objects, the main interaction is occlusion. That is, objects hide themselves depending on their respective positions with respect to the eye or the camera. A simple stochastic model for occlusion is given by the dead leaves model, which is therefore useful for the modeling of natural images [68, 28]. When objects are transparent, their interaction may be modeled by Formula (6.1). This is well known in the field of computer graphics, see e.g. [52] where the same principle is used for the creation of synthetic scenes. In this case, transparency is a source of heavy computations, especially in cases where objects are numerous (typically of the order of several thousands), e.g. in the case of grass, fur, smoke, fabrics, etc. The transparency phenomenon may also be encountered in other imag-

ing modality where images are obtained through successive reflexion-transmission steps, as in microscopy or ultrasonic imaging. A related non-linear image formation principle is at work in the field of radiography. In such cases, it is useful to rely on accurate stochastic texture models in order to be able to detect abnormal images. The TDL may be an interesting alternative to Gaussian fields that are traditionally used, see e.g. [69, 132].

In this paper, we first define the transparent dead leaves model in Section 6.2 and give some elementary properties in Section 6.3, where we also address the problem of simulating the process and show some realizations. The TDL covariance is then computed in Section 6.4. Eventually, it is shown in Section 6.5 that the normalized TDL converges, as α tends to zero, to a Gaussian process having the same covariance function as the shot noise associated with the grain X and with intensity one. Thus the TDLs with varying transparency coefficient α provide us with a family of models ranging from the dead leaves model to Gaussian fields.

6.2   Definition of the TDL Process

As explained in the introduction, the TDL process is obtained as the superimposition of transparent shapes. Formally it is defined from a marked Poisson point process, in a way similar to the dead leaves model (see Section 5.4 or [18]). Let $\mathcal{F}$ denote the set of closed sets of $\mathbb{R}^d$. On the state space

$$S := (-\infty, 0) \times \mathbb{R}^d \times \mathcal{F} \times \mathbb{R},$$

we define the point process[1]

$$\Phi := \sum_i \delta_{(t_i, x_i, X_i, a_i)}, \tag{6.2}$$

where

- $\{(t_i, x_i)\}$ is a stationary Poisson point process of intensity 1 in the half space $(-\infty, 0) \times \mathbb{R}^d$,

- $(X_i)_i$ is a sequence of i.i.d. random closed sets (RACS) with distribution P_X which is independent of the other random objects,

- $(a_i)_i$ is a sequence of i.i.d. real random variables (r.v.) with distribution P_a which is also independent of the other random objects.

Equivalently, by Theorem B.4, Φ is a Poisson point process with intensity measure $\mu := \lambda \otimes \mathcal{L}^d \otimes P_X \otimes P_a$, where λ denotes the restriction of the one-dimensional Lebesgue measure over $(-\infty, 0)$ and $\mathcal{L}^d$ denotes the d-dimensional Lebesgue measure over $\mathbb{R}^d$.

---

[1]Appendix B recalls basic definitions and properties of Poisson point processes useful for this chapter.

Each point $(t_i, x_i, X_i, a_i) \in \Phi$ is called a *leaf*. Having fixed a transparency coefficient $\alpha \in (0, 1]$, the TDL process f is defined by sequentially combining the elements of Φ according to Formula (6.1).

Definition 6.1 (Transparent Dead Leaves process). *The* Transparent Dead Leaves *process with transparency coefficient α associated to the Poisson process Φ defined by Equation (6.2) is the random field $f : \mathbb{R}^d \to \mathbb{R}$ defined by*

$$f(y) = \sum_{i \in \mathbb{N}} \mathbb{1}\left(y \in x_i + X_i\right) \alpha a_i \left(1 - \alpha\right)^{\left(\sum_{j \in \mathbb{N}} \mathbb{1}\left(t_j \in (t_i, 0) \text{ and } y \in x_j + X_j\right)\right)}. \qquad (6.3)$$

Let us justify that Formula (6.3) agrees with the informal description of the TDL process. Let y be a fixed point in $\mathbb{R}^d$, and let (t_i, x_i, X_i, a_i) be any leaf of the Poisson process Φ. If $y \notin x_i + X_i$ the contribution to $f(y)$ of the random shape $x_i + X_i$ is clearly 0. Otherwise, if $y \in x_i + X_i$ the contribution to $f(y)$ of the leaf (t_i, x_i, X_i, a_i) is αa_i multiplied by $(1 - \alpha)$ to the number of leaves fallen on the point y after the leaf (t_i, x_i, X_i, a_i), that is after time $t = t_i$. This number is exactly the exponent of $(1 - \alpha)$ in Equation (6.3):

$$\sum_{j \in \mathbb{N}} \mathbb{1}\left(t_j \in (t_i, 0) \text{ and } y \in x_j + X_j\right).$$

Remark (Variable transparency). For the sake of simplicity, the transparency parameter α is assumed to be the same for all objects. However, one may attach a random transparency α_i to every objects in Definition 6.1 and generalize the results of Sections 6.3 and 6.4, as will be briefly commented thereafter.

Since the distribution of the Poisson process Φ is invariant under shifts of the form $(t, x, X, a) \mapsto (t, x + y, X, a)$, the TDL process f is strictly stationary. Before establishing further properties of the TDL process f, let us introduce some notation and specify several assumptions.

Notations: Define $\beta := 1 - \alpha$ and let X and a denote respectively a RACS with distribution P_X and a r.v. with distribution P_a which are both independent of all the other random objects. The expectation with respect to the distribution of Φ is denoted by $\mathbb{E}$ (e.g. $\mathbb{E}(f(y))$) whereas the expectation with respect to the distributions $P_X \otimes P_a$ of the marks (X, a) is denoted by E (e.g. $E\left(\mathcal{L}^d(X)\right)$, $E(a)$). Finally, γ_X denotes the mean covariogram of the RACS X, that is the function defined by $\gamma_X(\tau) = E\left(\mathcal{L}^d(X \cap \tau + X)\right)$, $\tau \in \mathbb{R}^d$ (we refer to Section 8.4 of Chapter 8 for properties of the mean covariogram; see also [110, 100]).

Assumptions: Throughout the chapter, it is assumed that

$$0 < E\left(\mathcal{L}^d(X)\right) < +\infty.$$

This hypothesis ensures that each point $y \in \mathbb{R}^d$ is covered by a countable infinite number of leaves of Φ, whereas the number of leaves falling on y during a finite time interval $[s_1, s_2]$ is a.s. finite. We also assume that $E(|a|^2) < \infty$.

6.3 First-Order Distribution and the TDL Process

In this section the distribution of the r.v. $f(y)$ is given and a simulation procedure is presented and illustrated.

6.3.1 The Poisson Process of the Leaves Intersecting a Set

As one can observe from Equation (6.3), the only leaves which have a contribution to the sum defining $f(y)$ are the leaves (t_i, x_i, X_i, a_i) such that $y \in x_i + X_i$. When considering the restriction of f to a Borel set G the only leaves of interest are the ones intersecting G, *i.e.* the leaves (t_i, x_i, X_i, a_i) such that $x_i + X_i \cap G \neq \emptyset$. The next proposition gives the distribution of such leaves, a result to be used further in this chapter. We first recall two notation: if A and B are two Borel sets then $\check{A} = \{-x : x \in A\}$ and $A \oplus B = \{x + y : x \in A \text{ and } y \in B\}$. Remark that $x + X \cap G \neq \emptyset \iff x \in G \oplus \check{X}$.

Proposition 6.1 (The Poisson process of the leaves intersecting a Borel set). *Let $G \subset \mathbb{R}^d$ be a Borel set such that $0 < E\left(\mathcal{L}^d\left(X \oplus \check{G}\right)\right) < +\infty$ and let Φ be the Poisson process on $S = (-\infty, 0) \times \mathbb{R}^d \times \mathcal{F} \times \mathbb{R}$ with intensity measure $\mu = \lambda \otimes \mathcal{L}^d \otimes P_X \otimes P_a$. Denote by Φ^G the point process of the leaves of Φ which intersect G, that is*

$$\Phi^G = \{(t, x, X, a) \in \Phi : x + X \cap G \neq \emptyset\},$$

and let us note $\mathcal{A}^G \subset \mathbb{R}^d \times \mathcal{F}$ the set $\mathcal{A}^G = \{(x, X) : x + X \cap G \neq \emptyset\}$. Then Φ^G is a Poisson process on S with intensity measure

$$\mu^G = \lambda \otimes \left(\mathcal{L}^d \otimes P_X\right)_{\llcorner \mathcal{A}^G} \otimes P_a.$$

It is an independently marked Poisson process with ground process $\Pi^G = \left\{t : (t, x, X, a) \in \Phi^G\right\}$, an homogeneous Poisson process on $(-\infty, 0)$ of intensity $E\left(\mathcal{L}^d\left(X \oplus \check{G}\right)\right)$, and with mark distribution

$$\frac{1}{E\left(\mathcal{L}^d\left(X \oplus \check{G}\right)\right)} \left(\mathcal{L}^d \otimes P_X\right)_{\llcorner \mathcal{A}^G} \otimes P_a.$$

Proof. Φ^G is the restriction of the Poisson process Φ to the measurable set

$$\left\{(t, x, X, a) \in (-\infty, 0) \times \mathbb{R}^d \times \mathcal{F} \times \mathbb{R} : (x, X) \in \mathcal{A}^G\right\},$$

thus Φ^G is a Poisson process and its intensity measure μ^G is the restriction of μ to the above set (see Proposition B.3). As for the interpretation of Φ^G as an independently marked one-dimensional Poisson process, it is based on the factorization of the intensity measure μ^G (see Corollary B.2 or [11, Section 1.8], [136, Section 3.5]). Indeed we have

$$0 < \mathcal{L}^d \otimes P_X \left(\mathcal{A}^G\right) = \int_{\mathcal{F}} \int_{\mathbb{R}^d} \mathbb{1}\left\{y \in G \oplus \check{Y}\right\} \mathcal{L}^d(dy) P_X(dY) = E\left(\mathcal{L}^d\left(X \oplus \check{G}\right)\right) < +\infty,$$

and thus we can write

$$\mu^G = E\left(\mathcal{L}^d\left(X \oplus \check{G}\right)\right) \lambda \otimes \left[\frac{1}{E\left(\mathcal{L}^d\left(X \oplus \check{G}\right)\right)} \left(\mathcal{L}^d \otimes P_X\right)_{\llcorner \mathcal{A}^G} \otimes P_a\right],$$

where the measure between square brackets is a probability distribution. $\qquad \square$

6.3.2   First-Order Distribution

Proposition 6.2 (First-order distribution). *Let y be a point in $\mathbb{R}^d$. Then there exists a subsequence $(a(y, k))_{k \in \mathbb{N}}$ of i.i.d. r.v. with distribution P_a such that*

$$f(y) = \alpha \sum_{k=0}^{+\infty} a(y, k)\beta^k.$$

In particular we have $\mathbb{E}(f(y)) = \mathbb{E}(a)$ and $\mathrm{Var}\,(f(y)) = \dfrac{\alpha}{2 - \alpha}\,\mathrm{Var}(a)$.

Proof. According to Proposition 6.1 the point process $\Phi^{\{y\}}$ of the leaves which cover y is an independently marked Poisson process, the ground process of which is a Poisson process on $(-\infty, 0)$ with intensity $E(\mathcal{L}^d(X)) < +\infty$. Hence the falling times of the leaves of $\Phi^{\{y\}}$ are a.s. distinct and we can number the leaves

$$(t(y, k), x(y, k), X(y, k), a(y, k)), \ \ k \in \mathbb{N},$$

according to an anti-chronological order:

$$0 > t(y, 0) > t(y, 1) > t(y, 2) > \ldots.$$

Proposition 6.1 also gives the distribution of the marks $(x(y, k), X(y, k), a(y, k))$, and in particular it shows that the r.v. $a(y, k)$, $k \in \mathbb{N}$ are i.i.d. with distribution P_a. As already mentioned, the only leaves involved in the sum which defines $f(y)$ are the leaves of $\Phi^{\{y\}}$. Besides, using the above numbering we have for all $k \in \mathbb{N}$

$$\sum_{(t_j, x_j, X_j, a_j) \in \Phi} \mathbb{1}\,(t_j \in (t(y, k), 0) \text{ and } y \in x_j + X_j) = k.$$

Hence Equation (6.3) becomes

$$f(y) = \alpha \sum_{k=0}^{+\infty} a(y, k)\beta^k,$$

and the result follows. $\qquad \square$

Remark (Influence of the transparency coefficient α). Let us write f_α for the TDL process with transparency coefficient $\alpha \in (0, 1]$. Proposition 6.2 shows that the expectation of f_α does not depend on α. As for the variance, $\mathrm{Var}\,(f_\alpha(y)) = \dfrac{\alpha}{2 - \alpha}\,\mathrm{Var}(a)$ decreases as α decreases. Besides $\mathrm{Var}\,(f_\alpha(y))$ tends to 0 as α tends

to 0 (recall that the model is not defined for $\alpha = 0$). However, a central limit theorem for random geometric series [20] shows that for all $y \in \mathbb{R}^d$ the family of r.v. $\left(\dfrac{f_\alpha(y) - \mathbb{E}(f_\alpha)}{\sqrt{\mathrm{Var}(f_\alpha)}} \right)_\alpha$ converges in distribution to a standard normal distribution as α tends to 0. This pointwise convergence result will be extended in Section 6.5, where it will be shown that the family of normalized random fields $\left(y \mapsto \dfrac{f_\alpha(y) - \mathbb{E}(f_\alpha)}{\sqrt{\mathrm{Var}(f_\alpha)}} \right)_\alpha$ converges in the sense of finite-dimensional distributions.

6.3.3 Simulation of the TDL Process

In this section we draw on Proposition 6.2 to obtain a simulation algorithm for the restriction of the TDL process f to a bounded domain $U \subset \mathbb{R}^d$. The algorithm is based on a coupling from the past procedure, as the algorithm developed by Kendall and Thönnes [90] for simulating the dead leaves model (see also [82, 100]). This algorithm consists in sequentially superimposing transparent random objects but, contrary to the forward procedure described by Equation (6.1), each new object is placed *below* the former objects. In the case of the dead leaves model, this yields a perfect simulation algorithm. For the TDL process f, simulation is not perfect since the values $f(y)$ are the limits of convergent series. Nevertheless, supposing that the intensities a_i are bounded, we propose for any $\varepsilon > 0$ an algorithm which produces an approximation $\tilde{f}$ of f. This approximation satisfies

$$\mathbb{P}\left(\sup_{y \in U} \left| f(y) - \tilde{f}(y) \right| \leq \varepsilon \right) = 1$$

therefore providing a kind of perfect simulation with precision $\varepsilon > 0$.

In the remaining of this section we suppose that the colors a_i are a.s. bounded by $A > 0$. The control of the precision is based on the following elementary lemma.

Lemma 6.1 (Precision associated to the leaves layer)**.** *Let $y \in \mathbb{R}^d$ and let*

$$\tilde{f}_n(y) = \alpha \sum_{k=0}^{n-1} a(y, k) \beta^k$$

be the restriction of the sum defining $f(y)$ to the n latest leaves which have fallen on y. Then

$$\left| f(y) - \tilde{f}_n(y) \right| \leq A\beta^n.$$

Lemma 6.1 shows that to approximate $f(y)$ with a tolerance $\varepsilon > 0$ it is enough to cover the point y with (at least) $N(\varepsilon)$ leaves, where $N(\varepsilon)$ is the smallest integer n such that $A\beta^n \leq \varepsilon$, that is $N(\varepsilon) = \left\lceil \dfrac{\log(\varepsilon/A)}{\log(\beta)} \right\rceil$. This yields the following algorithm.

Algorithm 6.1 (Simulation of the TDL process with tolerance $\varepsilon > 0$)**.** *Let $U \subset \mathbb{R}^d$ be a bounded set such that $0 < E\left(\mathcal{L}^d \left(X \oplus \check{U} \right) \right) < +\infty$ and let $\varepsilon > 0$. Given a precision $\epsilon > 0$, an approximation $\tilde{f}$ of the TDL process f is computed by controlling the number of leaves L at each point:*

- **Initialization:** *For all $y \in U$, $\tilde{f}(y) \leftarrow 0$; $L(y) \leftarrow 0$;*

- **Computation of the required number of leaves:** $N(\varepsilon) = \left\lceil \dfrac{\log(\varepsilon/A)}{\log(\beta)} \right\rceil$;

- **Iteration:** *While $\left(\inf_{y \in U} L(y) < N(\varepsilon) \right)$ add a new leaf:*

  1. **Draw a leaf (x, X, a) hitting U:**
     (a) *Draw $X \sim P_X$;*
     (b) *Draw x uniformly in $U \oplus \check{X}$;*
     (c) *Draw $a \sim P_a$;*
  2. **Add the leaf (x, X, a) to $\tilde{f}$:** *for all $y \in U$, $\tilde{f}(y) \leftarrow \tilde{f}(y) + \mathbb{1}(y \in x + X)\, \alpha a \beta^{L(y)}$;*
  3. **Update the leaves layer L:** *for all $y \in U$, $L(y) \leftarrow L(y) + \mathbb{1}(y \in x + X)$;*

Clearly Algorithm 6.1 a.s. converges if every point of U is covered by $N(\varepsilon)$ leaves in an a.s. finite time. This is always the case if U is a discrete set, since $E\left(\mathcal{L}^d(X)\right) > 0$. It is also true for any bounded set U if there exists a non empty open ball B such that $E\left(\mathcal{L}^d(X \ominus B)\right) > 0$ [18], where $X \ominus B = \{x \in X, \ x + B \subset X\}$ is the erosion of X by B [110, 100].

Several realizations of some TDL processes are represented in Fig. 6.2. Remark that as soon as $\alpha < 1$, the TDL process is not piecewise constant: any region is intersected by the boundaries of some leaves, producing discontinuities.

6.4   Covariance of the TDL Process

This section is devoted to the computation of the covariance of the TDL. A classical way to achieve this would be to rely on Palm calculus, yielding relatively heavy computations in this case. Instead, we chose an alternative way relying on some no-memory property of the TDL, as explained below. For comparison, the computation of the TDL covariance using Palm calculus is reproduced in the companion appendix on the TDL process (see Section D.2 of Appendix D).

The following proposition is an extension of the fact that if $0 > t_0 > t_1 > t_2 > \ldots$ is an homogeneous Poisson process on $(-\infty, 0)$ then the shifted process $0 > t_1 - t_0 > t_2 - t_0 > t_3 - t_0 > \ldots$ is also a Poisson process with the same distribution [91, Chapter 4]. The proof of this proposition is given in Section B.2.2 of Appendix B.

Proposition 6.3 (Last hitting leaf and the Poisson process preceding the last hit)**.**
Let Ψ be a Poisson process in $(-\infty, 0) \times E$ with intensity measure of the form $\lambda \otimes \mu$ where λ is the one-dimensional Lebesgue measure on $(-\infty, 0)$ and μ is a measure on E. Let $A \subset E$ be a measurable set such that $0 < \mu(A) < +\infty$. Define

$$t_0 = \sup\{t_i \mid (t_i, y_i) \in \Psi \cap ((-\infty, 0) \times A)\},$$

(a) Original shape   (b) $\alpha = 1$ (occlusion)   (c) $\alpha = 0.7$

(d) $\alpha = 0.4$ (e) $\alpha = 0.05$ (f) $\alpha = 0.05$, enhanced contrast
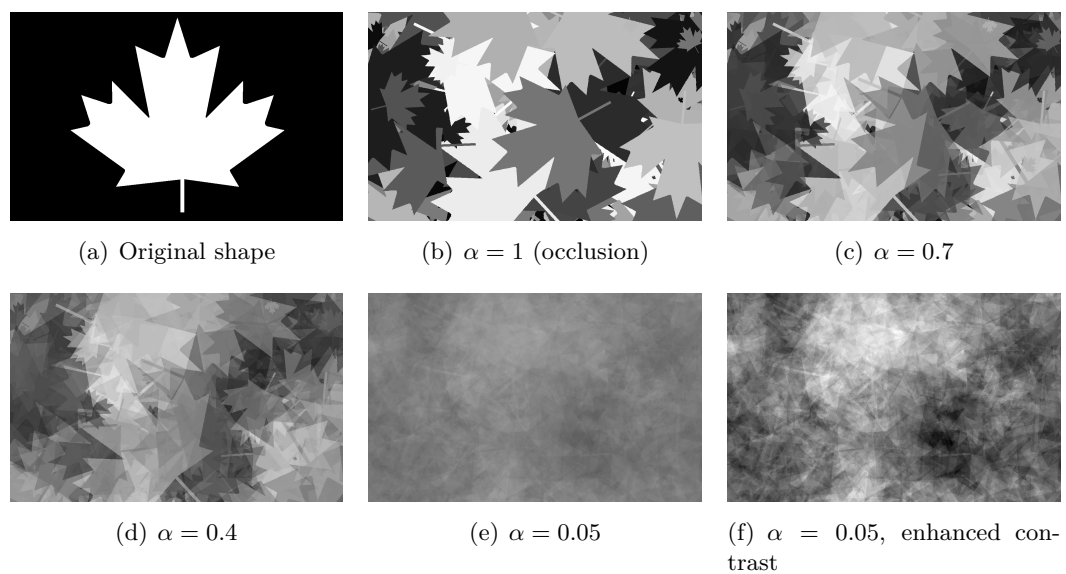
Figure 6.2: TDL realizations with various transparency coefficients α. The RACS X_i are all obtained from the original shape of Fig. 6.2(a) in applying a rotation of angle $\theta \sim Unif(0, 2\pi)$ and a homothety of factor $r \sim Unif(0,1)$, and $P_a = Unif(0,255)$. For $\alpha = 1$, one obtains a colored dead leaves model. As soon as the leaves are transparent ($\alpha < 1$), one can distinguish several layers of leaves and not only the leaves on top. For $\alpha = 0.05$, the variance of the TDL process is nearly 0 (see Proposition 6.2). Enhancing the contrast of the image (Fig.6.2(f)) reveals the structure of the image.

y_0 *the a.s. unique* $y \in E$ *such that* $(t_0, y) \in \Psi \cap ((-\infty, 0) \times A)$, *and*

$$\Psi_{t_0} = \sum_{(t_i, y_i) \in \Psi} \mathbb{1} \left(t_i < t_0 \right) \delta_{(t_i - t_0, y_i)}.$$

Then

- t_0, y_0, *and* Ψ_{t_0} *are mutually independent.*

- $-t_0$ *has an exponential distribution with parameter* $\mu(A)$.

- y_0 *has distribution* Q_A *defined for all* $B \in \mathcal{B}(E)$ *by* $Q_A(B) = \dfrac{\mu(B \cap A)}{\mu(A)}$.

- Ψ_{t_0} *is a Poisson process with intensity measure* $\lambda \otimes \mu$, *i.e.* Ψ_{t_0} *has the same distribution as* Ψ.

In the following of this section, Proposition 6.3 will be applied to the Poisson process Φ of the colored leaves to compute some statistics of the TDL process f. As a first example, let us reobtain the expectation of f by using Proposition 6.3. Let $y \in \mathbb{R}^d$ and let us note (t_0, x_0, X_0, a_0) the leaf which hits y at the maximal time t_0. Then one can decompose $f(y)$ into

$$f(y) = \alpha a_0 + \beta f_{t_0}(y), \tag{6.4}$$

where f_{t_0} is the TDL process associated to the time-shifted point process Φ_{t_0}. According to Proposition 6.3, a_0 has distribution P_a and both point processes Φ and Φ_{t_0} have the same distribution. Consequently, $f(y)$ and $f_{t_0}(y)$ also have the same distribution, and in particular the same expectation. Hence the above decomposition of $f(y)$ yields to the equation

$$\mathbb{E}\left(f(y)\right) = \alpha E(a) + \beta \mathbb{E}\left(f(y)\right),$$

which gives $\mathbb{E}\left(f(y)\right) = E(a)$, in accordance with Proposition 6.2.

The very same method is used below to compute the covariance of f. Besides, this method will be applied in Section D.1.3.1 to derive a decomposition of the multivariate characteristic function of the TDL process. The same method will also be applied in Chapter 9 to compute the mean total variation of the TDL process (see Section 9.6).

Recall that $\gamma_X(\tau) = E\left(\mathcal{L}^d(X \cap \tau + X)\right)$ is the mean covariogram of X.

Proposition 6.4 (Covariance of the TDL process)**.** *The TDL process f is a square-integrable stationary random field and its covariance is given by*

$$\mathrm{Cov}(f)(\tau) = \frac{\alpha \gamma_X(\tau)}{2E(\mathcal{L}^d(X)) - \alpha \gamma_X(\tau)} \, \mathrm{Var}(a), \ \tau \in \mathbb{R}^d.$$

Proof. Let y and z be such that $z - y = \tau$. Let us note (t_0, x_0, X_0, a_0) the last leaf which hits y or z at the maximal time t_0, and let Φ_{t_0} be the corresponding time-shifted Poisson process. According to Proposition 6.3, (x_0, X_0, a_0) is independent of Φ_{t_0}. In addition $\Phi_{t_0} \overset{d}{=} \Phi$, and consequently, noting f_{t_0} the TDL associated with Φ_{t_0}, $(f_{t_0}(y), f_{t_0}(z)) \overset{d}{=} (f(y), f(z))$. Proposition 6.3 also shows that a_0 has distribution P_a. As for the distribution of (x_0, X_0), a straightforward computation shows that

$$\mathcal{L}^d \otimes P_X\left(\{(x, X), \ \{y, z\} \cap x + X \neq \emptyset\}\right) = E\left(\mathcal{L}^d\left(X \oplus \{-y, -z\}\right)\right) = 2\gamma_X(0) - \gamma_X(\tau)$$

and

$$\mathcal{L}^d \otimes P_X\left(\{(x, X), \ \{y, z\} \subset x + X\}\right) = E\left(\mathcal{L}^d\left(-y + X \cap -z + X\right)\right) = \gamma_X(\tau).$$

Hence we have

$$\mathbb{P}\left(\{y, z\} \subset x_0 + X_0\right) = \frac{\mathcal{L}^d \otimes P_X\left(\{(x, X), \ \{y, z\} \subset x + X\}\right)}{\mathcal{L}^d \otimes P_X\left(\{(x, X), \ \{y, z\} \cap x + X \neq \emptyset\}\right)} = \frac{\gamma_X(\tau)}{2\gamma_X(0) - \gamma_X(\tau)},$$
$$(6.5)$$

and by symmetry and complementarity

$$\mathbb{P}\left(y \in x_0 + X_0 \text{ and } z \notin x_0 + X_0\right) = \mathbb{P}\left(z \in x_0 + X_0 \text{ and } y \notin x_0 + X_0\right) = \frac{\gamma_X(0) - \gamma_X(\tau)}{2\gamma_X(0) - \gamma_X(\tau)}.$$

As a shorter notation we write $m = \mathbb{E}(a) = \mathbb{E}(f)$. We have to compute $\mathrm{Cov}\left(f(y), f(z)\right) = \mathbb{E}\left((f(y) - m)(f(z) - m)\right)$. Conditioning with respect to the coverage of the last leaf (t_0, x_0, X_0, a_0) we have

$$\mathbb{E}\left((f(y) - m)(f(z) - m)\right)$$
$$= \mathbb{E}\left((f(y) - m)(f(z) - m) \,|\, \{y, z\} \subset x_0 + X_0\right) \frac{\gamma_X(\tau)}{2\gamma_X(0) - \gamma_X(\tau)}$$
$$+ \mathbb{E}\left((f(y) - m)(f(z) - m) \,|\, y \in x_0 + X_0 \text{ and } z \notin x_0 + X_0\right) \frac{\gamma_X(0) - \gamma_X(\tau)}{2\gamma_X(0) - \gamma_X(\tau)}$$
$$+ \mathbb{E}\left((f(y) - m)(f(z) - m) \,|\, z \in x_0 + X_0 \text{ and } y \notin x_0 + X_0\right) \frac{\gamma_X(0) - \gamma_X(\tau)}{2\gamma_X(0) - \gamma_X(\tau)}.$$

By symmetry it is clear that the two last terms of the above sum are equal. On the event $\{\{y, z\} \subset x_0 + X_0\}$ we have

$$f(y) - m = \alpha(a_0 - m) + \beta\left(f_{t_0}(y) - m\right) \text{ and } f(z) - m = \alpha(a_0 - m) + \beta\left(f_{t_0}(z) - m\right),$$

so that

$$(f(y) - m)(f(z) - m) = \alpha^2(a_0 - m)^2 + \beta^2\left(f_{t_0}(y) - m\right)\left(f_{t_0}(z) - m\right)$$
$$+ \alpha\beta(a_0 - m)\left(\left(f_{t_0}(y) - m\right) + \left(f_{t_0}(z) - m\right)\right).$$

By Proposition 6.3, a_0, (x_0, X_0), and $(f_{t_0}(y), f_{t_0}(z))$ are mutually independent, hence

$$\mathbb{E}\left((f(y) - m)(f(z) - m) \,|\, \{y, z\} \subset x_0 + X_0\right)$$
$$= \alpha^2 \mathbb{E}\left((a_0 - m)^2\right) + \beta^2 \mathbb{E}\left((f_{t_0}(y) - m)(f_{t_0}(z) - m)\right)$$
$$= \alpha^2 \mathrm{Var}(a) + \beta^2 \mathrm{Cov}\left(f(y), f(z)\right).$$

On the event $\{y \in x_0 + X_0 \text{ and } z \notin x_0 + X_0\}$ we have

$$f(y) - m = \alpha(a_0 - m) + \beta\left(f_{t_0}(y) - m\right) \quad \text{and} \quad f(z) - m = f_{t_0}(z) - m.$$

Using the above arguments,

$$\mathbb{E}\left(\left(f(y) - m\right)\left(f(z) - m\right) | y \in x_0 + X_0 \text{ and } z \notin x_0 + X_0\right) = \beta \operatorname{Cov}\left(f(y), f(z)\right).$$

Coming back to the above decomposition of $\mathbb{E}\left(\left(f(y) - m\right)\left(f(z) - m\right)\right)$, one obtains an equation involving the covariance $\operatorname{Cov}\left(f(y), f(z)\right)$, the values $\gamma_X(0)$ and $\gamma_X(\tau)$ of the mean covariogram of X, and the variance $\operatorname{Var}(a)$. Simplifying this equation one obtains the enunciated formula. $\square$

Remark (Variable transparency and second order property)**.** The technique used in this section enables to generalize second order formulas to the case where the transparency parameter α is assumed to be different for each object, that is, when it is assumed that each object X_i is assigned a transparency α_i distributed as a random variable α and independent of other objects. First, it is straightforward to show that in this case we still have $\mathbb{E}(f(y)) = E(a)$. Then, a simple application of Formula (6.4) yields $\operatorname{Var}\left(f(y)\right) = E(\alpha^2)\operatorname{Var}(a)(2E(\alpha) - E(\alpha^2))^{-1}$. Observe that a direct computation starting from the definition of f would be much more painful. Eventually, applying the same technique enables to show that the covariance of the model with variable transparency satisfies, for $\tau \in \mathbb{R}^d$,

$$\operatorname{Cov}(f)(\tau) = \frac{E(\alpha^2)\gamma_X(\tau)}{2E(\alpha)E(\mathcal{L}^d(X)) - E(\alpha^2)\gamma_X(\tau)} \operatorname{Var}(a).$$

6.5 Gaussian Convergence as the Objects Tend to Be Fully Transparent

Recall that the TDL process with transparency coefficient α is denoted f_α.

Theorem 6.1 (Normal convergence of the TDL process)**.** *Suppose that* $\operatorname{Var}(a) > 0$. *Then, as the transparency coefficient α tends to 0, the family of random fields* $\left(\dfrac{f_\alpha - \mathbb{E}\left(f_\alpha\right)}{\sqrt{\operatorname{Var}\left(f_\alpha\right)}}\right)_\alpha$ *converges in the sense of finite-dimensional distributions to a centered stationary Gaussian random field with covariance function*

$$C(\tau) = \frac{\gamma_X(\tau)}{E(\mathcal{L}^d(X))} = \frac{\gamma_X(\tau)}{\gamma_X(0)}.$$

The proof of Theorem 6.1 is postponed to the companion appendix (see Section D.1 of Appendix D). It relies on on a the method of moments for convergence in distribution and, as for the computation of the covariance of the TDL process (see Proposition 6.4), it involves a conditioning with respect to the coverage of a last hitting leaf. This theorem involves families of r.v. having a controlled dependency

(a) $\alpha = 1$ (b) $\alpha = 0.5$ (c) $\alpha = 0.2$

(d) $\alpha = 0.1$ (e) $\alpha = 0.01$ (f) Limit Gaussian r.f.
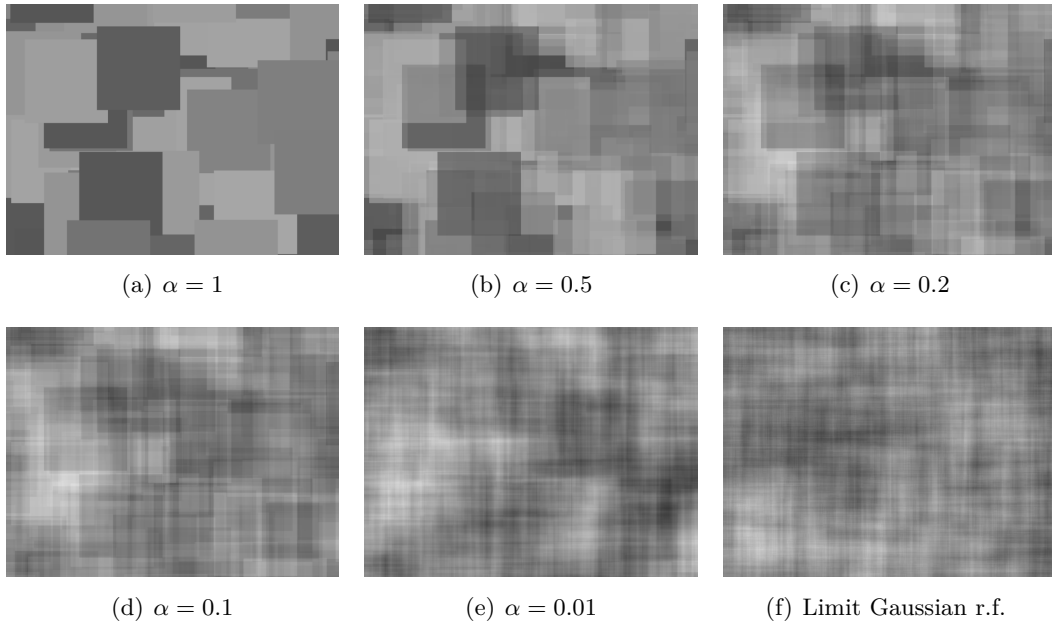
Figure 6.3: From colored dead leaves to Gaussian random fields: Visual illustration of the normal convergence of the normalized TDL processes $\left(\frac{f_\alpha - \mathbb{E}\left(f_\alpha\right)}{\sqrt{\operatorname{Var}\left(f_\alpha\right)}} \right)_\alpha$ (see Theorem 6.1). As α decreases to 0 the normalized TDL realizations look more and more similar to the Gaussian texture 6.3(f).

structure. Here this control is basically obtained from the obvious observation that a leaf covers at most once each considered points (see Section D.1 for the details).

The normal convergence of the normalized family of r.v. $\left(\frac{f_\alpha - \mathbb{E}\left(f_\alpha\right)}{\sqrt{\operatorname{Var}\left(f_\alpha\right)}} \right)_\alpha$ is illustrated by Fig. 6.3. The five first images are normalized TDL realizations obtained from the same random colored leaves but with various transparency coefficients α. The last image is a realization of the limit Gaussian random field given by Theorem 6.1. Observe that this Gaussian field is also the limit of the normalized shot noise associated with the grain distribution P_X when the intensity of germs tends to infinity (see Theorem 3.1 or [75]).

6.6 Conclusion

The transparent dead leaves model has been introduced and studied. It has been shown that, when varying the transparency coefficient α, the TDL process provides a family of r.f. which ranges from the colored dead leaves r.f. to Gaussian r.f.

The presented study of the TDL process might be extended in several ways. In Chapter 9, relying on the method introduced for the computation of the TDL covariance, the mean variation of the TDL process will be computed (see Section 9.6). It

might also be of interest to study the properties of the TDL model when the size of the grains varies according to a scaling law since, for both the dead leaves model and the shot noise model, scaling laws yield non Gaussian limit regimes [68, 15, 88, 16]. Another direction would be to investigate for possible applications of this theoretical study in computer graphics where the superimposition of numerous transparent objects is used to simulate certain materials [52].

Part III

Variation of Random Fields

General Introduction of Part III: Variation of Random Fields

Functions of bounded variation are an important model in image processing. Ever since the seminal paper of Rudin, Osher and Fatemi [133], the total variation has been widely used for various tasks such as denoising with the $TV - L^2$ and $TV - L^1$ models [133, 30, 117, 7, 32], zooming [71] or also deconvolution [33].

Concerning textures, the total variation generally appears in the problem of decomposing on image in a cartoon part (or geometric part) and a textural part following the framework proposed by Meyer [112]. For this problem it is considered that the total variation of a textural part should be high or even infinite, whereas the total variation of the cartoon part should be low, in comparison with another norm adapted to oscillatory images [112, 148, 8, 9, 23]. Another work which relates total variation and textures is the texture synthesis method proposed by Fadili and Peyré [55]. Their algorithm, which belongs to the general framework described in [125], consists in projecting a texture image on the set of images $\{f, \ TV(f) \leq c\}$ while preserving the histogram of the initial texture (by alternate projections). Starting from white noise, this procedure permits to generate generic piecewise smooth textures presenting sharp edges [55].

Even though the total variation of textures is generally considered to be high or even infinite, to the best of our knowledge little is known on the total variation of classic texture models such as Gaussian random fields, shot noises, or the other germ-grain models presented in Chapters 5 and 6. However, the random geometric images displayed in Chapter 5 are images of bounded variation, and intuitively their total variation depends on the geometry of the grains. Hence it is natural to ask the following question: **What is the mean total variation of the germ-grain models presented in Chapters 5 and 6?**

Even though the above question is intuitively simple, provide a solution to the problem raised by this question necessitates the development of several theoretical results, and it will be a central subject of the last three chapters of this thesis.

To the best of our knowledge random fields (r.f.) of bounded variation over $\mathbb{R}^d$ have never been studied for $d \geq 2$, with the exception of the short paper [80]. The object of Chapter 7 is to properly define random fields of bounded variation, to give practical necessary and sufficient conditions characterizing r.f. of bounded variation, as well as to establish simple expression for their mean total variation.

Let us recall that, by definition, the variation of an indicator function is its perimeter [6, 54]. Hence as a particular case of our results on the mean variation of r.f., one obtains formulas for the mean perimeter of random sets. These formulas extend known results from the theory of random sets which are due to Matheron [107, 110, 100]. In order to focus on the specificities of random sets as well as to discuss the links with the rich literature on the subject, a separated chapter is devoted to the variation of random sets (Chapter 8).

Finally, in Chapter 9, we will demonstrate the interest of the general results of

Chapters 7 and 8 in computing the mean variation of various random field models, namely Gaussian random fields, the germ-grain models presented in Chapter 5, as well as the transparent dead leaves model introduced in Chapter 6.

Random Fields of Bounded Variation

Contents

Abstract: The main purpose of this chapter is to define random fields of bounded variation and to study their mean total variation. Simple formulas are obtained for the mean total directional variation of random fields, based on known formulas for the directional variation of deterministic functions. It is also shown that the mean variation of stationary random fields is proportional to the Lebesgue measure. An expression of the constant of proportionality, called the *variation intensity*, is established. This expression shows in particular that the variation intensity only depends on the family of two-dimensional distributions of the stationary random field.

7.1   Introduction

This chapter is devoted to the general study of random fields (r.f.) of bounded variation. To avoid difficulties related to boundary conditions and since we are mostly interested into stationary r.f., we restrict ourselves to the case of r.f. defined on the whole space $\mathbb{R}^d$.

For a r.f. f, our general strategy is first to deal with directional variations $|D_u f|$, $u \in S^{d-1}$ and then integrate over all directions $u \in S^{d-1}$ to obtain results on the variation $|Df|$. The advantage of dealing with directional variations is that it yields simple expressions and also provides information on the anisotropy of the r.f. f.

The first section of this chapter is devoted to functions of bounded directional variation. Relations between the directional variation $|D_u f|$ of a function f and the integral of its difference quotients are emphasized, yielding to the fundamental relation

$$|D_u f| \left(\mathbb{R}^d \right) = \lim_{r \to 0} \int_{\mathbb{R}^d} \frac{|f(x + ru) - f(x)|}{|r|} dx.$$

Since the stated results are not found in the reference textbooks on the subject (e.g. [6, 54]), they are presented with a complete proof.

After this preliminary study of deterministic functions of bounded directional variation, random fields of (locally) bounded (directional) variation are defined and characterized. In particular, one defines the *directional variation intensity measure* $\Theta_{V_u}(f, \cdot)$ of a r.f. f as the expectation of the directional variation of f, and, in the case where the r.f. f is a.s. of bounded variation over the whole space $\mathbb{R}^d$, it is shown that

$$\Theta_{V_u} \left(f, \mathbb{R}^d \right) = \mathbb{E} \left(|D_u f| \left(\mathbb{R}^d \right) \right) = \lim_{r \to 0} \int_{\mathbb{R}^d} \frac{\mathbb{E} \left(|f(x + ru) - f(x)| \right)}{|r|} dx.$$

A particular interest is then given to stationary r.f. f of locally bounded (directional) variation. If f is such a r.f., it is proved that the mean directional variation of f on every domain U is proportional to the Lebesgue measure of U. The constant of proportionality is called the *directional variation intensity* of the stationary r.f. f and is denoted $\theta_{V_u}(f)$. Along with the definition of $\theta_{V_u}(f)$, a practical formula is derived:

$$\theta_{V_u}(f) = \lim_{r \to 0} \frac{\mathbb{E}(|f(ru) - f(0)|)}{|r|}.$$

In particular, the directional variation intensity $\theta_{V_u}(f)$ only depends on the family of two-dimensional distributions of the stationary random field f.

As mentioned above, we are aware of only one general result on the variation of r.f. which is due to Ibragimov [80]. Ibragimov's theorem shows that if a r.f. is *Lipschitz in mean*, that is if there exists $K > 0$ such that for all $x, h \in \mathbb{R}^d$,

$$\mathbb{E}(|f(x + h) - f(x)|) \leq K|h|,$$

then f has a.s. bounded variation. After recalling this theorem, we establish an equivalent of Ibragimov's theorem for r.f. of bounded directional variation. Besides,

we demonstrate that the converse of Ibragimov's theorem holds when the r.f. are stationary: a stationary r.f. has bounded variation with a finite variation intensity if and only if it has finite expectation and is Lipschitz in mean.

The plan of this chapter is as follows. In Section 7.2, several results from the theory of functions of bounded directional variation are recalled. Random fields of bounded (directional) variation are then defined in Section 7.3, and characterization theorems for these r.f are established. Finally, in Section 7.4 a special interest is given to stationary r.f. of bounded variation for which the variation intensity measure is shown to be proportional to the Lebesgue measure.

7.2 Functions of Bounded Directional Variation and Difference Quotients

This section gathers several necessary results from the theory of functions of bounded variation, with a particular interest in functions of bounded directional variation. For a general treatment of the subject we refer to the textbook of Ambrosio, Fusco and Pallara [6]. In a first part, some basic definitions are recalled. In a second part, relations between the directional variation of a function and the integral of its difference quotients are emphasized. Although the stated results are well-known in the calculus of variations community[1], they are not, to the best of our knowledge, presented in any reference textbooks on the subject (e.g. [6, 54]). This is why each result of this second part is presented with a complete proof.

7.2.1 Functions of Bounded Variation

For any open subset $U \subset \mathbb{R}^d$, $\mathcal{B}(U)$ denotes the set of Borel subsets of U, and we write $V \subset\subset U$ if $V \subset U$ is open and relatively compact in U.

Definition 7.1 (Functions of bounded variation)**.** *Let U be an open set of $\mathbb{R}^d$. We say that $f \in L^1(U)$ is a* function of bounded variation *in U if the distributional derivative of f is representable by a finite Radon measure, i.e. if there exists a $\mathbb{R}^d$-valued Radon measure[2], noted $Df = (D_1 f, \ldots, D_d f)$, such that $|Df|(U) < +\infty$ and for all $\varphi = (\varphi_1, \ldots, \varphi_d) \in \mathcal{C}_c^\infty(U, \mathbb{R}^d)$*

$$\int_U f(x)\operatorname{div}\varphi(x)dx = -\sum_{i=1}^d \int_U \varphi_i(x)D_i f(dx).$$

The vector space of all functions of bounded variation in U is denoted by $BV(U)$.

A function $f \in L^1_{\text{loc}}(U)$ has locally bounded variation *in U if $f \in BV(V)$ for all open set $V \subset\subset U$. The space of functions of locally bounded variation in U is denoted by $BV_{\text{loc}}(U)$.*

---

[1] Luigi Ambrosio, personal communication.

[2] The definition of vector-valued Radon measures is recalled in Appendix C.

In what follows, S^{d-1} denotes the unit Euclidean sphere in $\mathbb{R}^d$. If $\varphi \in \mathcal{C}^1\left(U, \mathbb{R}\right)$ and $u \in S^{d-1}$, we write

$$\frac{\partial \varphi}{\partial u}(x) = \langle \nabla \varphi(x), u \rangle, \ x \in \mathbb{R}^d,$$

for the directional derivative of φ in the direction u.

Definition 7.2 (Functions of bounded directional variation). *Let U be an open set of $\mathbb{R}^d$ and let $u \in S^{d-1}$. $f \in L^1\left(U\right)$ is a function of bounded directional variation in U in the direction u if the directional distributional derivative of f in the direction u is representable by a finite Radon measure, i.e. if there exists a signed Radon measure[3], noted $D_u f$, such that $|D_u f|(U) < +\infty$ and for $\varphi \in \mathcal{C}_c^\infty\left(U, \mathbb{R}\right)$*

$$\int_U f(x) \frac{\partial \varphi}{\partial u}(x) dx = - \int_U \varphi(x) D_u f(dx).$$

The corresponding space is denoted by $BV_u(U)$.

The space $BV_{u,\mathrm{loc}}(U)$ is defined as the subspace of functions $f \in L^1_{\mathrm{loc}}\left(U\right)$ such that $f \in BV_u(V)$ for all open set $V \subset\subset U$.

If $f \in BV(U)$ then $|Df|(U)$ is called the *variation* of f in U. Similarly, if $f \in BV_u(U)$, $|D_u f|(U)$ is called the *directional variation* of f in the direction u in U.

In what follows, $\mathcal{H}^{d-1}$ denotes the Hausdorff measure of index $d-1$.

Proposition 7.1 (Variation and directional variations). *Let U be an open set of $\mathbb{R}^d$ and let $f \in L^1(U)$. Then, the three following assertions are equivalent:*

(i) $f \in BV(U)$.

(ii) $f \in BV_u(U)$ for all $u \in S^{d-1}$.

(iii) For all vector e_i of the canonical basis, $f \in BV_{e_i}(U)$.

In addition, if $f \in BV(U)$ we have for all measurable set $A \in \mathcal{B}(U)$,

$$D_u f(A) = \langle Df(A), u \rangle = \sum_{i=1}^d u_i D_i f(A), \ u = (u_1, \dots, u_d) \in S^{d-1},$$

and

$$|Df|(A) = \frac{1}{2\omega_{d-1}} \int_{S^{d-1}} |D_u f|(A) \mathcal{H}^{d-1}(du), \tag{7.1}$$

where ω_{d-1} denotes the Lebesgue measure of the unit ball in $\mathbb{R}^{d-1}$.

---

[3]The definition of signed Radon measures is recalled in Appendix C.

Proof. This proposition is mostly from [34]. It is reproduced for the convenience of the reader. Clearly, Assertion (ii) implies Assertion (iii). Let us show that (i) implies (ii). Let $f \in BV(U)$, let $Df = (D_1 f, \ldots, D_d f)$ be the Radon measure representing its distributional derivative, and let $u \in S^{d-1}$. Then $\langle Df, u \rangle := \sum_{i=1}^{d} u_i D_i f$ is a signed Radon measure which represents the directional derivative of f in the direction u, and by the Cauchy-Schwarz inequality

$$|\langle Df, u \rangle| (U) \leq \sum_{i=1}^{d} |u_i| |D_i f|(U) \leq |u| |Df|(U) = |Df|(U) < +\infty.$$

Hence $f \in BV_u(U)$. Let us now show that (iii) implies (i). For all vector e_i of the canonical basis, $f \in BV_{e_i}\left(\mathbb{R}^d\right)$ and there exists a signed Radon measure $D_{e_i} f$ which represents the distributional partial derivatives of f. But then one easily checks that $(D_{e_1} f, \ldots, D_{e_d} f)$ is a $\mathbb{R}^d$-valued finite Radon measure which represents the distributional derivative of f, and thus $f \in BV(U)$. As for the two announced equalities, note that we have already shown that $D_u f = \langle Df, u \rangle$. To finish let us show Formula (7.1). Let $f \in BV(U)$ and let $A \in \mathcal{B}(U)$. By the polar decomposition theorem [6, Corollary 1.29] there exists a unique $|Df|$-integrable function $\sigma : U \to S^{d-1}$ such that $Df = \sigma |Df|$. With this notation, observe that for all $u \in S^{d-1}$

$$D_u f(A) = \langle Df, u \rangle(A) = \int_A \langle \sigma(x), u \rangle |Df|(dx).$$

Hence, by [6, Proposition 1.23]

$$|D_u f|(A) = \int_A |\langle \sigma(x), u \rangle| \, |Df|(dx).$$

For all $\nu \in S^{d-1}$ we have the following well-known identity

$$\int_{S^{d-1}} |\langle \nu, u \rangle| \, \mathcal{H}^{d-1}(du) = 2\omega_{d-1}.$$

Hence by Fubini's theorem

$$\int_{S^{d-1}} |D_u f|(A) \mathcal{H}^{d-1}(du) = \int_A \left(\int_{S^{d-1}} |\langle \sigma(x), u \rangle| \, \mathcal{H}^{d-1}(du) \right) |Df|(dx)$$
$$= 2\omega_{d-1} |Df|(A).$$

$\square$

7.2.2 Directional Variation and Difference Quotients

In this section we enunciate characterization theorems for functions of bounded variation in terms of difference quotient. To ensure that the difference quotients $x \mapsto \frac{f(x+ru)-f(x)}{r}$ are well-defined, we restrict ourselves to the case where the function f is defined over the whole Euclidean space $\mathbb{R}^d$. Since stationary random fields are by definition defined over $\mathbb{R}^d$, this restriction is of no consequence for the targeted applications.

Theorem 7.1 (Characterization of functions of bounded directional variation in terms of difference quotient). *Let $f \in L^1_{\text{loc}}\left(\mathbb{R}^d\right)$, and let $u \in S^{d-1}$. Then, the three following assertions are equivalent:*

(i) $f \in BV_{u,\text{loc}}\left(\mathbb{R}^d\right)$.

(ii) For all $U \subset\subset \mathbb{R}^d$, the family of functions

$$x \mapsto \frac{f(x + ru) - f(x)}{r}, \ r \neq 0,$$

is uniformly bounded in $L^1(U)$ as r tends to 0.

(iii) For all $U \subset\subset \mathbb{R}^d$, there exists a sequence (r_n), $r_n \neq 0$, converging to 0 such that the sequence of functions

$$x \mapsto \frac{f(x + r_n u) - f(x)}{r_n}, \ n \in \mathbb{N},$$

is uniformly bounded in $L^1(U)$.

Proof. Clearly (ii) implies (iii). Let us show that (i) implies (ii). Let $f \in BV_{u,\text{loc}}\left(\mathbb{R}^d\right)$, let $(\rho_\varepsilon)_{\varepsilon>0}$ be a family of mollifiers, for all $\varepsilon > 0$ define $f_\varepsilon = f * \rho_\varepsilon$, and let $U \subset\subset \mathbb{R}^d$. Since $f_\varepsilon \in \mathcal{C}^1_{\text{loc}}\left(\mathbb{R}^d, \mathbb{R}\right)$, for all $x \in \mathbb{R}^d$ and $r \neq 0$,

$$f_\varepsilon(x + ru) - f_\varepsilon(x) = \int_0^1 \frac{\partial f_\varepsilon}{\partial u}(x + tru)r\,dt.$$

Hence

$$\int_U \frac{|f_\varepsilon(x + ru) - f_\varepsilon(x)|}{|r|}\,dx \leq \int_U \int_0^1 \left|\frac{\partial f_\varepsilon}{\partial u}(x + tru)\right| dt\,dx$$

$$\leq \int_0^1 \int_{tru+U} \left|\frac{\partial f_\varepsilon}{\partial u}(x)\right| dx\,dt$$

$$\leq \int_0^1 |D_u f_\varepsilon|\,(tru + U)\,dt$$

$$\leq |D_u f_\varepsilon|\,(U \oplus B(0, |r|)),$$

where in the last step we used that $tru + U \subset U \oplus B(0, |r|)$ for all $t \in [0, 1]$. According to [6, Theorem 2.2 p. 42] for all open set $G \subset \mathbb{R}^d$,

$$|D_u f_\varepsilon|\,(G) \leq |D_u f|\,(G \oplus B(0, \varepsilon)).$$

From this property we obtain

$$|D_u f_\varepsilon|\,(U \oplus B(0, |r|)) \leq |D_u f|\,(U \oplus B(0, |r| + \varepsilon)).$$

Hence we have shown that

$$\int_U \frac{|f_\varepsilon(x + ru) - f_\varepsilon(x)|}{|r|}\,dx \leq |D_u f|\,(U \oplus B(0, |r| + \varepsilon)).$$

Letting ε tends to zero, we first get, since f_ε converges to f in $L^1_{\text{loc}}\left(\mathbb{R}^d\right)$,

$$\lim_{\varepsilon \to 0} \int_U \frac{|f_\varepsilon(x+ru) - f_\varepsilon(x)|}{|r|} dx = \int_U \frac{|f(x+ru) - f(x)|}{|r|} dx.$$

Moreover, since by hypothesis $|D_u f|$ is a Radon measure,

$$\lim_{\varepsilon \to 0} |D_u f| \left(U \oplus B(0, |r| + \varepsilon)\right) = |D_u f| \left(\bigcap_{\varepsilon > 0} U \oplus B(0, |r| + \varepsilon)\right)$$

$$= |D_u f| \left(\overline{U \oplus B(0, |r|)}\right).$$

Hence for all $r \neq 0$ and for all $U \subset\subset \mathbb{R}^d$,

$$\int_U \frac{|f(x+ru) - f(x)|}{|r|} dx \leq |D_u f| \left(\overline{U \oplus B(0, |r|)}\right) \tag{7.2}$$

Since $|D_u f| \left(\overline{U \oplus B(0, |r|)}\right)$ is a non-increasing function of r, the integrals of the difference quotients are uniformly bounded in r as r tends to 0.

To conclude the proof let us now show that (iii) implies (i). Let $f \in L^1_{\text{loc}}\left(\mathbb{R}^d\right)$ and $u \in S^{d-1}$. Let $U \subset\subset \mathbb{R}^d$ and let us show that $f \in BV_u(U)$. By hypothesis, there exists a sequence (r_n), $r_n \neq 0$, converging to 0 such that the sequence of functions

$$x \mapsto \frac{f(x+r_n u) - f(x)}{r_n}, \ n \in \mathbb{N},$$

is uniformly bounded in $L^1(U)$. For all $n \in \mathbb{N}$, denote by μ_n the signed Radon measure on U

$$\mu_n : A \mapsto \int_A \frac{f(x+r_n u) - f(x)}{r_n} dx, \ A \in \mathcal{B}(U).$$

For all $n \in \mathbb{N}$, the total variation of μ_n is

$$|\mu_n|(U) = \int_U \frac{|f(x+r_n u) - f(x)|}{|r_n|} dx,$$

and thus by hypothesis $\sup \{|\mu_n|(U), \ n \in \mathbb{N}\} < +\infty$. By weak* compactness[4] (see Theorem C.2 or [6, Theorem 1.59 p. 27]), there exists a subsequence (r_{n_k}) such that (μ_{n_k}) weakly* converges to a Radon measure μ. Hence for all function $\psi \in \mathcal{C}^0_c(U, \mathbb{R})$, we have

$$\lim_{k \to +\infty} \int_U \psi(x) \frac{f(x+r_{n_k} u) - f(x)}{r_{n_k}} dx = \int_U \psi(x) \mu(dx).$$

On the other hand, for all $k \in \mathbb{N}$ and for all $\varphi \in \mathcal{C}^\infty_c(U, \mathbb{R})$,

$$\int_U \varphi(x) \frac{f(x+r_{n_k} u) - f(x)}{r_{n_k}} dx = \int_U \frac{\varphi(x-r_{n_k} u) - \varphi(x)}{r_{n_k}} f(x) dx,$$

---

[4] The definition of weak* convergence signed Radon measures as well as weak* compactness are recalled in Appendix C.

and by dominated convergence,

$$\lim_{k\to+\infty} \int_U \frac{\varphi(x - r_{n_k}u) - \varphi(x)}{r_{n_k}} f(x)dx = -\int_U \frac{\partial\varphi}{\partial u}(x)f(x)dx.$$

All in all, we have for all $\varphi \in \mathcal{C}_c^\infty(U, \mathbb{R})$,

$$\int_U \varphi(x)\mu(dx) = -\int_U \frac{\partial\varphi}{\partial u}(x)f(x)dx.$$

Hence the distributional directional derivative of f over U is representable by the Radon measure μ. Besides, by lower semicontinuity of the total variation over open sets with respect to the weak* convergence (see Corollary C.1),

$$|\mu|(U) \le \liminf_{k\to+\infty} |\mu_{n_k}|(U) < +\infty.$$

Hence $f \in BV_u(U)$. This is true for any $U \subset\subset \mathbb{R}^d$ and thus concludes the proof. $\quad\square$

The remaining of this section consists of a series of corollaries of Theorem 7.1, which would eventually yield to the identity (see Corollary 7.4)

$$|D_u f|\left(\mathbb{R}^d\right) = \lim_{r\to 0} \int_{\mathbb{R}^d} \frac{|f(x + ru) - f(x)|}{|r|}dx.$$

This identity will be central in our study of random fields of bounded variation.

Corollary 7.1. *Let $f \in L^1_{\mathrm{loc}}\left(\mathbb{R}^d\right)$ and $u \in S^{d-1}$. Then $f \in BV_{u,\mathrm{loc}}\left(\mathbb{R}^d\right)$ if and only if for all $U \subset\subset \mathbb{R}^d$,*

$$\liminf_{r\to 0} \int_U \frac{|f(x + ru) - f(x)|}{|r|}dx < +\infty.$$

Proof. By Theorem 7.1, if $f \in BV_{u,\mathrm{loc}}\left(\mathbb{R}^d\right)$ then $\int_U \frac{|f(x+ru)-f(x)|}{|r|}dx$ is uniformly bounded as r tends to 0, and thus it has a finite lim inf. Conversely, suppose that for all $U \subset\subset \mathbb{R}^d$

$$\liminf_{r\to 0} \int_U \frac{|f(x + ru) - f(x)|}{|r|}dx < +\infty.$$

Let $U \subset\subset \mathbb{R}^d$. Then there exists a sequence (r_n) converging to 0 such that

$$\lim_{n\to+\infty} \int_U \frac{|f(x + r_n u) - f(x)|}{|r_n|}dx = \liminf_{r\to 0} \int_U \frac{|f(x + ru) - f(x)|}{|r|}dx.$$

Since a convergent sequence is bounded, there exists a constant C such that

$$\int_U \frac{|f(x + r_n u) - f(x)|}{|r_n|}dx \le C, \ n \in \mathbb{N}.$$

Hence for all $U \subset\subset \mathbb{R}^d$, there exists a sequence (r_n) converging to 0 such that the functions $x \mapsto \frac{f(x+r_n u)-f(x)}{r_n}$ are uniformly bounded in $L^1(U)$. By Theorem 7.1, $f \in BV_{u,\mathrm{loc}}\left(\mathbb{R}^d\right)$.

$\square$

Corollary 7.2 (local weak* convergence of difference quotients). *Let $f \in L^1_{\mathrm{loc}}\left(\mathbb{R}^d\right)$, and let $u \in S^{d-1}$. For all $r \neq 0$, denote μ_r the signed Radon measure*

$$\mu_r : A \mapsto \int_A \frac{f(x+ru) - f(x)}{r} dx, \ A \in \mathcal{B}\left(\mathbb{R}^d\right).$$

Then $f \in BV_{u,\mathrm{loc}}\left(\mathbb{R}^d\right)$ if and only if the family of measures (μ_r) locally weakly converges to some signed Radon measure μ, and in this case $D_u f = \mu$.*

Proof. First a preliminary remark: By dominated convergence, for all $\varphi \in \mathcal{C}^\infty_c\left(\mathbb{R}^d, \mathbb{R}\right)$,

$$\lim_{r \to 0} \int_{\mathbb{R}^d} \varphi(x) \mu_r(dx) = \lim_{r \to 0} \int_{\mathbb{R}^d} \frac{\varphi(x-ru) - \varphi(x)}{r} f(x) dx = -\int_{\mathbb{R}^d} \frac{\partial \varphi}{\partial u}(x) f(x) dx.$$

Let us suppose that (μ_r) locally weakly* converges to μ. By definition of the local weak* convergence, for all $\varphi \in \mathcal{C}^0_c\left(\mathbb{R}^d, \mathbb{R}\right)$,

$$\lim_{r \to 0} \int_{\mathbb{R}^d} \varphi(x) \mu_r(dx) = \int_{\mathbb{R}^d} \varphi(x) \mu(dx).$$

Hence for all $\varphi \in \mathcal{C}^\infty_c\left(\mathbb{R}^d, \mathbb{R}\right)$,

$$\int_{\mathbb{R}^d} \varphi(x) \mu(dx) = -\int_{\mathbb{R}^d} \frac{\partial \varphi}{\partial u}(x) f(x) dx,$$

that is $f \in BV_{u,\mathrm{loc}}\left(\mathbb{R}^d\right)$ and $D_u f = \mu$.

Let us now turn to the converse implication. Suppose that $f \in BV_{u,\mathrm{loc}}\left(\mathbb{R}^d\right)$. Let (r_n) be some sequence converging to 0 and note $\mu_n = \mu_{r_n}$. Then, according to Theorem 7.1, for all open set $U \subset\subset \mathbb{R}^d$, $|\mu_n|(U)$ is uniformly bounded. But then, for any compact set $K \subset \mathbb{R}^d$, $|\mu_n|(K)$ is also uniformly bounded and thus $\sup\{|\mu_n|(K), \ n \in \mathbb{N}\} < +\infty$. By local weak* compactness (see Corollary C.1) there exists a subsequence (r_{n_k}) of (r_n) such that μ_{n_k} locally weakly* converges to some signed Radon measure μ. Hence for all $\varphi \in \mathcal{C}^\infty_c\left(\mathbb{R}^d, \mathbb{R}\right)$,

$$\int_{\mathbb{R}^d} \varphi(x) \mu(dx) = \lim_{k \to +\infty} \int_{\mathbb{R}^d} \varphi(x) \mu_{n_k}(dx) = -\int_{\mathbb{R}^d} \frac{\partial \varphi}{\partial u}(x) f(x) dx,$$

that is $f \in BV_{u,\mathrm{loc}}\left(\mathbb{R}^d\right)$ and $D_u f = \mu$. Besides, according to the preliminary remark, for all $\varphi \in \mathcal{C}^\infty_c\left(\mathbb{R}^d, \mathbb{R}\right)$,

$$\lim_{r \to 0} \int_{\mathbb{R}^d} \varphi(x) \mu_r(dx) = \int_{\mathbb{R}^d} \varphi(x) \mu(dx).$$

By the density of $\mathcal{C}^\infty_c\left(\mathbb{R}^d, \mathbb{R}\right)$ in $\mathcal{C}^0_c\left(\mathbb{R}^d, \mathbb{R}\right)$ for the uniform convergence, the above equality extends to all $\varphi \in \mathcal{C}^0_c\left(\mathbb{R}^d, \mathbb{R}\right)$, which shows that the whole family (μ_r) locally weakly* converges to μ.

$\square$

The next corollary uses arguments from the proof of Theorem 7.1 to establish useful inequalities involving the directional variation and the integral of difference quotients.

Corollary 7.3. *Let* $f \in BV_{u,\mathrm{loc}}\left(\mathbb{R}^d\right)$ *and* $u \in S^{d-1}$. *For all* $U \subset\subset \mathbb{R}^d$ *and for all* $r \neq 0$,

$$\int_U \frac{|f(x+ru) - f(x)|}{|r|} dx \leq |D_u f|\left(\overline{U \oplus B(0,|r|)}\right).$$

Besides the following chain of inequalities holds:

$$|D_u f|(U) \leq \liminf_{r \to 0} \int_U \frac{|f(x+ru) - f(x)|}{|r|} dx$$

$$\leq \limsup_{r \to 0} \int_U \frac{|f(x+ru) - f(x)|}{|r|} dx \leq |D_u f|\left(\overline{U}\right).$$

Proof. Let $U \subset\subset \mathbb{R}^d$ and $r \neq 0$. Then Equation (7.2) in the proof of Theorem 7.1 ensures that

$$\int_U \frac{|f(x+ru) - f(x)|}{|r|} dx \leq |D_u f|\left(\overline{U \oplus B(0,|r|)}\right).$$

Since

$$\limsup_{r \to 0} |D_u f|\left(\overline{U \oplus B(0,|r|)}\right) = |D_u f|\left(\overline{U}\right),$$

we deduce that

$$\limsup_{r \to 0} \int_U \frac{|f(x+ru) - f(x)|}{|r|} dx \leq |D_u f|\left(\overline{U}\right).$$

To conclude, by Corollary 7.2, the signed Radon measures

$$\mu_r : A \mapsto \int_A \frac{f(x+ru) - f(x)}{r} dx, \ A \in \mathcal{B}\left(\mathbb{R}^d\right),$$

locally weakly* converge to $D_u f$. But since the application $\nu \mapsto |\nu|(U)$ is lower-semicontinuous with respect to the local weak* convergence (see Corollary C.1) we have

$$|D_u f|(U) \leq \liminf_{r \to 0} |\mu_r|(U) = \liminf_{r \to 0} \int_U \frac{|f(x+ru) - f(x)|}{|r|} dx.$$

$\square$

For functions of bounded directional variation in $\mathbb{R}^d$, Corollary 7.3 yields to a new practical expression for the total directional variation $|D_u f|\left(\mathbb{R}^d\right)$.

Corollary 7.4 (The directional variation is the limit of the integrated difference quotient)**.** *Let* $f \in L^1\left(\mathbb{R}^d\right)$ *and* $u \in S^{d-1}$. *Then the following assertions are equivalent:*

(i) $f \in BV_u\left(\mathbb{R}^d\right)$.

(ii) $\displaystyle\liminf_{r\to 0} \int_{\mathbb{R}^d} \frac{|f(x+ru)-f(x)|}{|r|} dx < +\infty.$

(iii) $\displaystyle\lim_{r\to 0} \int_{\mathbb{R}^d} \frac{|f(x+ru)-f(x)|}{|r|} dx$ exists and is finite.

If any of these assertions holds, then for all $r \neq 0$,

$$\int_{\mathbb{R}^d} \frac{|f(x+ru)-f(x)|}{|r|} dx \le |D_u f|\left(\mathbb{R}^d\right),$$

and

$$|D_u f|\left(\mathbb{R}^d\right) = \lim_{r\to 0} \int_{\mathbb{R}^d} \frac{|f(x+ru)-f(x)|}{|r|} dx. \tag{7.3}$$

Besides, Formula (7.3) is also valid in the degenerate case: if f is not in $BV_u\left(\mathbb{R}^d\right)$, then

$$\lim_{r\to 0} \int_{\mathbb{R}^d} \frac{|f(x+ru)-f(x)|}{|r|} dx = +\infty.$$

Proof. First remark that (iii) $\Rightarrow$ (ii) is trivial. Let us show that (i) $\Rightarrow$ (iii). Let $f \in BV_u\left(\mathbb{R}^d\right)$. By Corollary 7.3, for all $U \subset \mathbb{R}^d$,

$$|D_u f|(U) \le \liminf_{r\to 0} \int_U \frac{|f(x+ru)-f(x)|}{|r|} dx \le \liminf_{r\to 0} \int_{\mathbb{R}^d} \frac{|f(x+ru)-f(x)|}{|r|} dx.$$

Letting U tends to $\mathbb{R}^d$ shows that

$$|D_u f|\left(\mathbb{R}^d\right) \le \liminf_{r\to 0} \int_{\mathbb{R}^d} \frac{|f(x+ru)-f(x)|}{|r|} dx.$$

On the other hand, still by Corollary 7.3, for all $U \subset \mathbb{R}^d$,

$$\int_U \frac{|f(x+ru)-f(x)|}{|r|} dx \le |D_u f|\left(\overline{U \oplus B(0,|r|)}\right) \le |D_u f|\left(\mathbb{R}^d\right).$$

Thus letting U tends to $\mathbb{R}^d$,

$$\int_{\mathbb{R}^d} \frac{|f(x+ru)-f(x)|}{|r|} dx \le |D_u f|\left(\mathbb{R}^d\right),$$

and in particular

$$\limsup_{r\to 0} \int_{\mathbb{R}^d} \frac{|f(x+ru)-f(x)|}{|r|} dx \le |D_u f|\left(\mathbb{R}^d\right).$$

Hence the limit of the integrated difference quotients exists and equals $|D_u f|\left(\mathbb{R}^d\right)$. Let us now show that (ii) $\Rightarrow$ (i). Suppose that $f \in L^1\left(\mathbb{R}^d\right)$ satisfies (ii). Then, by Corollary 7.1 $f \in BV_{u,\text{loc}}\left(\mathbb{R}^d\right)$. Besides, the above argument shows that

$$|D_u f|\left(\mathbb{R}^d\right) \le \liminf_{r\to 0} \int_{\mathbb{R}^d} \frac{|f(x+ru)-f(x)|}{|r|} dx < +\infty,$$

and thus $f \in BV_u\left(\mathbb{R}^d\right)$. To conclude, let us deal with the degenerate case. Remark that it is enough to show that

$$\liminf_{r \to 0} \int_{\mathbb{R}^d} \frac{|f(x + ru) - f(x)|}{|r|} dx = +\infty. \tag{7.4}$$

First, if $f \notin BV_{u,\mathrm{loc}}\left(\mathbb{R}^d\right)$, then by Corollary 7.1 there exists $U \subset\subset \mathbb{R}^d$ such that

$$\liminf_{r \to 0} \int_U \frac{|f(x + ru) - f(x)|}{|r|} dx = +\infty,$$

which ensures (7.4). Second, if $f \in BV_{u,\mathrm{loc}}\left(\mathbb{R}^d\right)$ but not in $BV_u\left(\mathbb{R}^d\right)$, then necessarily, $|D_u f|\left(\mathbb{R}^d\right) = +\infty$. Besides, by Corollary 7.3, for all $U \subset\subset \mathbb{R}^d$,

$$|D_u f|(U) \leq \liminf_{r \to 0} \int_{\mathbb{R}^d} \frac{|f(x + ru) - f(x)|}{|r|} dx.$$

Letting U tends to $\mathbb{R}^d$, one obtains (7.4). $\qquad\square$

7.3 Random Fields of Bounded Variation

7.3.1 Measurable Random Fields

Following the generally approved definition, a *random field* (r.f.) of $\mathbb{R}^d$ is a a family of random variables $\xi_x : (\Omega, \mathcal{A}) \to (\mathbb{R}, \mathcal{B}(\mathbb{R}))$ indexed by $x \in \mathbb{R}^d$ (see e.g. [47, p. 46] or [63, p. 41]). The study of the variation of a r.f. requires an additional hypothesis, namely that the r.f. is measurable.

Definition 7.3 (Measurable random field). *Let $(\Omega, \mathcal{A}, \mathbb{P})$ be a probability space. A (jointly) measurable random field of $\mathbb{R}^d$ is a (jointly) measurable function*

$$f : \left(\Omega \times \mathbb{R}^d, \mathcal{A} \otimes \mathcal{B}\left(\mathbb{R}^d\right)\right) \to (\mathbb{R}, \mathcal{B}(\mathbb{R})).$$

Let us recall that if a r.f. ξ_x is continuous in probability, then there exists a jointly measurable version $f(\omega, x)$ of $\xi_x(\omega)$ (see [47, p. 61] or [63, p. 171]). In our context the measurability assumption is necessary to ensure that the weak derivatives of f, that is the integrals of the form

$$\int_{\mathbb{R}^d} f(\omega, x)\varphi(x)dx, \; \varphi \in \mathcal{C}_c^0\left(\mathbb{R}^d, \mathbb{R}\right),$$

are well-defined random variables. Indeed, if the restrictions of f on the sets $\Omega \times U$, $U \subset\subset \mathbb{R}^d$ are integrable, this is a direct consequence of Fubini's theorem [63, p. 173]. Hence **in what follows all the considered random fields will be supposed to be measurable**. When needed, random fields in the sense of the usual definition will be denoted by ξ_x (and not by f), and they will be referred to as (non necessarily measurable) random fields. Let us mention that the measurability assumption is also made in the recent paper [135] to study r.f. having sample paths in Sobolev spaces of index $p = 2$.

7.3.2   Definition of Random Fields of Bounded Variation

Definition 7.4 (Random field of bounded variation)**.** *Let $U \subset \mathbb{R}^d$ be an open set. An a.s. integrable random field $f : \Omega \times U \to \mathbb{R}$ is a* random field of bounded variation *in U if there exists some random $\mathbb{R}^d$-valued Radon measure $Df = (D_1 f, \ldots, D_d f)$ such that $|Df|(U)$ is a.s. finite and for all $\varphi = (\varphi_1, \ldots, \varphi_d) \in \mathcal{C}_c^\infty \left(U, \mathbb{R}^d \right)$,*

$$\int_{\mathbb{R}^d} f(x) \operatorname{div} \varphi(x) dx = -\sum_{i=1}^d \int_{\mathbb{R}^d} \varphi_i(x) D_i f(dx) \ a.s..$$

An a.s. locally integrable r.f. $f : \Omega \times U \to \mathbb{R}$ is a r.f. of locally bounded variation *in U if for all $V \subset\subset U$ the restriction of f to $\Omega \times V$ is a r.f. of bounded variation in V.*

Definition 7.5 (**Variation intensity measure**)**.** *Let $U \subset \mathbb{R}^d$ be an open set and f be a r.f. of locally bounded variation in U. Then the intensity measure of the variation $|Df|$, that is the measure $A \mapsto \mathbb{E}\left(|Df|(A)\right)$, is called the* variation intensity measure *of f and is denoted $\Theta_V(f, \cdot)$.*

The variation intensity measure is an important characteristic of a r.f. f of bounded variation: for all measurable set A, $\Theta_V(f, A)$ is the mean variation of f in A. The mean variation $\Theta_V(f, U)$ on the whole domain U will be called the *mean total variation* of f.

Definition 7.6 (Random field of bounded directional variation)**.** *Let $U \subset \mathbb{R}^d$ be an open set and let $u \in S^{d-1}$. An a.s. integrable random field $f : \Omega \times U \to \mathbb{R}$ is a* r.f. of bounded directional variation *in U if there exists some random signed Radon measure $D_u f$ such that $|D_u f|(U)$ is a.s. finite and for all $\varphi \in \mathcal{C}_c^\infty (U, \mathbb{R})$,*

$$\int_{\mathbb{R}^d} f(x) \frac{\partial \varphi}{\partial u}(x) dx = -\int_{\mathbb{R}^d} \varphi(x) D_u f(dx).$$

An a.s. locally integrable r.f. $f : \Omega \times U \to \mathbb{R}$ is a r.f. of locally bounded directional variation *in U if for all $V \subset\subset U$ the restriction of f to $\Omega \times V$ is a r.f. of bounded variation in V.*

Definition 7.7 (**Directional variation intensity measure**)**.** *Let $U \subset \mathbb{R}^d$ be an open set, let $u \in S^{d-1}$, and let f be a r.f. of locally bounded directional variation in U. Then the intensity measure of the variation $|D_u f|$, that is the measure $A \mapsto \mathbb{E}\left(|D_u f|(A)\right)$, is called the* directional variation intensity measure *of f in the direction u and is denoted $\Theta_{V_u}(f, \cdot)$.*

$\Theta_{V_u}(f, U)$ will be called the *mean total directional variation* of f in the direction u. One easily establishes the analog of Proposition 7.1 for the case of r.f. of bounded variation. In particular we have the following formula.

Proposition 7.2 (Integral geometric formula for directional variation intensity measures)**.** *Let $U \subset \mathbb{R}^d$ be an open set, and let f be a r.f. of bounded variation*

in U. Then f is a r.f. of bounded directional variation in U for all directions $u \in S^{d-1}$, and for all $A \in \mathcal{B}(U)$,

$$\Theta_V(f, A) = \frac{1}{2\omega_{d-1}} \int_{S^{d-1}} \Theta_{V_u}(f, A) du.$$

Proof. As for Proposition 7.1, if Df is a random $\mathbb{R}^d$-valued Radon measure representing the distributional derivative of f then $\langle Df, u \rangle$ is a random signed Radon measure which represents the directional distributional derivative of f. Hence f is a r.f. of bounded directional variation in U for all directions $u \in S^{d-1}$. The integral geometric formula is obtained in applying Fubini's theorem to Formula (7.1). □

We conclude this section in showing that the proposed definition of r.f. of bounded variation is equivalent with a more instinctive one: a r.f. has bounded variation if its sample paths have a.s. bounded variation.

Proposition 7.3 (Sample paths of r.f. of bounded variation). *Let $f \in L^1_{\mathrm{loc}}\left(\mathbb{R}^d\right)$ a.s. and let $u \in S^{d-1}$. Then f is a r.f. of locally bounded directional variation in the direction u (in the sense of Definition 7.6) if and only if the sample paths $x \mapsto f(\omega, x)$ are in $BV_{u,\mathrm{loc}}\left(\mathbb{R}^d\right)$ for $\mathbb{P}$-a.e. $\omega \in \Omega$. Similarly, f is a r.f. of locally bounded directional variation in $\mathbb{R}^d$ if and only if the sample paths $x \mapsto f(\omega, x)$ are in $BV_{\mathrm{loc}}\left(\mathbb{R}^d\right)$ for $\mathbb{P}$-a.e. $\omega \in \Omega$. If in addition $f \in L^1\left(\mathbb{R}^d\right)$, then f is a r.f. of bounded directional variation in the direction u (resp. of bounded variation) if and only if its sample paths are a.s. in $BV_u\left(\mathbb{R}^d\right)$ (resp. in $BV\left(\mathbb{R}^d\right)$).*

Proof. Let us first show the equivalence for r.f. of locally bounded directional variation. The direct sense is immediate from the definition: since $D_u f$ is a.s. a Radon measure, the sample paths are a.s. in $BV_{u,\mathrm{loc}}\left(\mathbb{R}^d\right)$. Conversely, note $\Omega' \subset \Omega$ the set of $\omega \in \Omega$ for which $x \mapsto f(\omega, x)$ are in $BV_{u,\mathrm{loc}}\left(\mathbb{R}^d\right)$. Then, for all $\omega \in \Omega'$, there exists a signed Radon measure $\mu(\omega, \cdot)$ such that for all $\varphi \in \mathcal{C}_c^\infty\left(\mathbb{R}^d, \mathbb{R}\right)$,

$$\int_{\mathbb{R}^d} f(\omega, x) \frac{\partial \varphi}{\partial u}(x) dx = -\int_{\mathbb{R}^d} \varphi(x) \mu(\omega, dx).$$

The only difficulty is to ensure that $\omega \mapsto \mu(\omega, \cdot)$ is a well-defined signed random measure, that is a measurable map. Let (r_n) be a sequence converging to 0. According to Corollary 7.2, for all $\omega \in \Omega'$, $\mu(\omega, \cdot)$ is the local weak* limit of the sequence of signed Radon measures

$$\mu_n(\omega, A) = \int_A \frac{f(\omega, x + r_n u) - f(\omega, x)}{r_n} dx, \ A \in \mathcal{B}\left(\mathbb{R}^d\right).$$

Hence by Proposition C.1 in Appendix C, μ is measurable since it is the a.s. limit of the weakly* convergent sequence of random signed Radon measures $(\mu_n)_{n \in \mathbb{N}}$.

The corresponding equivalence for r.f. of locally bounded variation is straightforward using the fact that $f(\omega, \cdot) \in BV_{\mathrm{loc}}\left(\mathbb{R}^d\right)$ if and only if $BV_{\mathrm{loc}, e_i}\left(\mathbb{R}^d\right)$ for all e_i in the canonical basis (see Proposition 7.1).

To conclude let us quickly deal with the case of r.f. of bounded variation. Suppose that $f \in L^1\left(\mathbb{R}^d\right)$. As before, if f is a r.f. of bounded variation, then as a consequence of Definition 7.4 its sample paths are a.s. in $BV\left(\mathbb{R}^d\right)$. Conversely, if the sample paths are a.s. in $BV\left(\mathbb{R}^d\right) \subset BV_{\text{loc}}\left(\mathbb{R}^d\right)$, then the first part of the proof ensures that f is a r.f. of locally bounded variation. Besides, since the sample paths are a.s. in $BV\left(\mathbb{R}^d\right)$, $|Df|\left(\mathbb{R}^d\right)$ is a.s. finite, and thus f is a r.f. of bounded variation. The case of r.f. of bounded directional variation is similar. $\qquad \square$

Remark (Notation)**.** Thanks to Proposition 7.3 we can use the notation $f \in BV\left(R^d\right)$ a.s., $f \in BV_{u,\text{loc}}\left(R^d\right)$ a.s., etc. to express that a r.f. f has bounded variation, locally bounded directional variation, etc.

7.3.3 Characterization in Terms of Difference Quotient

Proposition 7.4 (Characterization of r.f. of locally bounded directional variation)**.** *Let $f \in L^1_{\text{loc}}\left(\mathbb{R}^d\right)$ a.s. and $u \in S^{d-1}$. Then $f \in BV_{u,\text{loc}}\left(\mathbb{R}^d\right)$ a.s. if and only if for all $U \subset\subset \mathbb{R}^d$,*

$$\liminf_{r \to 0} \int_U \frac{|f(x + ru) - f(x)|}{|r|} dx < +\infty \ a.s.$$

Proof. Note that this proposition is an adaptation of Corollary 7.1 for random fields. If $f \in BV_{u,\text{loc}}\left(\mathbb{R}^d\right)$ a.s. then by Corollary 7.1, for all $U \subset\subset \mathbb{R}^d$,

$$\liminf_{r \to 0} \int_U \frac{|f(x + ru) - f(x)|}{|r|} dx < +\infty \text{ a.s.}.$$

Conversely, suppose that for all $U \subset\subset \mathbb{R}^d$,

$$\liminf_{r \to 0} \int_U \frac{|f(x + ru) - f(x)|}{|r|} dx < +\infty \text{ a.s.}.$$

For all $n \geq 1$ note B_n the ball of center 0 and of radius n, define

$$A_n = \left\{ \omega \in \Omega : \ f(\omega, \cdot) \in L^1_{\text{loc}}\left(\mathbb{R}^d\right) \text{ and } \liminf_{r \to 0} \int_{B_n} \frac{|f(\omega, x + ru) - f(\omega, x)|}{|r|} dx < +\infty \right\}.$$

and denote by A the intersection $A = \bigcap_{n \geq 1} A_n$. Clearly $A_{n+1} \subset A_n$ and by hypothesis $\mathbb{P}(A_n) = 1$, and consequently $\mathbb{P}(A) = 1$. Remark that for all $\omega \in A$, $f(\omega, \cdot) \in L^1_{\text{loc}}\left(\mathbb{R}^d\right)$ and for all open set $U \subset\subset \mathbb{R}^d$,

$$\liminf_{r \to 0} \int_U \frac{|f(x + ru) - f(x)|}{|r|} dx < +\infty,$$

since $U \subset B_n$ for some $n \in \mathbb{N}$. Hence for all $\omega \in A$ Corollary 7.1 applies to $f(\omega, \cdot)$ and thus for all $\omega \in A$, $f(\omega, \cdot) \in BV_{u,\text{loc}}\left(\mathbb{R}^d\right)$. $\qquad \square$

In the case where the r.f. has bounded directional variation, one obtains an integral expression of the mean total directional variation $\Theta_{V_u}\left(f, \mathbb{R}^d\right)$.

Proposition 7.5 (Characterization of r.f. of bounded directional variation)**.** *Let* $f \in L^1\left(\mathbb{R}^d\right)$ *a.s. and* $u \in S^{d-1}$*. Then the three following assertions are equivalent:*

(i) $f \in BV_u\left(\mathbb{R}^d\right)$ *a.s.*

(ii) $\liminf\limits_{r \to 0} \int_{\mathbb{R}^d} \dfrac{|f(x+ru)-f(x)|}{|r|} dx < +\infty$ *a.s.*

(iii) $\lim\limits_{r \to 0} \int_{\mathbb{R}^d} \dfrac{|f(x+ru)-f(x)|}{|r|} dx$ *exists and is finite a.s.*

If any of these conditions holds, then

$$\Theta_{V_u}\left(f, \mathbb{R}^d\right) = \lim_{r \to 0} \int_{\mathbb{R}^d} \frac{\mathbb{E}\left(|f(x+ru)-f(x)|\right)}{|r|} dx. \qquad (7.5)$$

Proof. This proposition is a transcription of Corollary 7.4 to the case of r.f. of bounded variation. The equivalence is straightforward thanks to Proposition 7.3. By Corollary 7.4

$$\lim_{r \to 0} \int_{\mathbb{R}^d} \frac{|f(x+ru)-f(x)|}{|r|} dx = |D_u f|\left(\mathbb{R}^d\right) \text{ a.s.,}$$

and

$$\int_{\mathbb{R}^d} \frac{|f(x+ru)-f(x)|}{|r|} dx \leq |D_u f|\left(\mathbb{R}^d\right) \text{ a.s..}$$

Hence if the r.v. $|D_u f|\left(\mathbb{R}^d\right)$ is integrable, Formula (7.5) is obtained by dominated convergence and Fubini's theorem. If $\mathbb{E}\left(|D_u f|\left(\mathbb{R}^d\right)\right) = \Theta_{V_u}\left(f, \mathbb{R}^d\right) = +\infty$, then Formula (7.5) is still valid since by Fatou's lemma

$$+\infty = \Theta_{V_u}\left(f, \mathbb{R}^d\right) = \mathbb{E}\left(\liminf_{r \to 0} \int_{\mathbb{R}^d} \frac{|f(x+ru)-f(x)|}{|r|} dx\right)$$

$$\leq \liminf_{r \to 0} \mathbb{E}\left(\int_{\mathbb{R}^d} \frac{|f(x+ru)-f(x)|}{|r|} dx\right).$$

$\square$

Remark (Degenerate case)**.** Formula (7.5) can be extended to the degenerate case where the limit on the right-hand side is infinite. However let us precise that this degenerate case is more subtle than in the deterministic case (see Corollary 7.4). Indeed there are two different cases for which the limit of Formula (7.5) is infinite: either the r.f. f is not of bounded variation or f is of bounded variation but its total variation $|D_u f|\left(\mathbb{R}^d\right)$ has infinite expectation. In both cases, it is coherent to say that the mean total variation of the process is infinite. This convention will be used in Chapter 8 where the mean perimeter of random sets will be computed (see Section 8.4).

7.3.4   A Sufficient Condition for Locally Bounded Directional Variation

As mentioned in the introduction, we are aware of only one result dealing with the variation of random fields defined over $\mathbb{R}^d$ for $d \geq 2$. This result, which is reproduced below, is due to Ibragimov [80] and it gives a sufficient condition for a r.f. to be of bounded variation. We will later demonstrate in Section 7.4 that this sufficient condition is also necessary for *stationary* r.f. (see Theorem 7.4).

Theorem 7.2 (Ibragimov's theorem [80])**.** *Let $U \subset\subset \mathbb{R}^d$ and let $f : \Omega \times U \to \mathbb{R}$ be a measurable and separable random field. Suppose that there exists $x_0 \in U$ such that $\mathbb{E}\left(f(x_0)\right) < +\infty$ and that there exists $K > 0$ such that for any $x, y \in U$*

$$\mathbb{E}\left(|f(x) - f(y)|\right) \leq K|x - y|.$$

Then the realizations of f are a.s. in $BV(U)$, and there is a constant $C > 0$ such that for all $A \in \mathcal{B}(U)$
$$\Theta_V\left(f, A\right) \leq C\mathcal{L}^d(A).$$

In the remaining of this section we will establish results similar to Ibragimov's theorem for both r.f. of bounded variation and r.f. of bounded directional variation. However we restrict ourself to random fields defined on the whole space $\mathbb{R}^d$. This is motivated by three reasons. First, this hypothesis yields to a simple proof which does not involve extensions of random fields, contrary to the proof of Ibragimov's theorem [80]. Second, in this framework we are able to give an optimal upper bound of the mean directional variation of any open subset of $\mathbb{R}^d$. Third, in the following we will be mainly interested in the study of stationary random fields of bounded variation which are consistently defined over the whole space $\mathbb{R}^d$.

Proposition 7.6 (A sufficient condition for locally bounded directional variation)**.** *Let $f \in L^1_{\mathrm{loc}}\left(\mathbb{R}^d\right)$ a.s., and let $u \in S^{d-1}$. Suppose that there exists a constant $K > 0$ such that for all $x \in \mathbb{R}^d$ and for all $r \in \mathbb{R}$,*

$$\mathbb{E}\left(|f(x + ru) - f(x)|\right) \leq K|r|. \tag{7.6}$$

Then f is a r.f. of locally bounded directional variation in the direction u and for all $U \subset\subset \mathbb{R}^d$,
$$\Theta_{V_u}(f, U) \leq K\mathcal{L}^d(U).$$

Proof. Let $U \subset\subset \mathbb{R}^d$. By Fatou's lemma and Fubini's theorem

$$\mathbb{E}\left(\liminf_{r \to 0} \int_U \frac{|f(x + ru) - f(x)|}{|r|} dx\right) \leq \liminf_{r \to 0} \mathbb{E}\left(\int_U \frac{|f(x + ru) - f(x)|}{|r|} dx\right)$$
$$\leq K\mathcal{L}^d(U) < +\infty.$$

In particular, $\liminf \int_U \frac{|f(x+ru)-f(x)|}{|r|} dx < +\infty$ a.s. This is valid for all $U \subset\subset \mathbb{R}^d$, and thus by Proposition 7.4, $f \in BV_{u,\mathrm{loc}}\left(\mathbb{R}^d\right)$ a.s. To finish, let us establish the

upper bound on $\Theta_{V_u}(f, U)$. By Corollary 7.3,

$$|D_u f|(U) \leq \liminf_{r \to 0} \int_U \frac{|f(x + ru) - f(x)|}{|r|} dx,$$

and thus by Fatou's lemma

$$\Theta_{V_u}(f, U) \leq \liminf_{r \to 0} \mathbb{E}\left(\int_U \frac{|f(x + ru) - f(x)|}{|r|} dx\right) \leq K\mathcal{L}^d(U).$$

$\square$

In the following, Property (7.6) will be referred to as *Lipschitzness in mean in the direction u*. Let us precise that the upper bound given in Proposition 7.6 is optimal. Indeed, as it will be shown later (see Theorem 7.4), any stationary r.f. f of bounded directional variation satisfies (7.6) for some constant K, and in the case where K is minimal $\Theta_{V_u}(f, U) = K\mathcal{L}^d(U)$.

The previous proposition can be adapted to deal with r.f. of bounded variation. It gives a new version of Ibragimov's theorem, with an optimal upper bound on the variation intensity. However, as previously noted, the result is restricted to r.f. defined over the whole space $\mathbb{R}^d$.

Proposition 7.7 (A sufficient condition for locally bounded variation). *Let $f \in L^1_{\text{loc}}\left(\mathbb{R}^d\right)$ a.s. Suppose that there exists a constant $K > 0$ such that for all x and $h \in \mathbb{R}^d$,*

$$\mathbb{E}\left(|f(x + h) - f(x)|\right) \leq K|h|.$$

Then f is a r.f. of locally bounded variation, and for all $U \subset\subset \mathbb{R}^d$,

$$\Theta_V(f, U) \leq \frac{d\omega_d}{2\omega_{d-1}} K\mathcal{L}^d(U).$$

Proof. By Proposition 7.6, f has a.s. bounded directional variation in the d directions of the canonical basis, and thus $f \in BV\left(\mathbb{R}^d\right)$ a.s. (see Proposition 7.1 or [6, Section 3.11]). In addition, Proposition 7.6 shows that for all $U \subset\subset \mathbb{R}^d$ and for all $u \in S^{d-1}$, $\Theta_{V_u}(f, U) \leq K\mathcal{L}^d(U)$. Hence, by Proposition 7.2, for all $U \subset\subset \mathbb{R}^d$,

$$\Theta_V(f, U) = \frac{1}{2\omega_{d-1}} \int_{S^{d-1}} \Theta_{V_u}(f, U)\mathcal{H}^{d-1}(du) \leq \frac{d\omega_d}{2\omega_{d-1}} K\mathcal{L}^d(U),$$

where we used that $\mathcal{H}^{d-1}\left(S^{d-1}\right) = d\omega_d$. $\square$

Similarly to the case of Proposition 7.6, the upper bound of the variation intensity of Proposition 7.7 is shown to be optimal for stationary and isotropic r.f. of locally bounded variation.

7.4 Stationary Random Fields of Bounded Variation

7.4.1 Stationary Measurable Random Fields

A r.f. is said to be stationary if its finite dimensional distributions are invariant by translation, that is for all $x_1, \ldots, x_n$ and $y \in \mathbb{R}^d$

$$(f(y+x_1), \ldots, f(y+x_n)) \stackrel{\mathcal{D}}{=} (f(x_1), \ldots, f(x_n)).$$

The following proposition shows that the sample paths of a stationary random field having finite expectation are a.s. locally integrable.

Proposition 7.8 (Integrability of stationary measurable random fields). *Let f be a stationary and measurable random field. If $\mathbb{E}(|f(x)|) < +\infty$, then $f \in L^1_{\mathrm{loc}}\left(\mathbb{R}^d\right)$ a.s.*

Proof. Let $B_n = B(0, n)$. By Fubini's theorem,

$$\mathbb{E}\left(\int_{B_n} |f(x)| dx\right) = \int_{B_n} \mathbb{E}\left(|f(x)|\right) dx = \mathbb{E}(|f(0)|)\mathcal{L}^d(B_n) < +\infty.$$

Thus f is a.s. integrable over B_n. Since $\mathbb{R}^d = \bigcup_n B_n$, f is a.s. integrable over every bounded open set $U \subset \mathbb{R}^d$, that is to say $f \in L^1_{\mathrm{loc}}\left(\mathbb{R}^d\right)$ a.s. $\qquad\square$

7.4.2 Definition and Computation of the Variation Intensities of Stationary Random Fields

The next theorem defines and gives an expression of the directional variation intensity $\theta_{V_u}(f)$ of a stationary r.f. f. This is the main result of this chapter.

Theorem 7.3 (Definition and computation of the directional variation intensity of a stationary r.f.). *Let $f : \Omega \times \mathbb{R}^d \to \mathbb{R}$ be a stationary r.f. with finite expectation and let $u \in S^{d-1}$. Then $f \in BV_{u,\mathrm{loc}}\left(\mathbb{R}^d\right)$ a.s. with a locally finite directional variation intensity measure $\Theta_{V_u}\left(f, \cdot\right)$ if and only if the limit*

$$\lim_{r \to 0} \frac{\mathbb{E}(|f(ru) - f(0)|)}{|r|}$$

exists and is finite. In this case the directional variation intensity measure $\Theta_{V_u}\left(f, \cdot\right)$ is proportional to the Lebesgue measure, and the constant of proportionality $\theta_{V_u}(f)$ is given by

$$\theta_{V_u}(f) = \lim_{r \to 0} \frac{\mathbb{E}(|f(ru) - f(0)|)}{|r|}.$$

*The constant $\theta_{V_u}(f)$ is called the **directional variation intensity** of f in the direction u. It is the mean amount of directional variation of f per unit volume.*

Instead of proving directly Theorem 7.3, we enunciate and prove the following proposition which is slightly more complete.

Proposition 7.9. *Let $f : \Omega \times \mathbb{R}^d \to \mathbb{R}$ be a stationary r.f. with finite expectation and let $u \in S^{d-1}$. The following assertions are equivalent:*

(i) *$f \in BV_{u,\mathrm{loc}}\left(\mathbb{R}^d\right)$ a.s. and its directional variation intensity measure $\Theta_{V_u}(f, \cdot)$ is locally finite.*

(ii) *$f \in BV_{u,\mathrm{loc}}\left(\mathbb{R}^d\right)$ a.s. and there exists a constant $\theta_{V_u}(f) \geq 0$ such that $\Theta_{V_u}(f, \cdot) = \theta_{V_u}(f)\mathcal{L}^d(\cdot)$, that is for all $A \in \mathcal{B}\left(\mathbb{R}^d\right)$, $\Theta_{V_u}(f, A) = \theta_{V_u}(f)\mathcal{L}^d(A)$.*

(iii) *$\displaystyle\liminf_{r\to 0} \frac{\mathbb{E}(|f(ru) - f(0)|)}{|r|} < +\infty.$*

(iv) *$\displaystyle\lim_{r\to 0} \frac{\mathbb{E}(|f(ru) - f(0)|)}{|r|}$ exists and is finite.*

If any of the above assertions holds, then

$$\theta_{V_u}(f) = \liminf_{r\to 0} \frac{\mathbb{E}(|f(ru) - f(0)|)}{|r|} = \lim_{r\to 0} \frac{\mathbb{E}(|f(ru) - f(0)|)}{|r|}.$$

Proof. We will show the following chain of implications:

$$\text{(i)} \Rightarrow \text{(iv)} \Rightarrow \text{(iii)} \Rightarrow \text{(i)} \Leftrightarrow \text{(ii)}.$$

First remark that (iv) $\Rightarrow$ (iii) and (i) $\Leftarrow$ (ii) are trivial. Now let us prove that (iii) $\Rightarrow$ (i). By stationarity of f, for all $U \subset\subset \mathbb{R}^d$,

$$\mathbb{E}\left(\int_U \frac{|f(x + ru) - f(x)|}{|r|}dx\right) = \frac{\mathbb{E}(|f(ru) - f(0)|)}{|r|}\mathcal{L}^d(U).$$

Hence, by Fatou's lemma,

$$\mathbb{E}\left(\liminf_{r\to 0} \int_U \frac{|f(x + ru) - f(x)|}{|r|}dx\right) \leq \liminf_{r\to 0} \frac{\mathbb{E}(|f(ru) - f(0)|)}{|r|}\mathcal{L}^d(U) < +\infty.$$

In particular, for all $U \subset\subset \mathbb{R}^d$ $\liminf \int_U \frac{|f(x+ru)-f(x)|}{|r|}dx$ is a.s. finite, and by Proposition 7.5 $f \in BV_{u,\mathrm{loc}}\left(\mathbb{R}^d\right)$ a.s. In addition, by Corollary 7.3 for all $U \subset\subset \mathbb{R}^d$

$$\Theta_{V_u}(f, U) \leq \liminf_{r\to 0} \frac{\mathbb{E}(|f(ru) - f(0)|)}{|r|}\mathcal{L}^d(U) < +\infty,$$

which shows that $\Theta_{V_u}(f, \cdot)$ is locally finite.

To conclude the proof it remains to show that (i) $\Rightarrow$ (iv) and (i) $\Rightarrow$ (ii). Hence let us suppose that $f \in BV_{u,\mathrm{loc}}\left(\mathbb{R}^d\right)$ a.s. and that $\Theta_{V_u}(f, \cdot)$ is locally finite. Let $B = B(y, \rho)$ be any open ball of $\mathbb{R}^d$. By Corollary 7.3,

$$\limsup_{r\to 0} \int_B \frac{|f(x + ru) - f(x)|}{|r|}dx \leq |D_u f|\left(\overline{B}\right) \quad \text{a.s..}$$

Besides, still by Corollary 7.3, for $|r| \leq R$ the integrals $\int_B \frac{|f(x+ru)-f(x)|}{|r|} dx$ are dominated by $|D_u f| \left(\overline{B \oplus B(0, R)} \right)$, which by hypothesis is a L^1-r.v. Hence, one can apply the reverse Fatou lemma, and using the stationarity of f,

$$
\begin{aligned}
\limsup_{r \to 0} \frac{\mathbb{E}\left(|f(ru) - f(0)|\right)}{|r|} \mathcal{L}^d(B) &= \limsup_{r \to 0} \mathbb{E}\left(\int_B \frac{|f(x+ru)-f(x)|}{|r|} dx \right) \\
&\leq \mathbb{E}\left(\limsup_{r \to 0} \int_B \frac{|f(x+ru)-f(x)|}{|r|} dx \right) \\
&\leq \mathbb{E}\left(|D_u f| \left(\overline{B} \right) \right) \\
&= \Theta_{V_u}\left(f, \overline{B} \right) < +\infty.
\end{aligned}
$$

$\limsup \frac{\mathbb{E}(|f(ru)-f(0)|)}{|r|}$ is thus finite, and consequently $\liminf \frac{\mathbb{E}(|f(ru)-f(0)|)}{|r|}$ is also finite. But then, as shown in the proof of (iii) $\Rightarrow$ (i), for all $\varepsilon > 0$,

$$
\Theta_{V_u}\left(f, B(y, \rho + \varepsilon) \right) \leq \liminf_{r \to 0} \frac{\mathbb{E}(|f(ru)-f(0)|)}{|r|} \mathcal{L}^d(B(y, \rho + \varepsilon)).
$$

We deduce that for all $\varepsilon > 0$,

$$
\limsup_{r \to 0} \frac{\mathbb{E}\left(|f(ru) - f(0)|\right)}{|r|} \leq \liminf_{r \to 0} \frac{\mathbb{E}(|f(ru)-f(0)|)}{|r|} \left(1 + \frac{\varepsilon}{|r|} \right)^d.
$$

Letting ε tends to 0 shows that the $\limsup$ is less than the $\liminf$, hence the limit exists and Assertion (iv) is proved. Let us note $C = \lim \frac{\mathbb{E}(|f(ru)-f(0)|)}{|r|}$. We have shown that for all $0 < \varepsilon < \rho$,

$$
C\mathcal{L}^d(B(y, \rho - \varepsilon)) \leq \Theta_{V_u}\left(f, B(y, \rho) \right) \leq C\mathcal{L}^d(B(y, \rho + \varepsilon)).
$$

Letting ε tends to 0 one obtains

$$
\Theta_{V_u}\left(f, B(y, \rho) \right) = C\mathcal{L}^d(B(y, \rho)).
$$

This identity extends to all Borel sets, which proves both Assertion (ii) and the formula

$$
\theta_{V_u}(f) = \liminf_{r \to 0} \frac{\mathbb{E}(|f(ru) - f(0)|)}{|r|} = \lim_{r \to 0} \frac{\mathbb{E}(|f(ru) - f(0)|)}{|r|}.
$$

The proof is complete. $\qquad\qquad\qquad\qquad\qquad\qquad\qquad\qquad\qquad\qquad\qquad \square$

Remark (Degenerate Case)**.** As for Proposition 7.5, one extends the definition of $\theta_{V_u}(f)$ to the degenerate case where $\lim \frac{\mathbb{E}(|f(ru)-f(0)|)}{|r|} = +\infty$.

Remark (Random fields with stationary increments)**.** Let us observe that the key point of the proof of Proposition 7.9 is not the stationarity of the r.f. f but rather the stationarity of the r.f. $x \mapsto f(x + ru) - f(x)$ for all $r \in \mathbb{R}$. Hence Theorem 7.3 straightforwardly extends to r.f. with stationary increments having integrable sample paths.

Integrating over all the directions, one obtains the equivalent of Theorem 7.3 for non directional variation.

Corollary 7.5 (Definition and computation of the variation intensity of a stationary r.f.)**.** *Let $f : \Omega \times \mathbb{R}^d \to \mathbb{R}$ be a stationary r.f. with finite expectation. Then $f \in BV_{\text{loc}}\left(\mathbb{R}^d\right)$ a.s. with a locally finite variation intensity measure $\Theta_V\left(f, \cdot\right)$ if and only if for all $u \in S^{d-1}$ the limit*

$$\lim_{r \to 0} \frac{\mathbb{E}(|f(ru) - f(0)|)}{|r|}$$

exists and is finite. In this case the variation intensity measure $\Theta_V\left(f, \cdot\right)$ is proportional to the Lebesgue measure, and the constant of proportionality $\theta_V(f)$ is given by

$$
\begin{aligned}
\theta_V(f) &= \frac{1}{2\omega_{d-1}} \int_{S^{d-1}} \theta_{V_u}(f) \mathcal{H}^{d-1}(du) \qquad\qquad\qquad (7.7)\\
&= \frac{1}{2\omega_{d-1}} \int_{S^{d-1}} \lim_{r \to 0} \frac{\mathbb{E}\left(|f(ru) - f(0)|\right)}{|r|} \mathcal{H}^{d-1}(du) \\
&= \lim_{r \to 0} \frac{1}{2\omega_{d-1}} \int_{S^{d-1}} \frac{\mathbb{E}\left(|f(ru) - f(0)|\right)}{|r|} \mathcal{H}^{d-1}(du).
\end{aligned}
$$

The constant $\theta_V(f)$ is called the **variation intensity** *of f.*

Proof. The results are straightforward consequences of Theorem 7.3 and the integral geometric formula of Proposition 7.2 which becomes Formula (7.7) in this context. The fact that the limit and the integral commute follows from the bounded convergence theorem using the bound

$$\frac{\mathbb{E}\left(|f(ru) - f(0)|\right)}{|r|} \leq \theta_{V_u}(f) \frac{\mathcal{L}^d\left(B(0, 1+r)\right)}{\mathcal{L}^d(B(0,1))} \leq \theta_{V_u}(f)(1 + R)^d, \ r \in (0, R],$$

given by Theorem 7.3 and Corollary 7.3. □

Let us remark that the directional variation intensities $\theta_{V_u}(f)$, $u \in S^{d-1}$, as well as the variation intensity $\theta_V(f)$ only depend on the two-dimensional distributions of the stationary r.f. f. Note that these second order distributions do not depend on the version of the r.f. f. More generally, if a (non necessarily measurable) r.f. ξ_x satisfies

$$\lim_{r \to 0} \frac{\mathbb{E}\left(|\xi_{ru} - \xi_0|\right)}{|r|} < +\infty$$

for all $u \in S^{d-1}$, then it is continuous in probability and thus it admits a measurable version (see [47, p. 61] or [63, p. 171]). By Corollary 7.5, this measurable version is necessarily a r.f. of bounded variation. This shows that the measurability assumption for the random fields f does not exclude any case of interest when dealing with stationary r.f.

7.4.3 Characterization via Directional Lipschitzness in Mean

In this last section, it is shown that the directional Lipschitzness in mean introduced in Section 7.3.4 is a necessary and sufficient condition for stationary r.f. having finite directional variation intensity.

Lemma 7.1 (Directional Lipschitzness in mean of stationary r.f.)**.** *Let $u \in S^{d-1}$ and let f be a stationary r.f. having finite expectation and being a.s. in $BV_{u,\mathrm{loc}}\left(\mathbb{R}^d\right)$. Then for all $x \in \mathbb{R}^d$ and all $r \in \mathbb{R}$,*

$$\mathbb{E}\left(|f(x + ru) - f(x)|\right) \leq \theta_{V_u}(f)|r|.$$

Proof. First recall that by stationarity for all $x \in \mathbb{R}^d$ and $r \in \mathbb{R}$, $\mathbb{E}\left(|f(x + ru) - f(x)|\right) = \mathbb{E}\left(|f(ru) - f(0)|\right)$. Let $\rho > 0$ and $r \neq 0$. By Corollary 7.3,

$$\int_{B(0,\rho)} \frac{|f(x + ru) - f(x)|}{|r|}dx \leq |D_u f|\left(\overline{B(0, \rho + |r|)}\right) \ \text{a.s.}.$$

Hence, by Fubini's theorem

$$\frac{\mathbb{E}\left(|f(ru) - f(0)|\right)}{|r|}\omega_d\rho^d \leq \theta_{V_u}(f)\omega_d(\rho + |r|)^d,$$

that is

$$\mathbb{E}\left(|f(ru) - f(0)|\right) \leq \theta_{V_u}(f)|r|\left(1 + \frac{|r|}{\rho}\right)^d.$$

Letting $\rho \to +\infty$ we obtain the result. $\qquad\square$

Combining the results of Proposition 7.6 and Lemma 7.1 we obtain that a stationary random field has finite directional variation intensity if and only if it is directionally Lipschitz in mean.

Theorem 7.4 (Characterization of stationary r.f. with locally bounded directional variation via directional Lipschitzness in mean)**.** *Let $f : \mathbb{R}^d \to \mathbb{R}$ be a stationary r.f. with finite expectation and let $u \in S^{d-1}$. The three following assertions are equivalent:*

(i) f has locally bounded variation in the direction u and its directional variation intensity $\theta_{V_u}(f)$ is finite.

(ii) There exists a constant $K > 0$ such that

$$\mathbb{E}\left(|f(x + ru) - f(x)|\right) \leq K|r|, \ x \in \mathbb{R}^d, \ r \in \mathbb{R}.$$

(iii) There exists a constant $K > 0$ and a real $R > 0$ such that

$$\mathbb{E}\left(|f(ru) - f(0)|\right) \leq K|r|, \ r \in [0, R).$$

Besides the directional variation intensity $\theta_{V_u}(f)$ is the least constant K such that (ii) *and* (iii) *hold.*

Proof. (i) $\Rightarrow$ (ii) has already been shown with Lemma 7.1: if f has locally bounded variation in the direction u with a finite directional variation intensity $\theta_{V_u}(f)$ then (ii) holds with $K = \theta_{V_u}(f)$. Clearly (ii) implies (iii). To finish, if (iii) holds, then

$$\liminf_{r \to 0} \frac{\mathbb{E}(|f(ru) - f(0)|)}{|r|} \leq K < +\infty,$$

and by Proposition 7.9 f has locally bounded variation and $\theta_{V_u}(f) \leq K$.

$\square$

As already mentioned in Section 7.3.4, Theorem 7.4 shows that the upper bound of Proposition 7.6 (resp. Proposition 7.7) becomes an equality for any stationary r.f. of bounded directional variation having a finite directional variation intensity (resp. any stationary and isotropic r.f. of bounded variation having a finite variation intensity).

7.5　Conclusion

In this chapter, general definitions and results related to random fields of (locally) bounded (directional) variation were presented. Our main result is Theorem 7.3 which shows that the directional variation intensity measure of any stationary r.f. f is equal to a constant, called the directional variation intensity $\theta_{V_u}(f)$, times the Lebesgue measure. This constant $\theta_{V_u}(f)$ is the mean directional variation of f per unit volume, and it is given by

$$\theta_{V_u}(f) = \lim_{r \to 0} \frac{\mathbb{E}(|f(ru) - f(0)|)}{|r|}.$$

In the next chapter, we will show that when restricting to the case of random sets, the results established in this chapter yield to rigorous generalizations of well-known results regarding the perimeter of random sets (see Chapter 8). Besides, it will be shown in Chapter 9 that the practical expression of $\theta_{V_u}(f)$ enables to compute the directional and non directional variation intensities of various classic r.f. models.

Several natural complements could enhance our results. First, as remarked earlier, the developed results for stationary r.f. are valid for r.f. with stationary increments. Second, one should be able to derive an expression of $\theta_{V_u}(f)$ from just one realization of f in the case where the stationary r.f. f is ergodic (in some sense to be made precise). Third, following [19, 40], one might use regularized difference quotients for the expression of $\theta_{V_u}(f)$.

As a starting point of our study of r.f. of bounded variation, the emphasis was on the mean variation of r.f. It might also be of interest to study the stochastic counterparts of the well-known geometric structures carried by any functions of bounded variation [6]. For example one might study the random set induced by the jumps of a r.f. of bounded variation.

Related to random fields of bounded variations are random fields with sample paths in Sobolev spaces. The recent paper [135] gives sufficient conditions for a second order r.f. to be in a Sobolev space $W_{\mathrm{loc}}^{s,2}\left(\mathbb{R}^d\right)$, $s > 0$. Using the same strategy as in this chapter, one might be able to establish necessary and/or sufficient conditions for stationary r.f. whose sample paths are in $W_{\mathrm{loc}}^{1,p}\left(\mathbb{R}^d\right)$, $p > 1$, and which have a finite mean Sobolev semi-norm.

Variation of Random Sets

Contents

Abstract: This chapter focuses on the mean directional and non directional variations of random sets. Applying the results of Chapter 7, one proves several formulas which equate the directional variations of random sets to the directional derivatives at the origin of functions related to the second-order property of random sets, namely the mean covariogram for random sets with finite mean Lebesgue measure and the variogram for stationary random sets. These formulas show that classical results on the mean perimeter of random closed sets due to Matheron [107, 110] extends rigorously to any measurable random set, provided that the perimeter is understood as the variational perimeter. In a last part, one also establishes a coarea formula for variation intensities: the mean total variation of a r.f. is equal to the integral of the mean perimeter of its excursion sets.

Most of the results of this chapter can be found in the accepted paper [58]. However the proofs presented in this paper do not rely on the results of Chapter 7 (which were not written at that time).

8.1   Introduction

When restricting to random sets, the general results on the mean variation of random fields established in Chapter 7 yield to identities for the mean directional vari-

ation and mean perimeter. The object of this chapter is to demonstrate that these identities provide rigorous generalization of well-known formulas of mathematical morphology due to Matheron [107, 110, 100]. The strength of the mean (variational) perimeter is that it provides formulas which are valid for any random set. In comparison, all the generalizations of Matheron's results for which the Steiner formula is involved rely on geometrical or topological hypotheses on the considered random sets.

The object of study of the first section of this chapter is the *covariogram*[1] g_A of a deterministic measurable set $A \subset \mathbb{R}^d$, that is the function defined for all $y \in \mathbb{R}^d$ by $g_A(y) = \mathcal{L}^d (A \cap (y + A))$.

Given the covariogram g_A of an unknown set A, a general inverse problem is to determine the geometric information on A that g_A contains. As an important example, Averkov and Bianchi have recently established Matheron's conjecture: up to a translation and a reflexion, **convex** bodies of $\mathbb{R}^2$ are fully determined by their covariogram (see [10] and the references within). Contrary to the above mentioned results, we focus on geometric information which is shown to be contained in the covariogram g_A of any measurable set A: the directional variations and the perimeter of A.

As our first main result will demonstrate, the right notion of perimeter which can be computed from the covariogram is the one from the theory of functions of bounded variation [6]. Let us recall that the perimeter $\mathrm{Per}(A)$ of a measurable set A is defined as

$$\mathrm{Per}(A) = \begin{cases} |D\mathbb{1}_A| \left(\mathbb{R}^d \right) & \text{if } \mathbb{1}_A \in BV \left(\mathbb{R}^d \right), \\ +\infty & \text{otherwise.} \end{cases}$$

Similarly the directional variation $V_u(A)$ in the direction $u \in S^{d-1}$ of A is

$$V_u(A) = \begin{cases} |D_u \mathbb{1}_A| \left(\mathbb{R}^d \right) & \text{if } \mathbb{1}_A \in BV_u \left(\mathbb{R}^d \right), \\ +\infty & \text{otherwise.} \end{cases}$$

Let us also recall that if A is a compact set with Lipschitz boundary (e.g. A is a convex body), then $\mathrm{Per}(A) = \mathcal{H}^{d-1} (\partial A)$, whereas in the general case we only have $\mathrm{Per}(A) \leq \mathcal{H}^{d-1} (\partial A)$ [6, Proposition 3.62]. However there is an alternative notion of boundary, the *essential boundary* $\partial_e A$, which is in accordance with the variational perimeter. Let us refer to [6, 54] for the definition of the essential boundary $\partial_e A$ and recall that $\partial_e A \subset \partial A$, and $\mathrm{Per}(A) = \mathcal{H}^{d-1} (\partial_e A)$, that is the variational perimeter is the $d-1$-Hausdorff measure of the essential boundary. This fundamental result shows that the variational perimeter is in accordance with the common notion of "perimeter".

We prove that for every measurable set A of finite Lebesgue measure,

$$\lim_{r \to 0} \frac{g_A(0) - g_A(ru)}{|r|} = \frac{1}{2} V_u(A), \ u \in S^{d-1}. \tag{8.1}$$

---

[1]Note that some authors prefer the terms *set covariance* or *covariance function* [25, 26, 129].

In addition, noting $(g_A^u)'(0) := \lim\limits_{r \to 0^+} \dfrac{g_A(ru) - g_A(0)}{r}$ the directional derivatives at the origin of the covariogram, it is shown that

$$\mathrm{Per}(A) = -\frac{1}{\omega_{d-1}} \int_{S^{d-1}} (g_A^u)'(0)\mathcal{H}^{d-1}(du). \tag{8.2}$$

Hence, for any measurable set A, the perimeter $\mathrm{Per}(A)$ can be computed from the directional derivatives at the origin of the covariogram g_A. As a by-product, it is also shown that a measurable set A has finite perimeter if and only if its covariogram g_A is Lipschitz, and in this case the Lipschitz constant is given by

$$\mathrm{Lip}\,(g_A) = \frac{1}{2} \sup_{u \in S^{d-1}} V_u(A).$$

Formula (8.1) has already been proved for certain classes of sets. It was well-known by the mathematical morphology school [106, 72, 110, 111] that the directional derivative at the origin of the covariogram g_A of a convex body is equal to the opposite of the length of the orthogonal projection of the set A. The convexity assumption was relaxed in [129] where Rataj extends the result to compact sets in $\mathcal{U}_{PR}$ satisfying a condition of full-dimensionality, $\mathcal{U}_{PR}$ being the family of locally finite unions of sets with positive reach such that all their finite intersections also have positive reach[2]. In this more general framework, the length of the orthogonal projection is replaced by the total projection $TP_u(A)$. One can easily verify that $V_u(A) = 2TP_u(A)$ by using a recent result due to Ambrosio, Colesanti and Villa [5]: a full-dimensional compact set with positive reach A satisfies $\mathrm{Per}(A) = 2\Phi_{d-1}(A)$ [5, Theorem 9], where $\Phi_{d-1}(A)$ denotes the $(d-1)$-total curvature of A [56]. Since Formula (8.1) is valid for any measurable set A such that $\mathcal{L}^d(A) < +\infty$, we claim that the directional variation is the relevant general concept when it comes to the derivative at the origin of the covariogram.

Formula (8.2) has been widely stated in the mathematical morphology literature [72, 110, 137, 100]. We rigorously show that it is valid for any measurable set A having finite Lebesgue measure, provided the perimeter $\mathrm{Per}(A)$ is understood as the variation of A (and not as $\mathcal{H}^{d-1}(\partial A)$).

The Lipschitzness of the covariogram seems to have received less attention in the literature. It is stated in [111] that the covariogram of a compact convex set is Lipschitz. The given upper bound of the Lipschitz constant is twice the actual Lipschitz constant.

The second section of this chapter (Section 8.4) transposes the above mentioned results to the case of random sets of finite mean Lebesgue measure. In this context, one defines the mean covariogram of a random set X as the function $\gamma_X(y) = \mathbb{E}\left(\mathcal{L}^d(X \cap y + X)\right)$. The mean covariogram of a random set X is of particular importance in stochastic geometry since it is related to the probability that two

---

[2]We refer to [56] and [130] for definitions and results regarding sets with positive reach and $\mathcal{U}_{PR}$-sets respectively

given points belong to X according to the following relation

$$\gamma_X(y) = \int_{\mathbb{R}^d} \mathbb{P}\left(x \in X \text{ and } x + y \in X\right) dx.$$

As a consequence the mean covariogram is systematically involved in second order statistics of the classical germ-grain models presented in Chapter 5. This is also the case for the transparent dead leaves model introduced in Chapter 6.

All the established properties of covariograms of deterministic sets extend to the case of mean covariograms of random sets. In particular, the stochastic equivalent of (8.1) and (8.2) show that the expectations of the variations of a random set X are proportional to the directional derivatives of its mean covariogram γ_X.

The following part of this chapter (Section 8.5) deals with the variation of stationary random sets. To be coherent with previous works [136], the directional variation intensity $\theta_{V_u}(X)$ of a random set X is also called *specific directional variation*, and similarly for the variation intensity $\theta_V(X)$ which is called *specific variation*. For a stationary random set X, the second-order function which is related to its variation is the *variogram* ν_X, that is the function defined by $\nu_X(y) = \mathbb{P}\left(y \in X, \ 0 \notin X\right)$. Our second main result shows that for any stationary random set X,

$$\theta_{V_u}(X) = 2 \lim_{r \to 0} \frac{\nu_X(ru)}{|r|}.$$

Again, noting $(\nu_X^u)'(0) = \lim \frac{\nu_X(ru)}{|r|}$ and integrating over all directions u, one obtains an expression of the specific variation $\theta_V(X)$ of X

$$\theta_V(X) = \frac{1}{\omega_{d-1}} \int_{S^{d-1}} (\nu_X^u)'(0) \mathcal{H}^{d-1}(du).$$

Like Formula (8.2), the above formula has been stated in the early works of Matheron [107, p. 30] [100, p. 26], but it was given without much detail on its validity. It should be emphasized that the specific variation is well-defined for any stationary random set, and that it can be easily computed as soon as one knows the probabilities $\mathbb{P}\left(ru \in X, 0 \notin X\right)$. As an illustration, the specific directional variations and the specific variation of homogeneous Boolean models will be computed in the next chapter (see Section 9.4). Because it is well-defined for any stationary RACS and easily computable, we claim that the specific variation is an interesting alternative to the usual specific surface area [136] when one deals with non $\mathcal{L}^d$-negligible random sets.

In the last part of this chapter, mean coarea formulas for mean total variation are established. In particular it is shown that the variation intensity of a stationary r.f. f is equal to the integral over t of the specific variation of its excursion sets $\{f > t\} := \{y \in \mathbb{R}^d, \ f(y) > t\}$, that is

$$\theta_{V_u}(f) = \int_{-\infty}^{+\infty} \theta_{V_u}(\{f > t\}) dt.$$

The plan of this chapter is as follows. Section 8.2 deals with covariograms of deterministic measurable sets and establishes the identities between the directional

derivative at the origin of covariogram and the directional variation. Then, in Section 8.3 our definition of (jointly) measurable sets and its link with the usual definition of random closed sets are discussed. Section 8.4 generalizes the results of Section 8.2 to the case of random sets with finite mean Lebesgue measure. Formulas for the specific directional and non directional variation of stationary random sets are established in Section 8.5, and its differences with the usual specific area is discussed. Finally, the mean coarea formulas for the total variation of random fields and for the variation intensity of stationary r.f. are proved in Section 8.6.

8.2 Covariogram of Measurable Sets and Variation

8.2.1 Covariogram of a Measurable Set

Definition 8.1 (Covariogram of a measurable set). *Let $A \subset \mathbb{R}^d$ be a $\mathcal{L}^d$-measurable set of finite Lebesgue measure. The* covariogram *of A is the function $g_A : \mathbb{R}^d \to [0, +\infty[$ defined for all $y \in \mathbb{R}^d$ by*

$$g_A(y) = \mathcal{L}^d \left(A \cap (y + A) \right) = \int_{\mathbb{R}^d} \mathbb{1}_A(x) \mathbb{1}_A(x + y) dx.$$

As initially noted by Matheron [106], the covariogram of A can be expressed as the convolution of the indicator functions of A and its symmetric $\check{A} = \{-x \mid x \in A\}$:

$$g_A = \mathbb{1}_A * \mathbb{1}_{\check{A}}.$$

As illustrated in the following proposition, this point of view is useful to establish some analytic properties of g_A.

Proposition 8.1. *Let $A \subset \mathbb{R}^d$ be a $\mathcal{L}^d$-measurable set of finite Lebesgue measure and g_A be its covariogram. Then*

1. *For all $y \in \mathbb{R}^d$, $0 \le g_A(y) \le g_A(0) = \mathcal{L}^d(A)$.*

2. *g_A is even: for all $y \in \mathbb{R}^d$, $g_A(-y) = g_A(y)$.*

3. *$\int_{\mathbb{R}^d} g_A(y) dy = \mathcal{L}^d(A)^2$.*

4. *g_A is uniformly continuous over $\mathbb{R}^d$ and $\lim_{|y| \to +\infty} g_A(y) = 0$.*

Proof. The three first points are elementary proved. The fourth property is obtained in applying the L^p-$L^{p'}$-convolution theorem to $g_A = \mathbb{1}_A * \mathbb{1}_{\check{A}}$ (see [1, Chapter 2] for example). $\qquad\square$

It is well-known that the covariogram is a positive-definite function [106, p. 22], [100, p. 23]. The next proposition improves slightly this result. In particular, it shows that for all $x \ne 0$, $g_A(x) < g_A(0)$.

Proposition 8.2 (Strict positive-definiteness of the covariogram)**.** *Let A be a $\mathcal{L}^d$-measurable set such that $0 < \mathcal{L}^d(A) < +\infty$. Then its covariogram g_A is a strictly positive-definite function, that is, for all $p \in \mathbb{N}^*$, for all p-tuple $(y_1, \ldots, y_p)$ of distinct vectors of $\mathbb{R}^d$, and for all $(w_1, \ldots, w_p) \in \mathbb{R}^p \setminus \{0\}$ we have*

$$\sum_{j,k=1}^{p} w_j w_k g_A(y_k - y_j) > 0.$$

Proof. By Lemma 8.1 below, the function $x \mapsto \sum_{j=1}^{p} w_j \mathbb{1}_A(x + y_j)$ is not a.e. equal to zero. Hence

$$\sum_{j,k=1}^{p} w_j w_k g_A(y_k - y_j) = \sum_{j,k=1}^{p} w_j w_k \int_{\mathbb{R}^d} \mathbb{1}_A(x) \mathbb{1}_A(x + y_k - y_j) dx$$

$$= \sum_{j,k=1}^{p} w_j w_k \int_{\mathbb{R}^d} \mathbb{1}_A(x + y_j) \mathbb{1}_A(x + y_k) dx$$

$$= \int_{\mathbb{R}^d} \left(\sum_{j=1}^{p} w_j \mathbb{1}_A(x + y_j) \right)^2 dx > 0.$$

$\square$

Lemma 8.1 (The translations of an integrable function are linearly independent)**.** *Let f be a non null function of $L^1\left(\mathbb{R}^d\right)$ and let $y_1, \ldots, y_p$ be p distinct vectors of $\mathbb{R}^d$. Then the functions $x \mapsto f(x + y_j)$, $j = 1, \ldots, p$, are linearly independent in $L^1\left(\mathbb{R}^d\right)$.*

Proof. Let $(w_1, \ldots, w_p) \in \mathbb{R}^p$ be such that $\sum_{j=1}^{p} w_j f(x + y_j) = 0$ for a.e. $x \in \mathbb{R}^d$. Applying the Fourier transform we have

$$\left(\sum_{j=1}^{p} w_j e^{i\langle \xi, y_j \rangle} \right) \hat{f}(\xi) = 0 \text{ for all } \xi \in \mathbb{R}^d.$$

Since f is non null and integrable, $\hat{f}$ is non null and continuous. Hence there exists $\xi_0 \in \mathbb{R}^d$ and $r > 0$ such that for all $\xi \in B(\xi_0, r)$, $\hat{f}(\xi) \neq 0$, and thus $\forall \xi \in B(\xi_0, r)$, $S(\xi) := \sum_{j=1}^{p} w_j e^{i\langle \xi, y_j \rangle} = 0$. One easily shows that the sum $S(\xi)$ is null for all $\xi \in \mathbb{R}^d$ in considering the one-dimensional restriction of S on the line containing ξ and ξ_0: by the identity theorem, this one-dimensional function is null since it is analytic and null over an open interval. Applying the inverse generalized Fourier transform to $S = 0$ shows that $\sum_{j=1}^{p} w_j \delta_{y_j} = 0$. This implies that $w_1 = \cdots = w_p = 0$, since by hypothesis the vectors y_j are distinct. $\square$

Proposition 8.3. *Let $A \subset \mathbb{R}^d$ be a $\mathcal{L}^d$-measurable set of finite Lebesgue measure and let g_A be its covariogram. Then for all $y, z \in \mathbb{R}^d$*

$$|g_A(y) - g_A(z)| \le g_A(0) - g_A(y - z).$$

Proof. First let us show that for all measurable sets A_1, A_2, and A_3

$$\mathcal{L}^d(A_1 \cap A_2) - \mathcal{L}^d(A_1 \cap A_3) \le \mathcal{L}^d(A_2 \setminus A_3) = \mathcal{L}^d(A_2) - \mathcal{L}^d(A_3 \cap A_2). \qquad (8.3)$$

We have

$$\mathcal{L}^d(A_1 \cap A_2) - \mathcal{L}^d(A_1 \cap A_3) \le \mathcal{L}^d(A_1 \cap A_2) - \mathcal{L}^d(A_1 \cap A_2 \cap A_3)$$
$$\le \mathcal{L}^d((A_1 \cap A_2) \setminus (A_1 \cap A_2 \cap A_3)).$$

Now using that $(A_1 \cap A_2) \setminus (A_1 \cap A_2 \cap A_3)$ is included in the set $A_2 \setminus A_3$, (8.3) is proved. Applying (8.3) to the sets $A_1 = A$, $A_2 = y + A$ and $A_3 = z + A$ we get

$$g_A(y) - g_A(z) = \mathcal{L}^d(A \cap (y + A)) - \mathcal{L}^d(A \cap (z + A))$$
$$\le \mathcal{L}^d(y + A) - \mathcal{L}^d((y + A) \cap (z + A))$$
$$\le \mathcal{L}^d(A) - \mathcal{L}^d(A \cap ((z - y) + A))$$
$$\le g_A(0) - g_A(z - y).$$

$\square$

Remark. The weaker inequality

$$|g_A(y) - g_A(z)| \le 2(g_A(0) - g_A(y - z))$$

was established by Matheron [111, p. 1].

Observe that the inequality of Proposition 8.3 shows that the Lipschitzness of the covariogram only depends on the behavior of the function at 0.

8.2.2   Directional Variation, Perimeter and Covariogram of Measurable Sets

Our main results relating the directional derivatives at the origin of the covariogram and the directional variation are established in this section (see Theorem 8.1 and Theorem 8.2).

Lemma 8.2 ([111])**.** *Let A be a $\mathcal{L}^d$-measurable set having finite Lebesgue measure and let g_A be its covariogram. Then for all $y \in \mathbb{R}^d$*

$$g_A(0) - g_A(y) = \frac{1}{2} \int_{\mathbb{R}^d} |\mathbb{1}_A(x + y) - \mathbb{1}_A(x)| \, dx.$$

Proof.

$$\int_{\mathbb{R}^d} |\mathbb{1}_A(x + y) - \mathbb{1}_A(x)| \, dx = \int_{\mathbb{R}^d} (\mathbb{1}_A(x + y) - \mathbb{1}_A(x))^2 \, dx = 2 \left(g_A(0) - g_A(y) \right).$$

$\square$

The identity of Lemma 8.2, which is due to Matheron [111], is the key point to apply the results from the theory of functions of bounded directional variations enunciated in Section 7.2.2. Especially of interest is Corollary 7.4 which ensures that for any $f \in L^1\left(\mathbb{R}^d\right)$

$$|D_u f|\left(\mathbb{R}^d\right) = \lim_{r \to 0} \int_{\mathbb{R}^d} \frac{|f(x + ru) - f(x)|}{|r|} dx.$$

First, one establishes Formula (8.1) and obtains a characterization of sets of finite directional variation. Recall that the directional variation $V_u(A)$ of a set A is defined by

$$V_u(A) = \begin{cases} |D_u \mathbb{1}_A|\left(\mathbb{R}^d\right) & \text{if } \mathbb{1}_A \in BV_u\left(\mathbb{R}^d\right), \\ +\infty & \text{otherwise.} \end{cases}$$

Theorem 8.1 (Directional variation and covariogram of measurable sets). *Let A be a $\mathcal{L}^d$-measurable set having finite Lebesgue measure, let g_A be its covariogram, and let $u \in S^{d-1}$. The following assertions are equivalent:*

(i) A has finite directional variation $V_u(A)$.

(ii) $\lim_{r \to 0} \dfrac{g_A(0) - g_A(ru)}{|r|}$ exists and is finite.

(iii) The one-dimensional restriction of the covariogram $g_A^u : r \mapsto g_A(ru)$ is Lipschitz.

In addition,

$$\mathrm{Lip}\left(g_A^u\right) = \lim_{r \to 0} \frac{g_A(0) - g_A(ru)}{|r|} = \frac{1}{2} V_u\left(A\right),$$

the second equality being valid both in the finite and infinite case.

Proof. Since from Lemma 8.2,

$$\frac{g_A(0) - g_A(ru)}{|r|} = \frac{1}{2} \int_{\mathbb{R}^d} \frac{|\mathbb{1}_A(x + ru) - \mathbb{1}_A(x)|}{|r|} dx,$$

by applying Corollary 7.4 with $f = \mathbb{1}_A$ one obtains the equivalence of *(i)* and *(ii)* as well as the formula $\lim_{r \to 0} \dfrac{g_A(0) - g_A(ru)}{|r|} = \dfrac{1}{2} V_u\left(A\right)$.

Let us show that *(i)* implies *(iii)*. By Proposition 8.3, for all r and $s \in \mathbb{R}$

$$|g_A(ru) - g_A(su)| \le g_A(0) - g_A((r - s)u) = \frac{1}{2} \int_{\mathbb{R}^d} |\mathbb{1}_A(x + (r - s)u) - \mathbb{1}_A(x)| \, dx.$$

Applying the inequality of Corollary 7.4 with $f = \mathbb{1}_A$,

$$|g_A(ru) - g_A(su)| \le \frac{1}{2}|r - s| \int_{\mathbb{R}^d} \frac{|\mathbb{1}_A(x + (r - s)u) - \mathbb{1}_A(x)|}{|r - s|} dx \le \frac{1}{2} V_u(A)|r - s|.$$

Hence g_A^u is Lipschitz and $\mathrm{Lip}\left(g_A^u\right) \le \frac{1}{2} V_u(A)$.

Let us now show that *(iii)* implies *(i)*. For all $r \neq 0$ we have

$$\operatorname{Lip}\left(g_A^u\right) \geq \frac{g_A(0) - g_A(ru)}{|r|} = \frac{1}{2} \int_{\mathbb{R}^d} \frac{|\mathbb{1}_A(x + ru) - \mathbb{1}_A(x)|}{|r|} dx.$$

By Corollary 7.4 the right-hand side tends towards $\frac{1}{2}V_u(A)$ as r tends to 0. Hence A has finite directional variation in the direction u and $\operatorname{Lip}\left(g_A^u\right) \geq \frac{1}{2}V_u(A)$. All in all we have shown that *(i)* and *(iii)* are equivalent and that $\operatorname{Lip}\left(g_A^u\right) = \frac{1}{2}V_u(A)$. $\square$

Considering all the possible directions $u \in S^{d-1}$, the results of the previous theorem yield to Formula (8.2) (reproduced below as Formula (8.4)) and a characterization of sets of finite perimeter.

Theorem 8.2 (Perimeter and covariogram of measurable sets)**.** *Let A be a $\mathcal{L}^d$-measurable set having finite Lebesgue measure, and let g_A be its covariogram. The following assertions are equivalent:*

(i) A has finite perimeter $\operatorname{Per}(A)$.

(ii) For all $u \in S^{d-1}$, $(g_A^u)'(0) := \lim\limits_{r \to 0^+} \dfrac{g_A(ru) - g_A(0)}{r}$ exists and is finite.

(iii) The covariogram g_A is Lipschitz.

In addition the following relations hold:

$$\operatorname{Lip}\left(g_A\right) = \frac{1}{2} \sup_{u \in S^{d-1}} V_u(A) \leq \frac{1}{2}\operatorname{Per}(A)$$

and

$$\operatorname{Per}(A) = -\frac{1}{\omega_{d-1}} \int_{S^{d-1}} (g_A^u)'(0)\mathcal{H}^{d-1}(du), \tag{8.4}$$

this last formula being valid both in the finite and infinite case.

Proof. The equivalence of *(i)* and *(ii)* as well as the integral geometric formula (8.4) derive from the integral geometric formula

$$\operatorname{Per}(A) = \frac{1}{2\omega_{d-1}} \int_{S^{d-1}} V_u(A)\mathcal{H}^{d-1}(du)$$

(see Proposition 7.1) and the identity

$$(g_A^u)'(0) = \lim_{r \to 0^+} \frac{g_A(ru) - g_A(0)}{r} = -\frac{1}{2}V_u(A).$$

Let us now show that *(i)* implies *(iii)*. Let $y, z \in \mathbb{R}^d$. Denote by u the direction of S^{d-1} such that $y - z = |y - z|u$. By Proposition 8.3 and Theorem 8.1

$$|g_A(y) - g_A(z)| \leq g_A(0) - g_A(y - z) \leq \frac{1}{2}V_u(A)|y - z| \leq \left(\frac{1}{2} \sup_{u \in S^{d-1}} V_u(A)\right)|y - z|.$$

Hence g_A is Lipschitz and $\mathrm{Lip}\,(g_A) \leq \frac{1}{2}\sup_u V_u(A)$. As for the converse implication and inequality, for all $u \in S^{d-1}$,

$$\mathrm{Lip}\,(g_A) \geq \lim_{r \to 0} \frac{g_A(0) - g_A(ru)}{|r|} = \frac{1}{2}V_u(A).$$

Hence for all $u \in S^{d-1}$, $V_u(A) < +\infty$ and $\mathrm{Lip}\,(g_A) \geq \frac{1}{2}\sup_u V_u(A)$. This concludes the proof. $\square$

Remark (Extension to the covariogram of functions?)**.** One natural question is whether Formula (8.4) extends to the case of functions. The answer to this question is negative. Indeed, if one considers a smooth function $f \in \mathcal{C}_c^1\left(\mathbb{R}^d\right)$, then its covariogram $g_f(y) = \int_{\mathbb{R}^d} f(x + y)f(x)dx$ is well-defined and is differentiable in 0. But since g_f is even, its derivative at the origin equals zero, and thus the variation of f is not equal to the integral of the directional derivatives of the covariogram g_f.

8.3   Measurable Random Sets

Definition 8.2 (Random sets)**.** *A random set X is a measurable subset of the measurable space $\left(\Omega \times \mathbb{R}^d, \mathcal{A} \otimes \mathcal{B}\left(\mathbb{R}^d\right)\right)$.*

The realizations of X are the sets $X(\omega) := \left\{x \in \mathbb{R}^d,\ (\omega, x) \in X\right\}$. One identifies a random set X with the measurable random indicator function $\mathbb{1}_X : (\omega, x) \mapsto \mathbb{1}_{X(\omega)}(x)$.

The above definition of random sets is the one evoked in [115, p. 41]. It is different and less standard than the one of random closed sets (RACS) [110, 115, 136]. Jointly measurable random sets are different than RACS since they are possibly non-closed sets. Let us precise that any RACS X defines a jointly measurable random set. Let $(\mathcal{F}, \mathcal{B}(\mathcal{F}))$ denotes the set of random closed sets of $\mathbb{R}^d$ equipped with the hit-or-miss topology, and let X be a RACS, that is a measurable map $X : (\Omega, \mathcal{A}) \to (\mathcal{F}, \mathcal{B}(\mathcal{F}))$. Then the map

$$\left(\Omega \times \mathbb{R}^d, \mathcal{A} \otimes \mathcal{B}\left(\mathbb{R}^d\right)\right) \quad \to \quad (\mathbb{R}, \mathcal{B}(\mathbb{R}))$$
$$(\omega, x) \quad \mapsto \quad \mathbb{1}_{X(\omega)}(x)$$

is measurable. Indeed it is the composition of the function

$$\left(\Omega \times \mathbb{R}^d, \mathcal{A} \otimes \mathcal{B}\left(\mathbb{R}^d\right)\right) \quad \to \quad \left(\mathcal{F} \times \mathbb{R}^d, \mathcal{B}(\mathcal{F}) \otimes \mathcal{B}\left(\mathbb{R}^d\right)\right)$$
$$(\omega, x) \quad \mapsto \quad (X(\omega), x),$$

which is trivially measurable, and the function

$$\left(\mathcal{F} \times \mathbb{R}^d, \mathcal{B}(\mathcal{F}) \otimes \mathcal{B}\left(\mathbb{R}^d\right)\right) \quad \to \quad (\mathbb{R}, \mathcal{B}(\mathbb{R}))$$
$$(X, x) \quad \mapsto \quad \mathbb{1}_X(x),$$

which is also measurable as proved in [115, p. 59]. To conclude, measurable random sets are more general than RACS, and any RACS defines a measurable random set. In particular all the following definitions and results which involve measurable random sets are also valid for RACS.

Let us also precise that dealing with this general definition for random sets is of interest. For example, an important class of generally not closed random sets are the level sets of a measurable random field f, that is the sets $\{f > u\} = \left\{(\omega, x) \in \Omega \times \mathbb{R}^d, \ f(\omega, x) > u\right\}$, $u \in \mathbb{R}$.

Definition 8.3 (Random sets of finite perimeter). *A random set X is a* random set of finite perimeter *if the random indicator function $\mathbb{1}_X : (\omega, x) \mapsto \mathbb{1}_{X(\omega)}(x)$ has a.s. finite bounded variation (as defined by Definition 7.4).*

One defines similarly *random sets of finite directional variation*, as well as *random set of locally finite perimeter* and random sets of locally finite directional variation. If X has locally finite variation, then we write $\Theta_V(X, \cdot) := \Theta_V(\mathbb{1}_X, \cdot)$ for its variation intensity measure. Similarly, for random sets of locally finite directional variation one writes $\Theta_{V_u}(X, \cdot) := \Theta_{V_u}(\mathbb{1}_X, \cdot)$.

8.4 Mean Covariogram and Variation of Random Sets

In this section we will consider random sets X for which $\mathbb{E}(\mathcal{L}^d(X)) < +\infty$. We will introduce the mean covariogram of random sets and generalize the results of Section 8.2 to the case of random sets.

Definition 8.4 (Mean covariogram of a random closed set). *Let X be a random closed set (RACS) of $\mathbb{R}^d$ having finite mean Lebesgue measure, that is $\mathbb{E}\left(\mathcal{L}^d(X)\right) < +\infty$. The* mean covariogram γ_X *of X is the function $\gamma_X : \mathbb{R}^d \to [0, \infty[$ defined by*

$$\gamma_X(y) = \mathbb{E}\left(\mathcal{L}^d\left(X \cap (y + X)\right)\right) = \int_{\Omega \times \mathbb{R}^d} \mathbb{1}_{X(\omega)}(x) \mathbb{1}_{X(\omega)}(x + y) \mathbb{P}(d\omega) dx.$$

All the results established for covariograms of deterministic sets can be adapted for mean covariograms of random sets.

Proposition 8.4 (Properties of mean covariograms). *Let X be a random set of $\mathbb{R}^d$ satisfying $\mathbb{E}\left(\mathcal{L}^d(X)\right) < +\infty$ and let γ_X be its mean covariogram. Then*

1. *For all $y \in \mathbb{R}^d$, $0 \le \gamma_X(y) \le \gamma_X(0) = \mathbb{E}\left(\mathcal{L}^d(X)\right)$.*

2. *γ_X is even.*

3. *$\gamma_X(y) = \int_{\mathbb{R}^d} \mathbb{P}\left(x \in X \text{ and } x + y \in X\right) dx.$*

4. *$\int_{\mathbb{R}^d} \gamma_X(y) dy = \mathbb{E}\left(\mathcal{L}^d(X)^2\right) \in [0, +\infty].$*

5. *If $\mathbb{E}\left(\mathcal{L}^d(X)\right) > 0$, then γ_X is a strictly positive-definite function.*

6. *For all $y, z \in \mathbb{R}^d$, $|\gamma_X(y) - \gamma_X(z)| \leq \gamma_X(0) - \gamma_X(y - z)$.*

7. *γ_X is uniformly continuous over $\mathbb{R}^d$ and $\lim\limits_{|y| \to +\infty} \gamma_X(y) = 0$.*

The proofs are omitted since they mostly consist in integrating the results of Section 8.2.1 with respect to ω.

As in the deterministic case, the directional derivatives of the mean covariogram of a random set are related to its mean directional variations.

Proposition 8.5 (Mean covariogram and mean variation)**.** *Let X be a random set of $\mathbb{R}^d$ satisfying $\mathbb{E}\left(\mathcal{L}^d(X)\right) < +\infty$ and let γ_X be its mean covariogram. Then for all $u \in S^{d-1}$,*

$$\lim_{r \to 0} \frac{\gamma_X(0) - \gamma_X(ru)}{|r|} = \frac{1}{2} \mathbb{E}\left(V_u(X)\right),$$

and, noting $(\gamma_X^u)'(0) = \lim\limits_{r \to 0^+} \dfrac{\gamma_X(ru) - \gamma_X(0)}{r}$,

$$-\frac{1}{\omega_{d-1}} \int_{S^{d-1}} (\gamma_X^u)'(0) \mathcal{H}^{d-1}(du) = \mathbb{E}\left(\mathrm{Per}(X)\right).$$

Proof. By Lemma 8.2,

$$\frac{\gamma_X(0) - \gamma_X(ru)}{|r|} = \frac{1}{2} \mathbb{E}\left(\int_{\mathbb{R}^d} \frac{|\mathbb{1}_X(x + ru) - \mathbb{1}(x)|}{|r|}\right),$$

hence the first formula is just a transcription of the identity of Proposition 7.5

$$\Theta_{V_u}\left(f, \mathbb{R}^d\right) = \lim_{r \to 0} \int_{\mathbb{R}^d} \frac{\mathbb{E}\left(|f(x + ru) - f(x)|\right)}{|r|} dx,$$

with $f = \mathbb{1}_X$. The second formula is obtained by integration over all the directions $u \in S^{d-1}$ and by applying the dominated convergence theorem, since by Corollary 7.4

$$\left|\frac{\gamma_X(ru) - \gamma_X(0)}{r}\right| \leq \frac{1}{2} \mathbb{E}\left(V_u(X)\right).$$

$\square$

8.5   Variogram and Specific Variation of Stationary Random Sets

A random set X is said to be *stationary* if its associated r.f. $\mathbb{1}_X : (\omega, x) \mapsto \mathbb{1}_{X(\omega)}(x)$ is stationary. Again, let us precise that if X is a stationary RACS (in the sense that for all $y \in \mathbb{R}^d$, $y + X$ and X have the same distribution over $(\mathcal{F}, \mathcal{B}(\mathcal{F}))$) then its associated measurable random field $\mathbb{1}_X : (\omega, x) \mapsto \mathbb{1}_{X(\omega)}(x)$ is stationary.

A stationary random set is said to be of *locally bounded variation* if the stationary random field $\mathbb{1}_X : (\omega, x) \mapsto \mathbb{1}_{X(\omega)}(x)$ is of locally bounded variation, and random sets of *locally bounded directional variation*. One writes $\theta_V(X) := \theta_V(\mathbb{1}_X)$

which is referred to as the *variation intensity* or the *specific variation* of the stationary random set X. Similarly, $\theta_{V_u}(X) := \theta_{V_u}(\mathbb{1}_X)$ is called the *directional variation intensity* or the *specific directional variation* in the direction u.

Definition 8.5 (Variogram of a stationary random set)**.** *Let X be a stationary random set. The variogram ν_X of X is the function $\nu_X : \mathbb{R}^d \to \mathbb{R}$ defined by*

$$\nu_X(y) = \mathbb{P}\left(y \in X, \ 0 \notin X\right).$$

Clearly $\nu_X(0) = 0$ and the variogram ν_X is even: indeed, by stationarity

$$\nu_X(-y) = \mathbb{P}\left(0 \notin X\right) - \mathbb{P}\left(-y \notin X, \ 0 \notin X\right) = \mathbb{P}\left(0 \notin X\right) - \mathbb{P}\left(0 \notin X, \ y \notin X\right) = \nu_X(y).$$

Besides, ν_X can be shown to be conditionally negative definite (see [100, Section 3.2] for details). As the next proposition shows, the variogram $\nu_X(y)$ plays the same role for stationary random sets as the difference $\gamma_X(0) - \gamma_X(y)$ for random sets of finite mean Lebesgue measure.

Proposition 8.6 (Specific variations and variogram)**.** *Let X be a stationary random set and let ν_X be its variogram. Then for all $u \in S^{d-1}$ the limit*

$$(\nu_X^u)'(0) := \lim_{r \to 0} \frac{1}{|r|} \nu_X(ru) \in [0, +\infty]$$

exists, and the specific directional variation $\theta_{V_u}(X)$ is given by

$$\theta_{V_u}(X) = 2\left(\nu_X^u\right)'(0) = 2 \lim_{r \to 0} \frac{1}{|r|} \mathbb{P}\left(ru \in X, 0 \notin X\right).$$

In other words, the specific directional variation is twice the directional derivative of the variogram at the origin. Integrating over all directions, one obtains the specific variation of X:

$$\theta_V(X) = \frac{1}{\omega_{d-1}} \int_{S^{d-1}} \left(\nu_X^u\right)'(0) \mathcal{H}^{d-1}(du). \tag{8.5}$$

Proof. Since X is a random set $|\mathbb{1}_X(ru) - \mathbb{1}_X(0)| \in \{0, 1\}$, hence for all $r \in \mathbb{R}$,

$$\mathbb{E}(|\mathbb{1}_X(ru) - \mathbb{1}_X(0)|) = \mathbb{P}(ru \in X, \ 0 \notin X) + \mathbb{P}(ru \notin X, \ 0 \in X) = 2\nu_X(ru).$$

By Theorem 7.3, the limit $\lim_{r \to 0} \frac{1}{|r|} \nu_X(ru)$ exists and

$$\theta_{V_u}(X) = 2 \lim_{r \to 0} \frac{1}{|r|} \nu_X(ru),$$

and the formula of $\theta_V(X)$ is given by Corollary 7.5. $\qquad\qquad\square$

Let us now discuss the terminology *specific variation* of X for the constant $\theta_V(X)$. Eq. (8.5) is exactly the formula given in [100, p. 26] and which originates from Matheron [107, p. 30]. In these references, the constant corresponding to the variation intensity $\theta_V(X)$ is called the *specific $(d-1)$-volume* of X (*specific*

perimeter if $d = 2$, *specific surface area* if $d = 3$). However, in the later works of Matheron [110] as well as on recent reference textbooks [142, 136], the *specific surface measure* refers to the surface measure that derives from Steiner's formula. This measure has different names, depending on its normalization and the degree of generalization: intrinsic volume of index $d - 1$ and Minkowski's content of index 1 for convex sets [136], total curvature of index $d - 1$ for sets with positive reach and $\mathcal{U}_{PR}$-sets [56, 130], or also in a more general setting outer Minkowski content [5, 149]; see also [79]. Even though the (variational) perimeter of a set and this notion of surface measure agree for convex sets [5], the distinction is important. Indeed their extensions to non convex sets have different behaviors. For example, the outer Minkowski content counts twice the isolated fine parts of a set having a bounded and $(d-1)$-rectifiable topological boundary, whereas these fine parts have no influence on the perimeter [149, Proposition 4.1] (here "isolated fine parts" denotes the part of the boundary which has Lebesgue density 0). In order to make a clear distinction between the (variational) perimeter and the surface measure from Steiner's formula, the constant $\theta_V(X)$ is named the *specific variation* of X and not its "specific perimeter".

As mentioned in the introduction, one should notice that, contrary to the specific surface area [136], the specific variation $\theta_V(X)$ is well-defined for any measurable random set, and in particular for any stationary RACS. Besides, Proposition 8.6 shows that the specific directional variations $\theta_{V_u}(X)$ and the specific variation $\theta_V(X)$ are easily computed as soon as one knows the variogram of X. This will be illustrated in the next chapter where the specific variations of homogeneous Boolean models are computed (see Section 9.4). However, we have to point out one limitation of the specific variation: it can only deals with d-dimensional random sets. This is a consequence of the fact that $\mathcal{L}^d(A) = 0$ implies $\mathrm{Per}(A) = 0$. On the opposite, the specific surface area derived form Steiner formula are adapted to deal with random sets of Hausdorff dimension lower than d (see e.g. [136, 4, 150] and the references therein).

8.6   Random Excursion Sets and Coarea Formula for Mean Variations

First let us recall the coarea formula for deterministic functions. In what follows, U is an open subset of $\mathbb{R}^d$. Recall that for any measurable set A, one defines the *perimeter* of A in U as the variation of the indicator function $\mathbb{1}_A$ in U, and one writes $\mathrm{Per}(A, U) := |D\mathbb{1}_A|(U)$. Similarly, one defines $V_u(A, U) := |D_u\mathbb{1}_A|(U)$ the directional variation of A in U.

If $f : U \to \mathbb{R}$ is a measurable function and $t \in \mathbb{R}$, $\{f > t\}$ denotes the set

$$\{x \in U, \ f(x) > t\} .$$

$\{f > t\}$ is called the *upper level set* of level t.

Proposition 8.7 (Coarea formula)**.** *Let $f \in L^1(U)$. Then $f \in BV(U)$ if and only if the sets $\{f > t\}$ are of finite perimeter for $\mathcal{L}^1$-a.a. $t \in \mathbb{R}$, and in this case*

$$|Df|(U) = \int_{-\infty}^{+\infty} \mathrm{Per}\left(\{f > t\}, U\right) dt.$$

We refer to [6, p. 145] for the proof of the coarea formula. Let us mention that the coarea formula remains valid if the upper level sets are replaced by other level sets: $\{f \geq t\}$, $\{f < t\}$ or $\{f \leq t\}$. Besides, a coarea formula also holds for directional variation:

$$|D_u f|(U) = \int_{-\infty}^{+\infty} D_u\left(\{f > t\}, U\right) dt, \; u \in S^{d-1}.$$

If f is a stationary random fields then its excursion sets $\{f > t\}$ are stationary random sets. Using the coarea formula (see Proposition 8.7), one obtains a relation between the variation intensity of f and the variation intensity of its level sets. Let us recall that by definition,

$$\Theta_{V_u}\left(f, \mathbb{R}^d\right) = \mathbb{E}\left(|D_u f|\left(\mathbb{R}^d\right)\right).$$

Proposition 8.8. *(Coarea formula for total variation intensity) Let f be a r.f. a.s. in $L^1\left(\mathbb{R}^d\right)$, and let $u \in S^{d-1}$. Then $f \in BV_u\left(\mathbb{R}^d\right)$ a.s. with finite mean total directional variation $\Theta_{V_u}\left(f, \mathbb{R}^d\right)$ if and only if for $\mathcal{L}^1$-a.e. $t \in \mathbb{R}$ its level sets $\{f > t\}$ have a.s. finite directional variation in the direction u and $t \mapsto \Theta_{V_u}\left(\{f > t\}, \mathbb{R}^d\right)$ is in $L^1(\mathbb{R})$, and in this case*

$$\Theta_{V_u}\left(f, \mathbb{R}^d\right) = \int_{-\infty}^{+\infty} \Theta_{V_u}\left(\{f > t\}, \mathbb{R}^d\right) dt.$$

Similarly, $f \in BV\left(\mathbb{R}^d\right)$ a.s. with finite mean total variation if and only if for $\mathcal{L}^1$-a.e. $t \in \mathbb{R}$ its level sets $\{f > t\}$ have a.s. finite variation and $t \mapsto \Theta_V\left(\{f > t\}, \mathbb{R}^d\right)$ is in $L^1(\mathbb{R})$, and in this case

$$\Theta_V\left(f, \mathbb{R}^d\right) = \int_{-\infty}^{+\infty} \Theta_V\left(\{f > t\}, \mathbb{R}^d\right) dt.$$

Proof. The proof consists in apply Fubini's and Lebesgue's theorem. First, let us justify that the function

$$
\begin{aligned}
g : \Omega \times \mathbb{R}^d \times \mathbb{R} &\rightarrow \{0, 1\} \\
(\omega, x, t) &\mapsto \mathbb{1}_{\{f > t\}}(\omega, x)
\end{aligned}
$$

is measurable. Let $(t_n)_{n \in \mathbb{N}}$ be a dense sequence of $\mathbb{R}$, then one easily checks that

$$g^{-1}(1) = \bigcup_{n \in \mathbb{N}} \{(\omega, x), \; f(\omega, x) > t_n\} \times (t_n, +\infty),$$

which is in the product σ-algebra $\mathcal{A} \otimes \mathcal{B}\left(\mathbb{R}^d\right) \otimes \mathcal{B}\left(\mathbb{R}\right)$. Second, we have the following elementary identity

$$|f(\omega, x + ru) - f(\omega, x)| = \int_{-\infty}^{+\infty} \left| \mathbb{1}_{\{f>t\}}(\omega, x + ru) - \mathbb{1}_{\{f>t\}}(\omega, x) \right| dt.$$

Hence, by Fubini's theorem

$$\int_{\mathbb{R}^d} \mathbb{E}\left(|f(x + ru) - f(x)|\right) dx = \int_{-\infty}^{+\infty} \int_{\mathbb{R}^d} \mathbb{E}\left(\left| \mathbb{1}_{\{f>t\}}(x + ru) - \mathbb{1}_{\{f>t\}}(x) \right| \right) dx dt.$$

Let us now suppose that for $\mathcal{L}^1$-a.e. $t \in \mathbb{R}$ the level sets $\{f > t\}$ have a.s. finite directional variation in the direction u and that $t \mapsto \Theta_{V_u}\left(\{f > t\}, \mathbb{R}^d\right)$ is in $L^1(\mathbb{R})$. Then, by Proposition 7.5,

$$\lim_{r \to 0} \int_{\mathbb{R}^d} \frac{\mathbb{E}\left(\left| \mathbb{1}_{\{f>t\}}(x + ru) - \mathbb{1}_{\{f>t\}}(x) \right| \right)}{|r|} dx = \Theta_{V_u}\left(\{f > t\}, \mathbb{R}^d\right) \quad \text{for } \mathcal{L}^1\text{-a.e. } t,$$

and by Corollary 7.3

$$\int_{\mathbb{R}^d} \frac{\mathbb{E}\left(\left| \mathbb{1}_{\{f>t\}}(x + ru) - \mathbb{1}_{\{f>t\}}(x) \right| \right)}{|r|} dx \leq \Theta_{V_u}\left(\{f > t\}, \mathbb{R}^d\right) \in L^1(\mathbb{R}).$$

Hence the Lebesgue theorem applies and

$$\lim_{r \to 0} \int_{\mathbb{R}^d} \frac{\mathbb{E}\left(|f(x + ru) - f(x)|\right)}{|r|} dx = \int_{-\infty}^{+\infty} \Theta_{V_u}\left(\{f > t\}, \mathbb{R}^d\right) dt < +\infty.$$

By Proposition 7.5 one deduces that f has a.s. bounded directional variation and that

$$\Theta_{V_u}\left(f, \mathbb{R}^d\right) = \int_{-\infty}^{+\infty} \Theta_{V_u}\left(\{f > t\}, \mathbb{R}^d\right) dt.$$

Let us now prove the converse implication. Let $f \in BV_u\left(\mathbb{R}^d\right)$ a.s. with $\Theta_{V_u}\left(f, \mathbb{R}^d\right) < +\infty$. Then, by Fatou's lemma and Fubini's theorem

$$\int_{-\infty}^{+\infty} \liminf_{r \to 0} \int_{\mathbb{R}^d} \frac{\mathbb{E}\left(\left| \mathbb{1}_{\{f>t\}}(x + ru) - \mathbb{1}_{\{f>t\}}(x) \right| \right)}{|r|} dx dt$$
$$\leq \liminf_{r \to 0} \int_{\mathbb{R}^d} \frac{\mathbb{E}\left(|f(x + ru) - f(x)|\right)}{|r|} dx$$
$$= \Theta_{V_u}\left(f, \mathbb{R}^d\right) < +\infty.$$

In particular, for L^1-a.e. $t \in \mathbb{R}$,

$$\liminf_{r \to 0} \int_{\mathbb{R}^d} \left| \mathbb{1}_{\{f>t\}}(x + ru) - \mathbb{1}_{\{f>t\}}(x) \right| dx dt < +\infty \text{ a.s.}$$

and Proposition 7.4 ensures that, for L^1-a.e. $t \in \mathbb{R}$, $\{f > t\}$ has a.s. locally bounded variation. Besides, as shown in the proof of Proposition 7.5 we have

$$\Theta_{V_u} \left(\{f > t\}, \mathbb{R}^d \right) \leq \liminf_{r \to 0} \int_{\mathbb{R}^d} \frac{\mathbb{E} \left(\left| \mathbb{1}_{\{f>t\}}(x + ru) - \mathbb{1}_{\{f>t\}}(x) \right| \right)}{|r|} dx,$$

and thus the above inequalities show that $\Theta_{V_u} \left(\{f > t\}, \mathbb{R}^d \right) \in L^1(\mathbb{R})$. To conclude, the case of non directional variation easily follows from the integral geometric formula of Proposition 7.2 and Fubini's theorem. $\qquad \square$

Proposition 8.9. *(Coarea formula for variation intensity of stationary r.f.) Let f be an integrable r.f. and let $u \in S^{d-1}$. Then $f \in BV_{u,\mathrm{loc}} \left(\mathbb{R}^d \right)$ a.s. with finite directional variation intensity $\theta_{V_u}(f)$ if and only if for $\mathcal{L}^1$-a.e. $t \in \mathbb{R}$ its level sets $\{f > t\}$ have a.s. locally finite directional variation in the direction u and $t \mapsto \theta_{V_u}(\{f > t\})$ is in $L^1(\mathbb{R})$, and in this case*

$$\theta_{V_u} (f) = \int_{-\infty}^{+\infty} \theta_{V_u}(\{f > t\}) dt.$$

Similarly, $f \in BV \left(\mathbb{R}^d \right)$ a.s. with finite mean total directional variation $\theta_V(f)$ if and only if for $\mathcal{L}^1$-a.e. $t \in \mathbb{R}$ its level sets $\{f > t\}$ have a.s. finite variation and $t \mapsto \theta_V(\{f > t\})$ is in $L^1(\mathbb{R})$, and in this case

$$\theta_V (f) = \int_{-\infty}^{+\infty} \theta_V (\{f > t\}) \, dt.$$

Proof. The proof of this proposition is similar to the previous one (Proposition 8.8), except that the dominated condition is replaced by

$$\frac{\mathbb{E} \left(\left| \mathbb{1}_{\{f>t\}}(ru) - \mathbb{1}_{\{f>t\}}(0) \right| \right)}{|r|} \leq \theta_V (\{f > t\}) (1 + R)^d, \quad |r| < R,$$

as in the proof of Proposition 7.9. $\qquad \square$

8.7 Conclusion

Several formulas relating the directional variation of random sets to the directional derivatives at the origin of their covariogram or their variogram have been established. It has been shown that they rigorously generalize classical results only established in restricted cases.

The relevance of these formulas will be illustrated in the next chapter (Chapter 9) where the variation intensities of the different germ-grain models presented in Chapter 5 will be computed.

This chapter has also introduced the notion of specific variation $\theta_V(X)$ of a stationary random set X as the variation intensity of the indicator stationary r.f. $\mathbb{1}_X$. The main advantage of the specific variation in comparison with the specific area

measure which stems from Steiner formula is that it is defined for any measurable random set, and in particular for any random closed set. Besides the directional and non directional specific variations are easily computed once the variogram of the stationary random set is known. Hence the specific variations are an interesting alternative to the usual specific area measure when dealing with d-dimensional random sets.

The good properties of the specific variation $\theta_V(X)$ of a stationary random set X opens new perspectives. As expressed in [150], a problem of interest in stochastic geometry is to define local mean surface densities for inhomogeneous (i.e. non stationary) random sets. The local surface densities introduced by Matheron [110, p. 50] and recently studied by Villa [150] is defined by

$$\sigma(X, y) := \lim_{r \to 0^+} \frac{\mathbb{P}\left(y \in X \oplus B(0, r) \setminus X\right)}{r}, \ y \in \mathbb{R}^d,$$

whenever the limit exists. Clearly, from Proposition 8.6, we should propose the alternative directional variation densities

$$\sigma_{V_u}(X, y) := \lim_{r \to 0} \frac{\mathbb{E}\left(|\mathbb{1}_X(y + ru) - \mathbb{1}_X(y)|\right)}{|r|} = \lim_{r \to 0} \frac{\mathbb{P}\left(y \in X \Delta(-ru + X)\right)}{|r|}, \ y \in \mathbb{R}^d,$$

where Δ denotes the symmetric difference, and the non directional variation density

$$\sigma_V(X, y) := \frac{1}{2\omega_{d-1}} \int_{S^{d-1}} \sigma_{V_u}(X, y) \mathcal{H}^{d-1}(du),$$

whenever these limits exist.

Another possible direction for further developments is to investigate the behavior of the variation of a set around its mean. An interesting particular case might be the behavior of the perimeter of excursion sets around their mean. A central limit theorem has recently been proved for the Lebesgue measure of excursion sets of certain Gaussian r.f. and shot noises [24], where the targeted application is a Gaussianity test for the surface of paper. As the author mention in conclusion, it might be of interest to investigate other "Minkowski's functionals" of the excursion sets, such as the perimeter.

Applications: Variation Intensities of Classical Germ-Grain Models

Contents

Abstract: Relying on the results of Chapter 7 and Chapter 8, the variation intensities of various stationary random field (r.f.) models are computed. In order of presentation, the considered stationary r.f. are: Gaussian r.f., Poisson shot noise of random sets, Boolean models, colored dead leaves r.f., transparent dead leaves process, and colored tessellations. In particular it is shown that if the sample paths of a stationary Gaussian r.f. are a.s. of bounded variation, then they are a.s. in the Sobolev space $W_{\text{loc}}^{1,1}\left(\mathbb{R}^d\right)$. Let us also mention that the derived formula for the specific variation of homogeneous Boolean random sets is valid for any grain distribution, and it generalizes known results in the case where the grains are convex sets.

9.1 Introduction

The goal of this chapter is to illustrate the results of Chapters 7 and 8 by computing the directional and non directional variation intensities of several stationary r.f. models. It particular an answer of the question "What is the mean total variation of the germ-grain models presented in Chapters 5 and 6?" raised in the general introduction of the present part of the thesis is provided.

We first study the variation of stationary Gaussian r.f. It is shown that a Gaussian r.f. f_G has finite variation intensity if and only if the one-dimensional restrictions of its covariance are twice differentiable at 0. According to [135], this condition also implies that the sample paths of f_G are a.s. in the Sobolev space $W^{1,1}_{\text{loc}}\left(\mathbb{R}^d\right)$, and in particular the variation $|Df_G|$ is a.s. absolutely continuous with respect to the Lebesgue measure.

The section on Gaussian r.f. is followed by a sequence of sections where the directional and non directional variation intensities are computed for the germ-grain r.f. of Chapter 5 and Chapter 6. In order of presentation, these r.f. models are: Poisson shot noise of random sets, Boolean models, colored dead leaves r.f., transparent dead leaves process, and colored tessellations.

Thanks to the results of Chapters 7 and 8, all the derived formulas for the specific variation of germ-grain models are established under very broad assumptions on the grain distribution. In particular, we provide a formula for the specific variation of homogeneous Boolean random sets that is valid for any grain distribution. This formula generalizes the corresponding classical result for Boolean random sets having convex grains [136].

For germ-grain models, the obtained formulas explicitly clarifies the somewhat intuitive relation between the geometry of the grains X and the total variation of the germ-grain r.f. Moreover, they show that for all the considered germ-grain models, there are only two geometric features of influence on the total variation of the germ-grain r.f.: the mean perimeter and the mean Lebesgue measure of the grains.

9.2   Gaussian Random Fields

A random field f_G is a *stationary Gaussian r.f.* with mean $\mu \in \mathbb{R}$ and covariance function $C : \mathbb{R}^d \to \mathbb{R}$ if for all $p \in \mathbb{N}$, for all $x_1, \ldots, x_p \in \mathbb{R}^d$, and for all $w_1, \ldots, w_p \in \mathbb{R}$ the r.v. $\sum_{i=1}^{p} w_i f_G(x_i)$ is normal with mean $\sum_{i=1}^{p} w_i \mu$ and variance $\sum_{i,j=1}^{p} w_i w_j C(x_j - x_i)$.

In what follows we will only consider stationary Gaussian r.f. whose covariance function is regular at the origin. Let us recall that as soon as the covariance function C is continuous in 0, the r.f. is continuous in probability and thus it has a measurable version (see [47, p. 61] or [63, p. 171]).

The computation of the directional and non directional variation intensities of f_G follows from the following lemma.

Lemma 9.1. *Let f_G be a stationary Gaussian r.f. with mean μ and covariance function C. Then for all $u \in S^{d-1}$ and $r \in \mathbb{R}$,*

$$\mathbb{E}\left(|f_G(ru) - f_G(0)|\right) = \frac{2}{\sqrt{\pi}}\sqrt{C(0) - C(ru)}.$$

Proof. We recall that if a r.v. Y has distribution $\mathcal{N}(0, \sigma^2)$ then $\mathbb{E}(|Y|) = \sqrt{\frac{2}{\pi}}\sigma$. Let f_G be a stationary r.f. with mean μ and covariance function C. Then for all $u \in S^{d-1}$ and $r \in \mathbb{R}$, $f_G(ru) - f_G(0)$ follows a normal distribution with mean 0 and variance $2(C(0) - C(ru))$. Hence

$$\mathbb{E}\left(|f_G(ru) - f_G(0)|\right) = \sqrt{\frac{2}{\pi}}\sqrt{2(C(0) - C(ru))} = \frac{2}{\sqrt{\pi}}\sqrt{C(0) - C(ru)}.$$

$\square$

Proposition 9.1 (Variation intensity of stationary Gaussian r.f.)**.** *Let f_G be a stationary Gaussian r.f. with mean μ and covariance C, and let $u \in S^{d-1}$. Then f_G has finite directional variation intensity $\theta_{V_u}(f_G)$ in the direction u if and only if the one-dimensional restriction of the covariance $C_u : r \mapsto C(ru)$ is twice differentiable at 0, and in this case, noting $C_u''(0)$ the second derivative in 0 of C_u,*

$$\theta_{V_u}(f_G) = \sqrt{\frac{-2C_u''(0)}{\pi}}.$$

Consequently, f_G has finite variation intensity $\theta_V(f_G)$ if and only if for all $u \in S^{d-1}$ the one-dimensional restrictions of the covariance $C_u : r \mapsto C(ru)$ are twice differentiable at 0, and in this case,

$$\theta_V(f_G) = \frac{1}{2\omega_{d-1}} \int_{S^{d-1}} \sqrt{\frac{-2C_u''(0)}{\pi}} \mathcal{H}^{d-1}(du).$$

Proof. This is a straightforward application of Theorem 7.3. By Lemma 9.1,

$$\lim_{r \to 0} \frac{\mathbb{E}\left(|f_G(ru) - f_G(0)|\right)}{|r|}$$

exists if and only if $\frac{C(0)-C(ru)}{r^2}$ admits a limit in 0, that is if and only if $C_u : r \mapsto C(ru)$ is twice differentiable at 0 with $C_u'(0) = 0$. But since C_u is even, if it is differentiable at 0 then necessarily $C_u'(0) = 0$. As for the expression of $\theta_{V_u}(f_G)$, note that

$$\lim_{r \to 0} \frac{C(0) - C(ru)}{r^2} = -\frac{C_u''(0)}{2},$$

hence by Theorem 7.3 and Lemma 9.1,

$$\theta_{V_u}(f_G) = \lim_{r \to 0} \frac{\mathbb{E}\left(|f_G(ru) - f_G(0)|\right)}{|r|} = \sqrt{\frac{-2C_u''(0)}{\pi}}.$$

The case of non directional variation follows from Corollary 7.5. $\square$

It is worth noticing that the necessary and sufficient condition for a stationary Gaussian r.f. to be of locally bounded variation implies a stronger regularity on the sample paths than just being of locally bounded variation. First, the differentiability

at the origin of the covariance implies that there exists $\rho > 0$ and $K > 0$ such that for all $x \in B(0, \rho)$

$$C(0) - C(x) \leq \frac{K}{|x|}.$$

In particular, there exists $\alpha > 0$ and $K' > 0$ such that for all $x \in B(0, \rho)$

$$C(0) - C(x) \leq \frac{K'}{|\log(|x|)|^{(1+\alpha)}},$$

and thus, according to Adler and Taylor [2, Theorem 1.4.1 p. 20], f has a.s. continuous sample paths. In addition, according to the recent paper of Scheuerer [135], the sample paths of a stationary Gaussian r.f. f_G are a.s. in the Sobolev space $W_{\text{loc}}^{1,2}\left(\mathbb{R}^d\right)$ if and only if the covariance function C is twice differentiable at the origin in every direction. Hence by Proposition 9.1 we have

$$f_G \in BV_{\text{loc}}\left(\mathbb{R}^d\right) \text{ a.s.} \Leftrightarrow f_G \in W_{\text{loc}}^{1,2}\left(\mathbb{R}^d\right) \text{ a.s.}$$

In particular if $f_G \in BV_{\text{loc}}\left(\mathbb{R}^d\right)$ a.s., then $f_G \in W_{\text{loc}}^{1,1}\left(\mathbb{R}^d\right)$ a.s., and consequently its variation intensity measure is absolutely continuous with respect to the Lebesgue measure. Hence, if $f_G \in BV_{\text{loc}}\left(\mathbb{R}^d\right)$ a.s. then it is a "smooth" function among the functions of bounded variation since its variation measure Df_G has neither a jump part nor a Cantor part (see [6, Section 3.9] for more details on the decomposition of the variation measure Df of functions of bounded variation).

We conclude this section in computing the specific perimeter of the excursion sets of stationary Gaussian r.f. For all $t \in \mathbb{R}$, we consider the random set $\{f_g > t\}$ and we note ν_t its variogram, that is the function defined for all $y \in \mathbb{R}^d$ by

$$\nu_t(y) = \mathbb{P}\left(f_G(y) > t, \ f_G(0) \leq t\right).$$

As stated in [100, p. 207] and initially shown by Matheron [109],

$$\nu_t(y) = \frac{1}{\pi} \int_0^{\arcsin\left(\sqrt{\frac{C(0)-C(y)}{2}}\right)} \exp\left(-\frac{t^2}{2}\left(1 + \tan^2 s\right)\right) ds. \qquad (9.1)$$

From this expression Lantuéjoul asserts that the excursion sets of f_G have finite "specific perimeter" if and only if $C(0) - C(y)$ is proportional to $|y|^2$ [100, p. 207]. Our next proposition completes this observation in computing the expression of the specific variations of the Gaussian excursion sets $\{f_G > t\}$.

Proposition 9.2 (Specific variation of Gaussian excursion sets). *Let f_G be a stationary Gaussian r.f. with mean μ and covariance C, let $t \in \mathbb{R}$, and let $u \in S^{d-1}$. Then $\{f_G > t\}$ has finite specific directional variation in the direction u if and only if the one-dimensional restriction C_u of the covariance is twice differentiable at 0, and in this case,*

$$\theta_{V_u}(\{f_G > t\}) = \frac{1}{\pi}\sqrt{-C_u''(0)} \exp\left(-\frac{t^2}{2}\right).$$

Consequently, $\{f_G > t\}$ has finite specific variation in the direction u if and only if for all $u \in S^{d-1}$ the one-dimensional restrictions $C_u : r \mapsto C(ru)$ are twice differentiable at 0, and in this case,

$$\theta_V(\{f_G > t\}) = \frac{1}{2\pi\omega_{d-1}} \left(\int_{S^{d-1}} \sqrt{-C_u''(0)} d\mathcal{H}^{d-1}(du) \right) \exp\left(-\frac{t^2}{2}\right).$$

Proof. By Proposition 8.6,

$$\theta_{V_u}(\{f_G > t\}) = 2 \lim_{r \to 0} \frac{\nu_t(ru)}{|r|}.$$

The function

$$h : x \mapsto \frac{1}{\pi} \int_0^{\arcsin(x)} \exp\left(-\frac{t^2}{2}\left(1 + \tan^2 s\right)\right) ds$$

is $\mathcal{C}^1$ at $x = 0$ and we have

$$h'(0) = \arcsin'(0) \frac{1}{\pi} \exp\left(-\frac{t^2}{2}\left(1 + \tan^2(\arcsin(0))\right)\right) = \frac{1}{\pi} \exp\left(-\frac{t^2}{2}\right).$$

Hence, thanks to Formula (9.1) one deduces that

$$\lim_{r \to 0} \frac{\nu_t(ru)}{|r|} = \frac{1}{\pi} \exp\left(-\frac{t^2}{2}\right) \lim_{r \to 0} \sqrt{\frac{C(0) - C(ru)}{2r^2}}.$$

As shown in the proof of Proposition 9.1, the limit on the right-hand side is finite if and only if C_u is twice differentiable, and in this case

$$\lim_{r \to 0} \sqrt{\frac{C(0) - C(ru)}{2r^2}} = \frac{1}{2}\sqrt{-C_u''(0)}.$$

The result follows. $\square$

Remark (Coarea formula)**.** Note that for all $t \in \mathbb{R}$ we have

$$\theta_{V_u}(\{f_G > t\}) = \theta_{V_u}(f_G) \frac{1}{\sqrt{2\pi}} \exp\left(-\frac{t^2}{2}\right)$$

and

$$\theta_V(\{f_G > t\}) = \theta_V(f_G) \frac{1}{\sqrt{2\pi}} \exp\left(-\frac{t^2}{2}\right).$$

In particular one checks that the coarea formula of Proposition 8.9 is satisfied.

9.3   Poisson Shot Noise

Let us now consider the Poisson shot noise model introduced in Chapter 3. Recall that the *Poisson shot noise* associated with the independently marked Poisson process $\Pi = \{(x_j, \kappa_j)\} \subset \mathbb{R}^d \times K$ and the *impulse function $h : \mathbb{R}^d \times K \to \mathbb{R}$* is the random field f_{SN} defined by

$$f_{SN}(x) = \sum_{(x_j, \kappa_j) \in \Pi} h(x - x_j, \kappa_j),$$

where $\Pi = \{(x_j, \kappa_j)\} \subset \mathbb{R}^d \times K$ is an independently marked Poisson process having intensity measure $\lambda \mathcal{L}^d \otimes P_\kappa$, $\lambda > 0$ and P_κ is the probability distribution of the marks. The impulse function $h : \mathbb{R}^d \times K \to \mathbb{R}$ is supposed to be $\mathcal{L}^d \otimes P_\kappa$-integrable, which ensures that f_{SN} is integrable by Campbell's theorem (see Theorem B.2).

We first show that if the impulse function h has a finite mean total variation then the shot noise f_{SN} has bounded variation and its variation intensity is finite.

Proposition 9.3 (Bound on the variation intensities of Poisson shot noises)**.** *Let $u \in S^{d-1}$ and suppose that $h(\cdot, \kappa) \in BV_u\left(\mathbb{R}^d\right)$ P_κ-a.s. with $E\left(|D_u h(\cdot, \kappa)|\left(\mathbb{R}^d\right)\right) < +\infty$. Then the shot noise f_{SN} has locally bounded directional variation in the direction u and*

$$\theta_{V_u}(f_{SN}) \leq \lambda E\left(|D_u h(\cdot, \kappa)|\left(\mathbb{R}^d\right)\right).$$

Consequently, if $h(\cdot, \kappa) \in BV\left(\mathbb{R}^d\right)$ P_κ-a.s. and $E\left(|Dh(\cdot, \kappa)|\left(\mathbb{R}^d\right)\right) < +\infty$ then f_{SN} has locally bounded variation and

$$\theta_V(f_{SN}) \leq \lambda E\left(|Dh(\cdot, \kappa)|\left(\mathbb{R}^d\right)\right).$$

Proof. Let $u \in S^{d-1}$ and $r \in \mathbb{R}$. Then

$$|f_{SN}(ru) - f_{SN}(0)| \leq \sum_{(x_j, \kappa_j) \in \Pi} |h(ru - x_j, \kappa_j) - h(-x_j, \kappa_j)|.$$

By Campbell's theorem (see Theorem B.2),

$$\mathbb{E}\left(|f_{SN}(ru) - f_{SN}(0)|\right) \leq \lambda \int_{\mathbb{R}^d \times K} |h(ru - x, \kappa) - h(-x, \kappa)| \, dx P_\kappa(d\kappa)$$

$$\leq \lambda E\left(\int_{\mathbb{R}^d} |h(ru - x, \kappa) - h(-x, \kappa)| \, dx\right).$$

By Corollary 7.3, P_κ-a.s.

$$\int_{\mathbb{R}^d} |h(ru - x, \kappa) - h(-x, \kappa)| \, dx \leq |D_u h(\cdot, \kappa)|\left(\mathbb{R}^d\right) |r|.$$

Hence

$$\mathbb{E}\left(|f_{SN}(ru) - f_{SN}(0)|\right) \leq \lambda E\left(|D_u h(\cdot, \kappa)|\left(\mathbb{R}^d\right)\right) |r|,$$

that is f_{SN} is directionally Lipschitz in mean. By Theorem 7.4, one concludes that f_{SN} is a.s. in $BV_{u,\mathrm{loc}}\left(\mathbb{R}^d\right)$ and $\theta_{V_u}(f_{SN}) \leq \lambda E\left(|D_u h(\cdot, \kappa)|\left(\mathbb{R}^d\right)\right)$. The upper bound on $\theta_V(f_{SN})$ is obtained in integrating over all directions $u \in S^{d-1}$. $\qquad\square$

Biermé and Desolneux [14] recently studied one-dimensional Poisson shot noise models of the form

$$f_\lambda(x) = \sum_{x_j \in \Pi_\lambda} h(x - x_j), \ x \in \mathbb{R},$$

where $h : \mathbb{R} \to \mathbb{R}$ is a deterministic $\mathcal{C}^2$ function such that h, h' and h'' are in $L^1(\mathbb{R})$, and Π_λ is a Poisson process over $\mathbb{R}$ of intensity λ. Among other results, they established that the variation intensity of these particular shot noises has the following asymptotic behavior [14, Corollary 3 p. 23]:

$$\frac{\theta_V(f_\lambda)}{\sqrt{\lambda}} = \sqrt{\frac{2C''(0)}{\pi}} + \mathcal{O}_{\lambda \to +\infty}\left(\frac{1}{\sqrt{\lambda}}\right),$$

where $C''(0)$ is the second derivative in 0 of the common covariance of the shot noises $\frac{f_\lambda}{\sqrt{\lambda}}$, that is

$$C : y \mapsto \int_{\mathbb{R}} h(x + y)h(x)dx.$$

First remark that this result is in accordance with the normal convergence of the Poisson shot noise (see Theorem 3.1): Indeed, the limit of the variation intensity is equal to the variation intensity of the limit Gaussian random field (see Proposition 9.1). Second, observe that in this case the upper bound given by Proposition 9.3 is really pessimistic when λ increases. This is due to the fact that the variations of the various smooth functions $h(\cdot - x_j)$ have locally opposite sign. Hence the variations does not simply add but rather compensate each other.

On the opposite, the next proposition shows that when the functions h are indicator functions of sets of finite perimeter, the upper bound of Proposition 9.3 is reached. Hence the upper bound of Proposition 9.3 cannot be improved in general.

Proposition 9.4 (Variation of shot noises of random indicator functions)**.** *Consider a shot noise of the form*

$$f(x) = \sum_{(x_j, X_j) \in \Pi} \mathbb{1}(x \in x_j + X_j),$$

where the Poisson process Π_λ has intensity measure $\lambda \otimes P_X$, $\lambda \geq 0$, P_X a probability distribution over the set $\mathcal{F}$ of closed subsets of $\mathbb{R}^d$. Suppose that the RACS $X \sim P_X$ is such that:

- *There exists a ball B such that $E\left(\mathcal{L}^d\left(X \oplus B\right)\right) < +\infty$.*

- *$\mathcal{L}^d(\partial X) = 0$ P_X-a.s.*

- *$E(\mathrm{Per}(X)) < +\infty$.*

Then f has a.s. bounded variation and $\theta_V(f) = \lambda E(\mathrm{Per}(X))$.

Proof. First, since $E(\mathrm{Per}(X)) < +\infty$ by Proposition 9.3 f has a.s. bounded varia-
tion and $\theta_V(f) \le \lambda E(\mathrm{Per}(X))$. Let B be a ball such that $E\left(\mathcal{L}^d\left(X \oplus B\right)\right) < +\infty$.
Recall that

$$B \cap x_j + X_j \ne \emptyset \Longleftrightarrow x_j \in B \oplus \check{X}.$$

Let us note Π^B the restriction of Π defined by

$$\Pi^B = \{(x_j, X_j),\ B \cap x_j + X_j \ne \emptyset\}.$$

By Proposition B.5, the expected number of point of Π^B is $E\left(\mathcal{L}^d\left(B \oplus \check{X}\right)\right) < +\infty$,
and the distribution of the points of Π^B under the events $\#\Pi^B = n$ is known.
Clearly, the only random sets of influence for the variation of f on the set B are
the random sets $x_j + X_j$ such that $(x_j, X_j) \in \Pi^B$. We have

$$Df(B) = \sum_{(x_j,X_j)\in\Pi^B} D\mathbb{1}_{x_j+X_j}(B).$$

To conclude we have to show that the different total variations $|D\mathbb{1}_{x_j+X_j}|$ are al-
most surely mutually singular. First, recall that for all set of finite perimeter Y,
$|D\mathbb{1}_Y|(A) \le \mathcal{H}^{d-1}(\partial Y \cap A)$, $A \in \mathcal{B}\left(\mathbb{R}^d\right)$. In particular, $|D\mathbb{1}_Y|\left(\mathbb{R}^d \setminus \partial Y\right) = 0$.
Hence to show that the measure $|D\mathbb{1}_Y|$ and another measure μ are mutually sin-
gular it is enough to show that $\mu(\partial Y) = 0$. Here we are interested in the measures
$|D\mathbb{1}_{x_j+X_j}|\llcorner B$. We will show that for any finite Radon measure μ,

$$\mu(x_j + \partial X_j \cap B) = 0 \text{ a.s.}$$

Let (x_j, X_j) be a point of Π^B given that $\#\Pi^B \ge 1$. Let us recall that all the
points of Π^B are i.i.d. Let us also recall that if ν is a finite Radon measure and
$A \in \mathcal{B}(\mathbb{R})$ then, by Fubini's theorem, the following translative integral geometric
formula holds [136, Theorem 5.2.1 p. 181]:

$$\int_{\mathbb{R}^d} \nu(x + A)dx = \mathcal{L}^d(A)\nu\left(\mathbb{R}^d\right).$$

Noting $\gamma = E\left(\mathcal{L}^d\left(B \oplus \check{X}\right)\right)$,

$$\begin{aligned}
\mathbb{E}\left(\mu(x_j + \partial X_j \cap B)\right) &= \frac{1}{\gamma}\int_{X\in\mathcal{F}}\int_{x\in B\oplus\check{X}} \mu(x + \partial X \cap B)dx P_X(dX) \\
&= \frac{1}{\gamma}\int_{X\in\mathcal{F}}\int_{x\in\mathbb{R}^d} \mu(x + \partial X \cap B)dx P_X(dX) \\
&= \frac{1}{\gamma}\int_{X\in\mathcal{F}} \mathcal{L}^d(\partial X)\mu(B) P_X(dX) \\
&= \frac{1}{\gamma}E\left(\mathcal{L}^d(\partial X)\right)\mu(B) \\
&= 0.
\end{aligned}$$

From this, thanks to the independence of the points of Π^B, we deduce that if (x_j, X_j)
and (x_k, X_k) are two distinct points then

$$\mathbb{E}\left(|D\mathbb{1}_{x_k+X_k}|(x_j + \partial X_j \cap B)\right) = 0,$$

and thus the two measures $\left|D\mathbb{1}_{x_j+X_j}\right| \llcorner B$ and $\left|D\mathbb{1}_{x_k+X_k}\right| \llcorner B$ are mutually singular. As a consequence, under the event $\left\{\#\Pi^B = n\right\}$, $n \geq 1$,

$$|Df|(B) = \sum_{k=1}^{n} \left|D\mathbb{1}_{x_k+X_k}\right|(B).$$

Let us compute the expectation of any of the terms $\left|D\mathbb{1}_{x_k+X_k}\right|(B)$.

$$
\begin{aligned}
\mathbb{E}(\left|D\mathbb{1}_{x_k+X_k}\right|(B)) &= \frac{1}{\gamma} \int_{X\in\mathcal{F}} \int_{x\in B\oplus\check{X}} |D\mathbb{1}_{x+X}|(B) dx P_X(dX) \\
&= \frac{1}{\gamma} \int_{X\in\mathcal{F}} \int_{x\in\mathbb{R}^d} |D\mathbb{1}_X|(-x+B) dx P_X(dX) \\
&= \frac{1}{\gamma} \int_{X\in\mathcal{F}} \mathcal{L}^d(B) |D\mathbb{1}_X|\left(\mathbb{R}^d\right) P_X(dX) \\
&= \frac{1}{\gamma} \mathcal{L}^d(B) E\left(\mathrm{Per}(X)\right).
\end{aligned}
$$

To conclude,

$$
\begin{aligned}
\mathbb{E}\left(|Df|(B)\right) &= \sum_{n=1}^{+\infty} \mathbb{E}\left(|Df|(B) \,\middle|\, \#\Pi^B = n\right) \mathbb{P}\left(\#\Pi^B = n\right) \\
&= \sum_{n=1}^{+\infty} \frac{n}{\gamma} \mathcal{L}^d(B) E\left(\mathrm{Per}(X)\right) \frac{\lambda^n \gamma^n}{n!} e^{-\lambda\gamma} \\
&= \lambda\mathcal{L}^d(B) E\left(\mathrm{Per}(X)\right) \sum_{n=1}^{+\infty} \frac{\lambda^{n-1}\gamma^{n-1}}{(n-1)!} e^{-\lambda\gamma} \\
&= \lambda\mathcal{L}^d(B) E\left(\mathrm{Per}(X)\right).
\end{aligned}
$$

Since $\mathbb{E}\left(|Df|(B)\right)$ is by definition equals to $\theta_V(f)\mathcal{L}^d(B)$, this concludes the proof. $\square$

9.4 Boolean Models

We now turn to the computation of the variation intensities of the Boolean models introduced in Section 5.3. Recall that the homogeneous *Boolean random set* with intensity λ and grain distribution P_X is the stationary random closed sets (RACS) Z_B defined by

$$Z_B = \bigcup_{j\in\mathbb{N}} x_j + X_j,$$

where $\{(x_j, X_j)\}$ is an independently marked stationary Poisson process in the space $\mathbb{R}^d \times \mathcal{F}$ having intensity measure $\lambda\mathcal{L}^d \otimes P_X$, $\lambda \geq 0$.

The avoiding functional of the Boolean model Z_B is well-known: for any compact $K \subset \mathbb{R}^d$ we have

$$\mathbb{P}\left(Z_B \cap K = \emptyset\right) = \exp\left(-\lambda\mathbb{E}\left(\mathcal{L}^d\left(X \oplus \check{K}\right)\right)\right), \tag{9.2}$$

where X denotes a RACS with distribution P_X (see e.g. [142, p. 65] or [100, p. 164]). Starting from the general Formula (9.2), which determines the distribution of Z_B, one easily derives the expression of the variogram ν_{Z_B} of Z_B. Indeed, specified for $K = \{0\}$, Formula (9.2) becomes

$$q := \mathbb{P}\left(0 \notin Z_B\right) = \exp\left(-\lambda \mathbb{E}\left(\mathcal{L}^d\left(X\right)\right)\right),$$

For $K = \{0, -ru\}$, $r \in \mathbb{R}$ and $u \in S^{d-1}$, remark that we have

$$\mathcal{L}^d\left(X \oplus \check{K}\right) = \mathcal{L}^d\left(X \cup ru + X\right) = 2\mathcal{L}^d(X) - \mathcal{L}^d\left(X \cap ru + X\right).$$

Hence in this case $\mathbb{E}\left(\mathcal{L}^d\left(X \oplus \check{K}\right)\right) = 2\mathbb{E}\left(\mathcal{L}^d\left(X\right)\right) - \gamma_X(ru)$. As a result the variogram ν_{Z_B} is equal to [142, p. 68], [100, p. 165]

$$
\begin{aligned}
\nu_{Z_B}(ru) = \mathbb{P}\left(-ru \in Z_B \text{ and } 0 \notin Z_B\right) &= \mathbb{P}\left(0 \notin Z_B\right) - \mathbb{P}\left(Z_B \cap \{0, -ru\} = \emptyset\right) \\
&= q - \exp\left(-\lambda\left(2\mathbb{E}\left(\mathcal{L}^d\left(X\right)\right) - \gamma_X(ru)\right)\right) \\
&= q - q\exp\left(-\lambda\left(\gamma_X(0) - \gamma_X(ru)\right)\right).
\end{aligned}
$$

Thanks to Proposition 8.6, one easily computes the specific variation intensities of Z_B from the expression of its variogram.

Proposition 9.5 (Specific variations of Boolean random sets)**.** *Let Z_B be the Boolean random set with Poisson intensity λ and grain distribution P_X, and let X be a RACS with distribution P_X. Then for all $u \in S^{d-1}$,*

$$\theta_{V_u}(Z_B) = \lambda\mathbb{E}\left(V_u(X)\right)\exp\left(-\lambda\mathbb{E}\left(\mathcal{L}^d\left(X\right)\right)\right)$$

and

$$\theta_V(Z_B) = \lambda\mathbb{E}\left(\mathrm{Per}(X)\right)\exp\left(-\lambda\mathbb{E}\left(\mathcal{L}^d\left(X\right)\right)\right). \tag{9.3}$$

Proof. By Proposition 8.6 and Proposition 8.5,

$$\theta_{V_u}(Z_B) = 2\left(\nu_{Z_B}^u\right)'(0) = 2q\lambda\left(\gamma_X^u\right)'(0) = q\lambda\mathbb{E}\left(V_u(X)\right),$$

and the result follows in replacing q by its expression. $\theta_V(Z_B)$ is obtained in integrating over all directions u. $\qquad\square$

Let us emphasize that Equation (9.3) is valid for *any* grain distribution P_X and that it generalizes known results for Boolean models with convex grains [136, p. 386]. Similar generalizations involving intensity of surface measures deriving from Steiner's formula have recently been established [79, 150], under some technical hypotheses on the RACS X. As already stressed out, our result is similar but not identical since the outer Minkowski content of a set differs from its (variational) perimeter [149].

Boolean random sets can be seen as a particular example of Boolean random fields also introduced in Section 5.3. Recall that a *Boolean random field* f_B is defined by

$$f_B(y) = \sup\left(\{0\} \cup \{a_j,\ y \in x_j + X_j\}\right),$$

where $\Phi = \{(x_j, X_j, a_j)\}$ be a Poisson process on $\mathbb{R}^d \times \mathcal{F} \times [0, +\infty)$ with intensity measure $\lambda \mathcal{L}^d \otimes P_X \otimes P_a$, $\lambda \geq 0$.

As already mentioned in Section 5.3, the upper-level sets of f_B are Boolean random sets: indeed, for all $t \geq 0$,

$$\{y, \ f_B(y) > t\} = \{y, \ \exists (x_j, X_j, a_j) \in \Phi, \ y \in x_j + X_j \text{ and } a_j > t\}$$
$$= \bigcup_{\Phi \cap \mathbb{R}^d \times \mathcal{F} \times (t, +\infty)} x_j + X_j,$$

that is to say $\{y, \ f_B(y) > t\}$ is the Boolean model associated with the Poisson process $\sum_\Phi \mathbb{1}(a_j > t)\, \delta_{x_j, X_j}$. Relying on this observation, by the coarea formula for variation intensities (see Proposition 8.9), one deduces an expression of the variation intensities of Boolean random fields.

Proposition 9.6 (Variation intensities of a Boolean random fields). *Let f_B be the Boolean random field with Poisson intensity λ, grain distribution P_X, and gray-level distribution P_a. Let X denote a RACS with distribution P_X and a a r.v. with distribution P_a. Then for all $u \in S^{d-1}$,*

$$\theta_{V_u}(f_B) = \lambda \mathbb{E}(V_u(A)) \int_0^{+\infty} P_a(\{a > t\}) \exp\left(-\lambda \mathbb{E}\left(\mathcal{L}^d(X)\right) P_a(\{a > t\})\right) dt$$

and

$$\theta_V(f_B) = \lambda \mathbb{E}(\mathrm{Per}(A)) \int_0^{+\infty} P_a(\{a > t\}) \exp\left(-\lambda \mathbb{E}\left(\mathcal{L}^d(X)\right) P_a(\{a > t\})\right) dt.$$

Proof. $\{y, \ f_B(y) > t\}$ is the Boolean model associated with the Poisson process $\sum_\Phi \mathbb{1}(a_j > t)\, \delta_{x_j, X_j}$. This Poisson process has grain distribution P_X and intensity $\lambda P_a(\{a > t\})$. Hence by Proposition 9.5

$$\theta_{V_u}(\{f_B > t\}) = \lambda \mathbb{E}(V_u(A)) P_a(\{a > t\}) \exp\left(-\lambda \mathbb{E}\left(\mathcal{L}^d(X)\right) P_a(\{a > t\})\right).$$

By the coarea formula for variation intensity (see Proposition 8.9)

$$\theta_{V_u}(f_B) = \lambda \mathbb{E}(V_u(A)) \int_0^{+\infty} P_a(\{a > t\}) \exp\left(-\lambda \mathbb{E}\left(\mathcal{L}^d(X)\right) P_a(\{a > t\})\right) dt.$$

$\square$

9.5 Colored Dead Leaves Model

This section establishes the expression of the variation intensities of colored dead leaves random fields. Let $\Phi = \{(t_j, x_j, X_j, a_j)\}$ be a Poisson point process of $(-\infty, 0) \times \mathbb{R}^d \times \mathcal{F} \times \mathbb{R}$ with intensity measure $\mathcal{L}^1 \otimes \mathcal{L}^d \otimes P_X \otimes P_a$. Recall that for each leaf (t_j, x_j, X_j, a_j), one defines the visible part V_j by

$$V_j = (x_j + X_j) \setminus \left(\bigcup_{(t_k, x_k, X_k, a_k) \in \Phi, \ t_k > t_j} x_k + X_k \right),$$

and that the *colored dead leaves r.f.* f_{CDL} is defined by

$$f_{CDL}(y) = \sum_{(t_j, x_j, X_j, a_j) \in \Phi} a_j \mathbb{1}(y \in V_j).$$

The next proposition gives the variation intensities of this r.f. model.

Proposition 9.7 (Variation intensities of the colored dead leaves r.f.)**.** *Suppose that $0 < E(\mathcal{L}^d(X)) < +\infty$ and that $a \in L^1$. Let a_1 and a_2 be two independent r.v. with distribution P_a. Then for all $u \in S^{d-1}$,*

$$\theta_{V_u}(f_{\mathrm{CDL}}) = \mathbb{E}(|a_1 - a_2|)\frac{E\left(V_u(X)\right)}{E\left(\mathcal{L}^d(X)\right)},$$

and

$$\theta_V(f_{\mathrm{CDL}}) = \mathbb{E}(|a_1 - a_2|)\frac{E\left(\mathrm{Per}(X)\right)}{E\left(\mathcal{L}^d(X)\right)}.$$

Proof. Let us first compute the expectation $\mathbb{E}\left(|f_{CDL}(ru) - f_{CDL}(0)|\right)$ for $r \in \mathbb{R}$ and $u \in S^{d-1}$. If ru and 0 are in the same visible part V_j, then $f_{CDL}(ru) = f_{CDL}(0)$. Otherwise, if ru and 0 are in different visible parts, then both $f_{CDL}(ru)$ and $f_{CDL}(0)$ have distribution P_a and they are independent. Hence,

$$\mathbb{E}\left(|f_{CDL}(ru) - f_{CDL}(0)|\right) = \mathbb{E}\left(|a_1 - a_2|\right) \mathbb{P}\left(\{ru \text{ and } 0 \text{ belong to different visible parts}\}\right).$$

Now, 0 and ru belong to different visible parts if the last leaf covering either ru or 0 does not cover both points. Hence, the probability

$$\mathbb{P}\left(\{ru \text{ and } 0 \text{ belong to different visible parts}\}\right)$$

has already been computed in Chapter 6 using Proposition 6.3[1]. More precisely, noting $x_0 + X_0$ the last leaf covering either 0 or ru, we have by Equation (6.5),

$$\mathbb{P}\left(\{ru \text{ and } 0 \text{ belong to different visible parts}\}\right) = 1 - \mathbb{P}\left(\{ru, 0\} \subset x_0 + X_0\right)$$

$$= 1 - \frac{\gamma_X(ru)}{2\gamma_X(0) - \gamma_X(ru)}$$

$$= 2\frac{\gamma_X(0) - \gamma_X(ru)}{2\gamma_X(0) - \gamma_X(ru)}.$$

Hence, by Theorem 7.3 and Proposition 8.5,

$$\theta_{V_u}(f_{\mathrm{CDL}}) = \lim_{r \to 0} \frac{\mathbb{E}\left(|f_{CDL}(ru) - f_{CDL}(0)|\right)}{|r|}$$

$$= \mathbb{E}\left(|a_1 - a_2|\right) \lim_{r \to 0} 2\frac{\gamma_X(0) - \gamma_X(ru)}{|r|} \frac{1}{2\gamma_X(0) - \gamma_X(ru)}$$

$$= \mathbb{E}(|a_1 - a_2|)\frac{E\left(V_u(X)\right)}{E\left(\mathcal{L}^d(X)\right)}.$$

$\square$

---

[1]Up to our slightly different definition of the visible parts, this probability is also given by the general Formula (12) of [18].

The expression of the variation intensity

$$\theta_V\left(f_{\mathrm{CDL}}\right) = \mathbb{E}(|a_1 - a_2|)\frac{E\left(\mathrm{Per}(X)\right)}{E\left(\mathcal{L}^d(X)\right)}.$$

is in accordance with our expectation: Indeed, $\mathbb{E}(|a_1 - a_2|)$ is the mean contrast between two distinct visible parts, whereas the ratio $\dfrac{E\left(V_u(X)\right)}{E\left(\mathcal{L}^d(X)\right)}$ is known to be the mean length of cell boundary per unit area when the RACS are random polygons [37].

9.6   Transparent Dead Leaves Process

As for the colored dead leaves model, the transparent dead leaves (TDL) process presented in Chapter 6 is obtained from the Poisson process $\Phi = \{(t_j, x_j, X_j, a_j)\}$ taking values in the state space $(-\infty, 0) \times \mathbb{R}^d \times \mathcal{F} \times \mathbb{R}$ and having intensity measure $\mathcal{L}^1 \otimes \mathcal{L}^d \otimes P_X \otimes P_a$. Given Φ, the TDL process f_{TDL} of transparency coefficient $\alpha \in (0, 1]$ is defined by

$$f_{TDL}(y) = \sum_{(t_j, x_j, X_j, a_j) \in \Phi} \mathbb{1}\left(y \in x_j + X_j\right) \alpha a_j \left(1 - \alpha\right)^{\left(\sum_{k \in \mathbb{N}} \mathbb{1}\left(t_k \in (t_j, 0)\ \text{and}\ y \in x_k + X_k\right)\right)}.$$

To compute the variation intensity of the TDL process we will use the same tools as for the computation of the TDL covariance (see Proposition 6.4), that is we will consider two points y and $z = y + ru$ and use a conditioning with respect to the coverage of the last leaf $x_0 + X_0$ hitting either y or z. Let us recall the properties which are essential for the above proof. Let $y, z \in \mathbb{R}^d$ and let us note $ru = z - y$. Consider the restriction $\Phi^{\{y,z\}}$ of the leaves of Φ which hit the set $\{y, z\}$, that is

$$\Phi^{\{y,z\}} = \left\{(t_j, x_j, X_j, a_j) \in \Phi,\ x_j + X_j \cap \{y, z\} \neq \emptyset\right\}.$$

According to Proposition 6.1[2], $\Phi^{\{y,z\}}$ is an independently marked Poisson process with ground process $\left\{t,\ (t, x, X, a) \in \Phi^{\{y,z\}}\right\}$ of intensity $2\gamma_X(0) - \gamma_X(ru)$ and marks (x_j, X_j, a_j). The marks a_j are i.i.d. with distribution P_a, and are independent of (x_j, X_j). As for the distributions of the marks (x_j, X_j) we are only interested in the following probabilities.

$$\mathbb{P}\left(\{y, z\} \subset x_j + X_j\right) = \frac{\mathcal{L}^d \otimes P_X\left(\{(x, X),\ \{y, z\} \subset x + X\}\right)}{\mathcal{L}^d \otimes P_X\left(\{(x, X),\ \{y, z\} \cap x + X \neq \emptyset\}\right)} = \frac{\gamma_X(ru)}{2\gamma_X(0) - \gamma_X(ru)}.$$

By symmetry and complementarity we have

$$\mathbb{P}\left(y \in x_i + X_i\ \text{and}\ z \notin x_i + X_i\right) = \mathbb{P}\left(z \in x_i + X_i\ \text{and}\ y \notin x_i + X_i\right) = \frac{\gamma_X(0) - \gamma_X(ru)}{2\gamma_X(0) - \gamma_X(ru)}.$$

Let us note (t_0, x_0, X_0, a_0) the last leaf of $\Phi^{\{y,z\}}$, that is the leaf such that

$$t_0 = \sup\left\{t_j,\ (t_j, x_j, X_j, a_j) \in \Phi^{\{y,z\}}\right\}.$$

---

[2]A proof of Proposition 6.1 is given in Section B.2.2 of Appendix B.

Then according to Proposition 6.3, (x_0, X_0, a_0) has the same distribution as any mark (x_j, X_j, a_j) of $\Phi^{\{y,z\}}$, the shifted Poisson process

$$\Phi_{t_0} = \{(t - t_0, x, X, a), \ (t, x, X, a) \in \Phi \text{ and } t < t_0\}$$

has the same distribution as Φ, and (x_0, X_0, a_0) and Φ_{t_0} are independent.

Proposition 9.8 (Variation intensities of the TDL process)**.** *Suppose that $0 < E\left(\mathcal{L}^d(X)\right) < +\infty$ and $a \in L^1$. Then for all $u \in S^{d-1}$,*

$$\theta_{V_u}(f_{TDL}) = C_\alpha \frac{E\left(V_u(X)\right)}{E\left(\mathcal{L}^d(X)\right)},$$

where C_α is the mean contrast between an independent leaf color and the TDL process, that is

$$C_\alpha = \mathbb{E}(|a - f_{TDL}(0)|) = E\left(\left|a - \sum_{k=0}^{+\infty} \alpha a_k \beta^k\right|\right),$$

where the r.v. a and $(a_k)_{k \in \mathbb{N}}$ are i.i.d. with distribution P_a. Consequently,

$$\theta_V(f_{TDL}) = C_\alpha \frac{E\left(\mathrm{Per}(X)\right)}{E\left(\mathcal{L}^d(X)\right)}.$$

Proof. To abbreviate notation, we note $f = f_{TDL}$ within this proof. As said above, we consider two points y and $z = y + ru$. First we give a lower and an upper bound of the expectation

$$\mathbb{E}\left(|f(z) - f(y)|\right).$$

One decomposes this expectation in conditioning with respect of the coverage of the last leaf $x_0 + X_0$ hitting either y or z,

$$\mathbb{E}\left(|f(z) - f(y)|\right) = \mathbb{E}\left(|f(z) - f(y)| \,|\{y, z\} \subset x_0 + X_0\right) \frac{\gamma_X(ru)}{2\gamma_X(0) - \gamma_X(ru)}$$

$$+ \mathbb{E}\left(|f(z) - f(y)| \,| y \in x_0 + X_0 \text{ and } z \notin x_0 + X_0\right) \frac{\gamma_X(0) - \gamma_X(ru)}{2\gamma_X(0) - \gamma_X(ru)}$$

$$+ \mathbb{E}\left(|f(z) - f(y)| \,| z \in x_0 + X_0 \text{ and } y \notin x_0 + X_0\right) \frac{\gamma_X(0) - \gamma_X(ru)}{2\gamma_X(0) - \gamma_X(ru)}.$$

By symmetry the two last terms of the above sum are equal. As in Chapter 6, let us note $\beta = 1 - \alpha$ and f_{t_0} the TDL process associated with the Poisson process Φ_{t_0}. Since Φ_{t_0} and Φ have the same distribution, f_{t_0} and f also have the same distribution. On the event $\{\{y, z\} \subset x_0 + X_0\}$ we have

$$f(y) = \alpha a_0 + \beta f_{t_0}(y) \quad \text{and} \quad f(z) = \alpha a_0 + \beta f_{t_0}(z),$$

so that

$$\mathbb{E}\left(|f(z) - f(y)| \,|\{y, z\} \subset x_0 + X_0\right) = \beta\mathbb{E}\left(|f_{t_0}(z) - f_{t_0}(y)|\right) = \beta\mathbb{E}\left(|f(z) - f(y)|\right).$$

On the event $\{y \in x_0 + X_0 \text{ and } z \notin x_0 + X_0\}$ we have

$$f(y) = \alpha a_0 + \beta f_{t_0}(y) \quad \text{and} \quad f(z) = f_{t_0}(z).$$

Hence

$$|f(z) - f(y)| = |f_{t_0}(z) - \alpha a_0 - \beta f_{t_0}(y)|$$
$$= |\alpha (f_{t_0}(z) - a_0) + \beta (f_{t_0}(z) - f_{t_0}(y))|.$$

Using the triangular inequality we have

$$\alpha |f_{t_0}(z) - a_0| - \beta |f_{t_0}(z) - f_{t_0}(y)| \leq |f(z) - f(y)| \leq \alpha |f_{t_0}(z) - a_0| + \beta |f_{t_0}(z) - f_{t_0}(y)|.$$

Now let us note $C_\alpha = \mathbb{E} (|f(0) - a|)$. We have, in taking expectation in the previous inequalities

$$\mathbb{E} (|f(z) - f(y)| \, | y \in x_0 + X_0 \text{ and } z \notin x_0 + X_0) \leq \alpha C_\alpha + \beta \mathbb{E} (|f(z) - f(y)|)$$

and

$$\mathbb{E} (|f(z) - f(y)| \, | y \in x_0 + X_0 \text{ and } z \notin x_0 + X_0) \geq \alpha C_\alpha - \beta \mathbb{E} (|f(z) - f(y)|).$$

Let us now establish the upper bound of $\mathbb{E} (|f(z) - f(y)|)$. From the initial decomposition of $\mathbb{E} (|f(z) - f(y)|)$ and the previous inequality,

$$\mathbb{E} (|f(z) - f(y)|)$$
$$\leq \beta \mathbb{E} (|f(z) - f(y)|) \frac{\gamma_X(ru)}{2\gamma_X(0) - \gamma_X(ru)} + 2 (\alpha C_\alpha + \beta \mathbb{E} (|f(z) - f(y)|)) \frac{\gamma_X(0) - \gamma_X(ru)}{2\gamma_X(0) - \gamma_X(ru)}.$$

Rearranging the terms we get

$$\mathbb{E} (|f(z) - f(y)|) \leq C_\alpha \frac{2 (\gamma_X(0) - \gamma_X(ru))}{2\gamma_X(0) - \gamma_X(ru)}.$$

Similarly we obtain the following lower bound

$$\mathbb{E} (|f(z) - f(y)|) \geq C_\alpha \frac{2\alpha (\gamma_X(0) - \gamma_X(ru))}{(4 - 2\alpha)\gamma_X(0) - (4 - 3\alpha)\gamma_X(ru)}.$$

Recall that $z = y + ru$. By Theorem 7.3, the directional variation intensity of the TDL process is equal to

$$\theta_{V_u}(f) = \lim_{r \to 0} \frac{\mathbb{E} (|f(y + ru) - f(y)|)}{|r|}.$$

On the other hand, by Proposition 8.5,

$$\lim_{r \to 0} \frac{\gamma_X(0) - \gamma_X(ru)}{|r|} = \frac{1}{2} E (V_u(X)).$$

Using this last property, observe that the two bounds of $\frac{\mathbb{E}(|f(y+ru)-f(y)|)}{|r|}$ both tends to $C_\alpha \frac{E(V_u(X))}{\gamma_X(0)}$ as r tends to 0. Hence

$$\theta_{V_u}(f) = C_\alpha \frac{E (V_u(X))}{E (\mathcal{L}^d(X))}.$$

Integrating this equality over all directions, one computes the variation intensity $\theta_V(f)$. □

Remark (Occlusion case)**.** Observe that when $\alpha = 1$, that is when the transparent leaves are opaque, the formulas of the variation intensities of the TDL process given by Proposition 9.8 boils down to the formulas of the variation intensities of the colored dead leaves r.f. given by Proposition 9.7.

9.7   Colored Tessellations

In this section we compute the variation intensities of colored tessellations. Not surprisingly, the variation intensity is proportional to the ratio mean perimeter over mean area of the typical cell.

   Recall that given a stationary tessellation $T = \sum_j \delta_{C_j}$ one constructs a stationary random field f_T by associating i.i.d. r.v. a_j to each cell C_j, and defining $f_T(x)$ as the color a_j of the a.s. unique cell C_j containing x (see Section 5.5).

   Before establishing the expression of variation intensities of f_T we need to introduce the fundamental notion of typical cell. First, one interprets a stationary tessellation as a point process in $\mathbb{R}^d$ marked with random sets by introducing a centroid map. Recall that $\mathcal{K}'$ denotes the set of non empty compact sets of $\mathbb{R}^d$. A *centroid map* is a measurable application $z : \mathcal{K}' \mapsto \mathbb{R}^d$ such that $z(x+C) = x+z(C)$. Second, given a centroid map z, any stationary tessellation $T = \sum_j \delta_{C_j}$ is decomposed into the stationary marked point process $\sum_j \delta_{(z(C_j), C_j - z(C_j))}$. According to [136, Section 4.1], one deduces that for any stationary tessellation T there exists a constant $\lambda > 0$ and a distribution Q over $\mathcal{K}'_0 = \{K \in \mathcal{K}', \ z(K) = 0\}$ such that for all measurable function $f : \mathcal{K}' \mapsto \mathbb{R}+$,

$$\mathbb{E}\left(\sum_j f(C_j)\right) = \lambda \int_{\mathcal{K}_0} \int_{\mathbb{R}^d} f(x + K) dx Q(dK). \tag{9.4}$$

λ is the intensity of the point process of cell centroids $\sum_j \delta_{z(C_j)}$, and, by definition, Q is the distribution of the *typical cell* of T denoted by $\mathcal{C}$. Applying (9.4) with $f : K \mapsto \mathcal{L}^d\left(K \cap [0,1]^d\right)$ shows that λ is equal to $\dfrac{1}{E\left(\mathcal{L}^d(\mathcal{C})\right)}$.

   The key result to compute the variation intensity of randomly colored stationary tessellations is the following proposition.

Proposition 9.9 (Stationary tessellations and mean covariogram)**.** *Let $T = \sum_j \delta_{C_j}$ be a stationary tessellation and let $\gamma_{\mathcal{C}} : h \mapsto E\left(\mathcal{C} \cap h + \mathcal{C}\right)$ be the mean covariogram of its typical cell $\mathcal{C}$. Then for all $h \in \mathbb{R}^d$,*

$$\mathbb{P}\left(\{0 \text{ and } h \text{ belong to the same cell}\}\right) = \frac{\gamma_{\mathcal{C}}(h)}{\gamma_{\mathcal{C}}(0)}.$$

Remark. Proposition 9.9 is stated without proof in [100]. The proof reproduced below is due to Calka[3].

---

[3]Personal communication. The author is thankful to Pierre Calka for his help for establishing this proof.

Proof of Proposition 9.9. Denote $\rho(h) = \mathbb{P}\left(\{0 \text{ and } h \text{ belong to the same cell}\}\right)$. First, by stationarity $\rho(h) = \mathbb{P}\left(\{-h \text{ and } 0 \text{ belong to the same cell}\}\right)$. Second, remark that for all $C \in \mathcal{K}$, $\{0, -h\} \subset C \iff 0 \in C \cap h + C$. Hence applying Formula (9.4) with $K \mapsto \mathbb{1}(0 \in K \cap h + K)$,

$$
\begin{aligned}
\rho(h) &= \mathbb{E}\left(\sum_j \mathbb{1}\left(0 \in C_j \cap h + C_j\right)\right) \\
&= \frac{1}{E\left(\mathcal{L}^d(\mathcal{C})\right)} \int_{\mathcal{K}_0} \int_{\mathbb{R}^d} \mathbb{1}\left(0 \in (x + K) \cap h + (x + K)\right) dx \, Q(dK) \\
&= \frac{1}{\gamma_{\mathcal{C}}(0)} \int_{\mathcal{K}_0} \int_{\mathbb{R}^d} \mathbb{1}\left(-x \in K \cap h + K\right) dx \, Q(dK) \\
&= \frac{1}{\gamma_{\mathcal{C}}(0)} \int_{\mathcal{K}_0} \mathcal{L}^d(K \cap h + K) Q(dK) \\
&= \frac{\gamma_{\mathcal{C}}(h)}{\gamma_{\mathcal{C}}(0)}.
\end{aligned}
$$

$\square$

Proposition 9.10 (Variation intensities of colored tessellations)**.** *Let* $T_c = \sum_j \delta_{(C_j, a_j)}$ *be a randomly colored stationary tessellation, let* f_T *be its associated stationary random field, and denote by* $\mathcal{C}$ *the typical cell of* T*. Let* a_1 *and* a_2 *be i.d.d. r.v. with distribution* P_a*. For all* $u \in S^{d-1}$*,*

$$
\theta_{V_u}(f_T) = E\left(|a_1 - a_2|\right) \frac{1}{2} \frac{E\left(V_u(\mathcal{C})\right)}{E\left(\mathcal{L}^d(\mathcal{C})\right)},
$$

and

$$
\theta_V(f_T) = E\left(|a_1 - a_2|\right) \frac{1}{2} \frac{E\left(\mathrm{Per}(\mathcal{C})\right)}{E\left(\mathcal{L}^d(\mathcal{C})\right)}.
$$

Proof. Let us compute $\mathbb{E}\left(|f_T(ru) - f_T(0)|\right)$. We have

$$
|f_T(ru) - f_T(0)| = \begin{cases} |a_k - a_j| & \text{if } 0 \in C_j \text{ and } ru \in C_k \text{ with } j \neq k, \\ 0 & \text{if } 0 \text{ and } ru \text{ belong to the same cell.} \end{cases}
$$

By Proposition 9.9, and since for $j \neq k$, a_j and a_k are independent,

$$
\begin{aligned}
\mathbb{E}\left(|f_T(ru) - f_T(0)|\right) &= E\left(|a_1 - a_2|\right) \mathbb{P}\left(\{0 \text{ and } ru \text{ are in different cells}\}\right) \\
&= E\left(|a_1 - a_2|\right) \frac{\gamma_{\mathcal{C}}(0) - \gamma_{\mathcal{C}}(h)}{\gamma_{\mathcal{C}}(0)}.
\end{aligned}
$$

By Proposition 8.5,

$$
\lim_{r \to 0} \frac{\gamma_{\mathcal{C}}(0) - \gamma_{\mathcal{C}}(h)}{|r|} = \frac{1}{2} E\left(V_u(\mathcal{C})\right).
$$

Hence, by Theorem 7.3,

$$
\theta_{V_u}(f_T) = \lim_{r \to 0} \frac{\mathbb{E}\left(|f_T(ru) - f_T(0)|\right)}{|r|} = E\left(|a_1 - a_2|\right) \frac{1}{2} \frac{E\left(V_u(\mathcal{C})\right)}{E\left(\mathcal{L}^d(\mathcal{C})\right)}.
$$

Integrating over all directions one obtains the expression of the variation intensity $\theta_V(f_T)$. $\square$

Observe that the formula

$$\theta_V\left(f_T\right) = E\left(|a_1 - a_2|\right)\frac{1}{2}\frac{E\left(\mathrm{Per}(\mathcal{C})\right)}{E\left(\mathcal{L}^d(\mathcal{C})\right)}.$$

of Proposition 9.10 is in accordance with our expectation: Indeed, $E\left(|a_1 - a_2|\right)$ is the mean contrast between two adjacent cells whereas $\frac{1}{2}\frac{E(\mathrm{Per}(\mathcal{C}))}{E\left(\mathcal{L}^d(\mathcal{C})\right)}$ is known to be the mean length of tessellations boundary per unit area [136, Section 10.1].

9.8   Conclusion

This chapter illustrated the results of Chapter 7 and Chapter 8 in computing the directional and non directional variation intensities of several stationary r.f. models. For germ-grain models, it formulates explicitly the intuitive relation between the geometry of the grains and the total variation. It is worthy to note that for all the studied models, there are only two geometric features of influence on the total variation of the germ-grain r.f.: the mean perimeter and the mean Lebesgue measure of the grains. Besides, for the colored dead leaves r.f., the transparent dead leaves r.f. and the colored tessellations, the mean variation is proportional to the ratio $\dfrac{E(\mathrm{Per}(X))}{E\left(\mathcal{L}^d(X)\right)}$. It is well-known that this ratio perimeter/area is related to the notion of scale (see e.g. [105, 48] and the references therein). Our formulas for the mean variation of these three germ-grain models are in accordance with the above statement: for a high perimeter/area ratio of the grains, the total variation of the concerned germ-grain r.f. is high and thus the r.f. corresponds to a texture, whereas for a low perimeter/area ratio of the grains the r.f. might not be perceived as a texture but rather as a piecewise constant image containing large objects.

All the r.f. models studied in this chapter are stationary. As mentioned in Chapter 7, the variation intensities can also be defined for r.f. with stationary increments. As a particular example of further developments, one might be able to extend to r.f. over $\mathbb{R}^d$ some results of Vervaat [147] where the variation of the sample paths of self-similar one-dimensional stochastic processes with stationary increments is studied.

As mentioned in the conclusion of Chapter 7, a problem of interest in stochastic geometry is to define local densities for inhomogeneous random sets, and the results of Chapter 7 lead to propose a definition for directional and non directional variation densities. As an important example, following the recent work of Villa [150], one could try to derive local variation densities of certain inhomogeneous Boolean models. This should yield to a local version of the expression of the variation intensities of homogeneous Boolean random sets established in this chapter.

Part IV

Appendix

Definition of the Periodic Plus Smooth Decomposition via Discrete Poisson Problems

Contents

This brief appendix shows that the periodic and the smooth component of a discrete image defined by Moisan [113] are both the unique solution of a discrete Poisson problem. As a consequence they both can be computed using the classic FFT-based Poisson solver [127, Section 20.4].

For the computation of the smooth component s, this boils down exactly to Moisan's original algorithm (see the megawave modulus **perdecomp.c** of [114], based on [113, Theorem 2]). For the periodic component p the advantages of this point of view are double. First it justifies that the periodic component p has locally the same behavior as the original image u. Indeed, it shows that both images have the "same" Laplacian, the only difference residing in the computation of the Laplacian at the boundary. This is a slightly more precise formulation of [113, Theorem 3 (*ii*)]. Second, and more importantly, it gives an algorithm to compute directly the DFT $\hat{p}$ of p in using only one call to the FFT algorithm. In comparison with the original algorithm proposed in [113, page 9], this saves one FFT call.

The proposed algorithm for the computation of the periodic component p and its DFT is the one which has been implemented for the on-line demo [60] of the random phase noise algorithm of Chapter 2. It is also used in the Gabor noise by example algorithm presented in Chapter 4. Documented ANSI C source codes are available on-line [60].

A.1   Variational Definition of the Periodic plus Smooth Decomposition

As in Chapter 2, we work on the space $\mathbb{R}^{M \times N}$ of discrete, real-valued and periodic rectangular images. The components of an image $f \in \mathbb{R}^{M \times N}$ are indexed on the set $\Omega = \{0, \ldots, M - 1\} \times \{0, \ldots, N - 1\}$, and by periodicity $f(x) = f(x_1 \mod M, x_2 \mod N)$ for all $x = (x_1, x_2) \in \mathbb{Z}^2$.

We reproduce below Theorem 1 of [113] that defines the periodic plus smooth decomposition.

Theorem A.1 (Definition of the periodic+smooth decomposition)**.** *Let $u \in \mathbb{R}^{M \times N}$ be a discrete gray-level image. There exists a unique couple of images $(p, s) \in \left(\mathbb{R}^{M \times N}\right)^2$ that minimizes*

$$E(p, s) = \sum_{x \in \Omega, \ y \in \mathbb{Z}^2 \setminus \Omega, \ |x - y| = 1} (p(x) - p(y))^2 + \sum_{x \in \Omega, \ y \in \Omega, \ |x - y| = 1} (s(x) - s(y))^2$$

under the constraint

$$u = p + s \quad and \quad \sum_{x \in \Omega} s(x) = 0.$$

p is called the periodic component *of u and s the* smooth component *of u.*

A.2   Periodic and Smooth Components as Solutions of Discrete Poisson Problems

In this section we prove that the periodic component p and the smooth component s are each the unique solution of a discrete Poisson problem. First let us define the discrete Laplacian operators.

Definition A.1 (Discrete Laplacians)**.** *Let $u \in \mathbb{R}^{M \times N}$. The* discrete Laplacian Δ *of u is defined as*

$$\Delta u(x) = \sum_{y \in N_x} (u(y) - u(x)) = -4u(x) + \sum_{y \in N_x} u(y), \ x \in \Omega,$$

where $N_x \subset \mathbb{Z}^2$ denotes the 4-connected neighborhood of x. The Laplacian Δ is split in two operators $\Delta = \Delta_i + \Delta_b$, where Δ_i contains only the differences between direct neighbors and Δ_b the differences between neighbors arising from periodization (i refers to interior and b to boundary). More precisely, the interior Laplacian *of u is*

$$\Delta_i u(x) = \sum_{y \in N_x \cap \Omega} (u(y) - u(x)) = -|N_x \cap \Omega| \, u(x) + \sum_{y \in N_x \cap \Omega} u(y), \ x \in \Omega,$$

where $|N_x \cap \Omega|$ denotes the number of neighbors of x that are in Ω.

Theorem A.2 (Periodic and Smooth Components as Solutions of Poisson Problems). *Let $u \in \mathbb{R}^{M \times N}$, and let p and s be respectively its periodic and smooth component. Then the image p is the unique solution of the Poisson problem*

$$\begin{cases} \Delta p = \Delta_i u, \\ \mathrm{mean}(p) = \mathrm{mean}(u), \end{cases} \tag{A.1}$$

where Δ is the usual discrete periodic Laplacian and Δ_i is the discrete Laplacian in the interior of the domain. Similarly the image s is the unique solution of the following Poisson problem

$$\begin{cases} \Delta s = \Delta_b u, \\ \mathrm{mean}(s) = 0. \end{cases} \tag{A.2}$$

Remark. Note that System (A.1) is just a slightly more precise formulation of [113, Theorem 3 (*ii*)]. However, as discussed in the next section, System (A.1) provides an algorithm to compute the DFT of p with only one call to the FFT.

The proof of Theorem A.2 relies on elementary relations between the discrete Laplacian operators and the corresponding gradient operators. It also provides a proof of Theorem A.1. Let us now precisely define the considered gradient operators.

Definition A.2 (Discrete gradients). *Let $u \in \mathbb{R}^{M \times N}$. Note $e_1 = (1,0)$ and $e_2 = (0,1)$. The* discrete gradient $\nabla : \mathbb{R}^{M \times N} \to \left(\mathbb{R}^2\right)^{M \times N}$ *is defined by*

$$\nabla u(x) = (u(x + e_1) - u(x), u(x + e_2) - u(x)).$$

As for the Laplacian, the gradient ∇ is spit in two disjoint operators $\nabla = \nabla_i + \nabla_b$, where ∇_i contains only the differences between direct neighbors and ∇_b the differences between neighbors arising from periodization. More precisely, for $x = (x_1, x_2) \in \Omega$, we have

$$\nabla_i u(x) = \begin{cases} (u(x + e_1) - u(x), u(x + e_2) - u(x)) & \text{if } x_1 \neq M - 1 \text{ and } x_2 \neq N - 1 \\ (u(x + e_1) - u(x), 0) & \text{if } x_1 \neq M - 1 \text{ and } x_2 = N - 1 \\ (0, u(x + e_2) - u(x)) & \text{if } x_1 = M - 1 \text{ and } x_2 \neq N - 1 \\ (0, 0) & \text{if } (x_1, x_2) = (M - 1, N - 1) \end{cases}$$

and

$$\nabla_b u(x) = \begin{cases} (0, 0) & \text{if } x_1 \neq M - 1 \text{ and } x_2 \neq N - 1 \\ (0, u(x + e_2) - u(x)) & \text{if } x_1 \neq M - 1 \text{ and } x_2 = N - 1 \\ (u(x + e_1) - u(x), 0) & \text{if } x_1 = M - 1 \text{ and } x_2 \neq N - 1 \\ (u(x + e_1) - u(x), u(x + e_2) - u(x)) & \text{if } (x_1, x_2) = (M - 1, N - 1) \end{cases}.$$

Some elementary properties of the gradient and Laplacian operators are listed below.

Lemma A.1. *The gradient and Laplacian operators satisfy the following properties:*

1. $\nabla_i^* \nabla_b = 0$ *and* $\nabla_b^* \nabla_i = 0$, *and thus* $\nabla^* \nabla = \nabla_i^* \nabla_i + \nabla_b^* \nabla_b$.

2. $\nabla^* \nabla = -\Delta$, $\nabla_i^* \nabla_i = -\Delta_i$ *and* $\nabla_b^* \nabla_b = -\Delta_b$,

3. $\ker \Delta$ *is the one-dimensional subspace of constant images,*

4.
$$\mathrm{Im}\, \Delta = \left\{ u \in \mathbb{R}^{M \times N} : \sum_{x \in \Omega} u(x) = 0 \right\},$$

5. $\mathrm{Im}\, \Delta_i \subset \mathrm{Im}\, \Delta$.

We can now prove Theorem A.2.

Proof of Theorem A.2. First remark that

$$E(p, s) = \|\nabla_b p\|_2^2 + \|\nabla_i s\|_2^2.$$

Define
$$F(p) = E(p, u - p) = \|\nabla_b p\|_2^2 + \|\nabla_i (u - p)\|_2^2.$$

(p, s) is solution of the constraint optimization problem if and only if $s = u - p$ and p minimizes F under the constraint $\mathrm{mean}(p) = \mathrm{mean}(u)$.

The functional $p \mapsto F(p)$ is convex and $\mathcal{C}^1$ so that p minimizes F (without constraint) if and only if the differential $DF(p) = 0$. By Lemma A.1,

$$\begin{aligned}
DF(p) &= 2 \nabla_b^* \nabla_b p + 2 \nabla_i^* \nabla_i (p - u) \\
&= 2 \left(\nabla_b^* \nabla_b + \nabla_i^* \nabla_i \right) p - 2 \nabla_i^* \nabla_i u \\
&= -2 \Delta p + 2 \Delta_i u.
\end{aligned}$$

Hence $DF(p) = 0 \iff \Delta p = \Delta_i u$. Now since $\mathrm{Im}\, \Delta_i \subset \mathrm{Im}\, \Delta$, the sets of images p satisfying $\Delta p = \Delta_i u$ is a one-dimensional affine subspace with direction $\ker \Delta$. Since $\ker \Delta$ is the subspace of constant images, there is one and only one image in $\left\{ p \in \mathbb{R}^{M \times N} : \Delta p = \Delta_i u \right\}$ such that $\mathrm{mean}(p) = \mathrm{mean}(u)$. If we note p this uniquely defined image, the resulting couple $(p, u - p)$ is the solution to the initial problem. Thus p is the unique solution of System (A.1), and by linearity $s = u - p$ is the unique solution of System (A.2). $\square$

Remark (Direct definition of s). According to Theorem A.2, s is the unique solution of System (A.2). Computing explicitly the second member $\Delta_b u = -\nabla_b^* \nabla_b u$ shows that $\nabla_b^* \nabla_b u$ is precisely the "boundary function" which is computed in the megawave modulus **perdecomp.c** of [114]. Indeed, for all $(v, u) \in \left(\mathbb{R}^2 \right)^{M \times N} \times \mathbb{R}^{M \times N}$,

$$\langle v, \nabla_b u \rangle = \sum_{k=0}^{M-1} (u(k, 0) - u(k, N-1)) v_1(k, N-1) + \sum_{l=0}^{N-1} (u(0, l) - u(M-1, l)) v_2(M-1, l).$$

Thus for all $v \in (\mathbb{R}^2)^{M \times N}$

$$\nabla_b^* v(x) = \begin{cases} v_1(x_1, N-1) & \text{if } x_2 = 0 \\ -v_1(x_1, N-1) & \text{if } x_2 = N-1 \\ 0 & \text{otherwise} \end{cases} + \begin{cases} v_2(M-1, x_2) & \text{if } x_1 = 0 \\ -v_2(M-1, x_2) & \text{if } x_1 = M-1 \\ 0 & \text{otherwise} \end{cases}.$$

Hence we have

$$\nabla_b^* \nabla_b u = \begin{cases} u(x_1, 0) - u(x_1, N-1) & \text{if } x_2 = 0 \\ u(x_1, N-1) - u(x_1, 0) & \text{if } x_2 = N-1 \\ 0 & \text{otherwise} \end{cases}$$

$$+ \begin{cases} u(0, x_2) - u(M-1, x_2) & \text{if } x_1 = 0 \\ u(M-1, x_2) - u(0, x_2) & \text{if } x_1 = M-1 \\ 0 & \text{otherwise} \end{cases}.$$

One can check that this is the "boundary function" which is computed in the megawave modulus **perdecomp.c** of [114].

A.3 FFT-based Poisson Solver

The periodic component p and the smooth component s are both the unique solution of a discrete Poisson problem of the form

$$\begin{cases} \Delta f = g, \\ \text{mean}(f) = m, \end{cases} \tag{A.3}$$

where Δ is the discrete periodic Laplacian, $g \in \text{Im}\,\Delta = \left\{ u \in \mathbb{R}^{M \times N} : \sum_{x \in \Omega} u(x) = 0 \right\}$, and $m \in \mathbb{R}$. This problem can be solved directly by the classic FFT-based Poisson solver [127, Section 20.4] since in the Fourier domain System (A.3) becomes

$$\begin{cases} \left(-4 + 2\cos\left(\frac{2\xi_1 \pi}{M}\right) + 2\cos\left(\frac{2\xi_2 \pi}{N}\right) \right) \hat{f}(\xi) = \hat{g}(\xi), \ \xi \in \Omega \setminus \{0\}, \\ \hat{f}(0) = m. \end{cases}$$

This yields an algorithm that computes directly the DFT of p and of s in using only one call to the FFT algorithm for each component. For example, for the periodic component p the algorithm is the following:

1. Compute Δu the discrete Laplacian of u.

2. Compute $m = \text{mean}(u)$.

3. Compute $\widehat{\Delta u}$ the DFT of Δu using the forward FFT.

4. Compute $\hat{p}$ defined by

$$\begin{cases} \hat{p}(\xi) = \dfrac{\widehat{\Delta u}(\xi)}{-4+2\cos\left(\frac{2\xi_1\pi}{M}\right)+2\cos\left(\frac{2\xi_2\pi}{N}\right)} & \text{for } \xi \neq 0 \\ \hat{p}(0) = m \end{cases}$$

5. Compute p using the backward FFT (if necessary).

Note that at the end of Step 4 of the above algorithm the DFT $\hat{p}$ of the periodic component p is computed with only one call to the FFT algorithm. In comparison the algorithm proposed in [113, page 9] uses two FFT calls to compute $\hat{p}$.

Poisson Point Processes

Contents

This appendix recalls basic definitions and properties regarding point processes and Poisson processes that have been used in one of the preceding chapters. After defining point processes and stating general properties of Poisson processes, a particular emphasis is given to marked Poisson processes upon which rely both the Poisson shot noise model of Chapters 3 and 4 and the germ-grain models of Chapters 5, 6 and 9. Except for the last section, the content of this chapter is taken from several reference textbooks, mostly [136], but also [89, 91, 11].

B.1 Poisson Point Processes

B.1.1 Framework and Notation

We will consider random measures and point processes defined on a space S called *state space*. Following [136, 89], this state space S is supposed to be a locally compact, second countable, and Hausdorff separable topological space. This means that every point in S has a compact neighborhood, that S has a countable base, and that distinct points of S may be separated by disjoint neighborhoods [89, p. 108]. Let us refer to such spaces as *admissible state spaces*. We will not discuss the necessity of these technical hypotheses. Let us just make three observations which are of interest for the following:

- The Euclidean space $\mathbb{R}^d$ is an admissible state space.

- The space $\mathcal{F} = \mathcal{F}\left(\mathbb{R}^d\right)$ of the closed subsets of $\mathbb{R}^d$ embedded with the hit or miss topology, also called the Fell topology, is also an admissible state space [110, 136].

- If S_1 and S_2 are two admissible state spaces, then the product space $S_1 \times S_2$ embedded with the product topology is also an admissible state space. In particular, $\mathbb{R}^d \times \mathcal{F}$ is an admissible state space.

In all the remaining of this appendix, S will denote an admissible state space and $\mathcal{B}(S)$ the set of Borel subsets of S. $\mathbf{M}^+ = \mathbf{M}^+(S)$ denotes the set of positive Radon measures[1], that is the set of positive measures ν on $(S, \mathcal{B}(S))$ such that $\nu(K) < +\infty$ for all relatively compact set $K \subset S$. $\mathbf{M}^+$ is supplied with the σ-algebra $\mathcal{M}^+$ generated by the evaluation maps $\nu \mapsto \nu(A)$, $A \in \mathcal{B}(S)$. As a special subclass of $\mathbf{M}^+$, $\mathbf{N}$ denotes the set of *counting measures*, that is the measures such that $\nu(A) \in \mathbb{N} \cup \{+\infty\}$ for all $A \in \mathcal{B}(S)$. The trace σ-algebra of $\mathcal{M}^+$ on $\mathbf{N}$ is denoted by $\mathcal{N}$. A counting measure ν is said to be *simple* if $\nu(\{x\}) \in \{0, 1\}$ for all $x \in S$. The set $\mathbf{N}_s$ of simple counting measures is a measurable subset of $\mathbf{N}$ [136, p.51]. It is equipped with $\mathcal{N}_s$, the trace σ-algebra of $\mathcal{N}$ on $\mathbf{N}_s$.

B.1.2 Point Processes

Definition B.1 (Random measure)**.** *A* random measure Φ *on S is a measurable map from some probability space $(\Omega, \mathcal{A}, \mathbb{P})$ into the measurable space $(\mathbf{M}^+, \mathcal{M}^+)$ of locally finite Borel measures. The* distribution of a random measure Φ *is the probability measure P_Φ on $\mathcal{M}^+$ defined by*

$$P_\Phi(B) = \mathbb{P}\left(\Phi \in B\right), \ B \in \mathcal{M}^+.$$

Definition B.2 (Point process)**.** *A* point process *is random measure which is almost surely concentrated on the set $\mathbf{N}$ of counting measure. A* point process *is said to be simple if it is a.s. in $\mathbf{N}_s$.*

For all $x \in S$, δ_x denotes the Dirac measure at point x, that is the measure defined for all $A \in \mathcal{B}(S)$ by $\delta_x(A) = 1$ if $x \in A$ and 0 otherwise. The following proposition shows that a point process can be represented as a sum of random Dirac measure.

Proposition B.1 (Representation of a point process)**.** *Let Φ be a point process on S. Then there exists a sequence of random variables $x_1, x_2, \dots$ such that*

$$\Phi(\omega, .) = \sum_{i=1}^{\Phi(\omega, S)} \delta_{x_i(\omega)}(.), \ \omega \in \Omega.$$

---

[1]Definitions relative to Radon measures are recalled in Chapter C where real-valued and vector-valued Radon measures are considered. However in this chapter the term measure implicitly refers to a positive measure.

References for the proof. It is a straightforward application of [136, Lemma 3.1.3 p. 49]. □

Thanks to the above proposition, a point process Φ can be viewed as a random measure $\Phi = \sum_i \delta_{x_i}$ but also as a (possibly redundant) random set of points $\Phi = \{x_i\}$.

One can apply several natural operations to point processes. For example, if Φ and Ψ are two point processes, then the *superposition* $\Phi + \Psi$ is also a point process. For all $A \in \mathcal{B}(S)$, the restriction $\Phi \llcorner A$ of a point process Φ is also a point process.

In several case of interest, point processes Φ can be translated by vector $x \in \mathbb{R}^d$ into shifted point processes $x + \Phi$ (e.g. when $S = \mathbb{R}^d$ or $S = \mathcal{F}$ the set of closed subsets of $\mathbb{R}^d$). A point process Φ is said to be *stationary* if $\Phi \overset{\mathcal{D}}{=} x + \Phi$ for all $x \in \mathbb{R}^d$.

Definition B.3 (Intensity measure)**.** *The intensity measure of random measure Φ (and in particular of a point process) is the measure μ defined by*

$$\mu(A) := \mathbb{E}\left(\Phi(A)\right), \ A \in \mathcal{B}(S).$$

The intensity measure is always defined but may be infinite. If Φ is stationary, its intensity measure is translation invariant. In particular, if $S = \mathbb{R}^d$, then there exists a constant $\lambda \in [0, +\infty)$ such that $\mu = \lambda \mathcal{L}^d$. λ is called the *intensity* of the stationary point process.

B.1.3 Poisson Distribution

This brief section recalls the definition of a Poisson distribution.

Definition B.4 (Poisson distribution)**.** *A random variable X has a Poisson distribution with parameter $\lambda \in (0, +\infty)$ if*

$$\forall n \in \mathbb{N}, \ \mathbb{P}(X = n) = \frac{\lambda^n e^{-\lambda}}{n!}.$$

This distribution is denoted by $\mathcal{P}(\lambda)$.

The family of Poisson distributions is extended to the degenerate cases $\lambda = 0$ and $\lambda = +\infty$: for $\lambda = 0$, $X = 0$ a.s. and for $\lambda = +\infty$, $X = +\infty$ a.s.

Proposition B.2 (Generating function of a Poisson distribution)**.** *Let $\lambda \in (0, +\infty)$ and $X \sim \mathcal{P}(\lambda)$. The generating function of X is*

$$G_\lambda(s) = \mathbb{E}\left(s^X\right) = e^{\lambda(s-1)}, \ s \in \mathbb{R}.$$

Proof.

$$\mathbb{E}\left(s^X\right) = \sum_{k=0}^{+\infty} s^k \mathbb{P}\left(X = k\right) = \sum_{k=0}^{+\infty} s^k \frac{\lambda^k}{k!} e^{-\lambda} = e^{\lambda(s-1)}.$$

□

B.1.4 Poisson Point Processes

Definition B.5 (Poisson point process)**.** *Let Φ be a point process on S and let μ be its intensity measure. Φ is a* Poisson (point) process *on S if:*

(i) *For any disjoint measurable subsets $A_1, A_2, \ldots, A_n$ of S, the random variables $\Phi(A_1), \Phi(A_2), \ldots, \Phi(A_n)$ are mutually independent.*

(ii) *For all measurable subset $A \subset S$, $\Phi(A)$ has the Poisson distribution with parameter $\mu(A) \in [0, +\infty]$, that is $\Phi(A) \sim \mathcal{P}(\mu(A))$.*

First let us remark that the restriction of a Poisson process is a Poisson process.

Proposition B.3 (Restriction of a Poisson process)**.** *Let Φ be a Poisson of measure μ and let $A \in \mathcal{B}(S)$. Then the restriction $\Phi \llcorner A$ of Φ to the set A is a Poisson process with intensity measure $\mu \llcorner A$.*

Proof. This is straightforward from the definition. $\qquad\square$

Now we turn to the fundamental result which establishes the existence and uniqueness of Poisson point processes.

Theorem B.1 (Existence and uniqueness of Poisson process)**.** *Let μ be a locally finite measure without atoms on S. Then there exists a unique Poisson process in S with intensity measure μ. Besides, this Poisson point process is simple.*

References for the proof. This theorem regroups Lemma 3.2.1 p. 59 and Theorem 3.2.1 p. 60 of [136]. $\qquad\square$

Proposition B.4 (Simplicity of Poisson processes)**.** *A Poisson process is simple if and only if its intensity measure has no atoms.*

References for the proof. This is a weaker version of [136, Lemma 3.2.1 p. 59]. $\quad\square$

As a consequence of the two above results, any simple Poisson process is characterized by its intensity measure. **In the remaining of this chapter we will always suppose that the considered intensity measures μ are locally finite and without atoms**, that is that the corresponding Poisson processes are simple.

The next proposition provides a better understanding of the randomness structure of Poisson processes (see [136, Theorem 3.2.2 (b) p. 62-63]).

Proposition B.5. *Let Φ be a Poisson in S with intensity measure μ. Let $A \subset S$ be a Borel set such that $0 < \mu(A) < +\infty$, and let $k \in \mathbb{N}$. Then*

$$\mathbb{P}\left(\Phi \llcorner A \in \cdot \,|\, \Phi(A) = k\right) = \mathbb{P}\left(\sum_{i=1}^{k} \delta_{\xi_i} \in \cdot\right)$$

where $\xi_1, \ldots, \xi_k$ are independent, identically distributed random points in S with distribution

$$P_\xi := \frac{\mu \llcorner A}{\mu(A)}.$$

We conclude this section with two elementary lemmas regarding the generating function of the counting variables $N_\Phi(A)$ which will be useful in Appendix D.

Lemma B.1. *Let Φ be a Poisson process on a state space S with intensity measure μ. Let $A \subset S$ be a measurable subset such that $0 < \mu(A) < +\infty$. Then for every $s \in \mathbb{R}$,*

$$\mathbb{E}\left(s^{N_\Phi(A)}\right) = e^{(s-1)\mu(A)}.$$

Proof. $\mathbb{E}\left(t^{N_\Phi(A)}\right)$ is the generating function of the r.v. $N_\Phi(A) \sim \mathcal{P}\left(\mu(A)\right)$. The result follows from Proposition B.2. $\qquad\square$

Lemma B.2. *Let Φ be a Poisson process on a state space S with intensity measure μ. Let $A, B \subset S$ be two measurable subsets such that $0 < \mu(A) < +\infty$ and $0 < \mu(B) < +\infty$. Then for every $s \in \mathbb{R}$,*

$$\mathbb{E}\left(s^{N_\Phi(A)+N_\Phi(B)}\right) = e^{(s-1)(\mu(A)+\mu(B))+(s-1)^2\mu(A\cap B)}.$$

Proof. Introduce the sets $A_1 = A \setminus B$ and $B_1 = B \setminus A$ and remark that

$$N_\Phi(A) + N_\Phi(B) = N_\Phi(A_1) + N_\Phi(B_1) + 2N_\Phi(A \cap B).$$

As the sets A_1, B_1 and $A\cap B$ are disjoint, the r.v. $N_\Phi(A_1)$, $N_\Phi(B_1)$ and $N_\Phi(A\cap B)$ are independent. Thus using Lemma B.1 we get

$$\begin{aligned}
\mathbb{E}\left(s^{N_\Phi(A)+N_\Phi(B)}\right) &= \mathbb{E}\left(s^{N_\Phi(A_1)}\right)\mathbb{E}\left(s^{N_\Phi(B_1)}\right)\mathbb{E}\left(s^{2N_\Phi(A\cap B)}\right)\\
&= e^{(s-1)\mu(A_1)}e^{(s-1)\mu(B_1)}e^{(s^2-1)\mu(A\cap B)}\\
&= e^{(s-1)(\mu(A)+\mu(B))+(s-1)^2\mu(A\cap B)},
\end{aligned}$$

where in the last step we used $\mu(A_1) + \mu(B_1) = \mu(A) + \mu(B) - 2\mu(A \cap B)$. $\qquad\square$

B.1.5 Sums over Poisson processes: Campbell's Theorem

The results of this section are taken from [91, Section 3.2]. Several of these results generalize to the case of non Poisson point processes (see e.g. [136, Theorem 3.1.2 p. 54] and [136, Theorem 3.1.3 p. 55]).

Theorem B.2 (Campbell's Theorem). *Let Φ be a Poisson process on the state space S with mean measure μ, and let $f : S \to \mathbb{R}$ be a measurable function. Then the sum*

$$\Sigma = \sum_{X\in\Phi} f(X)$$

is absolutely convergent with probability 1 if and only if

$$\int_S \min\left(|f(x)|, 1\right)\mu(dx) < +\infty. \tag{B.1}$$

If this condition holds, then

$$\mathbb{E}\left(e^{\theta\Sigma}\right) = \exp\left(\int_S \left(e^{\theta f(x)} - 1\right)\mu(dx)\right)$$

for any complex θ for which the integral on the right converges, and in particular whenever θ is pure imaginary. Moreover

$$\mathbb{E}\left(\Sigma\right) = \int_S f(x)\mu(dx) \tag{B.2}$$

in the sense that the expectation exists if and only if the integral converges, and they are then equal. If (B.2) converges, then

$$\mathrm{Var}(\Sigma) = \int_S f(x)^2 \mu(dx),$$

finite or infinite.

Corollary B.1 (Covariance of two sums over the same Poisson process)**.** *If $f_1, f_2, \ldots, f_p$ are measurable functions satisfying Hypothesis (B.1), so that the sums*

$$\Sigma_j = \sum_{X \in \Phi} f_j(X), \ \ j = 1, \ldots, p,$$

converge with probability 1, then

$$\mathbb{E}\left(e^{it_1\Sigma_1 + \cdots + it_p\Sigma_p}\right) = \exp\left(\int_S \left(e^{it_1 f_1(x) + \cdots + it_p f_p(x)} - 1\right)\mu(dx)\right).$$

In addition if the functions f_j satisfy

$$\int_S f_j(x)^2 \mu(dx) < +\infty,$$

then

$$\mathrm{Cov}\left(\Sigma_j, \Sigma_k\right) = \int_S f_j(x) f_k(x)\mu(dx).$$

B.1.6 Laplace Transform of Random Measures

This section introduces the concept of Laplace transform of random measures [89].

Definition B.6 (Laplace transform of a random measure)**.** *Let Φ be a random measure. The Laplace transform of Φ is the functional $\mathcal{L}_\Phi$*

$$f \mapsto \mathcal{L}_\Phi(f) := \mathbb{E}\left(\exp\left(-\int_S f(x)\Phi(dx)\right)\right),$$

where f describes the set of non negative measurable functions defined over S.

The Laplace transform of a random measure is an important analytic tool since, like the Laplace transform of a random variable, it characterizes the distribution of a random measure.

Theorem B.3 (Laplace transform and equality in distribution)**.** *Let Φ and Ψ be two random measures. Then the following assertions are equivalent:*

(i) $\Phi \overset{\mathcal{D}}{=} \Psi$.

(ii) $\mathcal{L}_\Phi(f) = \mathcal{L}_\Psi(f)$ *for all non negative measurable functions* $f : S \mapsto [0, +\infty)$.

(iii) $\mathcal{L}_\Phi(f) = \mathcal{L}_\Psi(f)$ *for all non negative and compactly supported continuous functions* $f : S \mapsto [0, +\infty)$.

References for the proof. (i) $\Rightarrow$ (ii) $\Rightarrow$ (iii) is straightforward. (iii) $\Rightarrow$ (i) is a part of [89, Theorem 3.1]. $\square$

Proposition B.6 (Laplace transform of a Poisson process)**.** *Let Φ be a Poisson process on the state space S with mean measure μ. Then for all non negative measurable functions $f : S \mapsto [0, +\infty)$,*

$$\mathcal{L}_\Phi(f) = \exp\left(-\int_S \left(1 - e^{-f(x)}\right) \mu(dx) \right).$$

Proof. Apply Campbell's theorem (Theorem B.2) to $\sum_{x_i \in \Phi} f(x_i)$ and specify the formula of the characteristic function in $\theta = -1$. $\square$

B.2 Independently Marked Poisson Processes

B.2.1 Independently Marked Point Processes

Within this section M denotes a locally compact and separable topological space with a countable base and the state space S is the product space $\mathbb{R}^d \times M$ provided with the product σ-algebra $\mathcal{B}\left(\mathbb{R}^d\right) \otimes \mathcal{B}(M)$. Our main reference is [136, Section 3.5]

Definition B.7 (Marked point process)**.** *A marked point process in $\mathbb{R}^d$ with mark space M is a simple point process Φ in $\mathbb{R}^d \times M$ with intensity measure μ satisfying*

$$\mu\left(C \times M\right) < +\infty \quad \text{for all compact set } C \subset \mathbb{R}^d.$$

Definition B.8 (Ground process)**.** *If Φ is a marked point process in $\mathbb{R}^d$ with mark space M, then the image $p(\Phi)$ of Φ under the projection $p : (x, m) \mapsto x$ is a point process in $\mathbb{R}^d$ called the* unmarked point process *or* ground process *of Φ.*

By Proposition B.1 a marked point process Φ in $\mathbb{R}^d$ with mark space M can be represented in the form

$$\Phi = \sum_{i=1}^{\Phi(\mathbb{R}^d \times M)} \delta_{(x_i, m_i)}, \tag{B.3}$$

where $(x_i, m_i)_i$ is a sequence of random variables in $\mathbb{R}^d \times M$. In general, the mark m_i may depend on the position x_i or even on the whole process[2] Φ. In the following we will restrict to the case where the marks are independent.

---

[2]This is for example the case with the particle process $\sum_i \delta_{(x_i, K_i)}$, $K_i \in \mathcal{K}'_0$, of Section 9.7 which defines a random tessellation (see [136, Section 10.1]).

Definition B.9 (Independently marked point process)**.** *A marked point process in $\mathbb{R}^d$ with mark space M is* independently marked *if it has a representation* (B.3) *where the random marks* $(m_i)_{i \in \mathbb{N}}$ *are i.i.d. and independent of* $\left((x_i)_{i \in \mathbb{N}}, \Phi(\mathbb{R}^d \times M) \right)$. *The common distribution Q of the r.v. m_i is then called the* mark distribution *of Φ.*

With this definition it might not be easy to show that a marked point process is independently marked. However when the ground process of Φ is a Poisson process we have the following characterization theorem.

Theorem B.4 (Characterization of independently marked Poisson processes)**.** *Let μ be the intensity measure of a Poisson process in $\mathbb{R}^d$, Q be a probability distribution over M and Φ be a marked point process in $\mathbb{R}^d$ with mark space M. Then the following assertions are equivalent :*

1. *Φ is independently marked with mark distribution Q and its ground process $p(\Phi)$ is a Poisson process with intensity measure μ.*

2. *Φ is a Poisson process in $\mathbb{R}^d \times M$ with intensity measure $\mu \otimes Q$.*

Bibliographic references for the proof. This theorem is stated in [11, Section 1.8] without proof. The implication (1)$\Rightarrow$(2) is given in the proof of [136, Theorem 3.5.7 p. 88]. The reverse is shown in slightly modifying the proof of [136, Theorem 3.5.8 p. 89], as the authors explain in the remark following the proof. □

Theorem B.4 is very useful because, as the next corollary explicitly shows, it permits to interpret some Poisson processes taking values in a product space as independently marked point processes.

Corollary B.2 (Decomposition of a Poisson process into an independently marked Poisson process)**.** *Let Φ be a Poisson process in $\mathbb{R}^d \times M$ with intensity measure $\mu = \mu_1 \otimes \mu_2$, where μ_1 is a measure over $\mathbb{R}^d$ without atoms and μ_2 is a measure over M. If $0 < \mu_2(M) < \infty$, then Φ is an independently marked Poisson process in $\mathbb{R}^d$ with mark distribution $\frac{1}{\mu_2(M)}\mu_2$ and ground Poisson process with intensity measure $\mu_2(M)\mu_1$.*

Proof. Write

$$\mu_1 \otimes \mu_2 = \mu_2(M)\mu_1 \otimes \frac{1}{\mu_2(M)}\mu_2$$

and use Theorem B.4. □

We conclude this general section in evoking stationary marked point processes. By definition, a marked point process is *stationary* if its ground process is stationary. It turns out that all stationary marked Poisson processes are necessarily independently marked.

Proposition B.7 (Stationary Poisson processes are independently marked). *Let Φ be a stationary Poisson process in $\mathbb{R}^d \times M$ with intensity measure satisfying*

$$\mu(C \times M) < +\infty \quad \text{for all compact set } C \subset \mathbb{R}^d.$$

Then Φ is necessarily independently marked.

Reference for the proof. This is [136, Theorem 3.5.8 p. 89]. □

B.2.2 The Poisson Process Preceding the Last Hit

The goal of this section is to prove Proposition 6.3 (reproduced below) which was been used in Chapter 6 to compute the covariance of the TDL process. It is an extension of the fact that if $0 > t_0 > t_1 > t_2 > \dots$ is an homogeneous Poisson process on $(-\infty, 0)$ then the shifted process $0 > t_1 - t_0 > t_2 - t_0 > t_3 - t_0 > \dots$ is also a Poisson process with the same distribution [91, Chapter 4].

Until the end of this section E denotes a locally compact and separable topological space with a countable basis.

Proposition 6.3 (Last hitting leaf and the Poisson process preceding the last hit). *Let Ψ be a Poisson process in $(-\infty, 0) \times E$ with intensity measure of the form $\lambda \otimes \mu$ where λ is the one-dimensional Lebesgue measure on $(-\infty, 0)$ and μ is a measure on E. Let $A \subset E$ be a measurable set such that $0 < \mu(A) < +\infty$. Define*

$$t_0 = \sup\{t_i | (t_i, y_i) \in \Psi \cap ((-\infty, 0) \times A)\},$$

y_0 the a.s. unique $y \in E$ such that $(t_0, y) \in \Psi \cap ((-\infty, 0) \times A)$, and

$$\Psi_{t_0} = \sum_{(t_i, y_i) \in \Psi} \mathbb{1}(t_i < t_0)\, \delta_{(t_i - t_0, y_i)}.$$

Then

- *t_0, y_0, and Ψ_{t_0} are mutually independent.*

- *$-t_0$ has an exponential distribution with parameter $\mu(A)$.*

- *y_0 has distribution Q_A defined for all $B \in \mathcal{B}(E)$ by $Q_A(B) = \dfrac{\mu(B \cap A)}{\mu(A)}$.*

- *Ψ_{t_0} is a Poisson process with intensity measure $\lambda \otimes \mu$, i.e. Ψ_{t_0} has the same distribution as Ψ.*

To prove Proposition 6.3 we first deals with the case where the time-shift is a r.v. independent of the Poisson process.

Lemma B.3 (Independent time shift). *Let Ψ be a Poisson process in $(-\infty, 0) \times E$ with intensity measure of the form $\lambda \otimes \mu$ where λ is the one-dimensional Lebesgue*

measure on $(-\infty, 0)$ and μ is a measure on E. Let T be a random variable independent of Ψ. Then the point process

$$\Psi_T = \sum_{(t_i, y_i) \in \Phi} \mathbb{1}\left(t_i < T\right) \delta_{(t_i - T, y_i)}$$

is a Poisson process with intensity measure $\lambda \otimes \mu$, i.e. Ψ_T has the same distribution as Ψ. Besides Ψ_T and T are independent.

Proof. For all non negative measurable function f, let us write

$$\mathcal{L}_\Psi(f) := \mathbb{E}\left(\exp\left(-\sum_{(t, y) \in \Psi} f(t, y)\right)\right)$$

the Laplace transform of Ψ, and for all $s \in [0, +\infty)$,

$$L_T(s) := \mathbb{E}\left(\exp(-sT)\right)$$

the Laplace transform of $T \in (-\infty, 0)$. As Ψ is a Poisson process with intensity measure $\lambda \otimes \mu$, by Proposition B.6

$$\mathcal{L}_\Psi(f) = \exp\left(-\int_{(-\infty, 0) \times E} \left(1 - e^{-f(t, y)}\right) dt\mu(dy)\right)$$

for all non negative measurable function f. By Theorem B.3 and following [91, Chapter 4], to prove that Ψ_T has the same distribution as Ψ and is independent of T, it is sufficient to prove that for all f and s we have

$$\mathbb{E}\left(\exp\left(-sT - \sum_{(t, y) \in \Psi_T} f(t, y)\right)\right) = L_T(s)\mathcal{L}_\Psi(f). \tag{B.4}$$

Let f be any non negative measurable function, and s be any non negative real. We have

$$\mathbb{E}\left(\exp\left(-sT - \sum_{(t, y) \in \Psi_T} f(t, y)\right)\right) = \mathbb{E}\left(\exp\left(-sT - \sum_{(t, y) \in \Psi} \mathbb{1}\left(t < T\right) f(t - T, y)\right)\right).$$

Since T is independent of Ψ, using Fubini theorem we can compute the last expectation in first integrating with respect to the distribution of Ψ and then integrating with respect to the distribution of T. Let us fix T and compute the integral

$$I_T = \int_{\mathbf{N}((-\infty, 0) \times E)} \exp\left(-sT - \sum_{(t, y) \in \phi} \mathbb{1}\left(t < T\right) f(t - T, y)\right) P_\Psi(\phi).$$

Introducing the function $g_T : (t, y) \mapsto \mathbb{1}\left(t < T\right) f(t - T, y)$ we see that $I_T = \exp(-sT)\mathcal{L}_\Psi(g_T)$. By Proposition B.6

$$\mathcal{L}_\Psi(g_T) = \exp\left(-\int_{(-\infty, 0) \times E} \left(1 - e^{-\mathbb{1}(t < T) f(t - T, y)}\right) dt\mu(dy)\right)$$

$$= \exp\left(-\int_{(-\infty, T) \times E} \left(1 - e^{-f(t - T, y)}\right) dt\mu(dy)\right).$$

By the change of variable $u = t - T$ we get

$$\mathcal{L}_\Psi(g_T) = \exp\left(-\int_{(-\infty,0)\times E}\left(1 - e^{-f(u,y)}\right)du\mu(dy)\right) = \mathcal{L}_\Psi(f).$$

Hence $I_T = \exp(-sT)\mathcal{L}_\Psi(f)$. Integrating I_T with respect to the distribution of T we obtain Equation (B.4), which concludes the proof. $\qquad\square$

Proof of Proposition 6.3. Note $\Psi_A = \{(t_i, y_i) \in \Psi : y_i \in A\} = \Psi \cap ((-\infty, 0) \times A)$. By Proposition B.3, Ψ_A is a Poisson process with intensity measure $\lambda \otimes (\mu \llcorner A)$. Since $0 < \mu(A) < +\infty$ we can write

$$\lambda \otimes (\mu \llcorner A) = \mu(A)\lambda \otimes Q_A,$$

where Q_A is the probability measure defined in the proposition. By Theorem B.4, Ψ_A is an independently marked Poisson process and its ground process is a one-dimensional homogeneous Poisson process on $(-\infty, 0)$ with intensity $\mu(A)$. This Poisson process on the line can be enumerated in decreasing order $t_0 > t_1 > t_2 > \dots$, along with the corresponding marks $y_0, y_1, y_2, \dots$ $-t_0$ is the length of the interval between 0 and the first point of this one-dimensional Poisson process. It is well-known that $-t_0$ has an exponential distribution with parameter $\mu(A)$ and that the shifted random set $\{t_i - t_0, \ i \geq 1\}$ is a Poisson process with intensity $\mu(A)$ which is independent of the original process $\{t_i, \ i \geq 0\}$ (see, for example, [91, Chapter 4]). Since Ψ_A is independently marked, the mark y_0 is independent of t_0 and has distribution Q_A. Besides, for the same reason, the process

$$\Psi_{t_0,A} := \Psi_{t_0} \cap ((-\infty, 0) \times A) = \{(t_i - t_0, y_i), \ i \geq 1\}$$

is an independently marked Poisson process with intensity measure $\mu(A)\lambda \otimes Q_A$. Let us now conclude the proof in considering the whole shifted point process

$$\Psi_{t_0} = \sum_{(t_i,y_i)\in\Psi} \mathbb{1}\left(t_i < t_0\right)\delta_{(t_i - t_0, y_i)}.$$

Decompose Ψ in $\Psi = \Psi_A \cup \Psi_{A^c}$, where $\Psi_{A^c} = \Psi \cap ((-\infty, 0) \times A^c)$, and use the same decomposition for $\Psi_{t_0} = \Psi_{t_0,A} \cup \Psi_{t_0,A^c}$. We have already shown that $\Psi_{t_0,A}$ has the same distribution as Ψ_A. Since Ψ is a Poisson process, Ψ_A and Ψ_{A^c} are independent. Consequently the couple (t_0, y_0) is independent of Ψ_{A^c}. Since t_0 is independent of Ψ_{A^c}, Lemma B.3 ensures that the shifted point process

$$\Psi_{t_0,A^c} = \sum_{(t_i,y_i)\in\Psi_{A^c}} \mathbb{1}\left(t_i < t_0\right)\delta_{(t_i - t_0, y_i)}$$

has the same distribution as Ψ_{A^c} and is independent of t_0. Besides $\Psi_{t_0,A}$ and Ψ_{t_0,A^c} are independent: Indeed by definition Ψ_{t_0,A^c} only depends of Ψ_{A^c} and t_0, and $\Psi_{t_0,A}$ is independent of the couple (t_0, Ψ_{A^c}). Eventually, the couple $(\Psi_{t_0,A}, \Psi_{t_0,A^c})$ has the same distribution as the couple (Ψ_A, Ψ_{A^c}), and so $\Psi_{t_0} = \Psi_{t_0,A} \cup \Psi_{t_0,A^c}$ has the same distribution as $\Psi = \Psi_A \cup \Psi_{A^c}$. As for the mutual independence of t_0, y_0 and Ψ_{t_0}, Ψ_{t_0} is independent of t_0 and y_0 is clearly independent of the couple (t_0, Ψ_{t_0}). $\qquad\square$

Signed Measures and Random Signed Measures

Contents

This chapter gathers necessary results related to signed and vector valued measures. Important examples of such measures are the weak derivatives of functions of bounded directional variation and functions of bounded variation respectively (see Section 7.2). First the definitions of signed Radon measures and vector-valued Radon measures are recalled. A second section deals with the notion of weak* convergence of signed Radon measure as well as the compactness for weak* convergence. To finish the definition of random signed measures is given. These random measures are at stake in the definition of random fields of bounded directional variation (see Chapter 7).

C.1   Definitions of Signed and Vector-Valued Measures

In this section we recall the definitions of signed and vector-valued Radon measures. Our reference is [6, Chapter 1]. In all the section $(X, \mathcal{A})$ denotes a measurable space.

Definition C.1 (Positive measures)**.** *A set function $\mu : \mathcal{A} :\to [0, +\infty]$ is a* positive measure *if*

- $\mu(\emptyset) = 0$.

- μ *is* additive*: for all $A, B \in \mathcal{A}$,*

$$A \cap B = \emptyset \implies \mu(A \cup B) = \mu(A) + \mu(B).$$

- μ *is σ-subadditive: for all $A, (A_n)_{n \in \mathbb{N}} \in \mathcal{A}$,*

$$A \subset \bigcup_{n=0}^{+\infty} A_n \implies \mu(A) \leq \sum_{n=0}^{+\infty} \mu(A_n).$$

μ *is said to be* finite *if* $\mu(X) < +\infty$. $A \in \mathcal{A}$ *is said to be* σ-finite *with respect to* μ *if* A *is the union of an increasing sequence of sets* A_n *such that* $\mu(A_n) < +\infty$.

Remark (σ-additivity)**.** It is straight forward to show that a set function $\mu : \mathcal{A} :\to [0, +\infty]$ is a measure if and only if μ is σ-*additive*, that is for any sequence of $(A_n)_{n\in\mathbb{N}}$ of pairwise disjoint elements of $\mathcal{A}$,

$$\mu\left(\bigcup_{n=0}^{+\infty} A_n\right) = \sum_{n=0}^{+\infty} \mu(A_n).$$

It is this property which permits to define real and vector-valued measures.

Definition C.2 (Real and vector-valued measures)**.** *A set function* $\mu : \mathcal{A} \to \mathbb{R}^m$, $m \geq 1$, *is a* measure *if*

- $\mu(\emptyset) = 0$.

- *For any sequence of* $(A_n)_{n\in\mathbb{N}}$ *of pairwise disjoint elements of* $\mathcal{A}$,

$$\mu\left(\bigcup_{n=0}^{+\infty} A_n\right) = \sum_{n=0}^{+\infty} \mu(A_n).$$

If $m = 1$ μ *is a* real measure *or* signed measure, *and if* $m > 1$ μ *is a* vector measure.

Let us remark that according to this definition, for all $A \in \mathcal{A}$, $|\mu(A)| < +\infty$, and all the series $\sum_{n=0}^{+\infty} \mu(A_n)$ are necessarily absolutely convergent since the union of sets does not depend on the order of its terms [6, p. 3]. In particular, note that a positive measure is not necessarily a real measure.

Let us now define the important notion of total variation of a real or vector-valued measures.

Theorem C.1 (Total variation)**.** *Let* μ *be a signed or vector measure over* $(X, \mathcal{A})$. *The total variation* $|\mu|$ *of* μ *is the set function defined for all* $A \in \mathcal{A}$ *by*

$$|\mu|(A) = \sup\left\{\sum_{n=0}^{+\infty} |\mu(A_n)|, \ (A_n)_{n\in\mathbb{N}} \in \mathcal{A} \text{ pairwise disjoint and } A = \bigcup_{n=0}^{+\infty} A_n\right\}.$$

The total variation $|\mu|$ *is a positive and finite measure on* $(X, \mathcal{A})$.

Reference for the proof. This is [6, Theorem 1.6 p. 5]. $\qquad\square$

We now turn to the definition of Borel and Radon measures which are measures defines on the Borel σ-algebra of a metric space. In the remaining of this section (S, d) denotes a locally compact and separable metric space[1], and $\mathcal{B}(S)$ denotes its Borel σ-algebra, that is the σ-algebra generated by the open sets for the topology induced by the distance d.

---

[1]Let us precise that if S is an admissible state space in the sense of Appendix B, that is a locally compact, second countable, and Hausdorff separable topological spaces, then it can be equipped with a distance d such that (S, d) is a locally compact and separable metric space [89, p. 168].

Definition C.3 (Borel measure and positive Radon measure)**.** *A positive measure on the measurable space* $(S, \mathcal{B}(S))$ *is called a* Borel measure*. If a Borel measure is finite on the compact sets, it is called a* positive Radon measure*.*

Definition C.4 (Real and Vector Radon measure)**.** *A real or vector-valued set function* μ *defined on the relatively compact Borel subsets of* S *which is a measure on* $(K, \mathcal{B}(K))$ *for every compact set* $K \subset S$ *is called a* real *or* vector Radon measure *on* S. *If* $\mu : \mathcal{B}(S) \to \mathbb{R}^m$ *is a real or vector-valued measure, then we say that* μ *is a* finite real *or* vector Radon measure*.*

Real Radon measures are also called *signed Radon measures.* We denote by $\mathbf{M}(S)$ (resp. $\mathbf{M}_F(S)$) the space of signed Radon measures (resp. finite signed Radon measures).

C.2 Weak* Convergence of Signed Radon Measures

This section recalls the definition of the weak* convergence of signed Radon measures, as well as the fundamental results of weak* compactness. All the above results extend to the case of vector-valued measure [6, p. 26-27].

As in the previous section, (S, d) is a locally compact and separable metric space (although we only use these results for $S = \mathbb{R}^d$), and $\mathbf{M}(S)$ and $\mathbf{M}_F(S)$ denote respectively the space of signed Radon measures and the space of finite signed Radon measures.

In what follows $\mathcal{C}_c(S)$ denotes the set of continuous functions $\varphi : S \to \mathbb{R}$ having compact support, and $\mathcal{C}_0(S)$ denotes the closure of $\mathcal{C}_c(S)$ for the sup norm.

Definition C.5 (Weak* convergence)**.** *We say that a sequence* $(\mu_n)_{n \in \mathbb{N}} \in \mathbf{M}(S)$ *locally weakly* converges to* $\mu \in \mathbf{M}(S)$ *is for every* $\varphi \in \mathcal{C}_c(S)$,

$$\lim_{n \to +\infty} \int_S \varphi(x) \mu_n(dx) = \int_S \varphi(x) \mu(dx).$$

In the case where the Radon measures are finite, we say that a sequence $(\mu_n)_{n \in \mathbb{N}} \in \mathbf{M}_F(S)$ *weakly* converges to* $\mu \in \mathbf{M}_F(S)$ *is for every* $\varphi \in \mathcal{C}_0(S)$,

$$\lim_{n \to +\infty} \int_S \varphi(x) \mu_n(dx) = \int_S \varphi(x) \mu(dx).$$

Theorem C.2 (Weak* compactness)**.** *If* $(\mu_n)_{n \in \mathbb{N}}$ *is a sequence of* $\mathbf{M}_F(S)$ *such that* $\sup \{|\mu_n|(S) < +\infty, \ n \in \mathbb{N}\} < +\infty$ *then* $(\mu_n)_{n \in \mathbb{N}}$ *has a weakly* converging subsequence. Moreover, the map* $\mu \mapsto |\mu|(S)$ *is lower semicontinuous with respect to the weak* convergence.*

Reference for the proof. This is [6, Theorem 1.59 p. 26]. □

Corollary C.1 (Local weak* compactness)**.** *Let* $(\mu_n)_{n \in \mathbb{N}}$ *is a sequence of* $\mathbf{M}(S)$ *such that* $\sup \{|\mu_n|(K) < +\infty, \ n \in \mathbb{N}\} < +\infty$ *for every compact* $K \subset S$. *Then* $(\mu_n)_{n \in \mathbb{N}}$ *has a locally weakly* converging subsequence. Moreover, for every open set* $U \subset S$, *the map* $\mu \mapsto |\mu|(U)$ *is lower semicontinuous with respect to the local weak* convergence.*

C.3   Random Signed Measures

As in the previous section, (S, d) is a locally compact and separable metric space (although we only use these results for $S = \mathbb{R}^d$). $\mathbf{M} := \mathbf{M}(S)$ and $\mathbf{M}_F := \mathbf{M}_F(S)$ denote respectively the space of signed Radon measures and the space of finite signed Radon measures.

In this section the formal definition of a random signed (Radon) measure is recalled as well as the fact that the total variation of a random signed Radon measure is a well-defined random positive Radon measure.

Following the usual construction of random objects, a random signed measure will be defined as a measurable function from a probability space $(\Omega, \mathcal{A}, \mathbb{P})$ to the space $\mathbf{M}$ of signed Radon measures equipped with an appropriate σ-algebra $\mathcal{M}$. Following [76], the σ-algebra $\mathcal{M}$ is defined in the same way as the σ-algebra $\mathcal{M}^+$ on the space $\mathbf{M}^+(S)$ of positive Radon measures (see Section B.1.1 or [89, 136, 76]). More precisely, $\mathcal{M}$ is the smallest σ-algebra for which the maps

$$\mu \mapsto \mu(A), \ A \in \mathcal{B}(S) \text{ relatively compact,}$$

are measurable.

Definition C.6 (Random signed (Radon) measures). *Let $(\Omega, \mathcal{A}, \mathbb{P})$ be a probability space. A random signed measure is a measurable map*

$$\mu : (\Omega, \mathcal{A}) \longrightarrow (\mathbf{M}, \mathcal{M}).$$

By [89, Lemma 1.3 p. 12], for all $\varphi \in \mathcal{C}_c(S)$, the map

$$\mu \mapsto \int_S \varphi(x)\mu(dx)$$

is measurable. Besides, by [89, Lemma 1.4 p. 12], the σ-algebra $\mathcal{M}$ is generated by all the maps of this form. From this we deduce the following proposition.

Proposition C.1 (Almost sure weak* convergence). *Let $(\mu_n)_{n \in \mathbb{N}}$ be a sequence of random signed measures such that for $\mathbb{P}$-almost all $\omega \in \Omega$, $\mu_n(\omega)$ is weakly* convergent to a measure $\mu(\omega)$. Then, the map $\omega \mapsto \mu(\omega)$ is measurable, that is to say, μ is a well-defined random signed measure.*

Proof. Let Ω' be a measurable subset of Ω such that $\mathbb{P}(\Omega') = 1$ and for all $\omega \in \Omega'$ $\mu_n(\omega)$ weakly* converge to some measure $\mu(\omega)$. Extend the definition of $\mu(\omega)$ to $\mu(\omega) = 0$ if $\omega \notin \Omega'$. Since $\mathcal{M}$ is generated by the maps $\mu \mapsto \int_S \varphi(x)\mu(dx)$, to show that the map $\omega \mapsto \mu(\omega)$ is measurable it is enough to show that for all $\varphi \in \mathcal{C}_c(S)$,

$$\omega \mapsto \int_S \varphi(x)\mu(\omega, dx)$$

is measurable. Now by hypothesis for all $\varphi \in \mathcal{C}_c(S)$ and $\omega \in \Omega'$,

$$\lim_{n \to +\infty} \int_S \varphi(x)\mu_n(\omega, dx) = \int_S \varphi(x)\mu(\omega, dx).$$

Hence the map $\omega \mapsto \int_S \varphi(x)\mu(\omega, dx)$ is measurable since it is the a.s. limit of a sequence of measurable maps. $\qquad\square$

We now consider the total variation of random signed measures.

Proposition C.2 (Measurability of the total variation). *Let $\mu : (\Omega, \mathcal{A}) \to (\mathbf{M}, \mathcal{M})$ be a random signed measure. Then the total variation of $|\mu| : \omega \mapsto |\mu(\omega)|$ is a random positive Radon measure.*

References for the proof. By Theorem C.1, for all ω, the total variation $|\mu(\omega)|$ is a positive Radon measure. The difficulty is to show that $\omega \mapsto |\mu(\omega)|$ is measurable. This has been proved by Horowitz [78, Theorem 1.1 p. 216] using Hahn's decomposition theorem [134]. $\qquad\square$

Technical Proofs Related to the TDL Process

Contents

    This appendix presents technical proofs related to the study of the transparent dead leaves (TDL) process developed in Chapter 6.

    The first section provides a fully detailed proof of the Gaussian convergence of the TDL process as the objects tend to be fully transparent (see Theorem 6.1). Our proof is based on a the method of moments for convergence in distribution.

    The second section proposes an alternative proof for the computation of the covariance (see Proposition 6.4) based on Palm calculus. The lengthy computations demonstrate the utility of our alternative strategy based on the conditioning with respect to the coverage of the last hitting leaf.

D.1 Proof of the Normal Convergence Theorem

This section provides the proof of Theorem 6.1 stated in Chapter 6. This theorem establishes the normal convergence of the TDL process as the objects tend to be fully transparent, as precisely recalled below.

Theorem 6.1 (Normal convergence of the TDL process)**.** *Suppose that* $\mathrm{Var}(a) > 0$. *Then, as the transparency coefficient* α *tends to* 0, *the family of random fields*

$\left(\dfrac{f_\alpha - \mathbb{E}\left(f_\alpha\right)}{\sqrt{\operatorname{Var}\left(f_\alpha\right)}} \right)_\alpha$ *converges in the sense of finite-dimensional distributions to a centered stationary Gaussian random field with covariance function*

$$C(\tau) = \frac{\gamma_X(\tau)}{E(\mathcal{L}^d(X))} = \frac{\gamma_X(\tau)}{\gamma_X(0)}.$$

D.1.1   Some Classical Results of Probability Theory

This section gathers the several classic theoretical results needed do prove Theorem 6.1. All these results are related to the method of moments to demonstrate a convergence in distribution.

D.1.1.1   Moments and Convergence in Distribution

Proposition D.1 (Moments and convergence in distribution)**.** *Let (f_n) be a sequence of centered random fields having finite moments of all order and let f_G be a centered stationary Gaussian r.f. with covariance function C. If for all $p \in \mathbb{N}$, for all (non necessarily distinct) $y_1, \ldots, y_p \in \mathbb{R}^d$,*

$$\lim_{n \to +\infty} \mathbb{E}\left(\prod_{j=1}^{p} f_n(y_j) \right) = \mathbb{E}\left(\prod_{j=1}^{p} f_G(y_j) \right),$$

then (f_n) converges to f_G in the sense of finite-dimensional distributions.

D.1.1.2   A Recurrence Relation for the Moments of a Multivariate Normal Distribution

Explicit expressions for the moments of a multivariate normal distribution are given by Isserlis' theorem recalled below.

Theorem D.1 (Isserlis' theorem)**.** *Let $Y_1, \ldots, Y_{2N+1}$, $N \geq 1$, be normalized, jointly Gaussian r.v. (i.e. $\mathbb{E}(Y_i) = 0$ and $\operatorname{Var}(Y_i) = \mathbb{E}(Y_i^2) = 1$). Then*

$$\mathbb{E}(Y_1 Y_2 \ldots Y_{2N}) = \sum \prod \mathbb{E}(Y_i Y_j) = \sum \prod \operatorname{Cov}(Y_i, Y_j),$$

and

$$\mathbb{E}(Y_1 Y_2 \ldots Y_{2N+1}) = 0,$$

where the notation $\sum \prod$ means summing over all distinct ways of partitioning the set $\{Y_1, \ldots, Y_{2N}\}$ into N pairs $\{Y_i, Y_j\}$ and take the product of the N terms $\mathbb{E}(Y_i Y_j) = \operatorname{Cov}(Y_i, Y_j)$.

From Isserlis' theorem one deduces a recurrence relation for the moments of a multivariate normal distribution.

Proposition D.2 (A recurrence relation for the moments of a multivariate normal distribution)**.** *Let* $Y = (Y_1, \ldots, Y_p)$, $p \geq 2$, *be a normalized Gaussian vector (i.e.* $\mathbb{E}(Y_i) = 0$, *and* $\mathrm{Var}(Y_i) = \mathbb{E}(Y_i^2) = 1$*). Then,*

$$\mathbb{E}\left(\prod_{j=1}^{p} Y_j\right) = \frac{2}{p} \sum_{\{j,k\} \subset \{1,\ldots,p\}} \mathrm{Cov}(Y_j, Y_k) \mathbb{E}\left(\prod_{l \in \{1,\ldots,p\} \setminus \{j,k\}} Y_l\right).$$

Proof. If $p \geq 2$ is odd, then by Isserlis' theorem the above formula is trivial. Hence, in the following we suppose that p is even. First let $j \in \{1, \ldots, p\}$. Factorizing with all the pairs containing j in Isserlis' identity, one obtains

$$\mathbb{E}\left(\prod_{j=1}^{p} Y_j\right) = \sum_{\substack{k=1 \\ k \neq j}}^{p} \mathrm{Cov}(Y_j, Y_k) \mathbb{E}\left(\prod_{l \in \{1,\ldots,p\} \setminus \{j,k\}} Y_l\right).$$

The above identity is valid for all $j \in \{1, \ldots, p\}$. Summing these p identities gives

$$\mathbb{E}\left(\prod_{j=1}^{p} Y_j\right) = \frac{1}{p} \sum_{j=1}^{p} \sum_{\substack{k=1 \\ k \neq j}}^{p} \mathrm{Cov}(Y_j, Y_k) \mathbb{E}\left(\prod_{l \in \{1,\ldots,p\} \setminus \{j,k\}} Y_l\right).$$

Now remark that in this double sum over (j, k), the terms $\mathrm{Cov}(Y_j, Y_k) \mathbb{E}\left(\prod_l Y_l\right)$ only depend on the pair $\{j, k\}$ but not on the order. Hence, the above expression simplifies to

$$\mathbb{E}\left(\prod_{j=1}^{p} Y_j\right) = \frac{2}{p} \sum_{\{j,k\} \subset \{1,\ldots,p\}} \mathrm{Cov}(Y_j, Y_k) \mathbb{E}\left(\prod_{l \in \{1,\ldots,p\} \setminus \{j,k\}} Y_l\right).$$

$\square$

D.1.1.3 Moments and Partial Derivatives of the Characteristic Function

If a random vector $(Y_1, \ldots, Y_p)$ has finite moments of all order, then its characteristic function

$$\phi : (t_1, \ldots, t_p) \mapsto \mathbb{E}\left(e^{i(t_1 Y_1 + \cdots + t_p Y_p)}\right)$$

is $\mathcal{C}^\infty$ and the multivariate moments of $(Y_1, \ldots, Y_p)$ are proportional to the partial derivatives of ϕ in $(0, \ldots, 0)$. Since this result will be used later, let us introduce notation for the partial derivatives of a function $f : (t_1, \ldots, t_n) \mapsto f(t_1, \ldots, t_n)$. In what follows, for every subset $\mathcal{I} = \{i_1, \ldots, i_k\} \subset \{1, \ldots, p\}$, we write $\#\mathcal{I} = k$ for the cardinal number of $\mathcal{I}$, and we adopt the short notation

$$\frac{\partial^k f}{\partial t_\mathcal{I}}(t_1, \ldots, t_p) := \frac{\partial^k f}{\partial t_{i_1} \partial t_{i_1} \ldots \partial t_{i_k}}(t_1, \ldots, t_p).$$

With these notation, one has

$$\frac{\partial^k \phi}{\partial t_\mathcal{I}}(0, \ldots, 0) = i^k \mathbb{E}\left(\prod_{j \in \mathcal{I}} Y_j\right).$$

As it will be needed later on, let us introduce further notation relative to partial derivatives. For $\mathcal{I} \subset \{1, \ldots, p\}$, $\mathcal{I}^c$ denotes the complementary set of indices $\mathcal{I}^c := \{1, \ldots, p\} \setminus \mathcal{I}$. Then, when differentiating a product $f(t) = g(t)h(t)$ we have the following formula

$$\frac{\partial^p f}{\partial t_1 \ldots \partial t_p}(t_1, \ldots, t_p) = \sum_{k=0}^{p} \sum_{\substack{\mathcal{I} \subset \{1, \ldots, p\} \\ \#\mathcal{I}=k}} \frac{\partial^k g}{\partial t_\mathcal{I}}(t_1, \ldots, t_p) \frac{\partial^{p-k} h}{\partial t_{\mathcal{I}^c}}(t_1, \ldots, t_p).$$

D.1.2 Notation and Plan of the Proof of Theorem 6.1

Let s be a real number such that $0 < s < \frac{1}{6}$ (this choice for s will be become clear later). For all $\alpha \in (0, 1]$, one defines the truncation operator

$$T_\alpha(b) = \begin{cases} b & \text{if } b \in [-\alpha^{-s}, \alpha^{-s}], \\ \alpha^{-s} & \text{if } b > \alpha^{-s}, \\ -\alpha^{-s} & \text{if } b < -\alpha^{-s}. \end{cases}$$

For all $\alpha \in (0, 1]$, f_α denotes the TDL process with transparency coefficient α and

$$g_\alpha(y) = \frac{f_\alpha(y) - \mathbb{E}(a)}{\sqrt{\mathrm{Var}(f_\alpha)}}$$

denotes its normalization. For all $\alpha \in (0, 1]$, f_α^T denotes the TDL process with transparency coefficient α associated to the Poisson process

$$\Phi^T = \{(t_i, x_i, X_i, T_\alpha(a_i)), (t_i, x_i, X_i, a_i) \in \Phi\},$$

that is the TDL process obtained by truncating the colors a_i of the leaves of Φ with the truncation operator T_α. We have

$$\mathbb{E}(f_\alpha^T) = E(T_\alpha(a)) \quad \text{and} \quad \mathrm{Var}(f_\alpha^T) = \frac{\alpha}{2 - \alpha} \mathrm{Var}(T_\alpha(a)).$$

As for the TDL f_α, one defines

$$g_\alpha^T(y) = \frac{f_\alpha^T(y) - \mathbb{E}(T_\alpha(a))}{\sqrt{\mathrm{Var}(f_\alpha^T)}}.$$

Thanks to the truncation, f_α^T is bounded by α^{-s}. In particular, for all $\alpha \in (0, 1]$, f_α^T and g_α^T have finite moments of all order.

We will note f_G a centered stationary Gaussian random field with covariance function $C : \tau \mapsto \frac{\gamma_X(\tau)}{\gamma_X(0)}$.

The proof of Theorem 6.1 is in two parts:

1. One shows that the normalized TDL with truncated colors g_α^T converges in distribution to f_G by the method of moments. More precisely the sufficient condition of Proposition D.1 will be shown to be true by induction over the number of points p.

2. One shows that the family $g_\alpha - g_\alpha^T$ converges to 0 in L^2.

By Slutsky's theorem, these two properties ensures that g_α converges in distribution to f_G.

D.1.3 Normal Convergence of the Normalized TDL Having Truncated Colors

With the above notation, by Proposition D.1, it is enough to show the following lemma.

Lemma D.1 (Convergence of Moments). *For all $p \in \mathbb{N}$, for all (non necessarily distinct) $y_1, \dots, y_p \in \mathbb{R}^d$,*

$$\lim_{\alpha \to 0} \mathbb{E}\left(\prod_{j=1}^p g_\alpha^T(y_j)\right) = \mathbb{E}\left(\prod_{j=1}^p f_G(y_j)\right).$$

We will show this lemma by induction over p. First note that, by definition of $g_\alpha^T(y_j)$, the statement is true for $p = 0$ and $p = 1$, and one easily checks that it is also true for $p = 2$ (but this is not necessary for the above proof).

For the proof by induction we now consider an integer $p \geq 2$ and p points $y_1, \dots, y_p$ of $\mathbb{R}^d$, and we suppose that the convergence of moments holds for all moments of order $k < p$.

D.1.3.1 Decomposition of the Multivariate Characteristic Function by Conditioning with Respect to the Coverage of the Last Hitting Leaf

We consider the random vector

$$\left(g_\alpha^T(y_1), \dots, g_\alpha^T(y_p)\right) = \left(\frac{f_\alpha^T(y_1) - \mathbb{E}(T_\alpha(a))}{\sigma_\alpha^T}, \dots, \frac{f_\alpha^T(y_p) - \mathbb{E}(T_\alpha(a))}{\sigma_\alpha^T}\right),$$

where $\sigma_\alpha^T = \sqrt{\mathrm{Var}(f_\alpha^T)}$. One denotes by $\phi_\alpha(t_1, \dots, t_p)$ the multivariate characteristic function of this random vector, that is

$$\phi_\alpha(t_1, \dots, t_p) = \mathbb{E}\left(e^{i\left(t_1 g_\alpha^T(y_1) + \dots + t_p g_\alpha^T(y_p)\right)}\right).$$

One denotes by ψ_α the characteristic function of the random variable $T_\alpha(a) - E(T_\alpha(a))$ where a follows the color distribution P_a, that is

$$\psi_\alpha(t) = E\left(e^{it(T_\alpha(a) - E(T_\alpha(a)))}\right).$$

In addition, we introduce the short notation $\mathcal{Y}$ for the set $\mathcal{Y} = \{y_1, \dots, y_p\}$.

In what follows we apply Proposition 6.3 in considering the leaves of Φ^T which hit the set $\mathcal{Y}$. Hence let $(t_0, x_0, X_0, T_\alpha(a_0))$ denote the last leaf covering at least

one point of $\mathcal{Y}$, and let us note g_{α,t_0}^T the corresponding time-shifted random field. Then for all $y_j \in \mathcal{Y}$, one has the decomposition

$$
g_\alpha^T(y_j) = \begin{cases} \alpha \frac{T_\alpha(a_0) - \mathbb{E}(T_\alpha(a))}{\sigma_\alpha^T} + \beta g_{\alpha,t_0}^T(y_j) & \text{if } y_j \in x_0 + X_0, \\ g_{\alpha,t_0}(y_j) & \text{otherwise}, \end{cases}
$$

which can also be written as follows

$$
g_\alpha^T(y_j) = \alpha \mathbb{1}(y_j \in x_0 + X_0) \frac{T_\alpha(a_0) - \mathbb{E}(T_\alpha(a))}{\sigma_\alpha^T} + \beta^{\mathbb{1}(y_j \in x_0 + X_0)} g_{\alpha,t_0}^T(y_j).
$$

Besides, by Proposition 6.3, g_{α,t_0}^T, (x_0, X_0) and a_0 are mutually independent.

To obtain a decomposition of the characteristic function ϕ_α we will condition with respect to the coverage of the last leaf $x_0 + X_0$. Hence, for all subset $\mathcal{X} \subset \mathcal{Y}$, $\mathcal{X} \neq \emptyset$, let us note $A_\mathcal{X} \subset \Omega$ the event

$$
A_\mathcal{X} = \{(x_0 + X_0) \cap \mathcal{Y} = \mathcal{X}\}
$$

and

$$
p_\mathcal{X} = \mathbb{P}(A_\mathcal{X}).
$$

The events $A_\mathcal{X}$, $\mathcal{X} \neq \emptyset$, form a partition of the probability space Ω, and in particular

$$
\sum_{\mathcal{X} \subset \mathcal{Y}, \mathcal{X} \neq \emptyset} p_\mathcal{X} = 1.
$$

Remark that on the event $A_\mathcal{X}$, the above decomposition of $g_\alpha^T(y_j)$ becomes

$$
g_\alpha^T(y_j) = \alpha \mathbb{1}(y_j \in \mathcal{X}) \frac{T_\alpha(a_0) - \mathbb{E}(T_\alpha(a))}{\sigma_\alpha^T} + \beta^{\mathbb{1}(y_j \in \mathcal{X})} g_{\alpha,t_0}^T(y_j).
$$

Hence, using the mutual independence of the different random variables,

$$
\begin{aligned}
\phi_\alpha(t_1, \ldots, t_p) &= \mathbb{E}\left(e^{i\left(t_1 g_\alpha^T(y_1) + \cdots + t_p g_\alpha^T(y_p)\right)} \right) \\
&= \sum_{\substack{\mathcal{X} \subset \mathcal{Y} \\ \mathcal{X} \neq \emptyset}} \mathbb{E}\left(e^{i\left(t_1 g_\alpha^T(y_1) + \cdots + t_p g_\alpha^T(y_p)\right)} \middle| A_\mathcal{X} \right) p_\mathcal{X} \\
&= \sum_{\substack{\mathcal{X} \subset \mathcal{Y} \\ \mathcal{X} \neq \emptyset}} \psi_\alpha\left(\frac{\alpha}{\sigma_\alpha^T} \sum_{j=1}^p \mathbb{1}(y_j \in \mathcal{X}) t_j \right) \phi_\alpha\left(\beta^{\mathbb{1}(y_1 \in \mathcal{X})} t_1, \ldots, \beta^{\mathbb{1}(y_p \in \mathcal{X})} t_p \right) p_\mathcal{X}.
\end{aligned}
$$

(D.1)

The next step of the proof consists in deriving the above decomposition of the multivariate characteristic function in order to obtain a recurrence relation for the moments of $\left(g_\alpha^T(y_1), \ldots, g_\alpha^T(y_p) \right)$.

D.1.3.2   A Recurrence Relation for the Moments of g_α^T

We refer to Section D.1.1.3 for short notation for partial derivatives and the corresponding formula for partial derivatives of a product function. Here to compute $\frac{\partial^p \phi_\alpha}{\partial t_1 \ldots \partial t_p}(t_1, \ldots, t_p)$ from Equation (D.1), one needs to derive with respect to each variable t_j the functions of the form

$$F_{\mathcal{X}}(t_1, \ldots, t_p) := \psi_\alpha\left(\frac{\alpha}{\sigma_\alpha^T}\sum_{j=1}^p \mathbb{1}(y_j \in \mathcal{X})t_j\right)\phi_\alpha\left(\beta^{\mathbb{1}(y_1 \in \mathcal{X})}t_1, \ldots, \beta^{\mathbb{1}(y_p \in \mathcal{X})}t_p\right).$$

We have

$$\frac{\partial^p F_{\mathcal{X}}}{\partial t_1 \ldots \partial t_p}(t_1, \ldots, t_p)$$

$$= \sum_{k=0}^p \sum_{\substack{\mathcal{I}\subset\{1,\ldots,p\}\\ \#\mathcal{I}=k}} \frac{\partial^k}{\partial t_{\mathcal{I}}}\left[\psi_\alpha\left(\frac{\alpha}{\sigma_\alpha^T}\sum_{j=1}^p \mathbb{1}(y_j \in \mathcal{X})t_j\right)\right]\frac{\partial^{p-k}}{\partial t_{\mathcal{I}^c}}\left[\phi_\alpha\left(\beta^{\mathbb{1}(y_1 \in \mathcal{X})}t_1, \ldots, \beta^{\mathbb{1}(y_p \in \mathcal{X})}t_p\right)\right]$$

$$= \sum_{k=0}^p \left(\frac{\alpha}{\sigma_\alpha^T}\right)^k \sum_{\substack{\mathcal{I}\subset\{1,\ldots,p\}\\ \#\mathcal{I}=k}}\left(\prod_{i\in\mathcal{I}}\mathbb{1}(y_i \in \mathcal{X})\right)\psi_\alpha^{(k)}\left(\frac{\alpha}{\sigma_\alpha^T}\sum_{j=1}^p \mathbb{1}(y_j \in \mathcal{X})t_j\right)$$

$$\left(\prod_{i\in\mathcal{I}^c}\beta^{\mathbb{1}(y_i \in \mathcal{X})}\right)\frac{\partial^{p-k}}{\partial t_{\mathcal{I}^c}}\phi_\alpha\left(\beta^{\mathbb{1}(y_1 \in \mathcal{X})}t_1, \ldots, \beta^{\mathbb{1}(y_p \in \mathcal{X})}t_p\right).$$

Summing over all subsets $\mathcal{X}$, one has the identity

$$\frac{\partial^p \phi_\alpha}{\partial t_1 \ldots \partial t_p}(t_1, \ldots, t_p)$$

$$= \sum_{k=0}^p \left(\frac{\alpha}{\sigma_\alpha^T}\right)^k \sum_{\substack{\mathcal{I}\subset\{1,\ldots,p\}\\ \#\mathcal{I}=k}}\sum_{\substack{\mathcal{X}\subset\mathcal{Y}\\ \mathcal{X}\neq\emptyset}}\left(\prod_{i\in\mathcal{I}}\mathbb{1}(y_i \in \mathcal{X})\right)\psi_\alpha^{(k)}\left(\frac{\alpha}{\sigma_\alpha^T}\sum_{j=1}^p \mathbb{1}(y_j \in \mathcal{X})t_j\right)$$

$$\left(\prod_{i\in\mathcal{I}^c}\beta^{\mathbb{1}(y_i \in \mathcal{X})}\right)\frac{\partial^{p-k}}{\partial t_{\mathcal{I}^c}}\phi_\alpha\left(\beta^{\mathbb{1}(y_1 \in \mathcal{X})}t_1, \ldots, \beta^{\mathbb{1}(y_p \in \mathcal{X})}t_p\right)p_{\mathcal{X}}.$$

Evaluating in $(t_1, \ldots, t_p) = (0, \ldots, 0)$, this gives

$$\frac{\partial^p \phi_\alpha}{\partial t_1 \ldots \partial t_p}(0, \ldots, 0)$$

$$= \sum_{k=0}^p \left(\frac{\alpha}{\sigma_\alpha^T}\right)^k \sum_{\substack{\mathcal{I}\subset\{1,\ldots,p\}\\ \#\mathcal{I}=k}}\sum_{\substack{\mathcal{X}\subset\mathcal{Y}\\ \mathcal{X}\neq\emptyset}}\left(\prod_{i\in\mathcal{I}}\mathbb{1}(y_i \in \mathcal{X})\right)\psi_\alpha^{(k)}(0)\left(\prod_{i\in\mathcal{I}^c}\beta^{\mathbb{1}(y_i \in \mathcal{X})}\right)\frac{\partial^{p-k}}{\partial t_{\mathcal{I}^c}}\phi_\alpha(0, \ldots, 0)p_{\mathcal{X}}$$

$$= \sum_{k=0}^p \left(\frac{\alpha}{\sigma_\alpha^T}\right)^k \psi_\alpha^{(k)}(0)\sum_{\substack{\mathcal{I}\subset\{1,\ldots,p\}\\ \#\mathcal{I}=k}}\frac{\partial^{p-k}}{\partial t_{\mathcal{I}^c}}\phi_\alpha(0, \ldots, 0)\left(\sum_{\substack{\mathcal{X}\subset\mathcal{Y}\\ \mathcal{X}\neq\emptyset}}\left(\prod_{i\in\mathcal{I}}\mathbb{1}(y_i \in \mathcal{X})\right)\left(\prod_{i\in\mathcal{I}^c}\beta^{\mathbb{1}(y_i \in \mathcal{X})}\right)p_{\mathcal{X}}\right).$$

In the above sum, remark that for $k = 0$, $\mathcal{I} = \emptyset$ and thus all the terms are proportional to $\frac{\partial^p \phi_\alpha}{\partial t_1 \ldots \partial t_p}(0, \ldots, 0)$. Besides, since $T_\alpha(a) - E(T_\alpha(a))$ is centered, $\psi_\alpha^{(1)}(0) = 0$, and thus for $k = 1$ all the terms are null. Hence we have the following equation

$$\frac{\partial^p \phi_\alpha}{\partial t_1 \ldots \partial t_p}(0, \ldots, 0) \left(1 - \sum_{\substack{\mathcal{X} \subset \mathcal{Y} \\ \mathcal{X} \neq \emptyset}} \left(\prod_{j=1}^p \beta^{\mathbb{1}(y_j \in \mathcal{X})} \right) p_\mathcal{X} \right) \tag{D.2}$$

$$= \sum_{k=2}^p \left(\frac{\alpha}{\sigma_\alpha^T} \right)^k \psi_\alpha^{(k)}(0) \sum_{\substack{\mathcal{I} \subset \{1, \ldots, p\} \\ \#\mathcal{I} = k}} \frac{\partial^{p-k}}{\partial t_{\mathcal{I}^c}} \phi_\alpha(0, \ldots, 0) \left(\sum_{\substack{\mathcal{X} \subset \mathcal{Y} \\ \mathcal{X} \neq \emptyset}} \left(\prod_{i \in \mathcal{I}} \mathbb{1}(y_i \in \mathcal{X}) \right) \left(\prod_{i \in \mathcal{I}^c} \beta^{\mathbb{1}(y_i \in \mathcal{X})} \right) p_\mathcal{X} \right).$$

D.1.3.3   Recurrence Relation for the Limit of the Moments

The next step of the proof consists in dividing by α and let α tends to 0 in Equation (D.2) above. First, recalling that $\beta = 1 - \alpha$, and using that $\sum p_\mathcal{X} = 1$, one has

$$1 - \sum_{\substack{\mathcal{X} \subset \mathcal{Y} \\ \mathcal{X} \neq \emptyset}} \left(\prod_{j=1}^p \beta^{\mathbb{1}(y_j \in \mathcal{X})} \right) p_\mathcal{X} = \sum_{\substack{\mathcal{X} \subset \mathcal{Y} \\ \mathcal{X} \neq \emptyset}} p_\mathcal{X} - \sum_{\substack{\mathcal{X} \subset \mathcal{Y} \\ \mathcal{X} \neq \emptyset}} \beta^{\#\mathcal{X}} p_\mathcal{X} = \sum_{\substack{\mathcal{X} \subset \mathcal{Y} \\ \mathcal{X} \neq \emptyset}} \left(1 - (1 - \alpha)^{\#\mathcal{X}} \right) p_\mathcal{X}.$$

Hence

$$\lim_{\alpha \to 0} \frac{1}{\alpha} \sum_{\substack{\mathcal{X} \subset \mathcal{Y} \\ \mathcal{X} \neq \emptyset}} \left(1 - (1 - \alpha)^{\#\mathcal{X}} \right) p_\mathcal{X} = \sum_{\substack{\mathcal{X} \subset \mathcal{Y} \\ \mathcal{X} \neq \emptyset}} (\#\mathcal{X}) p_\mathcal{X}.$$

Now by definition of $p_\mathcal{X}$,

$$\sum_{\substack{\mathcal{X} \subset \mathcal{Y} \\ \mathcal{X} \neq \emptyset}} (\#\mathcal{X}) p_\mathcal{X} = \mathbb{E}\left(\# \left((x_0 + X_0) \cap \mathcal{Y} \right) \right) = \mathbb{E}\left(\sum_{j=1}^p \mathbb{1}(y_j \in x_0 + X_0) \right) = p \frac{E\left(\mathcal{L}^d(X) \right)}{E\left(\mathcal{L}^d\left(\mathcal{Y} \oplus \check{X} \right) \right)} \neq 0.$$

Let us now turn to the limit of the right-hand side of Equation (D.2) when dividing by α and letting α tends to 0. First let us show that all the terms for which $k \geq 3$ will tend to 0. By induction for all $k \geq 2$, the terms $\frac{\partial^{p-k}}{\partial t_{\mathcal{I}^c}} \phi_\alpha(0, \ldots, 0)$ have a finite limit when α tends to 0. Besides, for all $k \geq 3$,

$$\left| \psi_\alpha^{(k)}(0) \right| = \left| i^k E\left((T_\alpha(a) - E(T_\alpha(a)))^k \right) \right| \leq E\left(|T_\alpha(a) - E(T_\alpha(a))|^k \right) \leq 2^k \alpha^{-sk}.$$

Hence, since

$$\sigma_\alpha^T = \sqrt{\frac{\alpha}{2 - \alpha} \mathrm{Var}(T_\alpha(a))} \underset{\alpha \to 0}{\sim} \sqrt{\frac{\mathrm{Var}(a)}{2}} \alpha^{\frac{1}{2}},$$

for all $k \geq 3$,

$$\frac{1}{\alpha} \left(\frac{\alpha}{\sigma_\alpha^T} \right)^k \psi_\alpha^{(k)}(0) \sum_{\substack{\mathcal{I} \subset \{1, \ldots, p\} \\ \#\mathcal{I} = k}} \frac{\partial^{p-k}}{\partial t_{\mathcal{I}^c}} \phi_\alpha(0, \ldots, 0) \left(\sum_{\substack{\mathcal{X} \subset \mathcal{Y} \\ \mathcal{X} \neq \emptyset}} \left(\prod_{i \in \mathcal{I}} \mathbb{1}(y_i \in \mathcal{X}) \right) \left(\prod_{i \in \mathcal{I}^c} \beta^{\mathbb{1}(y_i \in \mathcal{X})} \right) p_\mathcal{X} \right)$$

$$= \underset{\alpha \to 0}{\mathcal{O}} \left(\alpha^{\frac{1}{2}k - sk - 1} \right).$$

But since $s < 1/6$, the above exponent $\frac{1}{2}k - sk - 1$ is positive for all $k \geq 3$. Hence all the terms for which $k \geq 3$ tends to 0.

Now for $k = 2$, we have $\psi_\alpha^{(2)}(0) = i^2 \operatorname{Var}(T_\alpha(a))$. Besides, by induction, noting $\mathcal{I} = \{j_1, j_2\}$ a subset $\mathcal{I} \subset \{1, \ldots, p\}$ of cardinal number 2,

$$\lim_{\alpha \to 0} \frac{\partial^{p-2}}{\partial t_{\{j_1, j_2\}^c}} \phi_\alpha(0, \ldots, 0) = (i)^{p-2} \mathbb{E}\left(\prod_{l \in \{1, \ldots, p\} \setminus \{j_1, j_2\}} f_G(y_l) \right).$$

Hence

$$\lim_{\alpha \to 0} \frac{1}{\alpha} \left(\frac{\alpha}{\sigma_\alpha^T} \right)^2 \psi_\alpha^{(2)}(0) \sum_{\substack{\mathcal{I} \subset \{1, \ldots, p\} \\ \#\mathcal{I} = 2}} \frac{\partial^{p-2}}{\partial t_{\mathcal{I}^c}} \phi_\alpha(0, \ldots, 0) \left(\sum_{\substack{\mathcal{X} \subset \mathcal{Y} \\ \mathcal{X} \neq \emptyset}} \left(\prod_{i \in \mathcal{I}} \mathbb{1}(y_i \in \mathcal{X}) \right) \left(\prod_{i \in \mathcal{I}^c} \beta^{\mathbb{1}(y_i \in \mathcal{X})} \right) p_\mathcal{X} \right)$$

$$= (i)^p 2 \sum_{\{j_1, j_2\} \subset \{1, \ldots, p\}} \mathbb{E}\left(\prod_{l \in \{1, \ldots, p\} \setminus \{j_1, j_2\}} f_G(y_l) \right) \left(\sum_{\substack{\mathcal{X} \subset \mathcal{Y} \\ \mathcal{X} \neq \emptyset}} \mathbb{1}(y_{j_1} \in \mathcal{X}) \mathbb{1}(y_{j_2} \in \mathcal{X}) p_\mathcal{X} \right).$$

In addition remark that

$$\sum_{\substack{\mathcal{X} \subset \mathcal{Y} \\ \mathcal{X} \neq \emptyset}} \mathbb{1}(y_{j_1} \in \mathcal{X}) \mathbb{1}(y_{j_2} \in \mathcal{X}) p_\mathcal{X} = \mathbb{P}\left(\{y_{j_1}, y_{j_2}\} \subset x_0 + X_0 \right) = \frac{\gamma_X(y_{j_1} - y_{j_2})}{E\left(\mathcal{L}^d \left(\mathcal{Y} \oplus \check{X} \right) \right)}.$$

Coming back to Equation (D.2), one sees that $\frac{\partial^p \phi_\alpha}{\partial t_1 \ldots \partial t_p}(0, \ldots, 0)$ admits a finite limit when α tends to 0. Noting $(i)^p L$ this finite limit so that

$$L = \lim_{\alpha \to 0} \mathbb{E}\left(\prod_{j=1}^p g_\alpha^T(y_j) \right),$$

we have

$$L = \frac{E\left(\mathcal{L}^d \left(\mathcal{Y} \oplus \check{X} \right) \right)}{pE\left(\mathcal{L}^d(X) \right)} 2 \sum_{\{j_1, j_2\} \subset \{1, \ldots, p\}} \mathbb{E}\left(\prod_{l \in \{1, \ldots, p\} \setminus \{j_1, j_2\}} f_G(y_l) \right) \frac{\gamma_X(y_{j_1} - y_{j_2})}{E\left(\mathcal{L}^d \left(\mathcal{Y} \oplus \check{X} \right) \right)}$$

$$= \frac{2}{p} \sum_{\{j_1, j_2\} \subset \{1, \ldots, p\}} \frac{\gamma_X(y_{j_1} - y_{j_2})}{E\left(\mathcal{L}^d(X) \right)} \mathbb{E}\left(\prod_{l \in \{1, \ldots, p\} \setminus \{j_1, j_2\}} f_G(y_l) \right).$$

This is exactly the recursive formula for the moments of a Gaussian vector given by Proposition D.2. Hence,

$$L = \lim_{\alpha \to 0} \mathbb{E}\left(\prod_{j=1}^p g_\alpha^T(y_j) \right) = \mathbb{E}\left(\prod_{j=1}^p f_G(y_j) \right),$$

which concludes the proof by induction of Lemma D.1.

D.1.4   Convergence in L^2 of the Difference of the Normalized Processes

At this stage to conclude the proof of Theorem 6.1 we have to demonstrate the following lemma.

Lemma D.2 (Convergence to 0 in L^2 of $g_\alpha - g_\alpha^T$). *Let g_α and g_α^T be respectively the normalized TDL process and the normalized TDL process with truncated colors. Then for all $y \in \mathbb{R}^d$,*

$$g_\alpha(y) - g_\alpha^T(y) \xrightarrow[\alpha \to 0]{\mathrm{L}^2} 0.$$

Proof. Since $a \in L^2(\Omega)$ and for all $b \in \mathbb{R}$, $|T_\alpha(b)| \leq b$ and $\lim_\alpha T_\alpha(b) = b$, by dominated convergence

$$\lim_{\alpha \to 0} \mathrm{Var}(a - T_\alpha(a)) = 0,$$

and in particular

$$\lim_{\alpha \to 0} \mathrm{Var}(T_\alpha(a)) = \mathrm{Var}(a).$$

Let $y \in \mathbb{R}^d$. Recall that

$$\mathrm{Var}(f_\alpha) = \frac{\alpha}{2 - \alpha} \mathrm{Var}(a) \quad \text{and} \quad \mathrm{Var}(f_\alpha^T) = \frac{\alpha}{2 - \alpha} \mathrm{Var}(T_\alpha(a)).$$

Let us write

$$
\begin{aligned}
g_\alpha(y) - g_\alpha^T(y) &= \frac{f_\alpha(y) - \mathbb{E}(a)}{\sqrt{\mathrm{Var}(f_\alpha)}} - \frac{f_\alpha^T(y) - \mathbb{E}(T_\alpha(a))}{\sqrt{\mathrm{Var}(f_\alpha^T)}} \\
&= \frac{f_\alpha(y) - \mathbb{E}(a)}{\sqrt{\mathrm{Var}(f_\alpha)}} - \frac{f_\alpha^T(y) - \mathbb{E}(T_\alpha(a))}{\sqrt{\mathrm{Var}(f_\alpha)}} + \frac{f_\alpha^T(y) - \mathbb{E}(T_\alpha(a))}{\sqrt{\mathrm{Var}(f_\alpha)}} - \frac{f_\alpha^T(y) - \mathbb{E}(T_\alpha(a))}{\sqrt{\mathrm{Var}(f_\alpha^T)}} \\
&= \underbrace{\frac{f_\alpha(y) - f_\alpha^T(y) - \mathbb{E}(a - T_\alpha(a))}{\sqrt{\mathrm{Var}(f_\alpha)}}}_{I_1(\alpha)} + \underbrace{\left(\frac{\sqrt{\mathrm{Var}(f_\alpha^T)}}{\sqrt{\mathrm{Var}(f_\alpha)}} - 1 \right) g_\alpha^T(y)}_{I_2(\alpha)}.
\end{aligned}
$$

Let us note $I_1(\alpha)$ and $I_2(\alpha)$ the two terms above. Remark that the numerator of $I_1(\alpha)$ is a TDL process with color distribution $a - T_\alpha(a) - \mathbb{E}(a - T_\alpha(a))$. Hence we have

$$\mathbb{E}(I_1(\alpha)^2) = \frac{\frac{\alpha}{2-\alpha} \mathrm{Var}(a - T_\alpha(a))}{\frac{\alpha}{2-\alpha} \mathrm{Var}(a)} = \frac{\mathrm{Var}(a - T_\alpha(a))}{\mathrm{Var}(a)} \xrightarrow[\alpha \to 0]{} 0.$$

In addition,

$$\mathbb{E}(I_2(\alpha)^2) = \left(\frac{\sqrt{\mathrm{Var}(f_\alpha^T)}}{\sqrt{\mathrm{Var}(f_\alpha)}} - 1 \right)^2 = \left(\frac{\sqrt{\mathrm{Var}(T_\alpha(a))}}{\sqrt{\mathrm{Var}(a)}} - 1 \right)^2 \xrightarrow[\alpha \to 0]{} 0.$$

Hence, $g_\alpha(y) - g_\alpha^T(y)$ is the sum of two r.v. which tends to 0 in $L^2(\Omega)$, which concludes the proof. $\square$

D.2 Computation of the Covariance of the TDL Process by Slivnyak-Mecke Formulas

In this section an alternative proof for the computation of the TDL covariance is proposed. It makes use of Palm calculus tools, more precisely the Slivnyak-Mecke formula [136, p. 67-68]. One would remark that the usage of this general technique yields to more painful computations than the method exposed in Section 6.4 and which consists in conditioning with respect to the coverage of the last hitting leaf.

The plan of this section is as follows. First, we recall the Slivnyak-Mecke formulas. Second, we first apply this formula to compute the expectation, which is an easier task to begin with. Finally, the covariance is computed using the Slivnyak-Mecke formula.

D.2.1 Slivnyak-Mecke Formulas

We reproduce here the Slivnyak-Mecke theorem of order one and two (see [136, p. 67-68] for a formulation for all order $n \geq 1$).

In this section we consider general point processes having values in a state space S being a locally compact and separable topological space with a countable basis. As in appendix B, the set of point processes over S is denoted by $\mathbf{N}$. Besides, if Ψ is a point process we note

$$\Psi^2_{\neq} = \{(x,y) \in \Psi \times \Psi : \ x \neq y\}.$$

Theorem D.2 (Slivnyak-Mecke formula). *Let Ψ be a Poisson process on S with intensity measure Θ.*

- *(Oder one) For all measurable function $g : S \times \mathbf{N} \to \mathbb{R}$ we have*

$$\mathbb{E}\left(\sum_{x \in \Psi} g(x, \Psi)\right) = \int_S \mathbb{E}\left(g\left(x, \Psi + \delta_x\right)\right) \Theta(dx)$$

  as soon as the integral on the right hand side is well-defined.

- *(Order two) For all measurable function $g : S \times S \times \mathbf{N} \to \mathbb{R}$ we have*

$$\mathbb{E}\left(\sum_{(x,y) \in \Psi^2_{\neq}} g(x, y, \Psi)\right) = \int_S \int_S \mathbb{E}\left(g\left(x, y, \Psi + \delta_x + \delta_y\right)\right) \Theta(dx)\Theta(dy)$$

  as soon as the integral on the right hand side is well-defined.

Let us mention that the Slivnyak-Mecke formula of order one is also refereed to as Mecke theorem [136, p. 67].

D.2.2 The Intensity Measure of Peculiar Sets

Following the notation of Chapter 6, μ denotes the intensity measure of the Poisson process of leaves, that is $\mu = \lambda \otimes \mathcal{L}^d \otimes P_X \otimes P_a$ over the state space $S = (-\infty, 0) \times \mathbb{R}^d \times \mathcal{F} \times \mathbb{R}$. In the following we would need to compute the measure $\mu(A)$ of certain subsets $A \subset S$.

Lemma D.3 (Leaves intersecting a point y after time t). *For any point $y \in \mathbb{R}^d$ and any time $t \in (-\infty, 0)$, let $A_y(t)$ denote the set*

$$A_y(t) = (t, 0) \times \left\{ y + \check{X} \times \{X\} \,|\, X \in \mathcal{F} \right\} \times \mathbb{R} \subset S.$$

We have

$$\mu\left(A_y(t)\right) = -tE\left(\mathcal{L}^d(X)\right).$$

Proof. We have

$$
\begin{aligned}
\mu\left(A_y(t)\right) &= \int_t^0 du \left(\int_{\mathcal{F}} \int_{\mathbb{R}^d} \mathbb{1}\left\{ y \in y + \check{Y} \right\} \mathcal{L}^d(dy) P_X(dY) \right) \int_{\mathbb{R}} P_a(db) \\
&= -tE\left(\mathcal{L}^d(y + \check{X})\right) \\
&= -tE\left(\mathcal{L}^d(X)\right).
\end{aligned}
$$

$\square$

Recall that $\gamma_X(\tau) := E\left(\mathcal{L}^d(X \cap \tau + X)\right)$ denotes the mean geometric covariogram of the RACS X.

Lemma D.4 (Two different points during two different periods). *Let $y_1, y_2 \in \mathbb{R}^d$ and $t_1, t_2 \in (-\infty, 0)$ and consider both sets $A_{y_1}(t_1)$ and $A_{y_2}(t_2)$. Then we have*

$$\mu(A_{y_1}(t_1) \cap A_{y_2}(t_2)) = \min(-t_1, -t_2)\gamma_X(y_2 - y_1).$$

Proof. We have

$$A_{y_1}(t_1) \cap A_{y_2}(t_2) = (\max(t_1, t_2), 0) \times \left\{ \left(y_1 + \check{X} \cap y_2 + \check{X} \right) \times \{X\} \,|\, X \in \mathcal{F} \right\} \times \mathbb{R}$$

thus

$$\mu(A_{y_1}(t_1) \cap A_{y_2}(t_2)) = \min(-t_1, -t_2)E\left(\mathcal{L}^d\left(y_1 + \check{X} \cap y_2 + \check{X}\right)\right).$$

By the invariance properties of the Lebesgue measure, we have

$$\mathcal{L}^d\left(y_1 + \check{X} \cap y_2 + \check{X}\right) = \mathcal{L}^d\left(X \cap y_2 - y_1 + X\right)$$

which shows that

$$E\left(\mathcal{L}^d\left(y_1 + \check{X} \cap y_2 + \check{X}\right)\right) = \gamma_X(y_2 - y_1).$$

$\square$

D.2.3 Computing the TDL Expectation Using Mecke Theorem

It has already been shown two times in Chapter 6 that $\mathbb{E}(f) = E(a)$ (See Proposition 6.2 and Section 6.4). Here we give another proof of this result in using Mecke theorem [136, p. 67]. The only interest of this third proof is to introduce the tools and notation that are necessary to compute the covariance of the TDL process by the Slivnyak-Mecke formula (see Section D.2.4).

Recall that the TDL process f is defined for all $y \in \mathbb{R}^d$ by

$$f(y) = \sum_{(t_i,x_i,X_i,a_i)\in\Phi} \mathbb{1}\left(y \in x_i + X_i\right) \alpha a_i \beta^{\sum_{(t_j,x_j,X_j,a_j)\in\Phi} \mathbb{1}(t_j\in(t_i,0) \text{ and } y\in x_j+X_j)},$$

where $\beta = 1 - \alpha$. Here the state space is $S = (-\infty, 0) \times \mathbb{R}^d \times \mathcal{F} \times \mathbb{R}$. For any $y \in \mathbb{R}^d$ define the function $g_y : S \times \mathbf{N}(S) \to \mathbb{R}$ by

$$g_y((t,x,X,a),\psi) = \mathbb{1}\left(x \in y + \check{X}\right) \alpha a \beta^{N_\psi(A_y(t))}$$

where, as in Lemma D.3, $A_y(t) \subset S$ equals

$$A_y(t) = (t,0) \times \left\{ y + \check{X} \times \{X\} \,|\, X \in \mathcal{F} \right\} \times \mathbb{R}.$$

With these notations we have

$$f(y) = \sum_{(t,x,X,a)\in\Phi} g_y((t,x,X,a),\Phi).$$

The Slivnyak-Mecke formula of order one (see Theorem D.2 or [136, p. 67]) ensures that[1]

$$\mathbb{E}(f(y)) = \int_S \mathbb{E}\left(g_y\left((t,x,X,a), \Phi + \delta_{(t,x,X,a)}\right)\right) \mu(d(t,x,X,a)).$$

Remark that for any $(t,x,X,a) \in S$, $(t,x,X,a) \notin A_y(t)$, hence for any $\psi \in \mathbf{N}(S)$

$$g_y\left((t,x,X,a), \psi + \delta_{(t,x,X,a)}\right) = g_y((t,x,X,a),\psi).$$

For any $(t,x,X,a) \in S$, we have

$$\mathbb{E}\left(g_y((t,x,X,a),\Phi)\right) = \mathbb{1}\left(x \in y + \check{X}\right) \alpha a \mathbb{E}\left(\beta^{N_\Phi(A_y(t))}\right).$$

By Lemma D.3 we have $\mu(A_y(t)) = -tE\left(\mathcal{L}^d(X)\right)$ and by Lemma B.1 we get

$$\mathbb{E}\left(\beta^{N_\Phi(A_y(t))}\right) = e^{(\beta-1)\mu(A_y(t))} = e^{t\alpha E\left(\mathcal{L}^d(X)\right)},$$

---

[1]To be totally rigorous one should first show that the considered function $((t,x,X,a),\Phi) \mapsto g_y\left((t,x,X,a), \psi + \delta_{(t,x,X,a)}\right)$ is integrable with respect $\mu \otimes P_\Phi$. This is easily shown in replacing g_y by its absolute value $|g_y|$ and following exactly the same steps as for the actual computation of the integral. This remark is also valid for the next section.

since $\alpha = 1 - \beta$. Hence integrating with respect to μ we get

$$
\begin{aligned}
\mathbb{E}(f(y)) &= \int_S \mathbb{1}\left(x \in y + \check{X}\right) \alpha a e^{t\alpha E\left(\mathcal{L}^d(X)\right)} \mu(d(t,x,X,a)) \\
&= \alpha E(a) E\left(\mathcal{L}^d\left(y + \check{X}\right)\right) \int_{-\infty}^0 e^{t\alpha E\left(\mathcal{L}^d(X)\right)} dt \\
&= \alpha E(a) E\left(\mathcal{L}^d(X)\right) \frac{1}{\alpha E\left(\mathcal{L}^d(X)\right)} \\
&= E(a).
\end{aligned}
$$

D.2.4   Computing the TDL Covariance by Slivnyak-Mecke Formulas

With Proposition 6.4 it has been established that

$$
\mathrm{Cov}(f)(\tau) = \frac{\alpha \gamma_X(\tau)}{2E(\mathcal{L}^d(X)) - \alpha \gamma_X(\tau)} \, \mathrm{Var}(a), \ \tau \in \mathbb{R}^d.
$$

Below we propose a new proof of this result based on Slivnyak-Mecke formulas of order one and two (see Theorem D.2 or [136, p. 68]).

Recall that for all $y \in \mathbb{R}^d$,

$$
f(y) = \sum_{(t,x,X,a) \in \Phi} g_y((t,x,X,a), \Phi),
$$

where $g_y : ((t,x,X,a), \psi) \mapsto \mathbb{1}\left(x \in y + \check{X}\right) \alpha a \beta^{N_\psi(A_y(t))}$, $A_y(t) \subset S$ being the set

$$
(t,0) \times \left\{ y + \check{X} \times \{X\} \,|\, X \in \mathcal{F} \right\} \times \mathbb{R}.
$$

From now on fix any couple $(y,z) \in \left(\mathbb{R}^d\right)^2$. We have

$$
\begin{aligned}
f(y)f(z) &= \left(\sum_{(t,x,X,a) \in \Phi} g_y((t,x,X,a), \Phi) \right) \left(\sum_{(t,x,X,a) \in \Phi} g_z((t,x,X,a), \Phi) \right) \\
&= \sum_{((t_1,x_1,X_1,a_1),(t_2,x_2,X_2,a_2)) \in \Phi^2} g_y((t_1,x_1,X_1,a_1), \Phi) g_z((t_2,x_2,X_2,a_2), \Phi) \\
&= \sum_{(t,x,X,a) \in \Phi} g_y((t,x,X,a), \Phi) g_z((t,x,X,a), \Phi) \\
&\quad + \sum_{((t_1,x_1,X_1,a_1),(t_2,x_2,X_2,a_2)) \in \Phi^2_{\neq}} g_y((t_1,x_1,X_1,a_1), \Phi) g_z((t_2,x_2,X_2,a_2), \Phi).
\end{aligned}
$$

The expectation of both sums in the last equality can be computed in using the Slivnyak-Mecke formulas of order 1 and 2.

First let us compute

$$I := \mathbb{E}\left(\sum_{(t,x,X,a)\in\Phi} g_y((t,x,X,a),\Phi)g_z((t,x,X,a),\Phi)\right).$$

Mecke theorem ensures that

$$I = \int_S \mathbb{E}\left(g_y\left((t,x,X,a),\Phi+\delta_{(t,x,X,a)}\right)g_z\left((t,x,X,a),\Phi+\delta_{(t,x,X,a)}\right)\right)\mu(d(t,x,X,a)).$$

As $(t,x,X,a) \notin A_y(t)$ and $(t,x,X,a) \notin A_z(t)$ for all $(t,x,X,a) \in S$ we have

$$g_y\left((t,x,X,a),\Phi+\delta_{(t,x,X,a)}\right) = g_y\left((t,x,X,a),\Phi\right)$$

and

$$g_z\left((t,x,X,a),\Phi+\delta_{(t,x,X,a)}\right) = g_z\left((t,x,X,a),\Phi\right).$$

Hence we need to compute $\mathbb{E}\left(g_y\left((t,x,X,a),\Phi\right)g_z\left((t,x,X,a),\Phi\right)\right)$. For all $t \in (-\infty,0)$ Lemmas D.3 and D.4 show that

$$\mu(A_y(t)) = \mu(A_z(t)) = -tE(\mathcal{L}^d(X)) = -t\gamma_X(0)$$

and

$$\mu(A_y(t)\cap A_z(t)) = -t\gamma_X(z-y).$$

Applying Lemma B.2 we get

$$\begin{aligned}
&\mathbb{E}\left(g_y\left((t,x,X,a),\Phi\right)g_z\left((t,x,X,a),\Phi\right)\right)\\
&= \mathbb{1}\left(x\in y+\check{X}\right)\mathbb{1}\left(x\in z+\check{X}\right)\alpha^2 a^2\mathbb{E}\left(\beta^{N_\Phi(A_y(t))+N_\Phi(A_y(t))}\right)\\
&= \alpha^2 a^2\mathbb{1}\left(x\in y+\check{X}\cap z+\check{X}\right)e^{(\beta-1)(\mu(A_y(t))+\mu(A_z(t)))+(\beta-1)^2(\mu(A_y(t)\cap A_z(t)))}\\
&= \alpha^2 a^2\mathbb{1}\left(x\in y+\check{X}\cap z+\check{X}\right)e^{t\alpha\left(2E(\mathcal{L}^d(X))-\alpha\gamma_X(z-y)\right)}.
\end{aligned}$$

Finally

$$\begin{aligned}
I &= \int_S \alpha^2 a^2\mathbb{1}\left(x\in y+\check{X}\cap z+\check{X}\right)e^{t\alpha\left(2E(\mathcal{L}^d(X))-\alpha\gamma_X(z-y)\right)}\mu(d(t,x,X,a))\\
&= \alpha^2 E(a^2)E\left(\mathcal{L}^d\left(y+\check{X}\cap z+\check{X}\right)\right)\int_{-\infty}^0 e^{t\alpha\left(2E(\mathcal{L}^d(X))-\alpha\gamma_X(z-y)\right)}dt\\
&= \alpha^2 E(a^2)\gamma_X(z-y)\frac{1}{\alpha\left(2E(\mathcal{L}^d(X))-\alpha\gamma_X(z-y)\right)}\\
&= \frac{\alpha\gamma_X(z-y)}{2E(\mathcal{L}^d(X))-\alpha\gamma_X(z-y)}E(a^2).
\end{aligned}$$

Let us now compute the second expectation

$$J := \mathbb{E}\left(\sum_{((t_1,x_1,X_1,a_1),(t_2,x_2,X_2,a_2))\in\Phi_{\neq}^2} g_y((t_1,x_1,X_1,a_1),\Phi)g_z((t_2,x_2,X_2,a_2),\Phi)\right).$$

To simplify the notations let us note $s_1 = (t_1, x_1, X_1, a_1)$ and $s_2 = (t_2, x_2, X_2, a_2)$. Applying the Slivnyak-Mecke formula of order two we have

$$J = \int_{S \times S} \mathbb{E} \left(g_y \left(s_1, \Phi + \delta_{s_1} + \delta_{s_2} \right) g_z \left(s_2, \Phi + \delta_{s_1} + \delta_{s_2} \right) \right) \mu(ds_1) \mu(ds_2).$$

As above, since $s_1 = (t_1, x_1, X_1, a_1) \notin A_y(t_1)$,

$$g_y \left(s_1, \Phi + \delta_{s_1} + \delta_{s_2} \right) = g_y \left(s_1, \Phi + \delta_{s_2} \right).$$

Besides,

$$N_{\Phi + \delta_{s_2}} (A_y(t_1)) = \begin{cases} N_\Phi(A_y(t_1)) + 1 & \text{if } s_2 = (t_2, x_2, X_2, a_2) \in A_y(t_1), \\ N_\Phi(A_y(t_1)) & \text{otherwise,} \end{cases}$$

hence

$$g_y \left(s_1, \Phi + \delta_{s_2} \right) = \beta^{\mathbb{1}\left((t_2, x_2, X_2, a_2) \in A_y(t_1) \right)} g_y \left(s_1, \Phi \right)$$
$$= \beta^{\mathbb{1}\left(t_2 \in (t_1, 0) \text{ and } x_2 \in y + \check{X}_2 \right)} g_y \left(s_1, \Phi \right).$$

By symmetry, we also have

$$g_z \left(s_2, \Phi + \delta_{s_1} + \delta_{s_2} \right) = \beta^{\mathbb{1}\left(t_1 \in (t_2, 0) \text{ and } x_1 \in z + \check{X}_1 \right)} g_z \left(s_2, \Phi \right).$$

Thus,

$$\mathbb{E} \left(g_y \left(s_1, \Phi + \delta_{s_1} + \delta_{s_2} \right) g_z \left(s_2, \Phi + \delta_{s_1} + \delta_{s_2} \right) \right)$$
$$= \beta^{\mathbb{1}\left(t_2 \in (t_1, 0) \text{ and } x_2 \in y + \check{X}_2 \right)} \beta^{\mathbb{1}\left(t_1 \in (t_2, 0) \text{ and } x_1 \in z + \check{X}_1 \right)} \mathbb{E} \left(g_y \left(s_1, \Phi \right) g_z \left(s_2, \Phi \right) \right)$$
$$= \alpha^2 a_1 a_2 \beta^{\mathbb{1}\left(t_2 \in (t_1, 0) \text{ and } x_2 \in y + \check{X}_2 \right)} \beta^{\mathbb{1}\left(t_1 \in (t_2, 0) \text{ and } x_1 \in z + \check{X}_1 \right)}$$
$$\times \mathbb{1} \left(x_1 \in y + \check{X}_1 \right) \mathbb{1} \left(x_2 \in z + \check{X}_2 \right) \mathbb{E} \left(\beta^{N_\Phi(A_y(t_1)) + N_\Phi(A_y(t_2))} \right).$$

Recalling that from Lemma D.4 we have $\mu(A_y(t_1) \cap A_z(t_2))) = \min(-t_1, -t_2) \gamma_X(z - y)$ and applying Lemma B.2 we obtain

$$\mathbb{E} \left(\beta^{N_\Phi(A_y(t_1)) + N_\Phi(A_y(t_2))} \right) = e^{(\beta-1)(\mu(A_y(t_1)) + \mu(A_z(t_2))) + (\beta-1)^2 (\mu(A_y(t_1) \cap A_z(t_2)))}$$
$$= e^{t_1 \alpha E(\mathcal{L}^d(X))} e^{t_2 \alpha E(\mathcal{L}^d(X))} e^{\min(-t_1, -t_2) \alpha^2 \gamma_X(z - y)}.$$

At this step we obtain the following expression for J

$$J = \alpha^2 \int_{S \times S} a_1 a_2 \beta^{\mathbb{1}\left(t_2 \in (t_1, 0) \text{ and } x_2 \in y + \check{X}_2 \right)} \beta^{\mathbb{1}\left(t_1 \in (t_2, 0) \text{ and } x_1 \in z + \check{X}_1 \right)} \mathbb{1} \left(x_1 \in y + \check{X}_1 \right)$$
$$\times \mathbb{1} \left(x_2 \in z + \check{X}_2 \right) e^{t_1 \alpha E(\mathcal{L}^d(X))} e^{t_2 \alpha E(\mathcal{L}^d(X))} e^{\min(-t_1, -t_2) \alpha^2 \gamma_X(z - y)} d\mu d\mu.$$

Next we divide $S \times S$ in two disjoint domains D_1 and D_2 where over D_1 we have $t_1 \leq t_2$ and over D_2 we have $t_1 > t_2$. This partition of $S \times S$ yields a decomposition of $J = J_1 + J_2$. By symmetry one easily shows that $J_1 = J_2$ so that $J = 2J_1$.

Besides, J_1 is easy to compute. Indeed, we have, after integrating with respect to a_1 and a_2

$$J_1 = \alpha^2 E(a)^2 \int_{t_2=-\infty}^{0} \int_{t_1=-\infty}^{t_2} \int_{X_1, X_2, x_1, x_2} \beta^{\mathbb{1}\left(x_2 \in y + \check{X}_2\right)} \mathbb{1}\left(x_1 \in y + \check{X}_1\right) \mathbb{1}\left(x_2 \in z + \check{X}_2\right)$$
$$\times \, e^{t_1 \alpha E(\mathcal{L}^d(X))} e^{t_2 \alpha E(\mathcal{L}^d(X))} e^{-t_2 \alpha^2 \gamma_X(z-y)} \mathcal{L}^d(dx_1) \mathcal{L}^d(dx_2) P_X(dX_1) P_X(dX_2) dt_1 dt_2.$$

Integrating with respect to t_1, x_1 and X_1 we get

$$J_1 = \alpha^2 E(a)^2 \frac{1}{\alpha E(\mathcal{L}^d(X))} E(\mathcal{L}^d(X)) \int_{t_2=-\infty}^{0} \int_{X_2, x_2} \beta^{\mathbb{1}\left(x_2 \in y + \check{X}_2\right)} \mathbb{1}\left(x_2 \in z + \check{X}_2\right)$$
$$\times \, e^{t_2 \left(2\alpha E(\mathcal{L}^d(X)) - \alpha^2 \gamma_X(z-y)\right)} \mathcal{L}^d(dx_2) P_X(dX_2) dt_2.$$

Then simplifying and integrating with respect to t_2 gives

$$J_1 = \alpha E(a)^2 \frac{1}{\alpha \left(2E(\mathcal{L}^d(X)) - \alpha \gamma_X(z-y)\right)}$$
$$\times \int_{X_2, x_2} \beta^{\mathbb{1}\left(x_2 \in y + \check{X}_2\right)} \mathbb{1}\left(x_2 \in z + \check{X}_2\right) \mathcal{L}^d(dx_2) P_X(dX_2).$$

This last integral is easy to compute as the integrand takes only the three values 0, β and 1.

$$\int_{X_2, x_2} \beta^{\mathbb{1}\left(x_2 \in y + \check{X}_2\right)} \mathbb{1}\left(x_2 \in z + \check{X}_2\right) \mathcal{L}^d(dx_2) P_X(dX_2)$$
$$= \int_{X_2} \beta \mathcal{L}^d\left((z + \check{X}_2) \cap (y + \check{X}_2)\right) + \mathcal{L}^d\left((z + \check{X}_2) \setminus (y + \check{X}_2)\right) P_X(dX_2)$$
$$= E(\mathcal{L}^d(X)) - \alpha \gamma_X(z-y),$$

where we used $\mathcal{L}^d\left((z + \check{X}_2) \setminus (y + \check{X}_2)\right) = \mathcal{L}^d\left((z + \check{X}_2)\right) - \mathcal{L}^d\left((z + \check{X}_2) \cap (y + \check{X}_2)\right)$. Finally,

$$J = 2 \frac{E(\mathcal{L}^d(X)) - \alpha \gamma_X(z-y)}{2E(\mathcal{L}^d(X)) - \alpha \gamma_X(z-y)} E(a)^2.$$

To conclude this proof write

$$\text{Cov}(f(y), f(z)) = \mathbb{E}(f(x)f(y)) - E(a)^2$$
$$= I + J - E(a)^2$$
$$= \frac{\alpha \gamma_X(z-y)}{2E(\mathcal{L}^d(X)) - \alpha \gamma_X(z-y)} \left(E\left(a^2\right) - E(a)^2\right)$$
$$= \frac{\alpha \gamma_X(z-y)}{2E(\mathcal{L}^d(X)) - \alpha \gamma_X(z-y)} \text{Var}(a).$$

Bibliography

[1] R. A. Adams and J. F. Fournier. *Sobolev Spaces*, volume 140 of *Pure and applied mathematics*. Elsevier Science, second edition, 2003. 159

[2] R. J. Adler and J. E. Taylor. *Random Fields and Geometry*. Springer Monographs in Mathematics. Springer, 2007. 176

[3] N. Ahuja and A. Rosenfeld. Mosaic models for textures. *IEEE Trans. Pattern Anal. Mach. Intell.*, 3(1):1 –11, 1981. `doi:10.1109/TPAMI.1981.4767045`. 5, 104

[4] L. Ambrosio, V. Capasso, and E. Villa. On the approximation of mean densities of random closed sets. *Bernoulli*, 15:1222–1242, 2009. `doi:10.3150/09-BEJ186`. 168

[5] L. Ambrosio, A. Colesanti, and E. Villa. Outer Minkowski content for some classes of closed sets. *Math. Ann.*, 342(4):727–748, 2008. `doi:10.1007/s00208-008-0254-z`. 157, 168

[6] L. Ambrosio, N. Fusco, and D. Pallara. *Functions of bounded variation and free discontinuity problems*. Oxford mathematical monographs. Oxford university press, 2000. 5, 127, 130, 131, 133, 134, 135, 146, 152, 156, 169, 176, 211, 212, 213

[7] F. Andreu-Vaillo, V. Caselles, and J. M. Mazon. *Parabolic Quasilinear Equations Minimizing Linear Growth Functionals*, volume 223 of *Progress in mathematics*. Birkhäusser, 2004. 5, 127

[8] J.-F. Aujol, G. Aubert, L. Blanc-Féraud, and A. Chambolle. Image decomposition into a bounded variation component and an oscillating component. *J. Math. Imag. Vis.*, 22:71 – 88, 2005. 10.1007/s10851-005-4783-8. 6, 127

[9] J.-F. Aujol and A. Chambolle. Dual norms and image decomposition models. *Int. J. Comput. Vis.*, 63:85–104, 2005. 10.1007/s11263-005-4948-3. 6, 127

[10] G. Averkov and G. Bianchi. Confirmation of Matheron's conjecture on the covariogram of a planar convex body. *J. Eur. Math. Soc.*, 11(6):1187–1202, 2009. `doi:10.4171/JEMS/179`. 156

[11] A. Baddeley. Spatial point processes and their applications. In W. Weil, editor, *Stochastic Geometry, Lectures given at the C.I.M.E. Summer School held in Martina Franca, Italy, September 13-18, 2004*, volume 1892 of *Lecture Notes in Mathematics*, pages 1–75. Springer, 2007. 80, 115, 199, 206

[12] C. Barakat, P. Thiran, G. Iannaccone, C. Diot, and P. Owezarski. Modeling internet backbone traffic at the flow level. *IEEE Trans. Signal Process.*, 51(8):2111 – 2124, 2003. `doi:10.1109/TSP.2003.814521`. 46

[13] J. Barral and B. B. Mandelbrot. Multifractal products of cylindrical pulses. *Probability Theory and Related Fields*, 124(3):409–430, 2002. `doi:10.1007/s004400200220`. 109, 112

[14] H. Biermé and A. Desolneux. Regularity and crossings of shot noise processes. Submitted, 2010. Available from: `http://hal.archives-ouvertes.fr/hal-00484118/en/`. 62, 67, 179

[15] H. Biermé and A. Estrade. Poisson random balls: self-similarity and x-ray images. *Adv. Appl. Prob.*, 38(4):853–872, 2006. `doi:10.1239/aap/1165414582`. 67, 124

[16] H. Biermé, A. Estrade, and I. Kaj. Self-similar random fields and rescaled random balls models. *Jour. Theor. Probab.*, 2009. `doi:10.1007/s10959-009-0259-x`. 67, 124

[17] G. Blanchet, L. Moisan, and B. Rougé. Measuring the global phase coherence of an image. In *ICIP 2008*, pages 1176 – 1179, 2008. `doi:10.1109/ICIP.2008.4711970`. 22

[18] C. Bordenave, Y. Gousseau, and F. Roueff. The dead leaves model: a general tessellation modeling occlusion. *Adv. Appl. Prob.*, 38(1):31–46, 2006. `doi:10.1239/aap/1143936138`. 5, 21, 107, 108, 109, 112, 113, 118, 184

[19] J. Bourgain, H. Brezis, and P. Mironescu. Another look at Sobolev spaces. In *Optimal control and partial differential equation*, pages 439–455, 2001. 152

[20] A. Bovier and P. Picco. A law of the iterated logarithm for random geometric series. *The Annals of Probability*, 21(1):168–184, 1993. `doi:10.1214/aop/1176989399`. 117

[21] A. Brix and W. S. Kendall. Simulation of cluster point processes without edge effects. *Adv. Appl. Prob.*, 34(2):267–280, 2002. `doi:10.1239/aap/1025131217`. 67

[22] P. E. Brown, P. J. Diggle, and R. Henderson. A non-gaussian spatial process model for opacity of flocculated paper. *Scand. J. Statist.*, 30(2):355–368, 2003. `doi:10.1111/1467-9469.00335`. 46

[23] A. Buades, T. M. Le, J.-M. Morel, and L. A. Vese. Fast cartoon + texture image filters. *IEEE Trans. Image Process.*, 19(8):1978 –1986, 2010. `doi:10.1109/TIP.2010.2046605`. 6, 127

[24] A. Bulinski, E. Spodarev, and F. Timmermann. Central limit theorems for the excursion sets volumes of weakly dependent random fields. Technical report, Institut für Stochastik, Universität Ulm, 2010. Available from: `http://arxiv.org/abs/1005.0483`. 172

[25] A. J. Cabo and R. H. P. Janssen. Cross-covariance functions characterise bounded regular closed sets. cwi BS-R9426, CWI, 1994. Available from: `http://oai.cwi.nl/oai/asset/5110/5110D.pdf`. 156

[26] A.J. Cabo and A.J. Baddeley. Line transects, covariance functions and set convergence. *Adv. Appl. Prob.*, 7:585–605, 1995. Available from: `http://www.jstor.org/stable/1428125`. 156

[27] P. Calka. Tessellations. In W. S. Kendall and I. Molchanov, editors, *New Perspectives in Stochastic Geometry*, pages 145–169. Oxford University Press, 2010. 109

[28] F. Cao, F. Guichard, and H. Hornung. Dead leaves model for measuring texture quality on a digital camera. In *Proc. SPIE*, volume 7537, 2010. `doi:10.1117/12.838902`. 112

[29] Pierre Chainais. Infinitely divisible cascades to model the statistics of natural images. *IEEE Trans. Pattern Anal. Mach. Intell.*, 29(12):2105–2119, 2007. `doi:10.1109/TPAMI.2007.1113`. 109, 112

[30] A. Chambolle. An algorithm for total variation minimization and applications. *J. Math. Imaging Vis.*, 20(1-2):89–97, 2004. `doi:10.1023/B:JMIV.0000011325.36760.1e`. 127

[31] A. Chambolle, R. A. DeVore, N.-Y. Lee, and B. J. Lucier. Nonlinear wavelet image processing: Variational problems, compression, and noise removal through wavelet shrinkage. *IEEE Trans. Image Process.*, 7:319–335, 1996. `doi:10.1109/83.661182`. 5

[32] T. F. Chan and S. Esedoglu. Aspects of total variation regularized l^1 function approximation. *SIAM J. Appl. Math.*, 65(5):1817–1837, 2005. `doi:10.1137/040604297`. 5, 127

[33] T. F. Chan and C. K. Wong. Total variation blind deconvolution. *IEEE Trans. Image Process.*, 7(3):370 – 375, 1998. `doi:10.1109/83.661187`. 127

[34] M. Chlebík. On variation of sets. preprint 44, Max-Planck-Institut für Mathematik in den Naturwissenschaften Leipzig, 1997. Available from: `http://www.mis.mpg.de/preprints/1997/preprint1997_44.pdf`. 133

[35] H. Choi and R. G. Baraniuk. Wavelet statistical models and Besov spaces. In *Proc. SPIE*, volume 3813, pages 489–501. SPIE, 1999. `doi:10.1117/12.366806`. 5

[36] R. L. Cook and T. DeRose. Wavelet noise. In *SIGGRAPH '05*, pages 803–811, New York, NY, USA, 2005. ACM. `doi:10.1145/1186822.1073264`. 4, 24, 39, 70, 71

[37] R. Cowan and A.K.L. Tsang. The falling-leaves mosaic and its equilibrium properties. *Adv. Appl. Prob.*, 26:54–62, 1994. Available from: `http://www.jstor.org/stable/1427578`. 107, 185

[38] G. R. Cross and A. K. Jain. Markov random field texture models. *IEEE Trans. Pattern Anal. Mach. Intell.*, 5(1):25 – 39, 1983. `doi:10.1109/TPAMI.1983.4767341`. 3

[39] W. B. Davenport and W. L. Root. *An Introduction to the Theory of Random Signals and Noise.* McGraw-Hill, 1958. 22, 46

[40] J. Dávila. On an open question about functions of bounded variation. *Calc. Var.*, 15:519–527, 2002. 10.1007/s005260100135. 152

[41] J. S. De Bonet. Multiresolution sampling procedure for analysis and synthesis of texture images. In *SIGGRAPH '97*, pages 361–368. ACM Press/Addison-Wesley Publishing Co., 1997. `doi:10.1145/258734.258882`. 3

[42] W. C. de Leeuw and J. J. van Wijk. Enhanced spot noise for vector field visualization. In *IEEE Visualization*, pages 233–239, 1995. `doi:10.1109/VISUAL.1995.480817`. 22

[43] C. R. Dietrich and G. N. Newsam. Fast and exact simulation of stationary Gaussian processes through circulant embedding of the covariance matrix. *SIAM Journal on Scientific Computing*, 18(4):1088–1107, 1997. `doi:10.1137/S1064827592240555`. 47

[44] J.-M. Dischler and D. Ghazanfarpour. A procedural description of geometric textures by spectral and spatial analysis of profiles. *Computer Graphics Forum*, 16:129–139, 1997. `doi:10.1111/1467-8659.16.3conferenceissue.14`. 4, 70

[45] Y. Dong, S. Lefebvre, X. Tong, and G. Drettakis. Lazy solid texture synthesis. In *Computer Graphics Forum (Proceedings of the Eurographics Symposium on Rendering)*, 2008. 4

[46] D. L. Donoho and I. M. Johnstone. Adapting to unknown smoothness via wavelet shrinkage. *J. Am. Stat. Assoc.*, 90(432):1200–1224, 1995. `doi:10.2307/2291512`. 5

[47] J. L. Doob. *Stochastic Processes.* John Wiley & Sons, 1953. 140, 150, 174

[48] V. Duval, J.-F. Aujol, and Y. Gousseau. The tvl1 model: A geometric point of view. *Multiscale Model. Simul.*, 8(1):154–189, 2009. `doi:10.1137/090757083`. 190

[49] D. S. Ebert, F. K. Musgrave, D. Peachey, K. Perlin, and S. Worley. *Texturing and Modeling: A Procedural Approach.* Morgan Kaufmann Publishers Inc., San Francisco, CA, USA, 2002. 4, 5, 29, 70, 71, 77, 79, 105

[50] A. A. Efros and W. T. Freeman. Image quilting for texture synthesis and transfer. In *SIGGRAPH '01*, pages 341–346, New York, NY, USA, 2001. ACM. `doi:10.1145/383259.383296`. 3, 39

[51] A. A. Efros and T. K. Leung. Texture synthesis by non-parametric sampling. In *ICIP 1999*, pages 1033 – 1038, September 1999. `doi:10.1109/ICCV.1999.790383`. 3, 9, 24, 39, 41

[52] E. Enderton, E. Sintorn, P. Shirley, and D. Luebke. Stochastic transparency. In *I3D '10*, pages 157–164, New York, NY, USA, 2010. ACM. `doi:10.1145/1730804.1730830`. 5, 13, 112, 124

[53] K. B. Eom. Synthesis of color textures for multimedia applications. *Multimedia Tools Appl.*, 12(1):81–98, 2000. `doi:10.1023/A:1009648414312`. 26, 29

[54] L. C. Evans and R. F. Gariepy. *Measure theory and fine properties of functions.* Studies in advanced mathematics. CRC Press, 1992. 127, 130, 131, 156

[55] J. Fadili and G. Peyre. An algorithm for total variation projection. *IEEE Trans. on Image Process.*, 2010. Available from: `http://hal.archives-ouvertes.fr/hal-00380491/`. 127

[56] H. Federer. Curvature measures. *Trans. Amer. Math. Soc.*, 93:418–491, 1959. Available from: `http://www.jstor.org/stable/1993504`. 157, 168

[57] W. Feller. *An Introduction to Probability and Its Applications*, volume 2. John Wiley & Sons, second edition, 1971. 53, 58, 62

[58] B. Galerne. Computation of the perimeter of measurable sets via their covariogram. Applications to random sets. Accepted for publication in Image Analysis and Stereology, 2010. Available from: `http://hal.archives-ouvertes.fr/hal-00480825/en/`. 16, 155

[59] B. Galerne and Y. Gousseau. The transparent dead leaves process. preprint 2010-15, CMLA, ENS Cachan, 2010. Submitted. Available from: `http://hal.archives-ouvertes.fr/hal-00505281/en/`. 16, 111

[60] B. Galerne, Y. Gousseau, and J.-M. Morel. Micro-Texture Synthesis by Phase Randomization. Image Processing on Line, `http://www.ipol.im/pub/algo/ggm_random_phase_texture_synthesis/`, 2009. [submitted]. 7, 9, 16, 24, 35, 37, 40, 193

[61] B. Galerne, Y. Gousseau, and J.-M. Morel. Random phase textures: Theory and synthesis. *IEEE Trans. Image Process.*, 2010. `doi:10.1109/TIP.2010.2052822`. 16, 20

[62] C. Gasquet and P. Witomski. *Fourier analysis and applications: filtering, numerical computation, wavelets.* Springer-Verlag, New York, NY, USA, 1999. 75, 85

[63] I. I. Gikhman and A. V. Skorokhod. *The theory of stochastic processes I.* Classics in mathematics. Springer, 1974. 140, 150, 174

[64] G. Gilet, J.-M. Dischler, and L. Soler. Procedural descriptions of anisotropic noisy textures by example. In *Eurographics (Short)*, 2010. 71, 87

[65] A. Goldberg, M. Zwicker, and F. Durand. Anisotropic noise. In *SIGGRAPH '08*, pages 1–8, New York, NY, USA, 2008. ACM. `doi:10.1145/1399504.1360653`. 4, 24, 39, 70

[66] Y. Gousseau. Texture synthesis through level sets. In *2nd international workshop on texture analysis and synthesis*, 2002. 5, 105

[67] Y. Gousseau and J.-M. Morel. Are natural images of bounded variation? *SIAM J. Math. Anal.*, 33(3):634–648, 2001. `doi:10.1137/S0036141000371150`. 6

[68] Y. Gousseau and F. Roueff. Modeling occlusion and scaling in natural images. *SIAM journal of Multiscale Modeling and Simulation*, 6(1):105–134, 2007. `doi:10.1137/060659041`. 5, 6, 112, 124

[69] B. Grosjean and L. Moisan. A-contrario detectability of spots in textured backgrounds. *J. Math. Imaging Vis.*, 33(3):313–337, 2009. `doi:10.1007/s10851-008-0111-4`. 113

[70] J. A. Gubner. Computation of shot-noise probability distributions and densities. *SIAM J. Sci. Comput.*, 17(3):750–761, 1996. `doi:10.1137/S1064827594268725`. 62

[71] F. Guichard and F. Malgouyres. Total variation based interpolation. In *Eusipco'98*, pages 1741–1744. Elsevier North-Holland, Inc, 1998. 127

[72] A. Haas, G. Matheron, and J. Serra. Morphologie mathématique et granulométries en place. *Annales des Mines*, 1967. Available from: `http://www.cg.ensmp.fr/bibliotheque/public/HAAS_Publication_00098.pdf`. 157

[73] J. C. Hart, N. Carr, M. Kameya, S. A. Tibbitts, and T. J. Coleman. Antialiased parameterized solid texturing simplified for consumer-level hardware implementation. In *HWWS '99*, pages 45–53. ACM, 1999. `doi:10.1145/311534.311575`. 72, 96

[74] D. J. Heeger and J. R. Bergen. Pyramid-based texture analysis/synthesis. In *SIGGRAPH '95*, pages 229–238, New York, NY, USA, 1995. ACM. doi: 10.1145/218380.218446. 3, 5, 29, 43, 71, 87

[75] L. Heinrich and V. Schmidt. Normal convergence of multidimensional shot noise and rates of this convergence. *Adv. Appl. Prob.*, 17:709–730, 1985. Available from: http://www.jstor.org/stable/1427084. 7, 10, 47, 50, 53, 55, 58, 67, 112, 123

[76] Gunnar Hellmund. Completely random signed measures. *Stat. Probab. Lett.*, 79(7):894 – 898, 2009. doi:10.1016/j.spl.2008.11.009. 214

[77] D. Holten, J.J. van Wijk, and J.-B. Martens. A perceptually based spectral model for isotropic textures. *ACM Trans. Appl. Percept.*, 3(4):376–398, 2006. doi:10.1145/1190036.1190039. 27

[78] J. Horowitz. Measure-valued random processes. *Probability Theory and Related Fields*, 70:213–236, 1985. doi:10.1007/BF02451429. 215

[79] D. Hug, G. Last, and W. Weil. A local Steiner-type formula for general closed sets and applications. *Math. Z.*, 246(1-2):237–272, 2004. doi:10.1007/s00209-003-0597-9. 168, 182

[80] I. A. Ibragimov. Remarks on variations of random fields. *J. Math. Sci.*, 75(5):1931–1934, 1995. doi:10.1007/BF02365084. 127, 130, 145

[81] D. Jeulin. Morphological modeling of images by sequential random functions. *Signal Process.*, 16:403–431, 1989. doi:10.1016/0165-1684(89)90033-9. 110

[82] D. Jeulin. Dead leaves models: from space tesselation to random functions. In D. Jeulin, editor, *Proc. of the Symposium on the Advances in the Theory and Applications of Random Sets*, pages 137–156. World Scientific Publishing Company, 1997. 107, 110, 112, 117

[83] D. Jeulin. Random texture models for material structures. *Statistics and Computing*, 10:121–132, 2000. doi:10.1023/A:1008942325749. 110

[84] J.-O. Johansson and O. Hössjer. A shot-noise model for paper fibres with non-uniform random orientations. *Scand. J. Statist.*, 32(3):351–363, 2005. doi:10.1111/j.1467-9469.2005.00449.x. 46

[85] B. Julesz. Visual pattern discrimination. *IRE transactions on information theory*, 8(2):84–92, February 1962. doi:10.1109/TIT.1962.1057698. 20

[86] B. Julesz. Spatial nonlinearities in the instantaneous perception of textures with identical power spectra. *Phil. Trans. R. Soc. London, Ser. B*, 290(1038):83–94, July 1980. 20

[87] B. Julesz. A theory of preattentive texture discrimination based on first-order statistics of textons. *Biological Cybernetics*, 41(2):131–138, August 1981. `doi:10.1007/BF00335367`. 20, 21

[88] I. Kaj, L. Leskelä, I. Norros, and V. Schmidt. Scaling limits for random fields with long-range dependence. *Ann. Probab.*, 35(2):528–550, 2007. `doi:10.1214/009117906000000700`. 67, 124

[89] 0. Kallenberg. *Random measures.* Akademie-Verlag, Berlin, fourth edition, 1986. 199, 204, 205, 212, 214

[90] W. S. Kendall and E. Thönnes. Perfect simulation in stochastic geometry. *Pattern Recognition*, 32(9):1569–1586, 1999. `doi:10.1016/S0031-3203(99)00021-7`. 117

[91] J. F. C. Kingman. *Poisson Processes.* Oxford studies in probability. Oxford university press, 1993. 118, 199, 203, 207, 208, 209

[92] V. Y. Korolev and I.G. Shevtsova. An improvement of the Berry-Esseen inequality with applications to Poisson and mixed Poisson random sums. *Scandinavian Actuarial Journal*, 2010. `doi:10.1080/03461238.2010.485370`. 10, 47, 54, 55

[93] V. Y. Korolev and I.G. Shevtsova. Sharpened upper bounds for the absolute constant in the Berry-Esseen inequality for mixed Poisson random sums. *Doklady Mathematics*, 81(2):180–182, 2010. `doi:10.1134/S1064562410020031`. 54

[94] V. Kwatra, A.Schödl, I. Essa, G. Turk, and A. Bobick. Graphcut textures: image and video synthesis using graph cuts. In *SIGGRAPH '03*, pages 277–286. ACM Press, 2003. `doi:10.1145/1201775.882264`. 3

[95] A. Lagae, S. Lefebvre, R. Cook, T. DeRose, G. Drettakis, D. S. Ebert, J. P. Lewis, K. Perlin, and M. Zwicker. State of the art in procedural noise functions. In H. Hauser and E. Reinhard, editors, *EG 2010 - State of the Art Reports.* Eurographics Association, 2010. 4, 9, 24, 28, 46, 47, 63, 70, 77, 82, 86, 99

[96] A. Lagae, S. Lefebvre, G. Drettakis, and P. Dutré. Procedural noise using sparse Gabor convolution. *SIGGRAPH '09*, 28(3), August 2009. `doi:10.1145/1576246.1531360`. 4, 7, 9, 11, 16, 24, 29, 39, 43, 46, 63, 64, 66, 67, 69, 70, 71, 72, 73, 77, 79, 83, 86, 96

[97] A. Lagae, S. Lefebvre, G. Drettakis, and P. Dutré. Procedural noise using sparse Gabor convolution - auxiliary material. Report CW 545, Department of Computer Science, K.U.Leuven, Celestijnenlaan 200A, 3001 Heverlee, Belgium, May 2009. `doi:10.1145/1576246.1531360`. 71, 72

[98] A. Lagae, S. Lefebvre, and P. Dutré. Improving Gabor noise. Report CW 569, Department of Computer Science, K.U.Leuven, Celestijnenlaan 200A, 3001 Heverlee, Belgium, November 2009. Available from: `http://www.cs.kuleuven.be/publicaties/rapporten/cw/CW569.abs.html`. 64, 66, 79, 99

[99] A. Lagae, P. Vangorp, T. Lenaerts, and P. Dutré. Procedural isotropic stochastic textures by example. *Computers & Graphics (Special issue on Procedural Methods in Computer Graphics)*, 2010. `doi:10.1016/j.cag.2010.05.004`. 4, 70, 71, 87

[100] C. Lantuéjoul. *Geostatistical simulation: models and algorithms.* Springer, 2002. 46, 71, 75, 104, 114, 117, 118, 127, 156, 157, 158, 159, 167, 176, 182, 188

[101] S. Lefebvre and H. Hoppe. Parallel controllable texture synthesis. In *SIGGRAPH '05*, pages 777–786. ACM, 2005. `doi:10.1145/1186822.1073261`. 4

[102] J.-P. Lewis. Texture synthesis for digital painting. In *SIGGRAPH '84*, pages 245–252, New York, NY, USA, 1984. ACM. `doi:10.1145/800031.808605`. 9, 27, 46, 63

[103] F. Liu and R. W. Picard. A spectral 2-D Wold decomposition algorithm for homogeneous random fields. In *ICASSP '99*, pages 3501–3504. IEEE Computer Society, 1999. `doi:10.1109/ICASSP.1999.757597`. 99

[104] M. Loève. *Probability Theory I*, volume 45 of *Graduate texts in mathematics.* Springer-Verlag, fourth edition, 1977. 53

[105] B. Luo, J.-F. Aujol, and Y. Gousseau. Local scale measure from the topographic map and application to remote sensing images. *Multiscale Model. Simul.*, 8(1):1–29, 2009. `doi:10.1137/080730627`. 190

[106] G. Matheron. *Les variables régionalisées et leur estimation.* Masson, Paris, 1965. Available from: `http://cg.ensmp.fr/bibliotheque/`. 157, 159

[107] G. Matheron. *Éléments pour une théorie des mileux poreux.* Masson, Paris, 1967. Available from: `http://cg.ensmp.fr/bibliotheque/`. 8, 15, 106, 127, 155, 156, 158, 167

[108] G. Matheron. Schéma booléen séquentiel de partition aléatoire. Technical Report 89, CMM, 1968. Available from: `http://cg.ensmp.fr/bibliotheque/`. 21, 107, 112

[109] G. Matheron. Compléments sur les modèles isofactoriels. Technical Report N-432, Centre de Géostatistique, Ecole des mines de Paris, 1975. Available from: `http://cg.ensmp.fr/bibliotheque/`. 176

[110] G. Matheron. *Random sets and integral geometry.* Wiley series in probability and mathematical statistics. John Wiley & Sons, 1975. 15, 106, 114, 118, 127, 155, 156, 157, 164, 168, 172, 200

[111] G. Matheron. Le covariogramme géométrique des compacts convexes de $\mathbb{R}^2$. Technical Report N/2/86/G, Centre de Géostatistique, Ecole des mines de Paris, 1986. Available from: http://cg.ensmp.fr/bibliotheque/. 157, 161, 162

[112] Y. Meyer. *Oscillating patterns in image processing and nonlinear evolution equations. The fifteenth Dean Jacqueline B. Lewis memorial lectures*, volume 22 of *Universtity lecture series.* American Mathematical Society, 2001. 6, 127

[113] L. Moisan. Periodic plus smooth image decomposition. preprint 2009-11, MAP5, Université Paris Descartes, 2009. Available from: http://www.mi.parisdescartes.fr/~moisan/p+s/. 7, 9, 11, 24, 31, 32, 70, 71, 87, 88, 193, 194, 195, 198

[114] L. Moisan. Periodic plus smooth image decomposition webpage, 2009. Available from: http://www.math-info.univ-paris5.fr/~moisan/p+s/. 193, 196, 197

[115] I. Molchanov. *Theory of Random Sets.* Probability and Its Applications. Springer, 2005. 164, 165

[116] J. Møller and G. L. Torrisi. Generalised shot noise Cox processes. *Adv. Appl. Prob.*, 37(1):48–74, 2005. doi:10.1239/aap/1113402399. 67

[117] M. Nikolova. A variational approach to remove outliers and impulse noise. *J. Math. Imag. Vis.*, 20:99–120, 2004. doi:10.1023/B:JMIV.0000011326.88682.e5. 127

[118] A. V. Oppenheim and J. S. Lim. The importance of phase in signals. In *Proceedings of the IEEE*, volume 69, pages 529–541, May 1981. 20

[119] A. Papoulis. High density shot noise and Gaussianity. *J. Appl. Probab.*, 8(1):118–127, 1971. Available from: http://www.jstor.org/stable/3211842. 10, 47, 51, 53, 55, 64

[120] A. Papoulis and S. U. Pillai. *Probability, Random Variables and Stochastic Processes.* McGraw-Hill, fourth edition, 2002. 28

[121] P. Pérez, M. Gangnet, and A. Blake. Poisson image editing. In *SIGGRAPH '03*, pages 313–318, New York, NY, USA, 2003. ACM. doi:10.1145/1201775.882269. 31

[122] P. Pérez, M. Gangnet, and A. Blake. Patchworks: Example-based region tiling for image editing. Technical Report MSR-TR-2004-04, Microsoft Research, 2004. 39

[123] K. Perlin. An image synthesizer. In *SIGGRAPH '85*, pages 287–296, New York, NY, USA, 1985. ACM. doi:10.1145/280811.280986. 4, 9, 24, 29, 39, 46, 70, 71

[124] G. Peyré. Texture synthesis with grouplets. *IEEE Trans. Pattern. Anal. Mach. Intell.*, 4(32):733–746, 2010. doi:10.1109/TPAMI.2009.54. 3

[125] J. Portilla and E. P. Simoncelli. A parametric texture model based on joint statistics of complex wavelet coefficients. *Int. J. Comp. Vis.*, 40(1):49–71, 2000. doi:10.1023/A:1026553619983. 3, 5, 127

[126] T. Pouli, D. W. Cunningham, and E. Reinhard. Image statistics and their applications in computer graphics. In H. Hauser and E. Reinhard, editors, *EG 2010 - State of the Art Reports*, pages 83–112. Eurographics Association, 2010. 20

[127] W. H. Press, S. A. Teukolsky, W. T. Vetterling, and B. P. Flannery. *Numerical Recipes 3rd Edition: The Art of Scientific Computing.* Cambridge University Press, New York, NY, USA, 2007. 31, 193, 197

[128] J. Rabin, G. Peyré, J. Delon, and M. Bernot. Wasserstein barycenter and its application to texture mixing. Technical report, 2010. Available from: http://hal.archives-ouvertes.fr/hal-00476064/en/. 3

[129] J. Rataj. On set covariance and three-point test sets. *Czechoslovak Math.*, 54(129)(1):205–214, 2004. doi:10.1023/B:CMAJ.0000027260.34288. 7f. 156, 157

[130] J. Rataj and M. Zähle. Curvatures and currents for unions of sets with positive reach, II. *Ann. Glob. Anal. Geom.*, 20(1):1–21, 2001. doi:10.1023/A:1010624214933. 157, 168

[131] J. Rice. On generalized shot noise. *Adv. Appl. Prob.*, 9:553–565, 1977. Available from: http://www.jstor.org/stable/1426114. 50, 67, 112

[132] F. Richard and H. Biermé. Statistical tests of anisotropy for fractional Brownian textures. Application to full-field digital mammography. *J. Math. Imaging Vis.*, 36(3):227–240, 2010. doi:10.1007/s10851-009-0181-y. 113

[133] L. I. Rudin, S. Osher, and E. Fatemi. Nonlinear total variation based noise removal algorithms. *Physica D: Nonlinear Phenomena*, 60(1-4):259 – 268, 1992. doi:10.1016/0167-2789(92)90242-F. 5, 127

[134] W. Rudin. *Real and Complex Analysis.* McGraw-Hill series in higher mathematics. McGraw-Hill, 1970. 215

[135] M. Scheuerer. Regularity of the sample paths of a general second order random field. *Stoch. Process. Appl.*, 120(10):1879 – 1897, 2010. `doi:10.1016/j.spa.2010.05.009`. 140, 153, 174, 176

[136] R. Schneider and W. Weil. *Stochastic and Integral Geometry*. Probability and Its Applications. Springer, 2008. 104, 106, 109, 112, 115, 158, 164, 168, 174, 180, 182, 188, 190, 199, 200, 201, 202, 203, 205, 206, 207, 214, 227, 229, 230

[137] J. Serra, editor. *Image Analysis and Mathematical Morphology*, volume 1. Academic press, London, 1982. 21, 157

[138] J. Serra, editor. *Image Analysis and Mathematical Morphology, volume 2 : theoretical advances*. Academic press, London, 1988. 106

[139] M. Shinozuka. Simulation of multivariate and multidimensional random processes. *J. Acoust. Soc. Am.*, 49(1B):357–368, 1971. `doi:10.1121/1.1912338`. 71, 75

[140] M. Shinozuka and C.-M. Jan. Digital simulation of random processes and its applications. *J. Sound Vibration*, 25(1):111 – 128, 1972. `doi:10.1016/0022-460X(72)90600-1`. 71, 75

[141] D. Stoyan. On generalized planar random tessellations. *Math. Nachr.*, 128(1):215–219, 1986. `doi:10.1002/mana.19861280118`. 109

[142] D. Stoyan, W. S. Kendall, and J. Mecke. *Stochastic geometry and its applications*. Wiley series in probability and mathematical statistics. John Wiley & Sons, second edition, 1995. 104, 106, 109, 112, 168, 182

[143] D. Stoyan and K. Mecke. The Boolean model: from Matheron till today. In Michel Bilodeau, Fernand Meyer, and Michel Schmitt, editors, *Space, Structure and Randomness*, volume 183 of *Lecture Notes in Statistics*, pages 151–181. Springer New York, 2005. `doi:10.1007/0-387-29115-6_8`. 106, 112

[144] X. Tang and W. K. Stewart. Optical and sonar image classification: wavelet packet transform vs Fourier transform. *Comput. Vis. Image Underst.*, 79(1):25–46, July 2000. `doi:10.1006/cviu.2000.0843`. 20

[145] I. Tyurin. New estimates of the convergence rate in the Lyapunov theorem. Submitted, 2009. Available from: `http://arxiv.org/abs/0912.0726`. 54

[146] J. J. van Wijk. Spot noise texture synthesis for data visualization. In *SIGGRAPH '91*, pages 309–318, New York, NY, USA, 1991. ACM. `doi:10.1145/122718.122751`. 4, 5, 7, 8, 9, 22, 27, 46, 63

[147] W. Vervaat. Sample path properties of self-similar processes with stationary increments. *The Annals of Probability*, 13(1):1–27, 1985. `doi:10.1214/aop/1176993063`. 190

[148] L. A. Vese and S. J. Osher. Modeling textures with total variation minimization and oscillating patterns in image processing. *Journal of Scientific Computing*, 19:553–572, 2003. 10.1023/A:1025384832106. 6, 127

[149] E. Villa. On the outer Minkowski content of sets. *Ann. Mat. Pura Appl.*, 188:619–630, 2009. `doi:10.1007/s10231-008-0093-2`. 168, 182

[150] E. Villa. Mean densities and spherical contact distribution function of inhomogeneous Boolean models. *Stoch. Anal. Appl.*, 28:480–504, 2010. `doi:10.1080/07362991003708812`. 168, 172, 182, 190

[151] Mingshi Wang and André Knoesen. Rotation- and scale-invariant texture features based on spectral moment invariants. *J. Opt. Soc. Am. A*, 24(9):2550–2557, 2007. `doi:10.1364/JOSAA.24.002550`. 20

[152] L.-Y. Wei, S. Lefebvre, V. Kwatra, and G. Turk. State of the art in example-based texture synthesis. In *Eurographics 2009, State of the Art Report, EG-STAR*. Eurographics Association, 2009. 1, 3, 24, 39, 70

[153] L. Y. Wei and M. Levoy. Fast texture synthesis using tree-structured vector quantization. In *SIGGRAPH '00*, pages 479–488. ACM Press/Addison-Wesley Publishing Co., 2000. `doi:10.1145/344779.345009`. 3

[154] H. Wendt, S. G. Rouxand S. Jaffard, and P. Abry. Wavelet leaders and bootstrap for multifractal analysis of images. *Signal Process.*, 89(6):1100–1114, 2009. `doi:10.1016/j.sigpro.2008.12.015`. 6

[155] A. T. A. Wood and G. Chan. Simulation of stationary Gaussian processes in $[0,1]^d$. *Journal of Computational and Graphical Statistics*, 3(4):409–432, December 1997. `doi:10.2307/1390903`. 47

[156] S. Worley. A cellular texture basis function. In *SIGGRAPH '96*, pages 291–294. ACM, 1996. `doi:10.1145/237170.237267`. 5, 105

[157] L. P. Yaroslavsky. Pseudo-random numbers, evolutionary models in image processing and biology and nonlinear dynamic systems. In *SPIE*, volume 2824, pages 46–55, Denver, CO, USA, 1996. `doi:10.1117/12.258138`. 26

[158] J. I. Yellott. Implications of triple correlation uniqueness for texture statistics and the julesz conjecture. *J. Opt. Soc. Am. A*, 10:777 – 793, May 1993. `doi:10.1364/JOSAA.10.000777`. 20

Stochastic Image Models and Texture Synthesis

Abstract:

This thesis is a study of stochastic image models with applications to texture synthesis. Most of the stochastic texture models under investigation are germ-grain models.

In the first part of the thesis, texture synthesis algorithms relying on the shot noise model are developed. In the discrete framework, two different random processes, namely the *asymptotic discrete spot noise* and the *random phase noise*, are theoretically and experimentally studied. A fast texture synthesis algorithm relying on these random processes is then elaborated. Numerous results demonstrate that the algorithm is able to reproduce a class of real-world textures which we call micro-textures. In the continuous framework, the Gaussian convergence of shot noise models is further studied and new bounds for the rate of this convergence are established. Finally, a new algorithm for procedural texture synthesis from example relying on the recent Gabor noise model is presented. This new algorithm permits to automatically compute procedural models for real-world micro-textures.

The second part of the thesis is devoted to the introduction and study of the *transparent dead leaves (TDL) process*, a new germ-grain model obtained by superimposing semi-transparent objects. The main result of this part shows that, when varying the transparency of the objects, the TDL process provides a family of models varying from the dead leaves model to a Gaussian random field.

In the third part of the thesis, general results on random fields with bounded variation are established with an emphasis on the computation of the mean total variation of random fields. As particular cases of interest, these general results permit the computation of the mean perimeter of random sets and of the mean total variation of classical germ-grain models.

Keywords: covariogram, functions of bounded variation, Gabor noise, germ-grain models, random fields, random phase, shot noise, texture synthesis, transparency